Université Fédérale
Toulouse Midi-Pyrénées

THÈSE

En vue de l'obtention du

DOCTORAT DE L'UNIVERSITÉ DE TOULOUSE

Délivré par : *l'Institut Supérieur de l'Aéronautique et de l'Espace (ISAE)*

Présentée et soutenue le *08 décembre 2016* **par :**

FLÁVIO LUIZ CARDOSO RIBEIRO

Port-Hamiltonian modeling and control of a fluid-structure system

Application to sloshing phenomena in a moving container coupled to a flexible structure

---

JURY

PAUL KOTYCZKA	Membre du Jury
LAURENT LEFÈVRE	Président du Jury
ALESSANDRO MACCHELLI	Rapporteur
BERNHARD MASCHKE	Rapporteur
DENIS MATIGNON	Directeur de thèse
VALÉRIE POMMIER-BUDINGER	Co-directrice de thèse
JEAN-SÉBASTIEN SCHOTTÉ	Membre du Jury

École doctorale et spécialité :
EDSYS : Automatique
Unité de Recherche :
Équipe d'accueil ISAE-ONERA CSDV
Directeur(s) de Thèse :
Denis MATIGNON et *Valérie POMMIER-BUDINGER*
Rapporteurs :
Bernhard MASCHKE et *Alessandro MACCHELLI*

Port-Hamiltonian modeling and control of a fluid-structure system
Application to sloshing phenomena in a moving container coupled to a flexible structure

Abstract — This thesis is motivated by an aeronautical issue: the fuel sloshing in tanks of very flexible wings. The vibrations due to these coupled phenomena can lead to problems like reduced passenger comfort and maneuverability, and even unstable behavior. This thesis aims at developing new models of fluid-structure interaction based on the theory of port-Hamiltonian systems (pHs). The pHs formalism provides a unified framework for the description of complex multi-physics systems and a modular approach for the coupling of subsystems thanks to interconnection ports. Furthermore, the design of controllers using pHs models is also addressed.

PHs models are proposed for the equations of liquid sloshing based on 1D and 2D Saint Venant equations and for the equations of structural dynamics. The originality of the work is to give pHs models of sloshing in moving containers. The interconnection ports are used to couple the sloshing dynamics to the structural dynamics of a beam controlled by piezoelectric actuators. After writing the partial differential equations of the coupled system using the pHs formalism, a finite-dimensional approximation is obtained by using a geometric pseudo-spectral method that preserves the pHs structure of the infinite-dimensional model at the discrete level. The thesis proposes several extensions of the geometric pseudo-spectral method, allowing the discretization of systems with second-order differential operators and with an unbounded input operator. Experimental tests on a structure made of a beam connected to a tank were carried out to validate both the pHs model of liquid sloshing in moving containers and the pseudo-spectral semi-discretization method. The pHs model was finally used to design a passivity-based controller for reducing the vibrations of the coupled system.

Keywords: port-Hamiltonian systems, sloshing, fluid-structure interactions, geometric semi-discretization, passivity-based control.

Modélisation et commande d'interaction fluide-structure sous forme de système Hamiltonien à ports

Application au ballottement dans un réservoir en mouvement couplé à une structure flexible

Résumé — Cette thèse est motivée par un problème aéronautique: le ballottement du carburant dans des réservoirs d'ailes d'avion très flexibles. Les vibrations induites par le couplage du fluide avec la structure peuvent conduire à des problèmes tels que l'inconfort des passagers, une manœuvrabilité réduite, voire même provoquer un comportement instable. Cette thèse a pour objectif de développer de nouveaux modèles d'interaction fluide-structure, en mettant en œuvre la théorie des systèmes Hamiltoniens à ports d'interaction (pHs). Le formalisme pHs fournit d'une part un cadre unifié pour la description des systèmes multi-physiques complexes et d'autre part une approche modulaire pour l'interconnexion des sous-systèmes grâce aux ports d'interaction. Cette thèse s'intéresse aussi à la conception de contrôleurs à partir des modèles pHs.

Des modèles pHs sont proposés pour les équations de ballottement du liquide en partant des équations de Saint Venant en 1D et 2D. L'originalité du travail est de donner des modèles pHs pour le ballottement dans des réservoirs en mouvement. Les ports d'interaction sont utilisés pour coupler la dynamique du ballottement à la dynamique d'une poutre contrôlée par des actionneurs piézo-électriques, celle-ci étant préalablement modélisée sous forme pHs. Après l'écriture des équations aux dérivées partielles dans le formalisme pHs, une approximation en dimension finie est obtenue en utilisant une méthode pseudo-spectrale géométrique qui conserve la structure pHs du modèle continu au niveau discret. La thèse propose plusieurs extensions de la méthode pseudo-spectrale géométrique, permettant la discrétisation des systèmes avec des opérateurs différentiels du second ordre d'une part et avec un opérateur d'entrée non borné d'autre part. Des essais expérimentaux ont été effectués sur une structure constituée d'une poutre liée à un réservoir afin d'assurer la validité du modèle pHs du ballottement du liquide couplé à la poutre flexible, et de valider la méthode pseudo-spectrale de semi-discrétisation. Le modèle pHs a finalement été utilisé pour concevoir un contrôleur basé sur la passivité pour réduire les vibrations du système couplé.

Mots clés : systèmes Hamiltoniens à ports, ballottement, interactions fluide-structure, semi-discrétisation géométrique, commande basée sur la passivité.

Acknowledgements

First, I would like to thank my thesis advisors Prof. Valérie Pommier-Budinger and Prof. Denis Matignon for their invaluable support, encouragement, and guidance throughout my doctorate studies. The doors to their offices were always open for me. They consistently allowed this thesis to be my own work but steered me in the right direction. Furthermore, I am profoundly grateful for their friendly care, helping me in everything I needed during my stay in France.

I would like also to acknowledge Denis Arzelier, for welcoming me in France and guiding me during my first year in Toulouse.

I would like to acknowledge the members of the thesis committee: Paul Kotyczka, Laurent Lefèvre, Alessandro Macchelli, Bernhard Maschke and Jean-Sebastien Schotté. Their participation in my thesis commitee was an honor for me. I am really grateful for their helpful feedback, questions, interesting insights and encouragements.

I would like to thank all the members of the departments of ISAE that were involved in my research activities (DISC, DCAS, and DEOS). In special, I am grateful to Laurent Alloza, for his technical support with the experimental setup. I am also grateful to the many technical, administrative, and academic staff members for their help, support and inspiration: Gilles Pérusot, Guillaume Beaugendre, Matthieu Berranger, Ghislain Haine, Joel Bordeneuve, Michel Salaun, Xavier Vasseur, Daniel Alazard, Yves Brière, Yves Gourinat, Youssef Diouane, Pierre de Saqui-Sannes, Caroline Chanel, Marie-Carmen Fauré, and Odile Riteau.

This work has been done partially in the framework of *Agence Nationale de la Recherche* (ANR) project HAMECMOPSYS. Thanks to this project, I had the opportunity to attend conferences, summer schools and meet so many interesting people. I am especially grateful to the members of the project, with whom I had many fruitful discussions.

I would like to express my sincere gratitude to the Brazilian taxpayers, who funded my studies in France: this thesis was funded by a scholarship *Ciência sem Fronteiras* from the Brazilian agency CNPq, *Conselho Nacional de Desenvolvimento Científico e Tecnológico*. I am also grateful to ITA, *Instituto Tecnológico de Aeronáutica*, for supporting my participation in this Ph.D. program. I also thank for the support of my colleagues from ITA, especially to my friend Prof. Mauricio Morales, who helped me on so many occasions.

I am grateful to Coursera, EDx and France Université Numérique for supporting free of charge, high-quality online courses. Special thanks to the professors who offered excellent online courses: Russ Tedrake, Krishna Garikipati, Emmanuel de Langre, Nathan Kutz, Randall J. LeVeque.

I am also grateful to the colleagues of ISAE, for their friendship, support, and long coffee breaks: Marie, Vincent, Michèle, Saïd, Francesco, Antoine, Pierrick, Gaël, Arthur, Jacobo,

Jose, Adrian, Leandro, Paulo, Igor.

Finally, I express my deep gratitude to my family, for their life-long support. I am especially grateful to my lovely wife Nastenka. This four-year stay in France was our common project. Her love and companionship made these years much easier and happier. I am looking forward to our next adventures together!

Contents

Acronyms

DAE	Differential-Algebraic Equation
DVF	Direct Velocity Feedback
ISAE	*Institut Supérieur de l'Aéronautique et de l'Espace*
HALE	High-Altitude Long Endurance
FEM	Finite Element Method
FSI	Fluid-Structure Interactions
IFF	Integral Force Feedback
LQR	Linear Quadratic Regulator
LQG	Linear Quadratic Gaussian
ODE	Ordinary Differential Equation
pHs	port-Hamiltonian systems
PDE	Partial Differential Equation
PPF	Positive Position Feedback
PZT	Lead Zirconate Titanate (piezoelectric ceramic material)
RANS	Reynolds-averaged Navier Stokes
SWE	Shallow Water Equations

Part I

Introduction and state of the art

Chapter 1

Introduction

1.1 General context

Several accidents were reported to be related to the coupling of fuel sloshing and airplane dynamics. The motion of fuel can severely affect the flight dynamics, leading to reduced handling qualities and even instabilities. For example, several Lockheed F-80C crashed during the Korean war without apparent reason. Indeed, flight tests verified that a coupling between the motion of fuel and short period rigid body dynamics led to unstable pitch motion. Similarly, in the 1950s, the Dutch roll mode of Douglas A4D Skyhawk exhibited undamped oscillations for partially filled fuel tank, for the same reason. Both cases are presented in Chapter 14 of Abzug and Larrabee (2002). The sloshing is still a major concern for modern aircraft design since recent jet airplanes tend to have high ratios of fuel to gross weight. For instance, fuel represents about 47% of the weight of Boeing 777-200ER during take-off.

Fuel sloshing is also a cause of major concern for liquid-fueled launch vehicles. Saturn I presented oscillations due to sloshing as presented in Bauer (1960) and Chapter 1 of Abramson (1966). More recently, Falcon 1 exhibited an unstable oscillation in the upper stage control system that prevented the rocket from reaching its intended orbit. The oscillation was very likely caused by the liquid oxygen sloshing, as reported by SpaceX (2007).

The economical and environmental impacts of fuel consumption in aviation lead to a constant quest for improving the performance characteristics of aircraft. One way of achieving this is by optimization of the structure, trying to reduce the airplane empty weight (e.g., by using lightweight materials such as carbon fiber materials). Another way of saving fuel is by improving the aerodynamic efficiency: reducing drag. The lift-to-drag ratio can be maximized by using wings with a high aspect ratio (long wings).

Both of these strategies (optimizing the structure and increasing the aspect ratio) contribute to increasing the structural flexibility of new designs. As a matter of fact, the new generation of airplanes (like Airbus 350 and Boeing Dreamliner 787) have higher aspect ratios and are more flexible than previous generations. It is very likely that this trend will continue.

In the past, the disciplines of flight dynamics, control, structural dynamics, and aerodynamics could be analyzed almost independently of each other. With airplanes subject to larger structural flexibility, this approach might not be sufficient. In addition, flexibility can lead to several different nonlinear phenomena that could be neglected when stiffer structures were

Figure 1.1: Photos of Airbus A350 (left) and Boeing Dreamliner 787 (right). Both airplanes have higher wing aspect ratio and exhibit larger structural flexibility than previous generations.

used (e.g., nonlinear structural deflections and nonlinear aerodynamics phenomena, coupling with fluid sloshing, etc.).

Indeed, a great attention has been given recently to the High-Altitude Long Endurance (HALE) aircraft (also known as *atmospheric satellites* or *pseudo-satellites*). To achieve the mission of flying for months without landing, the performance requirements become even more critical. Thus, most HALE airplanes have wings with aspect ratios several times bigger than usual. This is the case, for example, of Facebook Aquila, Airbus Zephyr and NASA HALE prototypes (Pathfinder, Centurion, and Helios). In the case of the Helios prototype, large structural deflections lead to the loss of aircraft, depicted in Fig. 1.2. The accident report (Noll et al., 2004) highlighted that *"lack of adequate analysis methods (...)"* related to the *" (...) complex interactions among the flexible structure, unsteady aerodynamics, flight control system, propulsion system, the environmental conditions, and vehicle flight dynamics (...)"* was among the root causes of the accident.

Figure 1.2: Photos of the Helios Prototype. A complex instability, involving the (nonlinear) flexible structure, the unsteady aerodynamics, the flight control system, the propulsion system, the vehicle flight dynamics, and the weather conditions, led to the loss of the aircraft.

Another trend for future airplane design is the use of smart materials, i.e., materials that are designed to have a certain response for given external stimuli. Among the possible applications that are foreseen for these materials, we can cite morphing structures that can

change the airplane shape in-flight to adapt for the different flight phases, vibration reduction, structural health monitoring, etc.

For all these reasons (airplanes with large fuel tanks, increased structural flexibility, new smart materials), new tools, that can be used for analyzing complex, multidisciplinary, coupled systems will be very useful in the future of the aerospace industry.

The use of port-based modeling (Breedveld, 2004) is a recent trend in the systems analysis and control. The methodology allows describing complex systems as composed of several simple subsystems which interact through a pair of variables, whose product equals power. The energy exchange between each subsystem is viewed as a common language for describing the interaction of systems of different domains (thermal, mechanical, electrical, etc.). Additionally, this framework leads to valuable tools for simulation, since the dynamic equations can be obtained in a straightforward (and automated) way (Karnopp, Margolis, and Rosenberg, 2012).

More recently, the port-Hamiltonian formulation (Duindam et al., 2009) combined the port-based modeling with Hamiltonian systems theory. It provides a modular, physically oriented approach for modeling complex nonlinear systems. It is also a natural framework for passivity-based control design.

In this context of more flexible airplanes with smart materials, the main goal of this thesis is to investigate the use of the port-Hamiltonian formalism as a new tool for modeling and control of fluid-structure coupled systems. We focus on an experimental device that consists of a flexible structure with piezoelectric actuators coupled to a tank partially filled with water. This device mimics the dynamics of a flexible wing with tip fuel tank.

1.2 Outline

This document is divided into five main parts.

Part I introduces the topic with a survey (Chapter 2) and presenting the experimental device (Chapter 3).

Part II is devoted to the port-Hamiltonian modeling of the fluid-structure interactions. Firstly, a recall of port-Hamiltonian systems (pHs) is presented in Chapter 4. Secondly, the piezoelectric beam equations are established in Chapter 5. Thirdly, the fluid equations are presented in Chapter 6. Then, the final coupled equations are presented in Chapter 7.

Part III is dedicated to spatial discretization methods that preserve the port-Hamiltonian structure. Firstly, we recall the existing methods in Chapter 8. Then, extensions to include distributed ports and higher-order differential operators are presented in Chapter 9. Numerical results and comparisons with experimental results are presented in Chapter 10.

Part IV is consecrated to vibrations control. Firstly, a recall on classical methods of

vibration control is presented in Chapter 11. Secondly, a simple method for damping injection is presented in Chapter 12.

The thesis ends with conclusions and discussions about further work.

1.3 Contributions

The main contributions of this thesis are:

- Extension of shallow water equations for moving containers using the port-Hamiltonian formulation in 1D and 2D;
- Proposition of simple piezoelectric beam models as pHs with both bending and torsion motions;
- Extension of the power-preserving pseudo-spectral spatial discretization methods to system with higher-order derivatives, and to systems with distributed ports with unbounded input operator;
- Proposition of a control technique by "passifivation" of non-collocated actuators/sensors using state-observer, with the goal of actively reducing vibrations.

Moreover, experimental data was used to validate the numerical results obtained with this methodology.

1.4 Publications and presentations

The following publications and presentations were a result of work conducted during doctoral study:

Presentations in conference with full papers published in Proceedings:

1. Cardoso-Ribeiro, F. L., Pommier-Budinger, V., Schotté, J.-S., and Arzelier, D. (2014). Modeling of a coupled fluid-structure system excited by piezoelectric actuators. In Proc. of the 2014 IEEE/ASME International Conference on Advanced Intelligent Mechatronics (pp. 216–221). Besançon, France.
2. Cardoso-Ribeiro, F. L., Matignon, D., and Pommier-Budinger, V. (2015). Control design for a coupled fluid-structure system with piezoelectric actuators. In Proc. of the 3rd CEAS EuroGNC. Toulouse, France.
3. Cardoso-Ribeiro, F. L., Matignon, D., and Pommier-Budinger, V. (2015). Modeling of a Fluid-structure coupled system using port-Hamiltonian formulation. In Proc. of the

5th IFAC Workshop on Lagrangian and Hamiltonian Methods for Nonlinear Control (LHMNC) (Invited Session) (Vol. 48, pp. 217–222). Lyon, France.

4. Cardoso-Ribeiro, F. L., Matignon, D., and Pommier-Budinger, V. (2016). Piezoelectric beam with distributed control ports : a power-preserving discretization using weak formulation. In Proc. of the 2nd IFAC Workshop on Control of Systems Governed by Partial Differential Equations (CPDE) (Invited Session) (pp. 290–297). Bertinoro, Italy.

5. Cardoso-Ribeiro, F. L., Matignon, D., and Pommier-Budinger, V. (2016). Modeling by interconnection and control by damping injection of a fluid-structure system with non-collocated actuators and sensors. In Proc. of the International Conference on Noise and Vibration Engineering ISMA (pp. 121-135). Leuven, Belgium.

Journal papers submitted:

1. Cardoso-Ribeiro, F. L., Matignon, D., and Pommier-Budinger, V. A port-Hamiltonian model of liquid sloshing in moving containers and application to a fluid-structure system. Journal of Fluids and Structures (accepted for publication).

2. Aoues, S., Cardoso-Ribeiro, F. L., Matignon, D., and Alazard, D. Modeling and control of a rotating flexible spacecraft: a port-Hamiltonian approach. Submitted to an international journal (under review).

Presentation in workshop without proceedings:

1. Cardoso-Ribeiro, F. L., Matignon, D., and Pommier-Budinger, V. (2016). Port-Hamiltonian modeling and control of a fluid-structure system. In Book of Abstracts of the Workshop on Energy Based Modeling, Simulation, and Control of Complex Physical Systems. Berlin, Germany.

Presentation in seminars:

1. Cardoso-Ribeiro, F. L. (2016). Modeling and control of fluid-structure coupled systems: a port-Hamiltonian approach. In: Seminar of Département Conception et Conduite des véhicules Aéronautiques et Spatiaux (DCAS). ISAE-SUPAERO. Toulouse, France.

2. Cardoso-Ribeiro, F. L. (2016). Ballottement: expérimentation, modélisation et simulation par systèmes Hamiltoniens à ports d'interaction. In: Journée Interactions Fluide-Structure. ISAE-SUPAERO. Toulouse, France.

3. Cardoso-Ribeiro, F. L., and Matignon, D. (2015). Modeling and control of fluid-structure coupled systems: a port-Hamiltonian approach. In: Seminar of Département Aérodynamique, Energétique et Propulsion (DAEP). ISAE-SUPAERO. Toulouse, France.

4. Cardoso-Ribeiro, F. L. (2015). Shallow water equations under rigid body motion. In: Seminar of HAMECMOPSYS. IRCAM. Paris, France.

5. Cardoso-Ribeiro, F. L. (2014). Modeling and control of a flexible/fluid coupled system. In: Doctoral school conference EDSYS. Toulouse, France.

Chapter 2

Literature review

This manuscript involves the modeling of structural dynamics with piezoelectric materials, fluid dynamics, and their interactions. In addition, we discuss the use of spatial discretization for simulation and also the control design for active vibration suppression. Since this document involves such multidisciplinary and broad fields, a full literature review about each of these topics is out of scope. For this reason, this chapter will first focus on modeling of fluid-structure systems with emphasis on liquid sloshing and aerospace applications in Section 2.1. Then, a literature review about port-Hamiltonian systems (pHs) and their applications is presented in Section 2.2. Finally, we have chosen to make the literature review on active vibration control within the Chapter 11, that address this topic.

2.1 Liquid sloshing in moving containers and aerospace applications

One of the first studies of the influence of sloshing in the airplane dynamics was performed by Smith Jr. (1948) who conducted an experimental study in wind tunnel, to verify the influence of the sloshing in the lateral stability of airplanes. He found that sloshing in tanks caused erratic lateral motions. The effect was most pronounced when the tanks were less than half full.

Analytical approaches and mechanical equivalent solutions for the fluid motion: Graham and Rodriguez (1951) proposed a simple analytical approach for modeling the fluid in moving containers. He used the assumption of inviscid incompressible fluid inside rectangular tanks. Then, he suggested equivalent mechanical systems which produce the same forces and moments as the oscillating fuel when the container is given an arbitrary motion. Schy (1952) derived equations for the flight dynamics of airplanes coupled with fluid sloshing in spherical tanks. The motion of the fuel was approximated by the motion of solid pendulums. Other similar results are recalled in Abramson (1966) (see also the updated version by Dodge (2000) and a more recent book by Ibrahim (2005)).

The analytical solutions and mechanical equivalent models of sloshing are only possible for linearized equations and simple tank geometries. Nevertheless, they still attract a great interest and are used in many applications. Abzug (1996) extended the fuel slosh coupling with aircraft dynamics to include tanks that are skewed to the direction of flights. He performed a numerical study based on the geometry of Boeing 747-100. Coupling between the

sloshing and the rigid body motion was observed. Depending on the configuration of the tanks, an unstable mode appeared (that was more severe for longer tanks). Cho and McClamrocht (2000) used pendulum models for modeling the sloshing of fuel in a spacecraft. Schotté and Ohayon (2003b) used a mass-spring equivalent sloshing model to couple with a flexible plate. Firouz-Abadi, Zarifian, and Haddadpour (2014) used a mass-spring-damper equivalent sloshing model to study the influence of sloshing in flutter speed of a flexible wing. Robles and Serrano (2014) used a mechanical model for representing sloshing in oil dispersant aerial systems, and verifying its influence in the handling qualities of the Airbus C295 aircraft.

Numerical approaches for the fluid motion: Advances in numerical methods and improvement of computer performance made the simulation of more complex phenomena possible. Hirt and Cook (1970) proposed a Lagrangian technique for computing the transient dynamics of viscous incompressible fluids having a free surface. Feng (1973) extended a marker-and-cell method (MAC) to simulate the flow of a moving liquid in a 3D container. Armenio and Michele (1996) used the MAC method to numerically solve both a 2D Reynolds-averaged Navier-Stokes (RANS) and Shallow Water Equations (SWE) of sloshing and made comparisons with experimental results. While the RANS model exhibited a very good agreement for small and moderate amplitudes of oscillations, SWE gave only good agreement for small filling ratios (lower than 15%). For low filling ratios of fluid and large amplitudes, better agreement was obtained using SWE. Celebi and Akyildiz (2002) studied the sloshing in a moving rectangular tank using a finite differences approximation of nonlinear Navier-Stokes. Chen, Djidjeli, and Price (2009) studied the sloshing phenomena using a RANS model with two incompressible fluids to describe the free surface. A finite difference scheme was used for discretization.

Sloshing and coupling with structural dynamics: In the case of Fluid-Structure Interactions (FSI), numerical methods are used by many researchers. Kiefling and Feng (1976) used a finite element scheme to simulate the liquid sloshing coupled to a flexible tank. Liu and Uras (1988) used a three-field variational approach for FSI with sloshing, seismic and body forces. Schotté and Ohayon (2003a) included rigid body modes and proposed a variational approach that took into account the coupling between the sloshing and the hydroelastic deformations of the tank. Schotté and Ohayon (2009) compared several strategies to model sloshing and its interaction with complex aerospace structures ("frozen liquid" mass model, hydroelastic added mass, hydroelastic model with gravity, and hydroelastic model with nonlinear prestress). Noorian, Firouz-Abadi, and Haddadpour (2012) used finite element method to describe the dynamics of elastic baffled tanks having arbitrary geometries. Using the modal analysis, a reduced order model for coupled dynamics of slosh and structure was developed.

Although less frequent, analytical models and equivalent mechanical systems have also been used to model structures coupled with sloshing. For instance, Robu (2010) used equivalent an mechanical system to simulate the sloshing and coupled it with a finite-dimensional state-space approximation of the plate equations. Schotté and Ohayon (2003b) used an equivalent mass-spring system to simulate a fluid with free surface coupled to a flexible structure.

Shallow Water Equations for sloshing: In spite of the simplifying assumptions, the use of SWE for sloshing still brings a considerable attention of researchers. As presented by Armenio and Michele (1996), the computational time needed for simulating SWE is just a small fraction of the time needed for simulating RANS. In addition, the nonlinear behavior is well represented using SWE, thus large amplitudes of excitation can be simulated. Petit and Rouchon (2002) proposed equations where the tank horizontal position and rotation angle are the control inputs of the system. Alemi Ardakani and Bridges (2010) studied the coupling between SWE equations with a horizontally moving vehicle. In this case, a Hamiltonian formulation is proposed and, consequently, a symplectic time-integration scheme can be used. Alemi Ardakani (2016) extended the method for a nonlinear spring. Alemi Ardakani and Bridges (2012), Alemi Ardakani and Bridges (2011) generalized the sloshing equations in moving tanks for 2D and 3D motions.

Influence of liquid in tanks in the airplane aeroelastic behavior: In aeronautics, one of the most important sources of fluid-structure interactions is given by the coupling of aerodynamics and structural dynamics (aeroelasticity, see, e.g., Bisplinghoff, Ashley, and Halfman (1996), and Hodges and Pierce (2011)). The consequences of these interactions might lead to many dangerous issues that might reduce maneuverability (like controls inversion), and cause unstable behavior (like divergence and flutter).

The liquid inside the tank can also have an influence on the aeroelastic behavior of airplanes. The influence of the fuel sloshing on the flutter speed was analyzed by several authors. Farhat et al. (2013) used two simplified models to represent the fluid (frozen mass, and added hydrostatic mass), and coupled to a FEM model of the airplane structure. Firouz-Abadi, Zarifian, and Haddadpour (2014) modeled the fuel sloshing as an equivalent mass-spring-damper system and coupled it to a Euler-Bernoulli beam subject to unsteady aerodynamics. If the first natural frequency is close to the instability frequency, the sloshing affects the flutter speed.

2.2 Port-Hamiltonian systems

Port-based modeling: The port-based modeling was originally proposed by Paynter (1961) in the form of the bond graph technique, which is a graphical technique for representing physical systems. This technique provides physical insight into modeling and control of complex systems and can be used to represent systems from multiple physical domains.

There are many examples of applications from different fields of study. For instance, Perelson (1976) modeled electrical networks, Allen (1978) modeled plant biosystems, Karnopp (1976) used the bond graphs to study the stability and control of vehicle (rigid body) dynamics, Sueur and Dauphin-Tanguy (1991) used the formulation for structural analysis of MIMO linear systems.

One of the interests of the bond graph approach is that it allows finding the differential

equations of the modeled system in a procedural way. Granda (1985) developed a computer program that automatically finds the differential equations from the bond graph representation of a physical system. The approach was used to simulate complex aerospace systems by Granda and Montgomery (2003).

Port-Hamiltonian systems: The port-Hamiltonian formalism was first introduced by Maschke and van der Schaft (1992). Inspired by the port-based modeling approach, it extended classical Hamiltonian systems by the introduction of external *interconnection ports*. Among its properties, it allows coupling multi-domain systems in a physically consistent way, i.e., using energy flow, so that interconnections are power-conserving. Resistive elements can be coupled to the pHs, such that dissipative phenomena can also be modeled. Furthermore, the formulation is appropriate for energy-based control methods (see, e.g. Maschke, Ortega, and van der Schaft (2000), Ortega, van der Schaft, and Maschke (2001), and Ortega et al. (2002)).

The method has been applied successfully for a large class of problems. Maschke, van der Schaft, and Breedveld (1995) modeled networks of LC-circuits. Escobar, van der Schaft, and Ortega (1999) modeled switching power converters. Duindam, Blankenstein, and Stramigioli (2004) used the approach to analyze the locomotion of a snakeboard. Duindam (2006) modeled and controlled bipedal walking robots. Recently, the pHs formulation was extended even for systems with memory (Jeltsema and Dòria-Cerezo, 2012), and irreversible systems (Ramirez, Maschke, and Sbarbaro, 2013).

Extension to distributed parameter systems: The formulation was also extended for distributed (infinite-dimensional) systems (see, e.g., (Maschke and van der Schaft, 2000), van der Schaft and Maschke (2002), Macchelli, van der Schaft, and Melchiorri (2004b), and Chapter 4 of Duindam et al. (2009)). In this case, the system exchanges energy with the environment by means of *boundary* ports. The extension motivated further study in boundary control of infinite-dimensional systems (see, e.g., Rodriguez, van der Schaft, and Ortega (2001), Macchelli, van der Schaft, and Melchiorri (2004c)).

Many linear and nonlinear PDE of physical systems can be written in this framework. Furthermore, the coupling between finite-dimensional and distributed pHs is also possible, leading to the mixed finite-infinite pHs (m-pHs, see, e.g., Macchelli and Melchiorri (2005), and Pasumarthy (2006)).

Thus, in the last years, many applications of distributed pHs and m-pHs have been studied. For instance, Navier-Stokes equations for a compressible fluid were modeled by van der Schaft and Maschke (2001), Korteweg de Vries and Boussinesq equations were addressed in Maschke and van der Schaft (2013). Beam equations were proposed by Macchelli and Melchiorri (2004), Macchelli, van der Schaft, and Melchiorri (2004a) modeled flexible structures with piezoelectric actuators. Voss and Scherpen (2011b) studied the stabilization and shape control of the piezoelectric Timoshenko beam. Hamroun (2009) rewrote the shallow water equations in the pHs framework, for modeling and controlling the flow in irrigation chan-

nels. Vu (2014) modeled and controlled the plasma dynamics in Tokamaks. Wu et al. (2014) modeled a nanotweezer for DNA manipulation. Falaize (2016) simulated multi-physics audio systems. Lopes (2016) simulated a robotized test bench for brass instruments.

Power-preserving spatial discretization: Another subject that brought great interest is the spatial discretization of infinite-dimensional pHs, such that the power-balance is preserved in the finite dimensional approximated system. A first method to discretize infinite-dimensional pHs was proposed by Golo et al. (2004). The method was originally applied for the transmission line (a 1D-wave equation) and a 2D-wave equation. The method was also applied to simulate (Hamroun, Lefèvre, and Mendes, 2007) and control (Hamroun, 2009; Hamroun et al., 2010) open irrigation channels with SWE. The power-preserving discretization of the SWE for open channels was also studied by Pasumarthy (2006), Pasumarthy, Ambati, and van der Schaft (2012).

Other applications include the Timoshenko beam (Voss and Scherpen (2011c), and Macchelli (2012)), geometrically non-linear Euler-Bernoulli beam (Macchelli, Melchiorri, and Stramigioli (2007), Voss and Scherpen (2009), and Voss (2010)) convection-diffusion equations (Voss and Weiland, 2011), adsorption processes (Baaiu et al., 2009) and even parabolic PDEs like the heat equation (Le Gorrec et al., 2011).

Based on the ideas of Golo et al. (2004), a generalization algorithm was suggested by Bassi, Macchelli, and Melchiorri (2007). It presented a reduction algorithm for general pHs with differential operators including first-order derivatives and an idea of an extension to higher-order derivatives.

More recently, another approach was proposed by Moulla, Lefèvre, and Maschke (2011), Moulla, Lefèvre, and Maschke (2012), Moulla (2010), which used a pseudo-spectral (interpolation) method to approximate the distributed equations. Thanks to the convergence characteristics of the pseudo-spectral methods (Boyd, 2001; Trefethen, 2000), they require only a small number of finite-dimensional states yet exhibiting very good precision.

Finally, Seslija, Scherpen, and van der Schaft (2014) proposed a different power preserving spatial discretization method based on the idea of simplicial complexes.

2.3 Conclusions

The port-Hamiltonian systems have been subject to active research in the last years. The subject motivated many researchers from different fields. The tools emerging from this approach bring many advantages in the modeling, simulation, and control of complex systems. The main goal of this thesis is to bring this formalism to the modeling and control of fluid-structure systems.

Chapter 3

Experimental setup

This brief chapter describes the experimental setup that is used to test the methods proposed in this thesis. The device (depicted in Figs. 3.1 and 3.2) is installed at the *Institut Supérieur de l'Aéronautique et de l'Espace* (ISAE-SUPAERO) in Toulouse, France. It consists of an aluminium plate connected to an acrylic glass tip tank that can be filled with water. This setup was designed to have natural frequencies similar to a flexible airplane wing with a tip tank. Two piezoelectric patches are attached near the clamped end of the plate, that are be used to control the device.

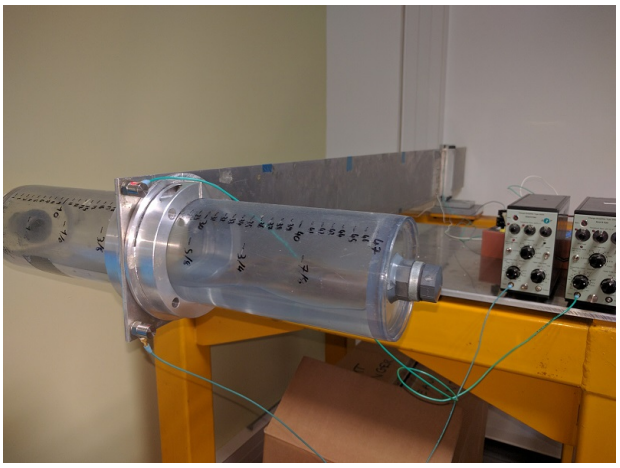

Figure 3.1: Experimental device

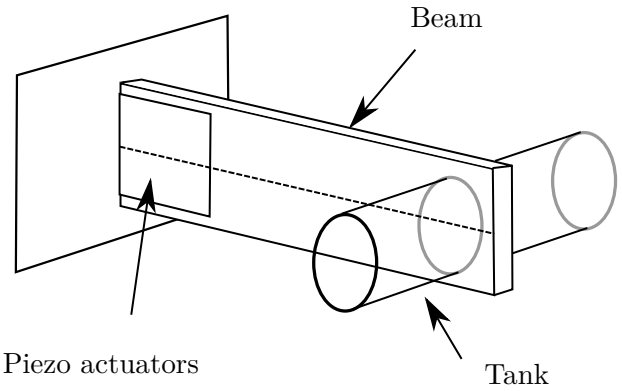

Figure 3.2: Experimental setup schematic representation

The plate dimensions and material characteristics are presented in Table 3.1. The plate has a hole with a diameter of 0.110 m, centered at 1.28 m from the clamped end of the plate.

Table 3.1: Aluminum plate data

Lenght	L	1.36 m
Width	l	0.16 m
Thickness	t	0.005 m
Density	ρ	2970 kgm^{-3}
Young modulus	E	75 GPa
Poisson coefficient	ν	0.33

The tank is symmetrically placed into the hole of the plate. The dimensions and material characteristics of the tank are presented in Table 3.2. Note the tips of the tank have a plug glued to a plastic disc. This plug can be removed, to fill or to release water of the tank. The "tip mass" presented in the table is the sum of the masses of the plug, glue and the plastic disc at each tip of the tank.

Table 3.2: Cylindric tank data

Exterior diameter	$D_{e,tank}$	0.110 m
Interior diameter	$D_{i,tank}$	0.105 m
Density	ρ_{PVC}	1180 kg/m^3
Tip mass	m_{tip}	156.5 g
Tank lenght	L_{tank}	0.5 m

In order to improve the fixation of the tank to the plate, two rings are attached to the structure (one at each side of the tank). The dimensions and material properties of these rings are presented in Table 3.3.

Table 3.3: Fixation rings data

Exterior diameter	$D_{e,fix}$	0.1445 m
Interior diameter	$D_{i,fix}$	0.11 m
Thickness	h_{fix}	0.02876 m
Density (Aluminum)	ρ	2970 kg/m^3

The sensors that are used to measure the motion of the structure are 4371 Bruel & Kjaer accelerometers (Fig. 3.3). Charge amplifiers (Type 2635, Fig. 3.4) are connected to the accelerometers. The amplifiers can provide a filtered signal of the speed for frequencies above 1 Hz, and a filtered signal of the acceleration for frequencies above 0.1 Hz.

The outputs of the amplifiers are connected to the inputs of the National Instruments BNC-2110 connector block (Fig. 3.5). The connector block is linked to a PC with an NI 6024-E board.

The piezoelectric actuators are PZT (Lead Zirconate Titanate) patches developed by PI Ceramic (model PIC 151). The dimensions and material properties of the patches are

presented in Table 3.4.

Table 3.4: PZT piezoelectric patches data

Lenght	L_p	0.14 m
Width	l_p	0.075 m
Thickness	t_p	0.0005 m
Density	ρ_p	2970 kg m^{-3}
Young modulus	E_p	67 GPa
Poisson coefficient	ν_p	0.33
Piezoelectric coefficient	d_{31}	$-2.1e-10$ mV^{-1}

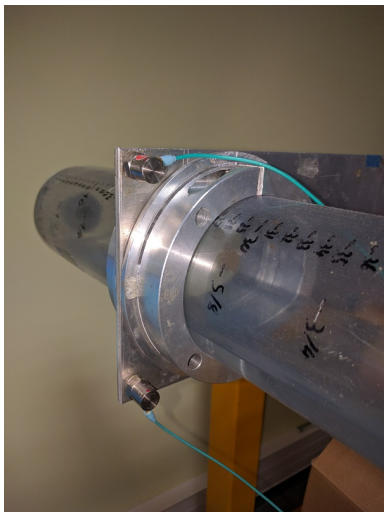

Figure 3.3: Accelerometers 4371 Bruel & Kjaer near the tip of the plate

Figure 3.4: Charge amplifier Type 2635 Bruel & Kjaer

The piezoelectric actuators are driven by the HVPZT Piezo Amplifier (Fig. 3.6). This high voltage amplifier multiplies the signal that comes from the PC (through the connector block) by a factor of 100.

The data acquisition and the implementation of the control laws are done using MATLAB Simulink, on Real-time Windows Target. A sampling time of 0.001s is used in all the experiments of this thesis.

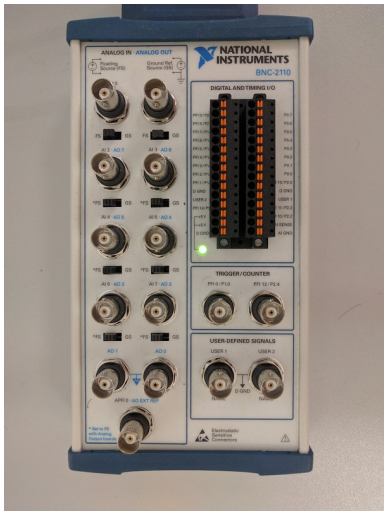

Figure 3.5: Connector block NI BNC-2110

Figure 3.6: HVPZT Piezo Amplifier

Part II

Port-Hamiltonian modeling of fluid-structure systems

Chapter 4

A recall on Port-Hamiltonian systems

The main goal of this chapter is to recall the basics of port-Hamiltonian systems (pHs). The tools presented in this chapter are used in the next chapters for the modeling of fluid-structure systems.

This chapter is organized as follows: a recall on finite-dimensional port-Hamiltonian systems is presented in section 4.1. Infinite-dimensional systems are recalled in section 4.2 using the wave equation as an example. Finally, section 4.3 recall some tools for interconnecting finite-dimensional pHs, as well as how to deal with constraints. One major property of pHs is that their power-preserving interconnection leads to a pHs. Indeed, the fluid-structure system presented in this thesis will be obtained from a combination of several pHs.

Contents

4.1 Finite-dimensional port-Hamiltonian systems

Before starting with the *port*-Hamiltonian systems, let us recall a very simple example of *classical* Hamiltonian systems (see, e.g., Lanczos (1970); Marsden and Ratiu (1999)). A concentrated mass connected to a spring without external force is considered. The system Hamiltonian (which, for this system, is equal to the total energy) is given by:

$$H(p,x) = \frac{1}{2m}p^2 + \frac{1}{2}kx^2\,, \tag{4.1}$$

where $p = m\dot{x}$ is the particle momentum, m is the mass, x is the position, k is the spring constant. The dynamic equations, obtained from Hamilton-Jacobi equations, are given by:

$$\frac{\mathrm{d}}{\mathrm{d}t}\begin{bmatrix} p \\ x \end{bmatrix} = \begin{bmatrix} 0 & -1 \\ 1 & 0 \end{bmatrix}\begin{bmatrix} \frac{\partial H}{\partial p} \\ \frac{\partial H}{\partial x} \end{bmatrix}\,. \tag{4.2}$$

One can easily verify that the Hamiltonian is constant along trajectories, i.e.:

$$\dot{H} = \frac{\partial H}{\partial p}\dot{p} + \frac{\partial H}{\partial x}\dot{x} = 0\,. \tag{4.3}$$

More generally, Hamiltonian systems can be represented as:

$$\dot{\boldsymbol{x}} = J(\boldsymbol{x})\nabla_{\boldsymbol{x}}H(\boldsymbol{x})\,, \tag{4.4}$$

where $\boldsymbol{x} \in \mathbb{R}^n$ is the vector of energy variables, $J(\boldsymbol{x})$ is an $n \times n$ skew-symmetric matrix and $\nabla_{\boldsymbol{x}}H(\boldsymbol{x})$ is the gradient of the Hamiltonian $H(\boldsymbol{x})$. Again, thanks to the skew-symmetry of $J(\boldsymbol{x})$, the Hamiltonian is constant along trajectories:

$$\begin{aligned} \dot{H} &= \left(\nabla_{\boldsymbol{x}}H(\boldsymbol{x})\right)^T\dot{\boldsymbol{x}}\,, \\ &= \left(\nabla_{\boldsymbol{x}}H(\boldsymbol{x})\right)^T J(\boldsymbol{x})\nabla_{\boldsymbol{x}}H(\boldsymbol{x})\,, \\ &= 0\,. \end{aligned} \tag{4.5}$$

Note that all the dynamics of the system of Eq. 4.4 is embedded in a scalar function (the Hamiltonian $H(\boldsymbol{x})$), together with the so-called *interconnection matrix* $J(\boldsymbol{x})$ (in the case of the mass-spring, this matrix *interconnects* the potential and kinetic energies).

While at first sight the simple mass-spring example might seem uninteresting from a practical point-of-view, since it can be easily derived from Newton's second law, the tools from analytical mechanics have many advantages when compared to Newtonian mechanics. For example:

- the variables $\boldsymbol{x}$ can be given in the so-called generalized coordinates (they are not necessarily Cartesian coordinates as in Newtonian mechanics): this provides straightforward methods for dealing with constrained systems;

- the structured form of the dynamical equations leads to straightforward ways to find constants of motion and symmetries;
- numerical methods that preserve some properties of the original Hamiltonian system have proved to be valuable tools for simulation (see e.g. Leimkuhler and Reich (2005)).

The port-Hamiltonian formalism is an extension of the Hamiltonian formalism by the introduction of interconnection ports. This concept was first introduced by Maschke, van der Schaft, and Breedveld (1992).[1] A typical representation of pHs is given by:

$$\begin{aligned} \dot{\boldsymbol{x}} &= J(\boldsymbol{x})\boldsymbol{e} + B(\boldsymbol{x})\boldsymbol{u}\,, \\ \boldsymbol{y} &= B^T(\boldsymbol{x})\boldsymbol{e}\,, \end{aligned} \tag{4.6}$$

where $\boldsymbol{x}(t) \in \mathbb{R}^n$ is the vector of energy variables, $\boldsymbol{e} := \nabla_{\boldsymbol{x}} H(\boldsymbol{x}) \in \mathbb{R}^n$ is the vector of co-energy variables, provided by the gradient of the system Hamiltonian $H(\boldsymbol{x})$, $\boldsymbol{u} \in \mathbb{R}^m$ is the input vector and $\boldsymbol{y} \in \mathbb{R}^m$ is the output vector. $J(\boldsymbol{x})$ is the $(n \times n)$ interconnection matrix, which must be skew-symmetric. The time-derivative of the Hamiltonian along trajectories is given by:

$$\begin{aligned} \dot{H}(\boldsymbol{x}(t)) &= \left(\nabla_{\boldsymbol{x}} H(\boldsymbol{x})\right)^T \dot{\boldsymbol{x}}\,, \\ &= \boldsymbol{e}^T \left(J\boldsymbol{e} + B\boldsymbol{u}\right)\,, \\ &= \underbrace{\boldsymbol{e}^T J \boldsymbol{e}}_{0} + \underbrace{\boldsymbol{e}^T B}_{\boldsymbol{y}^T}\boldsymbol{u}\,, \\ &= \boldsymbol{y}^T \boldsymbol{u}\,. \end{aligned} \tag{4.7}$$

Since the Hamiltonian usually represents the system total energy, its time derivative is equal to the power that flows into the system (power balance). The input $\boldsymbol{u}$ and output $\boldsymbol{y}$ are said to be (power-) conjugate. This is exactly the kind of variables that are used for interconnection in the bond graph method.

It is also possible to rewrite Eq. 4.6 as:

$$\begin{bmatrix} -\dot{\boldsymbol{x}} \\ \boldsymbol{y} \end{bmatrix} = \underbrace{\begin{bmatrix} -J(\boldsymbol{x}) & -B(\boldsymbol{x}) \\ B(\boldsymbol{x})^T & 0 \end{bmatrix}}_{S(\boldsymbol{x})} \begin{bmatrix} \boldsymbol{e} \\ \boldsymbol{u} \end{bmatrix}\,. \tag{4.8}$$

Note the dynamics of the port-Hamiltonian system is provided by an *interconnection* structure (here given by the $S(\boldsymbol{x})$ matrix), together with the Hamiltonian $H(\boldsymbol{x})$ (which allows obtaining the co-energy variables $\boldsymbol{e}$). Indeed, a more general representation of port-Hamiltonian system is provided by an abstract interconnection structure called Dirac structure. This structure, as presented later in this section, allows the representation of implicit port-Hamiltonian systems.

This section is divided as follows: firstly, one simple example is presented in § 4.1.1 (a

[1] In the first papers, the method was called Port-Controlled Hamiltonian systems (PCHS). A different approach for including input and output ports in Hamiltonian systems was presented before by Brockett in 1977 as recalled by van der Schaft (1989). There, the system Hamiltonian is a function of the external inputs.

mass-spring with external force). Secondly, § 4.1.2 briefly recalls the Euler-Lagrange equations of motion, and presents them in the port-Hamiltonian form. Thirdly, the introduction of dissipation in the port-Hamiltonian systems is recalled in § 4.1.3. An example of systems with constraints is presented in § 4.1.4. Finally, the Dirac structure is defined in § 4.1.5.

4.1.1 Example: mass-spring system

As a very simple example of a mechanical system written using the port-Hamiltonian framework, let us consider a lumped mass with two forces f_1 and f_2. The system Hamiltonian (total energy) is given by its kinetic energy:

$$H^m(p) = \frac{1}{2m} p^2 \,, \tag{4.9}$$

where $p = mv$ is the particle momentum, m is the mass and v is the speed. The dynamic equations, obtained from Hamiltonian formulation, are given by:

$$\begin{aligned} \dot{p} &= 0 \, \frac{\partial H^m}{\partial p} + \begin{bmatrix} 1 & 1 \end{bmatrix} \begin{bmatrix} f_1 \\ f_2 \end{bmatrix} \,, \\ \begin{bmatrix} v_1 \\ v_2 \end{bmatrix} &= \begin{bmatrix} 1 \\ 1 \end{bmatrix} \frac{\partial H^m}{\partial p} \,. \end{aligned} \tag{4.10}$$

Note that this system is written exactly as Eq. 4.6, where the inputs are the forces $\boldsymbol{u} = \begin{bmatrix} f_1 & f_2 \end{bmatrix}^T$, the outputs are the speeds $\boldsymbol{y} = \begin{bmatrix} v_1 & v_2 \end{bmatrix}^T$, $J = 0$, $B = \begin{bmatrix} 1 & 1 \end{bmatrix}$. The energy variable is the momentum p, and the co-energy variable is the speed $\frac{\partial H^m}{\partial p} = v$. Besides, the power balance is given by:

$$\dot{H}^m(p) = v_1 f_1 + v_2 f_2 = v(f_1 + f_2) \,. \tag{4.11}$$

Similarly, consider a linear spring with displacement x, speed v_s and subject to a force f_s. The system Hamiltonian is provided by the potential energy:

$$H^s(x) = \frac{k}{2} x^2 \,, \tag{4.12}$$

and the equations in the port-Hamiltonian framework are simply given by:

$$\begin{aligned} \dot{x} &= 0 \, \frac{\partial H^s}{\partial x} + 1 \, v_s \,, \\ f_s &= 1 \, \frac{\partial H^s}{\partial x} \,, \end{aligned} \tag{4.13}$$

where now the input is the speed v_s, and the output is the spring force f_s. The energy variable is the spring displacement x, and the co-energy variable is the spring force $\frac{\partial H^s}{\partial x} = kx$. The power balance is thus:

$$\dot{H}^s(x) = v_s f_s \,. \tag{4.14}$$

The mass and spring can be interconnected, by using the following kinematic and dynamic constraints:

$$\begin{aligned} v_s &= v_1 \,, \\ f_s &= -f_1 \,, \end{aligned} \tag{4.15}$$

which lead to the coupled equations:

$$\begin{aligned} \frac{\mathrm{d}}{\mathrm{d}t}\begin{bmatrix} p \\ x \end{bmatrix} &= \begin{bmatrix} 0 & -1 \\ 1 & 0 \end{bmatrix}\begin{bmatrix} \frac{\partial H}{\partial p} \\ \frac{\partial H}{\partial x} \end{bmatrix} + \begin{bmatrix} 1 \\ 0 \end{bmatrix} f_2 \,, \\ \dot{x} &= \begin{bmatrix} 1 & 0 \end{bmatrix}\begin{bmatrix} \frac{\partial H}{\partial p} \\ \frac{\partial H}{\partial x} \end{bmatrix} \,, \end{aligned} \tag{4.16}$$

where $H(p, x) = H^m(p) + H^s(x)$. Notice that Eq. 4.16 is also a port-Hamiltonian system (as Eq. 4.6), with input port the force f_2 and output port the speed v_2. One can easily verify that the power balance of this system is given by $\dot{H} = f_2 v_2$.

This simple example shows one of the interests of using the port-Hamiltonian formulation as a modeling tool. By interconnecting simple modules, the approach provides a systematic way for modeling more complex systems and guarantees the energy is preserved in each interconnection. In the previous example, only linear systems were considered. However, the same formalism can be used for nonlinear systems. For instance, a non-quadratic Hamiltonian could be used to represent a nonlinear spring:

$$H^s = k_p \cosh x \,. \tag{4.17}$$

Thus, the force is given by:

$$f_s = \frac{\partial H^s}{\partial x} = k_p \sinh x \,. \tag{4.18}$$

In the case of the nonlinear spring, the *interconnection structure* of Eq. 4.16 remains unchanged, and the only difference lies in the Hamiltonian.

4.1.2 From Euler-Lagrange equations to port-Hamiltonian systems

The classical framework of Lagrangian and Hamiltonian dynamics can be extended to port-Hamiltonian systems (as presented in Section 2.1 of van der Schaft (2005) and Section 1.3.1 of Hamroun (2009)). The Euler-Lagrange equations are given by:

$$\frac{d}{dt}\left(\frac{\partial L}{\partial \dot{q}_i}(q_i, \dot{q}_i)\right) - \frac{\partial L}{\partial q_i}(q_i, \dot{q}_i) = \tau_i(t), \tag{4.19}$$

where $q_i(t)$ $(i = 1, 2, ..., k)$ are the generalized coordinates for the system with k degrees of freedom, $\tau_i(t)$ are the generalized forces, L is the system Lagrangian (equals to the difference between the kinetic energy K and potential energy V, $L := K - V$). The kinetic energy K is

usually given by:

$$K(\dot{q}) = \frac{1}{2}\dot{\boldsymbol{q}}^T M(\boldsymbol{q})\dot{\boldsymbol{q}}\,, \tag{4.20}$$

where $\boldsymbol{q}(t) = [q_1(t) \quad q_2(t) \quad ... \quad q_k(t)]^T$ is the vector of system generalized coordinates, $\dot{\boldsymbol{q}}$ is the vector of generalized velocities and $M(\boldsymbol{q})$ is the $k \times k$ inertia matrix, which is symmetric and positive definite (for all $\boldsymbol{q}$). The potential energy is assumed to depend only on the generalized coordinates: $V = V(\boldsymbol{q})$. After defining the generalized momenta $\boldsymbol{p}(t) = [p_1(t) \quad p_2(t) \quad ... \quad p_k(t)]^T$ as:

$$\boldsymbol{p} := \nabla_{\dot{\boldsymbol{q}}} L = M(\boldsymbol{q})\dot{\boldsymbol{q}}\,, \tag{4.21}$$

the Hamiltonian can be obtained from the Legendre transform as:

$$H = \dot{\boldsymbol{q}}^T\boldsymbol{p} - L(\boldsymbol{q}, \dot{\boldsymbol{q}})\,. \tag{4.22}$$

Then, it can be rewritten as a function of $\boldsymbol{q}$ and $\boldsymbol{p}$:

$$\begin{aligned} H(\boldsymbol{q},\boldsymbol{p}) =& \frac{1}{2}\boldsymbol{p}^T M^{-1}(\boldsymbol{q})\boldsymbol{p} + V(\boldsymbol{q})\,, \\ =& K(\boldsymbol{q},\boldsymbol{p}) + V(\boldsymbol{q})\,, \end{aligned} \tag{4.23}$$

so, the Hamiltonian represents the total energy of the mechanical system. From the definition of p and H, we can re-write Euler-Lagrange equations as a set of first-order differential equations:

$$\begin{bmatrix} \dot{\boldsymbol{q}}(t) \\ \dot{\boldsymbol{p}}(t) \end{bmatrix} = \begin{bmatrix} 0 & I \\ -I & 0 \end{bmatrix} \begin{bmatrix} \nabla_{\boldsymbol{q}} H \\ \nabla_{\boldsymbol{p}} H \end{bmatrix} + \begin{bmatrix} 0 \\ \boldsymbol{\tau}(t) \end{bmatrix}\,. \tag{4.24}$$

By computing the time-derivative of the Hamiltonian, we verify that the following power balance holds:

$$\begin{aligned} \dot{H}(\boldsymbol{q},\boldsymbol{p}) &= \begin{bmatrix} \nabla_{\boldsymbol{q}}^T H & \nabla_{\boldsymbol{p}}^T H \end{bmatrix} \begin{bmatrix} \dot{\boldsymbol{q}} \\ \dot{\boldsymbol{p}} \end{bmatrix} \\ &= \underbrace{\begin{bmatrix} \nabla_{\boldsymbol{q}}^T H & \nabla_{\boldsymbol{p}}^T H \end{bmatrix} \begin{bmatrix} 0 & I \\ -I & 0 \end{bmatrix} \begin{bmatrix} \nabla_{\boldsymbol{q}} H \\ \nabla_{\boldsymbol{p}} H \end{bmatrix}}_{0} + \left(\nabla_{\boldsymbol{p}}^T H\right)\boldsymbol{\tau}\,, \\ &= \left(\nabla_{\boldsymbol{p}}^T H\right)\boldsymbol{\tau}\,. \end{aligned} \tag{4.25}$$

It is also easy to verify that $\nabla_{\boldsymbol{p}} H = M^{-1}(\boldsymbol{q})\boldsymbol{p} = \dot{\boldsymbol{q}}$. Thus, the system exchange of energy with the environment is given by the product of external forces and generalized speeds: $\dot{H} = \dot{\boldsymbol{q}}^T\boldsymbol{\tau}$. By choosing the input port $\boldsymbol{u}(t) := \boldsymbol{\tau}(t)$, and the output port $\boldsymbol{y}(t) := \dot{\boldsymbol{q}}$, the energy flow becomes $\dot{H} = \boldsymbol{y}^T\boldsymbol{u}$. We note that Eq. 4.24, together with these newly defined input and output ports, give exactly a pHs, as presented in Eq. 4.6.

More generally, we can re-write the system for the case where $\boldsymbol{\tau} = B(\boldsymbol{q})\boldsymbol{u}$ (in fact, the inputs of real systems are not usually the generalized forces). $B(\boldsymbol{q})$ is a $k \times m$ matrix, where m is the number of control inputs $\boldsymbol{u} \in \mathbb{R}^m$. In case $m < k$, the system is called underactuated. If $m = k$ and $B(\boldsymbol{q})$ is invertible (for any q), then the system is called fully actuated.

$$\begin{aligned}\begin{bmatrix}\dot{\boldsymbol{q}}\\ \dot{\boldsymbol{p}}\end{bmatrix} &= \begin{bmatrix}0 & I\\ -I & 0\end{bmatrix}\begin{bmatrix}\nabla_{\boldsymbol{q}}H\\ \nabla_{\boldsymbol{p}}H\end{bmatrix} + \begin{bmatrix}0\\ B(\boldsymbol{q})\end{bmatrix}\boldsymbol{u}\,,\\ \boldsymbol{y} &= \begin{bmatrix}0 & B(\boldsymbol{q})^T\end{bmatrix}\begin{bmatrix}\nabla_{\boldsymbol{q}}H\\ \nabla_{\boldsymbol{p}}H\end{bmatrix}\,.\end{aligned} \tag{4.26}$$

This choice of $\boldsymbol{u}$ and $\boldsymbol{y}$ leads again to the power balance: $\dot{H} = \boldsymbol{y}^T\boldsymbol{u}$. The previous system is clearly a pHs, as presented in Eq. 4.6.

4.1.3 Systems with dissipative elements

Port-Hamiltonian systems represented as Eq. 4.6 are conservative, i.e., no dissipation exists and the energy is preserved. In order to include dissipation, it is possible to interconnect a pHs with resistive (or dissipative) elements. Firstly, let us re-define the port-Hamiltonian system as:

$$\begin{aligned}\dot{\boldsymbol{x}} &= J(\boldsymbol{x})\nabla_{\boldsymbol{x}}H + B(\boldsymbol{x})\boldsymbol{u} + B_R(\boldsymbol{x})\boldsymbol{u}_R\,,\\ \boldsymbol{y} &= B^T(\boldsymbol{x})\nabla_{\boldsymbol{x}}H\,,\\ \boldsymbol{y}_R &= B_R^T(\boldsymbol{x})\nabla_{\boldsymbol{x}}H\,,\end{aligned} \tag{4.27}$$

where $\boldsymbol{u}_R \in \mathbb{R}^{n_R}$ and $\boldsymbol{y}_R \in \mathbb{R}^{n_R}$ are ports used for interconnection with resistive elements, $B_R(\boldsymbol{x})$ is an $n \times n_R$ matrix. By choosing the closure relation $\boldsymbol{u}_R = -D(\boldsymbol{x})\,\boldsymbol{y}_R$, where $D(\boldsymbol{x})$ is an $n_R \times n_R$ positive semi-definite matrix, the energy flow of the system becomes:

$$\begin{aligned}\dot{H} &= \boldsymbol{y}^T\boldsymbol{u} + \boldsymbol{y}_R^T\boldsymbol{u}_R\,,\\ &= \boldsymbol{y}^T\boldsymbol{u} \underbrace{-\boldsymbol{y}_R^T D(\boldsymbol{x})\boldsymbol{y}_R}_{\leq 0(\text{dissipative})}\,,\\ &\leq \boldsymbol{y}^T\boldsymbol{u}\,.\end{aligned} \tag{4.28}$$

Then, it is clear that the system from Eq. 4.27 becomes dissipative. In addition, pHs with dissipative terms are commonly written as:

$$\begin{aligned}\dot{\boldsymbol{x}} &= \left(J(\boldsymbol{x}) - R(\boldsymbol{x})\right)\nabla_{\boldsymbol{x}}H + B(\boldsymbol{x})\boldsymbol{u}\,,\\ \boldsymbol{y} &= B^T(\boldsymbol{x})\nabla_{\boldsymbol{x}}H\,,\end{aligned} \tag{4.29}$$

where $R(\boldsymbol{x}) = B_R(\boldsymbol{x})D(\boldsymbol{x})B_R^T(\boldsymbol{x})$ is an $n \times n$ matrix. Note that, even if $D(\boldsymbol{x})$ is an $n_R \times n_R$ positive-definite matrix, $R(\boldsymbol{x})$ is usually only positive semi-definite, since usually $n_R < n$ (the number of dissipation ports is smaller than the number of energy variables).

4.1.4 Constrained port-Hamiltonian systems

Let us consider another simple example to motivate the study of pHs with algebraic constraints. Given two particles with masses m_1 and m_2, with kinetic energies given by $H_1(p_1) = \frac{p_1^2}{2m_1}$ and $H_2(p_2) = \frac{p_2^2}{2m_2}$, where p_1 and p_2 are the linear momentum as defined in the example of § 4.1.1. The first particle is subject to a force $f_{1,i}$, the second particle is subject to two forces $f_{2,i}$ and $f_{2,e}$. The equations for each particle are given by:

$$\begin{aligned} \dot{p}_1 &= f_{1,i}\,, \\ \dot{p}_2 &= f_{2,i} + f_{2,e}\,, \end{aligned} \tag{4.30}$$

which can be rewritten using the port-Hamiltonian form as:

$$\begin{cases} \dot{p_1} = \underbrace{0}_{J_1}\dfrac{\partial H}{\partial p_1} + \underbrace{1}_{B_1} f_{1,i}\,, \\ \qquad\quad \dot{x}_{1,i} = \underbrace{1}_{B_1^T}\dfrac{\partial H}{\partial p_1}\,, \\ \qquad \text{with: } \dot{H}_1 = f_{1,i}\dot{x}_1\,, \end{cases} \quad , \quad \begin{cases} \dot{p_2} = \underbrace{0}_{J_2}\dfrac{\partial H}{\partial p_2} + \underbrace{\begin{bmatrix}1 & 1\end{bmatrix}}_{B_2}\begin{bmatrix} f_{2,i} \\ f_{2,e}\end{bmatrix}\,, \\ \qquad \begin{bmatrix}\dot{x}_{2,i} \\ \dot{x}_{2,e}\end{bmatrix} = \underbrace{\begin{bmatrix}1 \\ 1\end{bmatrix}}_{B^T}\dfrac{\partial H}{\partial p_2}\,, \\ \qquad \text{with: } \dot{H}_2 = (f_{1,i} + f_{2,e})\dot{x}_2\,. \end{cases} \tag{4.31}$$

The coupling of these particles is obtained by the following dynamic and kinematic constraints:

$$\begin{aligned} f_{1,i} &= -f_{2,i}\,, \\ \dot{x}_1 &= \dot{x}_2\,, \end{aligned} \tag{4.32}$$

which is obviously power-preserving since: $f_{1,i}\,\dot{x}_1 + f_{2,i}\,\dot{x}_2 = 0$, and since the Hamiltonian of the coupled system is given by the sum of each Hamiltonian, the power balance of the coupled system is given by:

$$\begin{aligned} \dot{H}(p_1, p_2) &= \dot{H}_1(p_1) + \dot{H}_2(p_2)\,, \\ &= f_{2,e}\,\dot{x}_2\,. \end{aligned} \tag{4.33}$$

Defining $\lambda := f_{1,i}$, using the interconnection of Eq. 4.32 in Eq. 4.31, the coupled equations become:

$$\begin{aligned} \begin{bmatrix}\dot{p}_1 \\ \dot{p}_2\end{bmatrix} &= \begin{bmatrix}0 & 0 \\ 0 & 0\end{bmatrix}\begin{bmatrix}\frac{\partial H}{\partial p_1} \\ \frac{\partial H}{\partial p_2}\end{bmatrix} + \begin{bmatrix}0 \\ 1\end{bmatrix} f_{2,e} + \begin{bmatrix}1 \\ -1\end{bmatrix}\lambda\,, \\ \dot{x}_2 &= \begin{bmatrix}0 & 1\end{bmatrix}\begin{bmatrix}\frac{\partial H}{\partial p_1} \\ \frac{\partial H}{\partial p_2}\end{bmatrix}\,, \end{aligned} \tag{4.34}$$

with the constraint ($\dot{x}_1 = \dot{x}_2$):

$$0 = \begin{bmatrix}1 & -1\end{bmatrix}\begin{bmatrix}\frac{\partial H}{\partial p_1} \\ \frac{\partial H}{\partial p_2}\end{bmatrix}\,. \tag{4.35}$$

Note that Eqs. 4.34 and 4.35 can be rewritten as:

$$\begin{bmatrix} -\dot{p}_1 \\ -\dot{p}_2 \\ \dot{x}_2 \\ 0 \end{bmatrix} = \begin{bmatrix} 0 & 0 & 0 & -1 \\ 0 & 0 & -1 & 1 \\ 0 & 1 & 0 & 0 \\ 1 & -1 & 0 & 0 \end{bmatrix} \begin{bmatrix} \frac{\partial H}{\partial p_1} \\ \frac{\partial H}{\partial p_2} \\ f_{2,e} \\ \lambda \end{bmatrix}, \tag{4.36}$$

highlighting that a skew-symmetric interconnection structure still exists in the constrained case.

By multiplying Eq. 4.34 by $\begin{bmatrix} 1 & 1 \end{bmatrix}$, it is possible to eliminate the λ. Additionally, by including the constraint and the output equation, we can find the following representation of this system that is independent of λ:

$$\begin{bmatrix} 1 & 1 & 0 \\ 0 & 0 & 1 \\ 0 & 0 & 0 \end{bmatrix} \begin{bmatrix} -\dot{p}_1 \\ -\dot{p}_2 \\ \dot{x}_2 \end{bmatrix} + \begin{bmatrix} 0 & 0 & 1 \\ 0 & -1 & 0 \\ 1 & -1 & 0 \end{bmatrix} \begin{bmatrix} e_1 \\ e_2 \\ f_{2,e} \end{bmatrix} = 0\,. \tag{4.37}$$

The previous equation is presented in what is called *Kernel* representation of port-Hamiltonian systems. In the next subsection we see that the interconnection structure of systems written in the explicit form of Eq. 4.6, the constrained form of Eqs. 4.34 and 4.35 and the Kernel representation of Eq. 4.37 can be generalized by the idea of Dirac structure. This structure will also allow defining other representations of implicit port-Hamiltonian systems.

4.1.5 Dirac structure

The following description was partially inspired from Golo (2002). Given the linear spaces $\mathcal{F}$ and $\mathcal{E}$, whose elements are labeled as $\boldsymbol{f}$ and $\boldsymbol{e}$, respectively[2]. The bond space (or power space) is defined as: $\mathcal{B} := \mathcal{F} \times \mathcal{E}$ with elements denoted by $\boldsymbol{b} := (\boldsymbol{f}, \boldsymbol{e})$. The spaces $\mathcal{F}$ and $\mathcal{E}$ are power conjugate. This means that there exists a map $\langle\ |\ \rangle$ defined as:

$$\begin{aligned} \langle\ |\ \rangle\ &: \mathcal{F} \times \mathcal{E} \mapsto \mathbb{R}\,, \\ &(\boldsymbol{f}, \boldsymbol{e}) \mapsto P = \langle \boldsymbol{e} | \boldsymbol{f} \rangle\,, \end{aligned} \tag{4.38}$$

where $\langle\ |\ \rangle$ is called power product. This product should satisfy the following conditions:

- it is a linear function of each coordinate,
- it is non-degenerate, that is:
  - if $\langle \boldsymbol{e} | \boldsymbol{f} \rangle = 0\,, \forall\, \boldsymbol{e} \in \mathcal{E}$, then $\boldsymbol{f} = 0$;
  - if $\langle \boldsymbol{e} | \boldsymbol{f} \rangle = 0\,, \forall\, \boldsymbol{f} \in \mathcal{F}$, then $\boldsymbol{e} = 0$,
- P has physical dimension of power.

[2] $\mathcal{F}$ is called flow space, and $\boldsymbol{f}$ flow variable; $\mathcal{E}$ is called effort space, and $\boldsymbol{e}$ effort variable; This terminology comes from the bond graph context.

One example of possible power product is the inner product of finite-dimensional vector spaces. Closely related to the definition of power product, there exist a symmetric bilinear form defined by:

$$\ll (\boldsymbol{f}^a, \boldsymbol{e}^a), (\boldsymbol{f}^b, \boldsymbol{e}^b) \gg := \langle \boldsymbol{e}^a | \boldsymbol{f}^b \rangle + \langle \boldsymbol{e}^b | \boldsymbol{f}^a \rangle, \\ (\boldsymbol{f}^a, \boldsymbol{e}^a), (\boldsymbol{f}^b, \boldsymbol{e}^b) \in \mathcal{F} \times \mathcal{E}. \tag{4.39}$$

One can easily see the relationship between the power product and the bilinear form:

$$\langle \boldsymbol{e}, \boldsymbol{f} \rangle = \frac{1}{2} \ll (\boldsymbol{f}, \boldsymbol{e}), (\boldsymbol{f}, \boldsymbol{e}) \gg, \quad \forall (\boldsymbol{f}, \boldsymbol{e}) \in \mathcal{B}. \tag{4.40}$$

Definition 4.1 (Dirac Structure)
A Dirac structure on $\mathcal{B} = \mathcal{F} \times \mathcal{E}$ is a subspace $\mathcal{D} \subset \mathcal{B}$, such that $\mathcal{D} = \mathcal{D}^{\perp}$, where $\perp$ denotes orthogonal complement with respect to the bilinear form $\ll, \gg$ (Eq. 4.39).

Let us recall the port-Hamiltonian system presented in Eq. 4.8, flow variables are defined as:

$$\boldsymbol{f} := \begin{bmatrix} -\dot{\boldsymbol{x}} \\ \boldsymbol{y} \end{bmatrix}, \boldsymbol{f} \in \mathcal{F}, \tag{4.41}$$

and effort variables as:

$$\boldsymbol{e} = \begin{bmatrix} \nabla_{\boldsymbol{x}} H \\ \boldsymbol{u} \end{bmatrix}, \boldsymbol{e} \in \mathcal{E}, \tag{4.42}$$

then a relationship between the flow and effort variables can be written as:

$$\boldsymbol{f} = S\boldsymbol{e}, \tag{4.43}$$

with S skew-symmetric.

It is easy to verify that the subspace of possible flow and space variables is a Dirac structure. We just need to verify that given any $(\boldsymbol{f}_a, \boldsymbol{e}_a)$ and $(\boldsymbol{f}_b, \boldsymbol{e}_b) \in \mathcal{B}$ that satisfies Eq. 4.43, the bilinear form (Eq. 4.39) is equal to zero. Using as power product the usual product ($\langle \boldsymbol{e}, \boldsymbol{f} \rangle := \boldsymbol{f}^T \boldsymbol{e}$) and from the definition of the bilinear form we get:

$$\begin{aligned} \ll (\boldsymbol{f}_a, \boldsymbol{e}_a), (\boldsymbol{f}_b, \boldsymbol{e}_b) \gg &= \boldsymbol{f}_b^T \boldsymbol{e}_a + \boldsymbol{f}_a^T \boldsymbol{e}_b \\ &= \boldsymbol{e}_b^T S^T \boldsymbol{e}_a + \boldsymbol{e}_a^T S^T \boldsymbol{e}_b \\ &= \boldsymbol{e}_a^T \underbrace{(S + S^T)}_{0} \boldsymbol{e}_b \\ &= 0. \end{aligned} \tag{4.44}$$

In the case of vector flow and effort spaces, with $\boldsymbol{f} \in \mathbb{R}^N$ and $\boldsymbol{e} \in \mathbb{R}^N$, several matrix representations are available for the Dirac structure, let us recall a few of them that appear throughout this thesis[3]:

[3]For more details, see, e.g., Chapter 5 of van der Schaft and Jeltsema (2014), Section 2.4.1 of Macchelli and

Kernel representation

$$\mathcal{D} = \{(\boldsymbol{f}, \boldsymbol{e}) \in \mathcal{F} \times \mathcal{E} | F\boldsymbol{f} + E\boldsymbol{e} = 0\}, \tag{4.45}$$

where F, E are $N \times N$ matrices satisfying: $EF^T + FE^T = 0$ and $\text{rank}[F|E] = \dim\mathcal{F}$.

It is straightforward to verify that the explicit representation of Eq. 4.43 satisfies the requirements. Using $F = I$ and $E = -S$, it follows that $S + S^T = 0$ and $\text{rank}[I|S] = N = \dim\mathcal{F}$. Additionally, it is easy to verify that the Kernel representation for the coupling of two particles, Eq. 4.37, with flow and effort variables given by $\boldsymbol{f} = \begin{bmatrix} -\dot{p}_1 & -\dot{p}_2 & \dot{x}_2 \end{bmatrix}^T$ and $\boldsymbol{e} = \begin{bmatrix} \frac{\partial H}{\partial p_1} & \frac{\partial H}{\partial p_1} & f_{2,e} \end{bmatrix}$, also satisfies both requirements.

Image representation

$$\mathcal{D} = \{(\boldsymbol{f}, \boldsymbol{e}) \in \mathcal{F} \times \mathcal{E} | \exists \lambda \in \mathbb{R}^N \text{ such that } \boldsymbol{f} = E^T\boldsymbol{\lambda}, \boldsymbol{e} = F^T\boldsymbol{\lambda}\}, \tag{4.46}$$

where F, E are $N \times N$ matrices satisfying: $EF^T + FE^T = 0$ and $\text{rank}[F|E] = \dim\mathcal{F}$.

Constrained input-output representation

$$\mathcal{D} = \{(\boldsymbol{f}, \boldsymbol{e}) \in \mathcal{F} \times \mathcal{E} | \exists \lambda \in \mathbb{R}^{N_\lambda} \text{ such that } \boldsymbol{f} = J\boldsymbol{e} + G\boldsymbol{\lambda}\,,\, G^T\boldsymbol{e} = 0\}, \tag{4.47}$$

where J is an $N \times N$ skew-symmetric matrix J, here λ is the vector of Lagrange multipliers, and G is an $N \times N_\lambda$ matrix.

Note: In the constrained pHs of Eq. 4.34 and Eq. 4.35, the flow and effort variables are defined as $\boldsymbol{f} =: \begin{bmatrix} -\dot{p}_1 & -\dot{p}_2 & \dot{x}_2 \end{bmatrix}^T$ and $\boldsymbol{e} =: \begin{bmatrix} \frac{\partial H}{\partial p_1} & \frac{\partial H}{\partial p_1} & f_{2,e} \end{bmatrix}$. The relationship between these variables is given by a constrained input-output representation of Dirac structure.

Finally, from the definition of Dirac structure, the following properties follow:

1. $\langle \boldsymbol{e}, \boldsymbol{f} \rangle = 0, \forall (\boldsymbol{e}, \boldsymbol{f}) \in \mathcal{D}$,

2. $\dim(\mathcal{B}) = \dim(\mathcal{F})$.

The first property means that the Dirac structure is power-preserving (the structure will not introduce/remove energy into/from the system). The second property can be connected with the fact that one half of the variables depends on the other half: it is not possible to impose two conjugate variables at the same time (e.g. speed and force, one is a consequence of the other).

Melchiorri (2004), and references therein.

4.2 Infinite-dimensional port-Hamiltonian Systems

The port-Hamiltonian formalism was extended to systems with distributed parameters by Maschke and van der Schaft (2000). This section starts with an example: the vibrating string is written as a port-Hamiltonian system in § 4.2.1, then the Stokes-Dirac structure is recalled in § 4.2.2. Finally, some comments about more general 1D infinite-dimensional port-Hamiltonian systems, well-posedness and coupling of pHs are addressed in § 4.2.3.

4.2.1 Example: the vibrating string

The vibrating string problem can be approximated using the well-known wave equation:

$$\mu(z)\frac{\partial^2}{\partial t^2}u(z,t) = \frac{\partial}{\partial z}\left(T(z)\frac{\partial}{\partial z}u(z,t)\right), 0 \leq z \leq L\,, \tag{4.48}$$

where $u(z,t)$ is the string vertical displacement, at point z and time t; $\mu(z)$ is the string mass per unit length, and $T(z)$ is the tension.

The total energy (Hamiltonian) associated with the string is given by the sum of kinetic energy and potential energy:

$$H = \frac{1}{2}\int_{z=0}^{L}\left(\mu(z)\left(\frac{\partial u}{\partial t}\right)^2 + T(z)\left(\frac{\partial u}{\partial z}\right)^2\right)\mathrm{d}z\,. \tag{4.49}$$

By defining the following variables: $\alpha_1 := \mu\frac{\partial u}{\partial t}$, which is the linear moment density; $\alpha_2 := \frac{\partial u}{\partial z}$, which is the local string tangent angle. The Hamiltonian becomes:

$$H[\alpha_1(z,t),\alpha_2(z,t)] = \frac{1}{2}\int_{z=0}^{L}\left(\frac{1}{\mu}{\alpha_1}^2 + T{\alpha_2}^2\right)\mathrm{d}z\,. \tag{4.50}$$

Remind that for finite-dimensional pHs, a skew-symmetric interconnection matrix appeared. For infinite-dimensional pHs, a similar form is available. However, here the interconnection is provided by a differential operator. In addition, instead of using the gradient of the Hamiltonian, variational derivatives are used (see e.g. Definition 4.1 of Olver (1993) , or Chapter 4 of Duindam et al. (2009)). The following definition of variational derivative is used:

Definition 4.2
Let us consider $H[u(z,t)]$, a functional of $u(z,t)$:

$$H[u(z,t)] = \int_{z=a}^{b}\mathcal{H}(u,z,t)\,\mathrm{d}z\,. \tag{4.51}$$

*Supposing a variation of $u = \bar{u} + \epsilon\eta(z)$. The **variational derivative** of H, $\frac{\delta H}{\delta u}$ is defined*

from the following expression:

$$H(\bar{u} + \epsilon\eta(z)) = H(\bar{u}) + \epsilon \int_{z=a}^{b} \frac{\delta H}{\delta u}\eta(z)\,\mathrm{d}z + O(\epsilon^2)\,. \tag{4.52}$$

Obs.: when the integrand $\mathcal{H}(u, z, t)$ can be written as an explicit function of u ($\mathcal{H}(u)$), which does not involve the derivatives of u, the variational derivative of H can be easily obtained by derivation of the integrand $\mathcal{H}$: $\frac{\delta H}{\delta u} = \frac{\partial \mathcal{H}}{\partial u}$.

The variational derivatives of the Hamiltonian (Eq. 4.50) are given by:

$$\begin{aligned}\frac{\delta H}{\delta \alpha_1} &= \frac{\alpha_1}{\mu} = \frac{\partial u}{\partial t}\,,\\ \frac{\delta H}{\delta \alpha_2} &= T\alpha_2 = T\frac{\partial u}{\partial z}\,.\end{aligned}$$

These variational derivatives are called co-energy variables: $e_1 := \frac{\delta H}{\delta \alpha_1}$ and $e_2 := \frac{\delta H}{\delta \alpha_2}$. In this case, we recognize that e_1 represents the local string speed ($\frac{\partial u}{\partial t}$) and e_2 the vertical component of the tension.

The wave equation can be rewritten in terms of α_1, α_2, e_1 and e_2:

$$\frac{\partial \alpha_1}{\partial t} = \frac{\partial}{\partial z}(T\alpha_2) = \frac{\partial}{\partial z}(e_2)\,, \tag{4.53}$$

and:

$$\frac{\partial \alpha_2}{\partial t} = \frac{\partial}{\partial t}\left(\frac{\partial u}{\partial z}\right) = \frac{\partial}{\partial z}\left(\frac{\partial u}{\partial t}\right) = \frac{\partial}{\partial z}(e_1)\,. \tag{4.54}$$

These two equations can be written as:

$$\begin{bmatrix} \frac{\partial \alpha_1}{\partial t} \\ \frac{\partial \alpha_2}{\partial t} \end{bmatrix} = \underbrace{\begin{bmatrix} 0 & \frac{\partial}{\partial z} \\ \frac{\partial}{\partial z} & 0 \end{bmatrix}}_{\mathcal{J}} \begin{bmatrix} e_1 \\ e_2 \end{bmatrix}, \tag{4.55}$$

which looks very similar to the finite-dimensional Hamiltonian equation: $\dot{\boldsymbol{x}} = J(\boldsymbol{x})\,\nabla_{\boldsymbol{x}} H$. Except that now $\mathcal{J}$ is a differential operator, and the Hamiltonian's variational derivatives are used instead of the gradient.

Next, the system energy exchange is considered, by analyzing the time derivative of the

Hamiltonian along a trajectory:

$$\begin{aligned}\frac{d}{dt}H &= \int_{z=0}^{L}\left(e_1\frac{\partial\alpha_1}{\partial t}+e_2\frac{\partial\alpha_2}{\partial t}\right)\mathrm{d}z\,,\\ &= \int_{z=0}^{L}\left(e_1\frac{\partial e_2}{\partial z}+e_2\frac{\partial e_1}{\partial z}\right)\mathrm{d}z\,,\\ &= \int_{z=0}^{L}\frac{\partial}{\partial z}(e_1e_2)\,\mathrm{d}z\,,\\ &= e_1(L,t)e_2(L,t)-e_1(0,t)e_2(0,t)\,.\end{aligned} \tag{4.56}$$

It is clear that the energy rate depends only on the boundary conditions of the system. This motivates the definition of "boundary ports". One possible choice of input ports is the following:

$$\boldsymbol{u}_\partial := \begin{bmatrix} e_1(L,t)\\ -e_2(0,t)\end{bmatrix}\,, \tag{4.57}$$

which leads to the following power-conjugated output:

$$\boldsymbol{y}_\partial = \begin{bmatrix} e_2(L,t)\\ e_1(0,t)\end{bmatrix}\,, \tag{4.58}$$

such that the energy flow is written as:

$$\frac{dH}{dt} = \boldsymbol{y}_\partial^T\boldsymbol{u}_\partial\,. \tag{4.59}$$

Note that this particular choice of input and output is only one among many possibilities. A description of all the possible choices of input/outputs that lead to well-posed problems is described by Le Gorrec, Zwart, and Maschke (2005).

In addition to energy conservation, another advantage of rewriting the wave equation as Eq. 4.55 is that two additional conservation laws become evident. By integrating the equations along the domain, we find:

$$\begin{aligned}\int_{z=0}^{L}\dot{\alpha_1}\,\mathrm{d}z &= e_2(L)-e_2(0)\,,\\ \int_{z=0}^{L}\dot{\alpha_2}\,\mathrm{d}z &= e_1(L)-e_1(0)\,.\end{aligned} \tag{4.60}$$

Finally, remember that for finite-dimensional port-Hamiltonian systems, matrix J is skew-symmetric. For infinite-dimensional pHs, $\mathcal{J}$ is a formally skew-symmetric operator. This means that:

$$\langle\mathcal{J}\boldsymbol{e},\boldsymbol{f}\rangle = -\langle\boldsymbol{e},\mathcal{J}\boldsymbol{f}\rangle, \tag{4.61}$$

where $\boldsymbol{e}(z)$, $\boldsymbol{f}(z)$ are functions of z with zero boundary conditions, $\langle,\rangle$ is the usual inner product (here: $\langle\mathbf{u}(z),\mathbf{v}(z)\rangle = \int_{z=0}^{L}\mathbf{u}^T(z)\mathbf{v}(z)\,\mathrm{d}z$). It is easy to verify that $\mathcal{J}$ is formally

skew-symmetric for the wave equation:

$$\begin{aligned}
\langle \mathcal{J}\boldsymbol{e}, \boldsymbol{f} \rangle &= \int_{z=0}^{L} (\mathcal{J}\boldsymbol{e})^T \boldsymbol{f} \, \mathrm{d}z \,, \\
&= \int_{z=0}^{L} (\begin{bmatrix} 0 & 1 \\ 1 & 0 \end{bmatrix} \partial_z \boldsymbol{e})^T \boldsymbol{f} \, \mathrm{d}z \,, \\
&= \int_{z=0}^{L} \partial_z \boldsymbol{e}^T \begin{bmatrix} 0 & 1 \\ 1 & 0 \end{bmatrix} \boldsymbol{f} \, \mathrm{d}z \,, \\
&= - \int_{z=0}^{L} \boldsymbol{e}^T \underbrace{\begin{bmatrix} 0 & 1 \\ 1 & 0 \end{bmatrix} \partial_z}_{\mathcal{J}} \boldsymbol{f} \, \mathrm{d}z + \underbrace{\boldsymbol{e}^T \begin{bmatrix} 0 & 1 \\ 1 & 0 \end{bmatrix} \boldsymbol{f}|_{z=0}^{L}}_{0} \,, \\
&= -\langle \boldsymbol{e}, \mathcal{J}\boldsymbol{f} \rangle \,.
\end{aligned} \tag{4.62}$$

4.2.1.1 Nonlinear case

Now let us consider the nonlinear wave equation, similar to the one presented in Section 12.2.1 of Leimkuhler and Reich (2005):

$$\frac{\partial^2 u}{\partial t^2} = \frac{\partial}{\partial z} \left(\sigma' \left(\frac{\partial u}{\partial z} \right) \right) \,, \quad z \in [0, L] \,, \tag{4.63}$$

where $\sigma(.)$ is a nonlinear smooth function (and $\sigma'(.)$ its derivative). Similarly to the previous section, let us define $\alpha_1 := \frac{\partial u}{\partial t}$, $\alpha_2 := \frac{\partial u}{\partial z}$, and the following Hamiltonian:

$$H[\alpha_1, \alpha_2] = \frac{1}{2} \int_{z=0}^{L} \left(\alpha_1^2 + \sigma(\alpha_2) \right) \mathrm{d}z \,. \tag{4.64}$$

The variational derivatives of this Hamiltonian are:

$$\begin{aligned}
e_1 &:= \frac{\delta H}{\delta \alpha_1} = \alpha_1 \,, \\
e_2 &:= \frac{\delta H}{\delta \alpha_2} = \sigma'(\alpha_2) \,.
\end{aligned} \tag{4.65}$$

Thus, the non-linear wave equation can be rewritten as:

$$\begin{bmatrix} \dot{\alpha}_1 \\ \dot{\alpha}_2 \end{bmatrix} = \underbrace{\begin{bmatrix} 0 & \partial_z \\ \partial_z & 0 \end{bmatrix}}_{\mathcal{J}} \begin{bmatrix} e_1 \\ e_2 \end{bmatrix} . \tag{4.66}$$

Again, $\mathcal{J}$ is a formally skew-symmetric (linear!) differential operator. The nonlinearity of the system comes from the non-quadratic form of the Hamiltonian.

By computing the energy balance of the non-linear system, the same result as before is

obtained:

$$\dot{H} = e_2(L,t)e_1(L,t) - e_2(0,t)e_1(0,t)\,. \tag{4.67}$$

It is important to remark that the operator $\mathcal{J}$ provides an interconnection structure between the co-energy variables ($e_i(z,t)$), the time-derivative of the energy variables ($\dot{\alpha}_i(z,t)$) and the boundary ports. In the sequel, it is shown that this structure is a Dirac structure as defined previously.

4.2.2 Stokes-Dirac structure

To verify that the differential operator presented before provides a Dirac structure, first, let us define the flow and effort variables as:

$$\begin{aligned} \boldsymbol{f} &:= (f_1(z,t),\, f_2(z,t),\, \boldsymbol{y}_\partial(t)) := (-\dot{\alpha}_1(z,t),\, -\dot{\alpha}_2(z,t),\, \boldsymbol{y}(t))\ , \\ \boldsymbol{e} &:= (e_1(z,t),\, e_2(z,t),\, \boldsymbol{u}_\partial(t)) := (e_1(z,t),\, e_2(z,t),\, \boldsymbol{u}(t))\ . \end{aligned} \tag{4.68}$$

Additionally, we define the following power product:

$$P := \langle \boldsymbol{e} | \boldsymbol{f} \rangle := \int_{z=0}^{L} \begin{bmatrix} e_1 & e_2 \end{bmatrix} \begin{bmatrix} f_1 \\ f_2 \end{bmatrix} \mathrm{d}z + \boldsymbol{y}_\partial^T \boldsymbol{u}_\partial\,, \tag{4.69}$$

The relationship between the flow and effort variables is given by the operator $\mathcal{J}$ (Eq. 4.55) together with the input/output boundary ports (Eqs. 4.57 and 4.58), which are recalled as follows:

$$\begin{aligned} \begin{bmatrix} f_1 \\ f_2 \end{bmatrix} &= \begin{bmatrix} 0 & -1 \\ -1 & 0 \end{bmatrix} \partial_z \begin{bmatrix} e_1 \\ e_2 \end{bmatrix}\ , \\ \boldsymbol{u}_\partial &= \begin{bmatrix} e_1(L,t) & -e_2(0,t) \end{bmatrix}^T\ , \\ \boldsymbol{y}_\partial &= \begin{bmatrix} e_2(L,t) & e_1(0,t) \end{bmatrix}^T\ . \end{aligned} \tag{4.70}$$

Then, computing the bilinear product as defined in Eq. 4.39 for $(\boldsymbol{f}^a, \boldsymbol{e}^a)$ and $(\boldsymbol{f}^b, \boldsymbol{e}^b)$, that satisfy Eq. 4.70, we get:

$$\begin{aligned} \ll (\boldsymbol{f}^a, \boldsymbol{e}^a), (\boldsymbol{f}^b, \boldsymbol{e}^b) \gg &= \int_{z=0}^{L} \begin{bmatrix} e_1^a & e_2^a \end{bmatrix} \begin{bmatrix} f_1^b \\ f_2^b \end{bmatrix} \mathrm{d}z + \boldsymbol{y}_\partial^{a,T} \boldsymbol{u}_\partial^b + \int_{z=0}^{L} \begin{bmatrix} e_1^b & e_2^b \end{bmatrix} \begin{bmatrix} f_1^a \\ f_2^a \end{bmatrix} \mathrm{d}z + \boldsymbol{y}_\partial^{b,T} \boldsymbol{u}_\partial^a\,, \\ &= \int_{z=0}^{L} \begin{bmatrix} e_1^a & e_2^a \end{bmatrix} \begin{bmatrix} 0 & -1 \\ -1 & 0 \end{bmatrix} \partial_z \begin{bmatrix} e_1^b \\ e_2^b \end{bmatrix} \mathrm{d}z + \boldsymbol{y}_\partial^{a,T} \boldsymbol{u}_\partial^b + \\ &\quad \int_{z=0}^{L} \begin{bmatrix} e_1^b & e_2^b \end{bmatrix} \begin{bmatrix} 0 & -1 \\ -1 & 0 \end{bmatrix} \partial_z \begin{bmatrix} e_1^a \\ e_2^a \end{bmatrix} \mathrm{d}z + \boldsymbol{y}_\partial^{b,T} \boldsymbol{u}_\partial^a\,, \end{aligned} \tag{4.71}$$

and after integration by parts of the first term, with $\boldsymbol{u}_\partial$ and $\boldsymbol{y}_\partial$ that satisfy Eq. 4.70:

$$\begin{aligned}
\ll (\boldsymbol{f}^a, \boldsymbol{e}^a), (\boldsymbol{f}^b, \boldsymbol{e}^b) \gg = & -\int_{z=0}^{L} \begin{bmatrix} e_1^b & e_2^b \end{bmatrix} \begin{bmatrix} 0 & -1 \\ -1 & 0 \end{bmatrix} \partial_z \begin{bmatrix} e_1^a \\ e_2^a \end{bmatrix} \mathrm{d}z + \\
& + \begin{bmatrix} e_1^a & e_2^a \end{bmatrix} \begin{bmatrix} 0 & -1 \\ -1 & 0 \end{bmatrix} \begin{bmatrix} e_1^b \\ e_2^b \end{bmatrix} |_{z=0}^{L} + \boldsymbol{y}_\partial^{a,T} \boldsymbol{u}_\partial^b + \\
& + \int_{z=0}^{L} \begin{bmatrix} e_1^b & e_2^b \end{bmatrix} \begin{bmatrix} 0 & -1 \\ -1 & 0 \end{bmatrix} \partial_z \begin{bmatrix} e_1^a \\ e_2^a \end{bmatrix} \mathrm{d}z + \boldsymbol{y}_\partial^{b,T} \boldsymbol{u}_\partial^a \,, \\
= & -(e_2^a e_1^b + e_1^a e_2^b)|_{z=0}^{L} + e_2^a(L) e_1^b(L) - e_1^a(0) e_2^b(0) + \\
& + e_2^b(L) e_1^a(L) - e_1^b(0) e_2^a(0) \\
= & 0 \,.
\end{aligned} \tag{4.72}$$

Thus, Eq. 4.70 gives a Dirac structure, that interconnects the flow and energy variables defined in Eq. 4.68.

As it happened in the finite-dimensional systems, the definition of the Dirac structure is independent of the definition of the Hamiltonian itself. Both finite and infinite-dimensional pHs are defined by a Dirac structure together with a Hamiltonian (and sometimes with other constitutive relations like those provided by dissipative elements, see § 4.1.3).

For infinite-dimensional systems, the Dirac structure is also known as Stokes-Dirac structure. The reason for that is that the Stokes theorem allows generalizing the computation of the energy flow by means of boundary ports for 2D and 3D systems.

4.2.3 Generalizations, well-posedness and coupling of infinite-dimensional port-Hamiltonian systems

More generally, 1D infinite-dimensional port-Hamiltonian systems can be written as:

$$\begin{aligned}
\dot{\boldsymbol{x}}(z,t) &= \mathcal{J}\boldsymbol{e}(z,t) \,, \\
\boldsymbol{u}_\partial(t) &= \mathcal{B}\boldsymbol{e}(z,t) \,, \\
\boldsymbol{y}_\partial(t) &= \mathcal{C}\boldsymbol{e}(z,t) \,,
\end{aligned} \tag{4.73}$$

where $\boldsymbol{x}(z,t)$ is the vector of energy variables, $\boldsymbol{e}(z,t)$ is the vector of co-energy variables, given by the variational derivatives of the Hamiltonian ($\boldsymbol{e} = \frac{\delta H}{\delta \boldsymbol{x}}$), $\mathcal{J}$ is a formally skew-adjoint operator, $\boldsymbol{u}_\partial$ and $\boldsymbol{y}_\partial$ are boundary ports, and $\mathcal{B}$ and $\mathcal{C}$ are boundary operators, such that $\dot{H} = \boldsymbol{y}_\partial^T \boldsymbol{u}_\partial$.

The differential operator $\mathcal{J}$ can be parametrized as follows:

$$\mathcal{J} = P_0 + \sum_{i=1}^{N} P_i \frac{\partial^i}{\partial z^i} \,, \tag{4.74}$$

where $P_i = (-1)^{i+1}(P_i)^T$. Using a procedure similar to the one presented in Eq. 4.62 for the wave equation, it is quite straightforward to prove that this parametrization of $\mathcal{J}$ leads to formally skew-symmetric operators (see, e.g., Le Gorrec, Zwart, and Maschke (2005); Villegas (2007)).

From a mathematical point of view, one of the main difficulties when dealing with partial differential equations is to check that the problem is well-posed, i.e., that solutions exist and are unique. Using semi-group theory (Curtain and Zwart, 1995), many results of well posedness of *linear*[4] infinite-dimensional port-Hamiltonian systems becomes quite straightforward (Jacob and Zwart, 2012).

Also in the case of linear infinite-dimensional systems, Le Gorrec, Zwart, and Maschke (2005) provided an algebraic criteria, which can be used to easily check the well-posedness of port-Hamiltonian systems.

Finally, many results exist on the coupling of pHs: Macchelli and Melchiorri (2005) discuss the regulation problem for a problem with two coupled pHs, one finite-dimensional and the other infinite-dimensional; Chapter 3 of Pasumarthy (2006) and Chapter 7 of Villegas (2007) present different interconnections between finite-dimensional and infinite-dimensional systems through boundary and distributed ports.

4.3 Tools for manipulating finite-dimensional port-Hamiltonian systems

In the next two chapters of this thesis, infinite-dimensional port-Hamiltonian representations of the fluid and structural dynamic equations will be obtained. Then, in Part III, semi-discretization methods will be presented, such that the distributed systems are approximated as finite-dimensional systems in a way that the pHs structure is preserved. Thus, each subsystem becomes represented as a finite-dimensional pHs (as, e.g., Eq. 4.6). Indeed, after discretization, the systems are manipulated in the computer as finite-dimensional pHs.

As explained before, one of the main interests of using the pHs is that it provides a modular approach for modeling complex systems. The approach is compatible with object-oriented programming paradigm. Each subsystem can be written as an object, and methods can be programmed to manipulate the pHs. This advantage is intrinsic to the pHs formulation. In this section, we recall two classical power-preserving interconnections (called "gyrator" and "transformer" interconnections). Then, we recall some methods for dealing with algebraic constraints that appear after "transformer" interconnections.

[4]For linear systems, the Hamiltonian is quadratic, i.e.: $H[\boldsymbol{x}] = \frac{1}{2}\int_{z=0}^{L} \boldsymbol{x}^T Q\boldsymbol{x}\,\mathrm{d}z$. And the co-energy variables are given by: $\boldsymbol{e} = Q\boldsymbol{x}$.

4.3.1 Gyrator and transformer interconnections

In § 4.1.1 and 4.1.4, two examples of interconnections were presented (given by a mass-spring system and two masses, respectively). Let us now repeat the interconnection procedure for a more general case. Consider two pHs, Σ_1 and Σ_2, written as:

$$\Sigma_1 \begin{cases} \dot{\boldsymbol{x}}_1 = (J_1 - R_1)\boldsymbol{e}_1 + B_{1,int}\boldsymbol{u}_{1,int} + B_{1,ext}\boldsymbol{u}_{1,ext}\,, \\ \boldsymbol{y}_{1,int} = B_{1,int}^T \boldsymbol{e}_1\,, \\ \boldsymbol{y}_{1,ext} = B_{1,ext}^T \boldsymbol{e}_1, \end{cases} \tag{4.75}$$

and

$$\Sigma_2 \begin{cases} \dot{\boldsymbol{x}}_2 = (J_2 - R_2)\boldsymbol{e}_2 + B_{2,int}\boldsymbol{u}_{2,int} + B_{2,ext}\boldsymbol{u}_{2,ext}\,, \\ \boldsymbol{y}_{2,int} = B_{2,int}^T \boldsymbol{e}_2\,, \\ \boldsymbol{y}_{2,ext} = B_{2,ext}^T \boldsymbol{e}_2, \end{cases} \tag{4.76}$$

where $\boldsymbol{x}_1(t) \in \mathbb{R}^{N_1}$ and $\boldsymbol{x}_2(t) \in \mathbb{R}^{N_2}$ are the vectors of energy variables, $\boldsymbol{e}_1 := \nabla_{x_1} H_1(\boldsymbol{x}_1)$ and $\boldsymbol{e}_2 := \nabla_{x_2} H_2(\boldsymbol{x}_2)$ are the vectors of co-energy variables. Each system has two pairs of input/output vectors, one that will be used for interconnection ($\boldsymbol{u}_{1,int}$, $\boldsymbol{y}_{1,int} \in \mathbb{R}^{M_{1,int}}$ and $\boldsymbol{u}_{2,int}$, $\boldsymbol{y}_{2,int} \in \mathbb{R}^{M_{2,int}}$) and the other will be left for external interactions ($\boldsymbol{u}_{1,ext}$, $\boldsymbol{y}_{1,ext} \in \mathbb{R}^{M_{1,ext}}$ and $\boldsymbol{u}_{2,ext}$, $\boldsymbol{y}_{2,ext} \in \mathbb{R}^{M_{2,ext}}$). As before, J_i are skew-symmetric matrices and R_i are positive semi-definite matrices.

There are two main power-preserving interconnections of interest during the coupling of physical systems. They are called "gyrator" and "transformer" interconnection.

Gyrator interconnection: The gyrator interconnection is depicted in Fig. 4.1. It is given by the following relationship between the interconnection ports:

$$\begin{aligned} \boldsymbol{u}_{1,int} &= -C\boldsymbol{y}_{2,int}\,, \\ \boldsymbol{u}_{2,int} &= C^T\boldsymbol{y}_{1,int}\,, \end{aligned} \tag{4.77}$$

where C is an $M_{2,int} \times M_{1,int}$ matrix. Since $\boldsymbol{u}_{1,int}^T\boldsymbol{y}_{1,int} + \boldsymbol{u}_{2,int}^T\boldsymbol{y}_{2,int} = 0$, this interconnection is power-preserving.

It is easy to verify that from this interconnection, we have:

$$\begin{aligned} \begin{bmatrix} \dot{\boldsymbol{x}}_1 \\ \dot{\boldsymbol{x}}_2 \end{bmatrix} &= \begin{bmatrix} J_1 - R_1 & -B_{1,int}CB_{2,int}^T \\ B_{2,int}C^TB_{1,int}^T & J_2 - R_2 \end{bmatrix} \begin{bmatrix} \boldsymbol{e}_1 \\ \boldsymbol{e}_2 \end{bmatrix} + \begin{bmatrix} B_{1,ext} & 0 \\ 0 & B_{2,ext} \end{bmatrix} \begin{bmatrix} \boldsymbol{u}_{1,ext} \\ \boldsymbol{u}_{2,ext} \end{bmatrix}, \\ \begin{bmatrix} \boldsymbol{y}_{1,ext} \\ \boldsymbol{y}_{2,ext} \end{bmatrix} &= \begin{bmatrix} B_{1,ext}^T & 0 \\ 0 & B_{2,ext}^T \end{bmatrix} \begin{bmatrix} \boldsymbol{e}_1 \\ \boldsymbol{e}_2 \end{bmatrix}, \end{aligned} \tag{4.78}$$

where $H = H_1 + H_2$. Note that the ports used for interconnection totally disappear in the previous equation: the resulting pHs is explicit. The power balance becomes dependent on the "external" ports only:

$$\dot{H} = \boldsymbol{u}_{1,ext}^T\boldsymbol{y}_{1,ext} + \boldsymbol{u}_{2,ext}^T\boldsymbol{y}_{2,ext}\,. \tag{4.79}$$

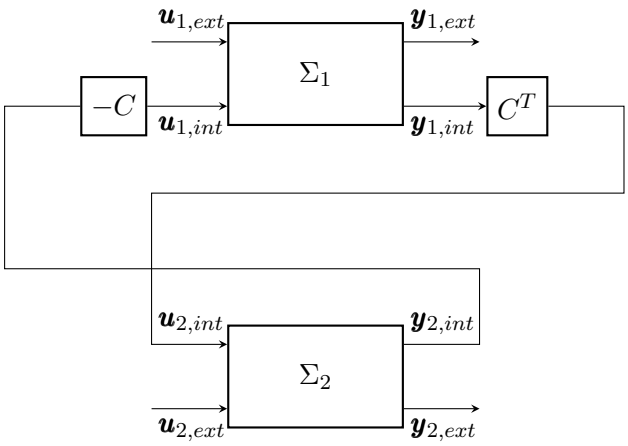

Figure 4.1: Gyrator interconnection

Transformer interconnection: The transformer interconnection is depicted in Fig. 4.2. It is given by the following relationship between the interconnection ports:

$$\begin{aligned} \boldsymbol{u}_{1,int} &= -C\boldsymbol{u}_{2,int}\,, \\ \boldsymbol{y}_{2,int} &= C^T\boldsymbol{y}_{1,int}\,, \end{aligned} \tag{4.80}$$

where C is an $M_{2,int} \times M_{1,int}$ matrix. Since $\boldsymbol{u}_{1,int}^T\boldsymbol{y}_{1,int} + \boldsymbol{u}_{2,int}^T\boldsymbol{y}_{2,int} = 0$, this interconnection is also power-preserving.

In this case, the equations of the coupled system become:

$$\begin{aligned} \begin{bmatrix} \dot{\boldsymbol{x}}_1 \\ \dot{\boldsymbol{x}}_2 \end{bmatrix} &= \begin{bmatrix} J_1 - R_1 & 0 \\ 0 & J_2 - R_2 \end{bmatrix} \begin{bmatrix} \boldsymbol{e}_1 \\ \boldsymbol{e}_2 \end{bmatrix} + \begin{bmatrix} B_{1,ext} & 0 \\ 0 & B_{2,ext} \end{bmatrix} \begin{bmatrix} \boldsymbol{u}_{1,ext} \\ \boldsymbol{u}_{2,ext} \end{bmatrix} + \begin{bmatrix} -B_{1,int}C \\ B_{2,int} \end{bmatrix} \boldsymbol{\lambda}\,, \\ \begin{bmatrix} \boldsymbol{y}_{1,ext} \\ \boldsymbol{y}_{2,ext} \end{bmatrix} &= \begin{bmatrix} B_{1,ext}^T & 0 \\ 0 & B_{2,ext}^T \end{bmatrix} \begin{bmatrix} \boldsymbol{e}_1 \\ \boldsymbol{e}_2 \end{bmatrix}\,, \\ 0 &= \begin{bmatrix} -C^T B_{1,int}^T & B_{2,int}^T \end{bmatrix} \begin{bmatrix} \boldsymbol{e}_1 \\ \boldsymbol{e}_2 \end{bmatrix}\,, \end{aligned} \tag{4.81}$$

which is no more explicit, but Eq. 4.81 is a Differential-Algebraic Equation (DAE), where $\boldsymbol{\lambda} = \boldsymbol{u}_{2,int}$ is the vector of Lagrange multipliers (unknowns) of the system. This system can be simulated using DAE solvers (Ascher and Petzold, 1998; Kunkel and Mehrmann, 2006). Other manipulations are also possible to avoid the constraints and find an equivalent set of Ordinary Differential Equations (ODEs) for this system, as explained in the following subsection.

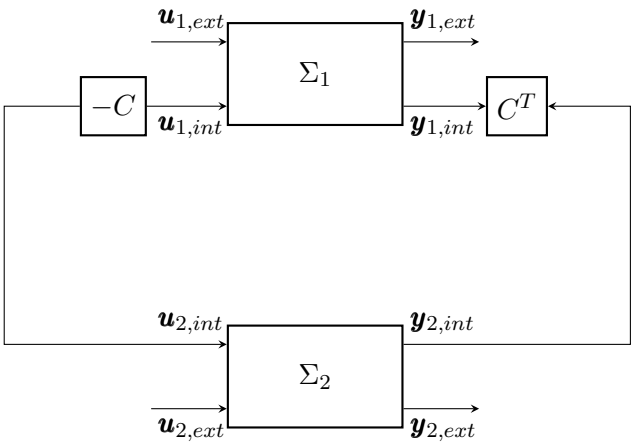

Figure 4.2: Transformer interconnection

4.3.2 Dealing with algebraic constraints

Port-Hamiltonian systems with algebraic constraints (van der Schaft, 2013), as those seen in § 4.1.4 and § 4.3.1, can be presented in the following form:

$$\begin{aligned} \dot{\boldsymbol{x}} &= (J-R)\nabla_{\boldsymbol{x}}H + B\boldsymbol{u} + G\boldsymbol{\lambda}\,, \\ \boldsymbol{y} &= B^T\nabla_{\boldsymbol{x}}H\,, \\ 0 &= G^T\nabla_{\boldsymbol{x}}H\,, \end{aligned} \tag{4.82}$$

where $\boldsymbol{x} \in \mathbb{R}^N$, $\boldsymbol{u}$, $\boldsymbol{y} \in \mathbb{R}^M$ and $\boldsymbol{\lambda} \in \mathbb{R}^{N_\lambda}$. The matrices J and R are $N \times N$, B is $N \times M$, and G is $N \times N_\lambda$ (G has full column rank N_λ).

In order to eliminate these N_λ algebraic constraints, it is possible to use changes of variables, reducing the number of states of the system (and still having a port-Hamiltonian system). In the linear case, a reduced-order set of ODEs can be obtained that preserves the port-Hamiltonian structure of the system. This section recalls how such a change of variable can be performed.

4.3.2.1 Finding a reduced-order explicit pHs by change of variables

The elimination of algebraic constraints is presented, e.g., by van der Schaft (2013) and Wu et al. (2014). Defining an $(N - N_\lambda) \times N$ matrix $G^\perp$, which is a left-annihilator of G (such that $G^\perp G = 0$), the $N \times N$ matrix

$$M := \begin{bmatrix} G^\perp \\ (G^TG)^{-1}G^T \end{bmatrix}\,, \tag{4.83}$$

and the new variable $\boldsymbol{z} \in \mathbb{R}^N$:

$$\boldsymbol{z} := M\boldsymbol{x} \Rightarrow \boldsymbol{x} = M^{-1}\boldsymbol{z}\,, \tag{4.84}$$

the dynamic equations can be rewritten as:

$$\begin{aligned}\dot{\boldsymbol{z}} &= M(J-R)\nabla_{\boldsymbol{x}}H + MB\boldsymbol{u} + MG\boldsymbol{\lambda}\,,\\ &= M(J-R)\nabla_{\boldsymbol{x}}H + MB\boldsymbol{u} + \begin{bmatrix} G^{\perp} \\ (G^TG)^{-1}G^T \end{bmatrix} G\boldsymbol{\lambda}\,,\\ &= M(J-R)\nabla_{\boldsymbol{x}}H + MB\boldsymbol{u} + \begin{bmatrix} 0 \\ I \end{bmatrix} \boldsymbol{\lambda}\,. \end{aligned} \tag{4.85}$$

The gradient of the Hamiltonian with respect to the new variable $\boldsymbol{z}$ can be computed as:

$$\begin{aligned}\nabla_{\boldsymbol{z}}H &= \left(\frac{\partial \boldsymbol{x}}{\partial \boldsymbol{z}}\right)^T \nabla_{\boldsymbol{x}}H\,,\\ &= M^{-T}\nabla_{\boldsymbol{x}}H\,, \end{aligned} \tag{4.86}$$

leading to the following equations:

$$\dot{\boldsymbol{z}} = M(J-R)M^T\nabla_{\boldsymbol{z}}H + MB\boldsymbol{u} + \begin{bmatrix} 0 \\ I \end{bmatrix} \boldsymbol{\lambda}\,. \tag{4.87}$$

Defining $\tilde{J} := MJM^T$ (which is still skew-symmetric), $\tilde{R} := MRM^T$ (which is still symmetric and positive semi-definite) and $\tilde{B} := MB$:

$$\dot{\boldsymbol{z}} = (\tilde{J}-\tilde{R})\nabla_{\boldsymbol{z}}H + \tilde{B}\boldsymbol{u} + \begin{bmatrix} 0 \\ I \end{bmatrix} \boldsymbol{\lambda}\,. \tag{4.88}$$

Similarly, the output equation can be rewritten as:

$$\begin{aligned}\boldsymbol{y} &= B^TM^T\nabla_{\boldsymbol{z}}H\,,\\ &= \tilde{B}^T\nabla_{\boldsymbol{z}}H\,, \end{aligned} \tag{4.89}$$

and the constraint equation as:

$$\begin{aligned} 0 &= G^TM^T\nabla_{\boldsymbol{z}}H\,,\\ &= (MG)^T\nabla_{\boldsymbol{z}}H\,,\\ &= \begin{bmatrix} 0 & I \end{bmatrix} \nabla_{\boldsymbol{z}}H\,. \end{aligned} \tag{4.90}$$

So, the dynamic equations with constraints can be written as:

$$\begin{aligned}\dot{\boldsymbol{z}} &= (\tilde{J}-\tilde{R})\nabla_{\boldsymbol{z}}H + \tilde{B}\boldsymbol{u} + \begin{bmatrix} 0 \\ I \end{bmatrix} \boldsymbol{\lambda}\,,\\ \boldsymbol{y} &= \tilde{B}^T\nabla_{\boldsymbol{z}}H\,,\\ 0 &= \begin{bmatrix} 0 & I \end{bmatrix} \nabla_{\boldsymbol{z}}H\,. \end{aligned} \tag{4.91}$$

The vector $\boldsymbol{z}$ can be split in two parts, $\boldsymbol{z}_1 \in \mathbb{R}^{(N-N_\lambda)}$ and $\boldsymbol{z}_2 \in \mathbb{R}^{N_\lambda}$:

$$\begin{cases} \begin{bmatrix} \dot{\boldsymbol{z}}_1 \\ \dot{\boldsymbol{z}}_2 \end{bmatrix} = \left(\begin{bmatrix} \tilde{J}_{11} & \tilde{J}_{12} \\ \tilde{J}_{21} & \tilde{J}_{22} \end{bmatrix} - \begin{bmatrix} \tilde{R}_{11} & \tilde{R}_{12} \\ \tilde{R}_{21} & \tilde{R}_{22} \end{bmatrix} \right) \begin{bmatrix} \nabla_{\boldsymbol{z}_1} H \\ \nabla_{\boldsymbol{z}_2} H \end{bmatrix} + \begin{bmatrix} \tilde{B}_1 \\ \tilde{B}_2 \end{bmatrix} \boldsymbol{u} + \begin{bmatrix} 0 \\ I \end{bmatrix} \boldsymbol{\lambda} \,, \\ \boldsymbol{y} = \begin{bmatrix} \tilde{B}_1 & \tilde{B}_2 \end{bmatrix}^T \begin{bmatrix} \nabla_{\boldsymbol{z}_1} H \\ \nabla_{\boldsymbol{z}_2} H \end{bmatrix} \,, \\ 0 = \begin{bmatrix} 0 & I \end{bmatrix} \begin{bmatrix} \nabla_{\boldsymbol{z}_1} H \\ \nabla_{\boldsymbol{z}_2} H \end{bmatrix} \,. \end{cases} \tag{4.92}$$

The constraints from the third equation implies that $\nabla_{\boldsymbol{z}_2} H(\boldsymbol{z}_1, \boldsymbol{z}_2) = 0$ and the equations can be simplified into:

$$\begin{cases} \dot{\boldsymbol{z}}_1 = (\tilde{J}_{11} - \tilde{R}_{11}) \frac{\partial H}{\partial \boldsymbol{z}_1}(\boldsymbol{z}_1, \boldsymbol{z}_2) + \tilde{B}_1 \boldsymbol{u} \,, \\ \boldsymbol{y} = \tilde{B}_1{}^T \frac{\partial H}{\partial \boldsymbol{z}_1}(\boldsymbol{z}_1, \boldsymbol{z}_2) \,, \\ 0 = \frac{\partial H}{\partial \boldsymbol{z}_2}(\boldsymbol{z}_1, \boldsymbol{z}_2) \,. \end{cases} \tag{4.93}$$

Note that the dynamical system has fewer dynamic states ($N - N_\lambda$), but an implicit equation has to be solved to find $\boldsymbol{z}_2$ at each time. In the linear case, the system can be simplified further. For linear pHs, the Hamiltonian is quadratic and its gradient can be written as:

$$\nabla_{\boldsymbol{x}} H = Q\boldsymbol{x} \,. \tag{4.94}$$

The gradient of H with respect to $\boldsymbol{z}$ is given by:

$$\nabla_{\boldsymbol{z}} H = M^{-T} Q M^{-1} \boldsymbol{z} \,, \tag{4.95}$$

Defining:

$$\tilde{Q} := M^{-T} Q M^{-1} \,, \tag{4.96}$$

we get:

$$\nabla_{\boldsymbol{z}} H = \tilde{Q}\boldsymbol{z} \,, \tag{4.97}$$

$$\begin{bmatrix} \nabla_{\boldsymbol{z}_1} H \\ \nabla_{\boldsymbol{z}_2} H \end{bmatrix} = \begin{bmatrix} \tilde{Q}_{11} & \tilde{Q}_{12} \\ \tilde{Q}_{21} & \tilde{Q}_{22} \end{bmatrix} \begin{bmatrix} \boldsymbol{z}_1 \\ \boldsymbol{z}_2 \end{bmatrix} \,. \tag{4.98}$$

So, the dynamic equations become:

$$\begin{cases} \dot{\boldsymbol{z}}_1 = \left(\tilde{J}_{11} - \tilde{R}_{11} \right) \left(\tilde{Q}_{11}\boldsymbol{z}_1 + \tilde{Q}_{12}\boldsymbol{z}_2 \right) + \tilde{B}_1 \boldsymbol{u} \,, \\ \boldsymbol{y} = \tilde{B}_1^T (\tilde{Q}_{11}\boldsymbol{z}_1 + \tilde{Q}_{12}\boldsymbol{z}_2) \,, \\ 0 = \tilde{Q}_{21}\boldsymbol{z}_1 + \tilde{Q}_{22}\boldsymbol{z}_2 \,. \end{cases} \tag{4.99}$$

Assuming that $\tilde{Q}$ is positive-definite (which is usually the case for mechanical systems), the

$N_\lambda \times N_\lambda$ matrix $\tilde{Q}_{22}$ is also positive-definite and thus invertible, such that:

$$\boldsymbol{z}_2 = -\tilde{Q}_{22}^{-1}\tilde{Q}_{21}\boldsymbol{z}_1\,. \tag{4.100}$$

Thus, the system can be written explicitly as:

$$\begin{aligned}\dot{\boldsymbol{z}}_1 &= (\tilde{J}_{11} - \tilde{R}_{11})\left(\tilde{Q}_{11} - \tilde{Q}_{12}\tilde{Q}_{22}^{-1}\tilde{Q}_{21}\right)\boldsymbol{z}_1 + \tilde{B}_1\boldsymbol{u}\,,\\ \boldsymbol{y} &= \tilde{B}_1^T\left(\tilde{Q}_{11} - \tilde{Q}_{12}\tilde{Q}_{22}^{-1}\tilde{Q}_{21}\right)\boldsymbol{z}_1\,.\end{aligned} \tag{4.101}$$

4.3.2.2 Finding the values of the Lagrange multipliers

An alternative method to find an explicit version of Eq. 4.82 consists in computing the values of the Lagrange multipliers $\boldsymbol{\lambda}$. This can be done by the time-derivation of the constraint equation:

$$0 = G^T\frac{\partial^2 H}{\partial \boldsymbol{x}^2}\dot{\boldsymbol{x}}\,, \tag{4.102}$$

where the $N \times N$ matrix $\frac{\partial^2 H}{\partial \boldsymbol{x}^2}(\boldsymbol{x})$ is the Hessian of the Hamiltonian evaluated at $\boldsymbol{x}$. From the substitution of the dynamical equation:

$$\begin{aligned}0 &= G^T\frac{\partial^2 H}{\partial \boldsymbol{x}^2}\left[(J-R)\nabla_{\boldsymbol{x}}H + G\boldsymbol{\lambda} + B\boldsymbol{u}\right]\,,\\ 0 &= G^T\frac{\partial^2 H}{\partial \boldsymbol{x}^2}\left[(J-R)\nabla_{\boldsymbol{x}}H + B\boldsymbol{u}\right] + G^T\frac{\partial^2 H}{\partial \boldsymbol{x}^2}G\boldsymbol{\lambda}\,,\end{aligned} \tag{4.103}$$

and assuming the $N_\lambda \times N_\lambda$ matrix $G^T\frac{\partial^2 H}{\partial \boldsymbol{x}^2}G$ is invertible, $\boldsymbol{\lambda}$ can be computed as:

$$\boldsymbol{\lambda} = -\left(G^T\frac{\partial^2 H}{\partial \boldsymbol{x}^2}G\right)^{-1}G^T\frac{\partial^2 H}{\partial \boldsymbol{x}^2}\left[(J-R)\nabla_{\boldsymbol{x}}H + B\boldsymbol{u}\right]\,. \tag{4.104}$$

Remark 4.1
If the system is linear, the Hamiltonian is quadratic: $H = \frac{1}{2}\boldsymbol{x}^T Q\boldsymbol{x}$. *Thus, the Hessian* $\frac{\partial^2 H}{\partial x^2} = Q$ *is constant, and the Lagrange multiplier reads:*

$$\boldsymbol{\lambda} = -\left(G^T Q G\right)^{-1}G^T Q\left[(J-R)Q\boldsymbol{x} + B\boldsymbol{u}\right]\,. \tag{4.105}$$

4.4 Conclusions

The main goal of this chapter was to provide a general overview of port-Hamiltonian systems *as a modeling technique*, and to recall the main tools that are used in the next chapters to model the fluid-structure system. Some characteristics of these systems that motivates their use are recalled here:

- it is physically motivated (by the classical Hamiltonian theory);
- it provides a modular way to model complex systems, which can be easily implemented in object-oriented computer languages, and used for simulation;
- it can be used for modeling nonlinear, multi-physics and distributed systems;
- after rewriting PDEs as the wave equation using the port-Hamiltonian formalism, several conservation laws become evident and physically relevant variables appear as interconnection ports (that can be used to interconnect with other systems);
- many results exist about well-posedness of 1D linear infinite-dimensional pHs.

Moreover, in the case of infinite-dimensional systems, semi-discretization methods that preserve port-Hamiltonian structure are available, as described in the Part III of this thesis.

Finally, another interest of port-Hamiltonian systems that was not treated in this chapter, but that is one of the main motivations for the study of pHs is that it also provides powerful tools for stability analysis and control design. Some of these aspects are recalled in Part IV.

Chapter 5

PHs model of a Piezoelectric beam

Many different approaches are available for modeling the structural dynamics. Beam (1D) and plate (2D) models are commonly used for many applications in aerospace industry. A 1D model is adequate for modeling our experimental device, since the structure has a large ratio between its length and width.

In the case of the beam model, two different dynamics must be represented: the bending and torsion motions.

Among the bending models, several alternatives exists, each one assuming different hypothesis. The most commons are:

1. Euler-Bernoulli: cross-section dimensions are negligible in comparison with length;
2. Rayleigh: rotation inertia of the section is included;
3. Timoshenko: both rotation inertia and shear stress is included.

Since the cross-section of our beam is small, and we are only interested on the low-frequency behavior of the dynamics, an Euler-Bernoulli model of the beam is used in this thesis.

For the torsion model, we use the Saint-Venant torsion model, which is equivalent to a wave equation.

Modeling of beams with piezoelectric patches is well known in the literature (see, e.g., Banks, Smith, and Wang (1996), Aglietti et al. (1997), and Preumont (2011)).

Several previous contributions were presented in the last years for modeling and discretization of a beam with piezoelectric patches as pHs (Macchelli, van der Schaft, and Melchiorri, 2004a; Voss, Scherpen, and van der Schaft, 2008; Voss, Scherpen, and Onck, 2008; Voss, 2010; Voss and Scherpen, 2011c; Voss and Scherpen, 2014; Morris and Ozer, 2013)).

In this contribution, voltage is used as an external control input of the piezoelectric material. This comes with a difficulty, since an unbounded input operator appears. This problem was avoided in the previous articles using two different strategies: 1) by including the electric field (which is equivalent to the voltage) as an extra dynamic variable, instead of an input; 2) by including the magnetic field dynamics. The first solution can be used for simulation, but leads to a finite-dimensional approximation that is not stabilizable (Voss, 2010; Voss and

Scherpen, 2011c). The second solution introduces dynamic states of high frequency (that usually does not affect the dynamics in the frequency range of interest in mechanical problems). After spatial discretization, both solutions lead to constrained state-space systems, in the form of Differential Algebraic Equations (DAE), since the piezoelectric voltage is an output of these systems.

This work uses only the mechanical variables as energy variables. The final finite-dimensional system has voltage as input. The finite-dimensional state-space obtained does not have any constraints related to the voltage. The unbounded operator that appears requires that a weak formulation be used before spatial discretization, as described in Chapter 9.

This chapter is organized as follows: firstly, the piezoelectric beam model for bending is presented in Section 5.1. Secondly, the torsion model is presented in 5.2. Then, Section 5.3 gathers both models in a single equation. The use of distributed ports to introduce damping in the model is presented in Section 5.4. Finally, comments and conclusions are adressed in Section 5.5.

Contents

5.1 Bending

This section is divided in two parts. Firstly, the partial differential equations for the piezoelectric beam in bending are obtained from the Hamilton principle. Secondly, the equations are written using the port-Hamiltonian formalism, and it is shown that the energy flows through the boundary and distributed ports.

5.1.1 Derivation of equations from Hamilton principle

A beam with a piezoelectric patch attached to its surface is considered as presented in Fig. 5.1. The beam has the following properties: length L, thickness t, width b, section area $S = bt$, density ρ, Young modulus E. The patch has the following properties: length $(b-a)$, thickness

t_p, width b_p, section area $S_p = b_p t_p$, density ρ_p, Young modulus E_p and the piezoelectric charge constant γ.

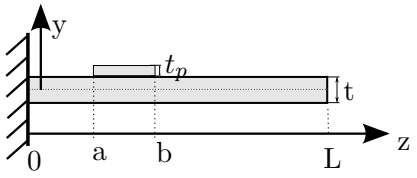

Figure 5.1: Beam with piezoelectric patch

Neglecting the rotational inertia, the kinetic energy is given by:

$$\begin{aligned} \mathcal{K} &= \frac{1}{2}\int_{\Omega} \rho \dot{w}^2 \,\mathrm{d}V\,, \\ &= \frac{1}{2}\int_{z=0}^{L} \left(\rho S + \rho_p S_p \Pi_{ab}(z)\right) \dot{w}^2 \,\mathrm{d}z\,, \end{aligned} \tag{5.1}$$

where $w(z,t)$ is the local deflection, $\dot{w}$ is its time-derivative and $\Pi_{ab}(z)$ is the rectangular function, defined as:

$$\Pi_{ab}(z) := \begin{cases} 0, & z \leq a\,, \\ 1, & a < z < b\,, \\ 0, & b \leq z\,. \end{cases} \tag{5.2}$$

It is assumed that the strain ϵ is only due to bending, such that: $\epsilon = -y\,\partial^2_{z^2} w(z,t)$. In this case, the potential elastic energy is:

$$\mathcal{P} = \frac{1}{2}\int_{\Omega} \sigma_{mec}\epsilon \,\mathrm{d}V\,, \tag{5.3}$$

where $\sigma_{mec} = E_i\,\epsilon$ is the mechanical stress. After integration over the cross-sectional area:

$$\mathcal{P} = \frac{1}{2}\int_{z=0}^{L} \left(EI + \Pi_{ab}(z) E_p I_p\right) \left(\partial^2_{z^2} w\right)^2 \mathrm{d}z\,, \tag{5.4}$$

where I and I_p are the area moments of inertia of the plate and the piezo, respectively, with respect to the neutral axis ($y = 0$):

$$\begin{aligned} I &= b\int_{y=-t/2}^{t/2} y^2 \,\mathrm{d}y = \frac{bt^3}{12}\,, \\ I_p &= b_p \int_{y=t/2}^{t/2+t_p} y^2 \,\mathrm{d}y = b_p\left(\frac{(t/2+t_p)^3}{3} - \frac{t^3}{24}\right)\,. \end{aligned} \tag{5.5}$$

The work due to the voltage $v(z,t)$ applied to the piezoelectric patch is given by:

$$\mathcal{W} = \frac{1}{2}\int_{\Omega} \sigma_{elec}\epsilon \,\mathrm{d}V\,, \tag{5.6}$$

where $\sigma_{elec} = -\gamma E_y(z,t)$ ($E_y(z,t)$ is the electric field in the y direction, γ is the piezoelectric

electro-mechanical constant). The electric field is proportional to the voltage applied to the piezoelectric patches, i.e.: $E_y(z,t) = \frac{v(z,t)}{t_p}$. This leads to the following work expression:

$$\mathcal{W} = \frac{1}{2}\int_{z=0}^{L} \gamma \frac{v(z,t)}{t_p} \Pi_{ab}(z) I_{p,1}\, \partial_{z^2}^2 w \, \mathrm{d}z \,, \tag{5.7}$$

where $I_{p,1}$ is the first moment of area of the piezoelectric patch, i.e.,

$$I_{p,1} = b_p \int_{y=t/2}^{t/2+t_p} y \, \mathrm{d}y = \frac{b_p t_p}{2}(t + t_p) \,. \tag{5.8}$$

Finally, using the Hamilton Principle, i.e.,

$$\delta \int_{t_1}^{t_f} (\mathcal{K} - \mathcal{P} + \mathcal{W}) \, \mathrm{d}t = 0 \,, \tag{5.9}$$

the following partial differential equation is obtained:

$$\mu(z)\ddot{w} = -\partial_{z^2}^2 \left(\kappa(z)\partial_{z^2}^2 w\right) + \partial_{z^2}^2 \left(\Pi_{ab}(z) k_p v(z,t)\right) \,, \tag{5.10}$$

where:

$$\begin{aligned} \mu(z) :=& \rho S + \rho_p S_p \Pi_{ab}(z) \,, \\ \kappa(z) :=& EI + \Pi_{ab}(z) E_p I_p \,, \\ k_p :=& \frac{\gamma I_{p,1}}{t_p} \,. \end{aligned} \tag{5.11}$$

5.1.2 Port-Hamiltonian representation

Equation 5.10 is rewritten using the port-Hamiltonian formalism as explained below. First, the system Hamiltonian is given by:

$$H^B[x_1^B, x_2^B] = \frac{1}{2}\int_{z=0}^{L} \left(\frac{x_1^B(z,t)^2}{\mu(z)} + \kappa(z) x_2^B(z,t)^2 \right) \mathrm{d}z \,, \tag{5.12}$$

where $x_1^B(z,t)$ and $x_2^B(z,t)$ are the energy variables, defined as follows:

$$\begin{aligned} x_1^B(z,t) &:= \mu(z)\dot{w}(z,t) \,, \\ x_2^B(z,t) &:= \partial_{z^2}^2 w(z,t) \,. \end{aligned} \tag{5.13}$$

The superscript B stands for *bending*. The first term of the Hamiltonian is the kinetic energy and the second is the potential energy.

The variational derivatives of the Hamiltonian (Eq. 5.12) with respect to x_1^B and x_2^B are

given by:

$$\begin{aligned} e_1^B(z,t) &:= \frac{\delta H^B}{\delta x_1^B} = \frac{x_1^B(z,t)}{\mu(z)} = \dot{w}(z,t)\,, \\ e_2^B(z,t) &:= \frac{\delta H^B}{\delta x_2^B} = \kappa(z) x_2^B(z,t)\,. \end{aligned} \tag{5.14}$$

Notice that e_1^B is the local vertical speed, and e_2^B is the local restoring torque (bending moment).

Using these newly defined energy and co-energy variables, Eq. 5.10 can thus be rewritten as:

$$\begin{bmatrix} \dot{x_1^B} \\ \dot{x_2^B} \end{bmatrix} = \underbrace{\begin{bmatrix} 0 & -\partial_{z^2}^2 \\ \partial_{z^2}^2 & 0 \end{bmatrix}}_{\mathcal{J}} \begin{bmatrix} e_1^B \\ e_2^B \end{bmatrix} + \begin{bmatrix} \partial_{z^2}^2 \\ 0 \end{bmatrix} \Pi_{ab}(z) k_p v(z,t)\,, \tag{5.15}$$

where $\mathcal{J}$ is a formally skew-symmetric operator.

The time-derivative of the Hamiltonian is computed as:

$$\begin{aligned} \dot{H}^B &= \int_{z=0}^{L} \left(e_1^B \dot{x_1^B} + e_2^B \dot{x_2^B} \right) \mathrm{d}z\,, \\ &= \int_{z=0}^{L} \left(e_1^B \left(-\partial_{z^2}^2 e_2^B + \partial_{z^2}^2 \Pi_{ab}(z) k_p v(z,t) \right) + e_2^B\, \partial_{z^2}^2 e_1^B \right) \mathrm{d}z\,, \\ &= \int_{z=0}^{L} \left(\partial_z \left(-e_1^B\, \partial_z(e_2^B) + \partial_z(e_1^B)\, e_2^B \right) + e_1^B\, \partial_{z^2}^2 \Pi_{ab}(z) k_p v(z,t) \right) \mathrm{d}z\,, \\ &= \left(-e_1^B\, \partial_z(e_2^B) + \partial_z(e_1^B) e_2^B \right) \Big|_{z=0}^{L} + \int_{z=a}^{b} k_p v(z,t)\, \partial_{z^2}^2 e_1^B \,\mathrm{d}z\,. \end{aligned} \tag{5.16}$$

The first part of $\dot{H}^B$ depends only on the boundary values of e_1^B (vertical speed), e_2^B (torque), $\partial_z e_1^B$ (rotation speed) and $\partial_z e_2^B$ (force). As in the example of the previous chapter, this motivates the definition of the boundary-ports. From Eq. 5.16, one possible definition is the following:

$$\boldsymbol{y}_\partial^B := \begin{bmatrix} f_{1\partial}^B \\ f_{2\partial}^B \\ f_{3\partial}^B \\ f_{4\partial}^B \end{bmatrix} := \begin{bmatrix} \partial_z e_2^B(0) \\ -e_2^B(0) \\ -e_1^B(L) \\ \partial_z e_1^B(L) \end{bmatrix}, \boldsymbol{u}_\partial^B = \begin{bmatrix} e_{1\partial}^B \\ e_{2\partial}^B \\ e_{3\partial}^B \\ e_{4\partial}^B \end{bmatrix} = \begin{bmatrix} e_1^B(0) \\ \partial_z e_1^B(0) \\ \partial_z e_2^B(L) \\ e_2^B(L) \end{bmatrix}. \tag{5.17}$$

Moreover, since the second part of $\dot{H}^B$ depends on the distributed voltage $v(z,t)$, it also motivates the definition of a power-conjugated output to $v(z,t)$ given by:

$$y^B(z,t) := k_p\, \partial_{z^2}^2 e_1^B\,, \quad a < z < b\,. \tag{5.18}$$

The final energy flow ($\dot{H}^B$) thus reads:

$$\dot{H}^B = \boldsymbol{y}_\partial^{B^T} \boldsymbol{u}_\partial^B + \int_{z=a}^{b} v(z,t) y^B(z,t)\,\mathrm{d}z\ . \tag{5.19}$$

This system is an infinite-dimensional pHs with boundary ports $\boldsymbol{u}_\partial^B$ and $\boldsymbol{y}_\partial^B$, and distributed ports $v(z,t)$ and $y^B(z,t)$.

A useful particular case: In practice, for a single piezoelectric patch $v(z,t) = v(t)$ (the voltage is uniform along the patch). In this case, $\dot{H}^B$ becomes:

$$\begin{aligned}\dot{H}^B &= \boldsymbol{y}_\partial^{B^T} \boldsymbol{u}_\partial^B + k_p \partial_z e_1^B \Big|_{z=a}^{b} v(t)\,, \\ &= \boldsymbol{y}_\partial^{B^T} \boldsymbol{u}_\partial^B + k_p \left(\partial_z e_1^B(b) - \partial_z e_1^B(a)\right) v(t)\,.\end{aligned} \tag{5.20}$$

This energy flow motivates the definition of y_v, which is the conjugate output of the applied voltage v:

$$y_v := k_p \left(\partial_z e_1^B(b) - \partial_z e_1^B(a)\right). \tag{5.21}$$

Finally, the full vector of inputs and outputs of the bending model can be defined as:

$$\boldsymbol{y}^B := \begin{bmatrix} \partial_z e_2^B(0) \\ -e_2^B(0) \\ -e_1^B(L) \\ \partial_z e_1^B(L) \\ y_v \end{bmatrix}, \boldsymbol{u}^B = \begin{bmatrix} e_1^B(0) \\ \partial_z e_1^B(0) \\ \partial_z e_2^B(L) \\ e_2^B(L) \\ v \end{bmatrix}, \tag{5.22}$$

and the energy flow is equal to $\dot{H}^B = (\boldsymbol{u}^B)^T \boldsymbol{y}^B$.

Remark 5.1
All the usual boundary conditions of the Euler-Bernoulli beam can be set using the previously defined boundary ports:

Case	*conditions*
Free	$w'' = 0$ *and* $w''' = 0 \iff e_2^B = 0$ *and* $\frac{\partial e_2^B}{\partial z} = 0$
Simply supported	$w'' = 0$ *and* $w =$ *constant* $\iff e_2^B = 0$ *and* $e_1^B = 0$
Clamped	$w' =$ *constant and* $w =$ *constant* $\iff \frac{\partial e_1^B}{\partial z} = 0$ *and* $e_1^B = 0$
Point force F	$w'' = 0$ *and* $EIw''' = F \iff e_2^B = 0$ *and* $\frac{\partial e_2^B}{\partial z} = F$
Point torque M	$EIw'' = M$ *and* $w''' = 0 \iff e_2^B = M$ *and* $\frac{\partial e_2^B}{\partial z} = 0$

In the case of the simply supported and clamped boundary conditions, the values of the position (w) and angle (w') at boundary conditions are constant. These constant values are equivalent

to zero speed (e_1^B) and angular speed ($\frac{\partial e_1^B}{\partial z}$).

Remark 5.2
The energy exchange depends on the system's boundary conditions and distributed ports. In the clamped-free beam, for example, the following boundary conditions apply:

- *Clamped end at $z = 0$: $e_1^B(0,t) = 0$ and $\frac{\partial}{\partial z} e_1^B(0,t) = 0$;*
- *Free end at $z = L$: $e_2^B(L,t) = 0$ and $\frac{\partial}{\partial z} e_2^B(L,t) = 0$.*

In this specific case: $\dot{H}^B = y_v(t)v(t)$. In our case, the flexible beam is connected to a rigid tank with fluid, so the free-end boundary conditions are:

$$\dot{H}^B = e_2^B(L)\partial_z e_1^B(L) - \partial_z e_2^B(L) e_1^B(L) + y_v(t)v(t). \tag{5.23}$$

Remark 5.3
The output $y_v(t)$, which is power conjugated to the input voltage $v(t)$, has dimension of current. However, it does not represent the total current that flows through the electrodes, but only a part of it. Physically, it represents the component of the current linked to the electromechanical coupling usually referred as "motional current".

5.2 Torsion

In this section, a simplified model for the torsion of the beam is considered using the Saint-Venant theory of torsion (see, e.g., Section 2.3.1 of Hodges and Pierce (2011)). In the sequel, the derivation of the dynamic equations from Hamilton principle is briefly recalled. Then, the equations are represented in the port-Hamiltonian form.

5.2.1 Derivation of equations from Hamilton principle

Defining $\theta(z,t)$ as the local torsional angle, z the position along the beam, t the time, the kinetic energy due to torsion is given by:

$$\begin{aligned} \mathcal{K} &= \frac{1}{2}\int_\Omega \rho(x\dot{\theta})^2 \,\mathrm{d}V\,, \\ &= \frac{1}{2}\int_{z=0}^{L} \rho I_p \dot{\theta}^2 \,\mathrm{d}z\,, \end{aligned} \tag{5.24}$$

where I_p is the section polar moment of inertia per unit length.

The potential (elastic) energy is given by:

$$\mathcal{P} = \frac{1}{2}\int_{z=0}^{L} GJ(\frac{\partial \theta}{\partial z})^2 \,\mathrm{d}z\,,$$

where G is the material shear constant and J is the section torsion constant.

From Hamilton principle, the following equation is obtained:

$$I_p \frac{\partial^2}{\partial t^2}\theta(z,t) = \frac{\partial}{\partial z}\left(GJ\frac{\partial}{\partial z}\theta(z,t)\right), \quad 0 \leq z \leq L\,, \tag{5.25}$$

which is a linear wave equation.

Remark 5.4
In the previous development, it is possible to include the external work due to the voltage applied to the piezoelectric patches. However, since we are assuming symmetric actuations with respect to the torsion axis, the total work is equal to zero. Further research should include the influence of the voltage in the torsion equation when excitations that are not symmetric. In this case, an additional term will appear in Eq. 5.25 (similar to $+\frac{\partial^2}{\partial z^2}\left(k_p^T \Pi_{ab}(z) v(z,t)\right)$*, as it happened for the bending equations).*

5.2.2 Port-Hamiltonian representation

Defining as energy variables $x_1^T := \frac{\partial \theta}{\partial z}$ and $x_2^T := -I\frac{\partial \theta}{\partial t}$, we get:

$$\frac{\partial}{\partial t}\begin{bmatrix} x_1^T \\ x_2^T \end{bmatrix} = \begin{bmatrix} 0 & -\partial_z \\ -\partial_z & 0 \end{bmatrix}\begin{bmatrix} e_1^T \\ e_2^T \end{bmatrix}, \tag{5.26}$$

where $e_1^T = GJx_1^T = GJ\frac{\partial \theta}{\partial z}$ and $e_2^T = \frac{x_2^T}{I} = -\frac{\partial \theta}{\partial t}$, which are the variational derivatives of the Hamiltonian, given by:

$$H^T(x_1^T, x_2^T) = \frac{1}{2}\int_{z=0}^{L}\left(GJ(x_1^T)^2 + \frac{(x_2^T)^2}{I_p}\right)dz. \tag{5.27}$$

Notice that e_1^T is the restoring torque (moment of twist) and e_2^T is the torsion angular velocity. The time-derivative of the Hamiltonian can be computed as:

$$\dot{H}^T = (\boldsymbol{u}^T)^T \boldsymbol{y}^T\,, \tag{5.28}$$

where:

$$\boldsymbol{y}^T = \begin{bmatrix} -e_2^T(L,t) \\ e_1^T(0,t) \end{bmatrix}, \; and \, \boldsymbol{u}^T = \begin{bmatrix} e_1^T(L,t) \\ e_2^T(0,t) \end{bmatrix}. \tag{5.29}$$

Remark 5.5
All usual boundary conditions for the torsion equation can be represented by set using the boundary ports:

Case	*conditions*
Free	$GJ\theta' = 0 \implies e_1^T = 0$
Fixed	$\theta = constant \implies e_2^T = 0$
Point torque M	$GJ\theta' = M \implies e_1^T = M$

Again, the constant value of the angle θ in the fixed boundary condition is equivalent to a zero angular speed e_2^T.

Remark 5.6
Again, it is possible to see that the energy flows through the boundaries.

In the fixed-free case, for example, the following boundary conditions apply:

- *Fixed end:* $e_2^T(0,t) = 0$*;*
- *Free end:* $e_1^T(L,t) = 0$*,*

and the system is power conserving: $\dot{H}^T = 0$*. In this work, the beam is clamped at* $z = 0$ *(*$e_2^T(0,t) = 0$*) and connected to the tank at* $z = L$*. For this reason,* $\dot{H}^T$ *is equal to:*

$$\dot{H}^T = -e_2^T(L,t)e_1^T(L,t). \tag{5.30}$$

5.3 Beam equations with both bending and torsion

It is possible to write both the bending and torsion equations together as a single port-Hamiltonian system. Firstly, the Hamiltonian is the sum of both Hamiltonians (Eqs. 5.12 and 5.27):

$$H^{BT}[x_1^B, x_2^B, x_1^T, x_2^T] = \frac{1}{2}\int_{z=0}^{L}\left(\frac{(x_1^B)^2}{\mu(z)} + \kappa(z)(x_2^B)^2 + GJ(x_1^T)^2 + \frac{(x_2^T)^2}{I_p}\right)\mathrm{d}z\,, \tag{5.31}$$

secondly, the equations are simply given by the concatenation of Eqs. 5.15 and 5.26:

$$\begin{bmatrix}\dot{x_1^B}\\ \dot{x_2^B}\\ \dot{x_1^T}\\ \dot{x_2^T}\end{bmatrix} = \begin{bmatrix}0 & -\partial_{z^2}^2 & 0 & 0\\ \partial_{z^2}^2 & 0 & 0 & 0\\ 0 & 0 & 0 & -\partial_z\\ 0 & 0 & -\partial_z & 0\end{bmatrix}\begin{bmatrix}e_1^B\\ e_2^B\\ e_1^T\\ e_2^T\end{bmatrix} + \begin{bmatrix}\partial_{z^2}^2\Pi_{ab}(z)k_p\\ 0\\ 0\\ 0\end{bmatrix} v(z,t)\,, \tag{5.32}$$

where the co-energy variables are given by the variational derivatives of the Hamiltonian, i.e., $\begin{bmatrix}e_1^B & e_2^B & e_1^T & e_2^T\end{bmatrix}^T := \begin{bmatrix}\frac{\delta H^{BT}}{\delta x_1^B} & \frac{\delta H}{\delta x_2^B} & \frac{\delta H}{\delta x_1^T} & \frac{\delta H}{\delta x_2^T}\end{bmatrix}^T$ with distributed output:

$$y^B(z,t) := k_p\,\partial_{z^2}^2 e_1^B\,, \quad a < z < b\,. \tag{5.33}$$

and boundary input/output:

$$\boldsymbol{y}_{\partial}^{BT} := \begin{bmatrix} \partial_z e_2^B(0) \\ -e_2^B(0) \\ -e_1^B(L) \\ \partial_z e_1^B(L) \\ -e_2^T(L) \\ e_1^T(0) \end{bmatrix}, \boldsymbol{u}_{\partial}^{BT} = \begin{bmatrix} e_1^B(0) \\ \partial_z e_1^B(0) \\ \partial_z e_2^B(L) \\ e_2^B(L) \\ e_1^T(L) \\ e_2^T(0) \end{bmatrix} . \tag{5.34}$$

Finally, the power-balance of the coupled system is given by:

$$\dot{H}^{BT} = (\boldsymbol{y}^{BT})^T \boldsymbol{u}^{BT} + \int_{z=a}^{b} y^B(z,t) v(z,t) \, \mathrm{d}z \, . \tag{5.35}$$

The bending and the torsion equations were modeled independently in the previous sections and consequently are decoupled in Eq. 5.32: the interconnection matrix has no coupling terms between the bending and torsion co-energy variables; and the Hamiltonian also has no coupling terms between the energy variables. In this thesis, the interactions between the two equations is made through the boundary conditions, that are used to couple the beam with the tank, as explained in Chapter 7.

Remark 5.7
By looking at the kinetic energy of the system under both bending $w(z,t)$ and torsion $\theta(z,t)$, it is found that:

$$\begin{aligned} K &= \frac{1}{2} \int_{\Omega} \rho \left(\dot{w} + y\dot{\theta} \right)^2 \, \mathrm{d}\Omega \, , \\ &= \frac{1}{2} \int_{\Omega} \rho \left(\dot{w}^2 + 2y\dot{w}\dot{\theta} + y^2\dot{\theta}^2 \right) \, \mathrm{d}\Omega \, , \\ &= \frac{1}{2} \int_{z=0}^{L} \left(\mu(z)\dot{w}^2 + 2I_1\dot{w}\dot{\theta} + I_p\dot{\theta}^2 \right) \, \mathrm{d}z \, , \end{aligned} \tag{5.36}$$

where $I_1 = \int_S \rho y \mathrm{d}S$ is the first moment of area, which is equal to zero in our symmetric plate with uniformly distributed parameters.

In a more general case, where the center of gravity of the section does not coincide with the elastic axis, $I_1 \neq 0$. In this latter case, the kinetic energy term from the Hamiltonian would couple the equations of bending and torsion.

5.4 Introducing damping through distributed dissipative ports

The beam equations presented before does not take into account any dissipation. In the real system, however, dissipative forces introduce damping in the dynamics of the structure. As recalled in § 4.1.3 for finite-dimensional systems, damping can be introduced in pHs

formulation by coupling with dissipative elements, given by constitutive relations between conjugate input and output ports of the pHs. A similar approach is possible for infinite-dimensional pHs, and different types of damping models are possible (see, e.g., Matignon and Hélie (2013)). Let us recall two of them here, namely, the viscous damping and the Kelvin-Voigt damping.

Viscous damping: In the case of the bending equations, it is possible to introduce a distributed vertical force $q(z,t)$. In the case of torsion, it is possible to introduce a distributed torque $\tau(z,t)$. The equations become:

$$\begin{bmatrix} \dot{x_1^B} \\ \dot{x_2^B} \\ \dot{x_1^T} \\ \dot{x_2^T} \end{bmatrix} = \begin{bmatrix} 0 & -\partial_{z^2}^2 & 0 & 0 \\ \partial_{z^2}^2 & 0 & 0 & 0 \\ 0 & 0 & 0 & -\partial_z \\ 0 & 0 & -\partial_z & 0 \end{bmatrix} \begin{bmatrix} e_1^B \\ e_2^B \\ e_1^T \\ e_2^T \end{bmatrix} + \begin{bmatrix} \partial_{z^2}^2 \Pi_{ab}(z) k_p \\ 0 \\ 0 \\ 0 \end{bmatrix} v(z,t) + \begin{bmatrix} 1 & 0 \\ 0 & 0 \\ 0 & 0 \\ 0 & 1 \end{bmatrix} \begin{bmatrix} q(z,t) \\ \tau(z,t) \end{bmatrix}, \quad (5.37)$$

with the following new distributed outputs:

$$\begin{bmatrix} y_q(z,t) \\ y_\tau(z,t) \end{bmatrix} = \begin{bmatrix} 1 & 0 & 0 & 0 \\ 0 & 0 & 0 & 1 \end{bmatrix} \begin{bmatrix} e_1^B \\ e_2^B \\ e_1^T \\ e_2^T \end{bmatrix}. \quad (5.38)$$

Thus, the power balance of this system becomes:

$$\dot{H}_d^{BT} := \dot{H}^{BT} + \int_{z=0}^{L} y_q(z,t) q(z,t)\, dz + \int_{z=0}^{L} y_\tau(z,t) \tau(z,t)\, dz\,. \quad (5.39)$$

Using the following constitutive relations:

$$\begin{bmatrix} q(z,t) \\ \tau(z,t) \end{bmatrix} = - \begin{bmatrix} d_1^B(z) & 0 \\ 0 & d_1^T(z) \end{bmatrix} \begin{bmatrix} y_q(z,t) \\ y_\tau(z,t) \end{bmatrix}, \quad (5.40)$$

where $d_1^B(z)$ and $d_1^T(z)$ are positive functions of z ($d_1^B(z)$, $d_1^T(z) > 0$, $\forall\, z \in [0,\, L]$), the power balance becomes:

$$\dot{H}_d^{BT} := \dot{H}^{BT} \underbrace{- \int_{z=0}^{L} d_1^B(z) y_q(z,t)^2\, dz}_{\leq 0} \underbrace{- \int_{z=0}^{L} d_1^T(z) y_\tau(z,t)^2\, dz}_{\leq 0}\,. \quad (5.41)$$

Recall that $y_q(z,t) = e_1^B(z,t)$ and $y_\tau = e_2^T(z,t)$ are the vertical and angular velocities of the beam, respectively. Thus, these two terms remove energy if the velocities are different from zero at some point.

The equations with dissipation can be rewritten without the dissipative ports as:

$$\begin{bmatrix} \dot{x}_1^B \\ \dot{x}_2^B \\ \dot{x}_1^T \\ \dot{x}_2^T \end{bmatrix} = \begin{bmatrix} -d_1^B(z) & -\partial_{z^2}^2 & 0 & 0 \\ \partial_{z^2}^2 & 0 & 0 & 0 \\ 0 & 0 & 0 & -\partial_z \\ 0 & 0 & -\partial_z & -d_1^T(z) \end{bmatrix} \begin{bmatrix} e_1^B \\ e_2^B \\ e_1^T \\ e_2^T \end{bmatrix} + \begin{bmatrix} \partial_{z^2}^2 \Pi_{ab}(z) k_p \\ 0 \\ 0 \\ 0 \end{bmatrix} v(z,t)\,. \tag{5.42}$$

Rewriting the original PDE of bending (Eq. 5.10), with the proposed damping, we get:

$$\mu(z)\ddot{w} = -\frac{\partial^2}{\partial z^2}\left(\kappa(z)\frac{\partial^2}{\partial z^2}w\right) + \frac{\partial^2}{\partial z^2}\left(\Pi_{ab}(z)k_p v(z,t)\right) - \underbrace{d_1^B(z)\dot{w}(z,t)}_{\text{viscous damping}}\,, \tag{5.43}$$

where the last term is classically known as viscous damping.

Similarly, for the torsion (Eq. 5.25), we get:

$$I_p\ddot{\theta}(z,t) = \frac{\partial}{\partial z}\left(GJ\frac{\partial}{\partial z}\theta(z,t)\right) - \underbrace{d_1^T(z)\dot{\theta}(z,t)}_{\text{viscous damping}}\,. \tag{5.44}$$

Kelvin-Voigt damping: Now we introduce four distributed ports q_1 and q_2 that act on the bending, τ_1 and τ_2 that act on the torsion. The pHs is written as follows (the voltage input is ignored to simplify the presentation):

$$\begin{bmatrix} \dot{x}_1^B \\ \dot{x}_2^B \\ \dot{x}_1^T \\ \dot{x}_2^T \end{bmatrix} = \begin{bmatrix} 0 & -\partial_{z^2}^2 & 0 & 0 \\ \partial_{z^2}^2 & 0 & 0 & 0 \\ 0 & 0 & 0 & -\partial_z \\ 0 & 0 & -\partial_z & 0 \end{bmatrix} \begin{bmatrix} e_1^B \\ e_2^B \\ e_1^T \\ e_2^T \end{bmatrix} + \begin{bmatrix} 1 & \partial_{z^2}^2 & 0 & 0 \\ 0 & 0 & 0 & 0 \\ 0 & 0 & 0 & 0 \\ 0 & 0 & 1 & \partial_z \end{bmatrix} \begin{bmatrix} q_1(z,t) \\ q_2(z,t) \\ \tau_1(z,t) \\ \tau_2(z,t) \end{bmatrix}\,, \tag{5.45}$$

with their conjugated outputs:

$$\begin{bmatrix} y_{q_1}(z,t) \\ y_{q_2}(z,t) \\ y_{\tau_1}(z,t) \\ y_{\tau_2}(z,t) \end{bmatrix} = \begin{bmatrix} 1 & 0 & 0 & 0 \\ \partial_{z^2}^2 & 0 & 0 & 0 \\ 0 & 0 & 0 & 1 \\ 0 & 0 & 0 & -\partial_z \end{bmatrix} \begin{bmatrix} e_1^B \\ e_2^B \\ e_1^T \\ e_2^T \end{bmatrix}\,, \tag{5.46}$$

and the following power balance:

$$\begin{aligned} \dot{H}_d^{BT} :=& \dot{H}^{BT} + \int_{z=0}^{L} y_{q_1}(z,t)q_1(z,t)\;dz + \int_{z=0}^{L} y_{\tau_1}(z,t)\tau_1(z,t)\;dz \\ &+ \int_{z=0}^{L} y_{q_2}(z,t)q_2(z,t)\;dz + \int_{z=0}^{L} y_{\tau_2}(z,t)\tau_2(z,t)\;dz\,. \end{aligned} \tag{5.47}$$

Now the following constitutive relations are used:

$$\begin{bmatrix} q_1(z,t) \\ q_2(z,t) \\ \tau_1(z,t) \\ \tau_2(z,t) \end{bmatrix} = - \begin{bmatrix} d_1^B(z) & 0 & 0 & 0 \\ 0 & d_2^B(z) & 0 & 0 \\ 0 & 0 & d_1^T(z) & 0 \\ 0 & 0 & 0 & d_2^T(z) \end{bmatrix} \begin{bmatrix} y_{q_1}(z,t) \\ y_{q_2}(z,t) \\ y_{\tau_1}(z,t) \\ y_{\tau_2}(z,t) \end{bmatrix}, \tag{5.48}$$

with positive $d_1^B(z)$, $d_1^T(z)$, $d_2^B(z)$ and $d_2^T(z)$. Thus, the power balance becomes:

$$\begin{aligned} \dot{H}_d^{BT} :=& \dot{H}^{BT} \underbrace{- \int_{z=0}^{L} d_1^B(z) y_q(z,t)^2 \, dz}_{\leq 0} \underbrace{- \int_{z=0}^{L} d_1^T(z) y_\tau(z,t)^2 \, dz}_{\leq 0} \\ & \underbrace{- \int_{z=0}^{L} d_2^B(z) \left(\frac{\partial^2}{\partial z^2} y_q(z,t) \right)^2 dz}_{\leq 0} \underbrace{- \int_{z=0}^{L} d_2^T(z) \left(\frac{\partial}{\partial z} y_\tau(z,t) \right)^2 dz}_{\leq 0} . \end{aligned} \tag{5.49}$$

In this case, the original PDEs become:

$$\mu(z)\ddot{w} = -\frac{\partial^2}{\partial z^2} \left(\kappa(z) \frac{\partial^2}{\partial z^2} w \right) + \frac{\partial^2}{\partial z^2} \left(\Pi_{ab}(z) k_p v(z,t) \right) - \underbrace{d_1^B(z)\dot{w}(z,t)}_{\text{viscous damping}} - \underbrace{\frac{\partial^2}{\partial z^2} \left(d_2^B(z) \frac{\partial^2}{\partial z^2} \dot{w}(z,t) \right)}_{\text{Kelvin-Voigt damping}}, \tag{5.50}$$

$$I_p \ddot{\theta}(z,t) = \frac{\partial}{\partial z} \left(GJ \frac{\partial}{\partial z} \theta(z,t) \right) - \underbrace{d_1^T(z)\dot{\theta}(z,t)}_{\text{viscous damping}} - \underbrace{\frac{\partial}{\partial z} \left(d_2^T(z) \frac{\partial}{\partial z} \dot{\theta}(z,t) \right)}_{\text{Kelvin-Voigt damping}} . \tag{5.51}$$

Remark 5.8
In the beam equations with external voltage as input (e.g., Eqs. 5.15 and 5.37), the input operator is unbounded and the rectangular function is discontinuous. Despite of these difficulties, existence and uniqueness results for such systems can be found in Chapter 4 of Banks, Smith, and Wang (1996). The conditions for well-posedness, presented in Theorem 4.1 of that reference, are satisfied when using Kelvin-Voigt damping. During the semi-discretization of these equations, a weak formulation has to be used to overcome these difficulties, as presented in Chapter 9.

5.5 Conclusions

The main goal of this chapter was to introduce the structural dynamic models that are used in this thesis for modeling the fluid-structure system. Thanks to the boundary ports, the structural dynamics will be coupled with the fluid dynamics and the tank in Chapter 7.

Previous work on port-Hamiltonian models of beams with piezoelectric actuators used two approaches for introducing the piezoelectric effect: 1) used the electric field as an energy

variable of the system. In this case, the voltage is an output of the system; 2) included magnetic field equations, and the voltage is applied in the boundary conditions. Differently from previous work, we used the voltage as an external control input. This lead to equations with fewer variables (since only mechanical energy variables are considered), and more simple boundary conditions (there are no boundary conditions related to the voltage). However, this choice leads to the appearance of an unbounded distributed control input, such that usual power-preserving discretization methods cannot be directly applied. This difficulty will be addressed in Chapter 9 by using a weak formulation.

Moreover, in the end of the chapter we discussed the introduction of damping on the beam models.

Chapter 6

PHs model of liquid sloshing in moving containers

Shallow Water Equations (SWE, also known as Saint-Venant equations) are probably the simplest infinite-dimensional mathematical representation for a fluid with free-surface. Nevertheless, these equations are still used for the modeling and control of sloshing in moving tanks. Petit and Rouchon (2002) proposed new equations, where the tank horizontal position and rotation angle are the control inputs of the system. Alemi Ardakani and Bridges (2010) and Alemi Ardakani (2016) studied the coupling between Saint-Venant equations with a horizontally moving vehicle. In this case, a Hamiltonian formulation is proposed, allowing the use of a symplectic integration scheme.

The SWE were also recently extended to the port-Hamiltonian framework, but with a different goal: modeling and controlling the flow on open channel irrigation systems (Hamroun, Lefèvre, and Mendes, 2007; Hamroun et al., 2010). In this latter case, there is neither rotation nor translation of the channels.

The main contribution of this chapter is that port-Hamiltonian models of SWE for the liquid sloshing in moving containers are proposed. Differently from previous work (that does not use the pHs framework), here the fluid and the tank are viewed as *open systems*, providing interconnection ports that allow coupling with arbitrarily complex mechanical systems.

This chapter is divided in two main parts. Firstly, the SWE in 1D are obtained using the port-Hamiltonian formalism in Section 6.1. These equations are used in the subsequent chapters for simulation and control of the fluid-structure system. Then, the equations are extended to 2D flows in Section 6.2. Finally, a discussion about the limitations and a possible alternative to this model is presented in Section 6.3.

Contents

Preliminary remark
It is important to recall that the tank of the experimental device presented in Chapter 3 is cylindrical. However, the equations are derived in the sequel for a rectangular tank. In order to find a good agreement of the liquid sloshing in a cylinder using a rectangular tank model, we consider that:

- *The dimensions of the free-surface in the cylindrical tank are preserved in the rectangular tank model;*
- *The total volume of fluid in the cylindrical tank is preserved.*

6.1 The 1D Shallow Water Equations

In this section, the fluid equations for a moving tank are presented. Firstly, in § 6.1.1, the equations obtained from Euler-Lagrange formulation, as presented by Petit and Rouchon (2002), are recalled. This leads to equations that can be used for simulating tanks with a prescribed trajectory. Then, in § 6.1.2 these equations are rewritten in the port-Hamiltonian formalism. The new equations provide interconnection ports that can be used to couple with other systems. One observation that is made in § 6.1.2.1 is that a rigid mass is necessary to allow writing the equations in this formalism. We could also include the other rigid body inertias of the tank. However, to emphasize the modularity of the pHs approach, the rigid body equations of the tank are presented separately in Appendix B.

6.1.1 Euler-Lagrange formulation

Our goal is to model the dynamics of a fluid in a moving tank, as presented in Fig. 6.1. The equations presented here were previously obtained by Petit and Rouchon (2002). The variable $D(t)$ represents the horizontal position of the tank (with respect to an inertial frame), $\theta(t)$ is the angle of the tank relative to horizontal. The height of fluid is given by $h(z,t)$, where z is the position along the tank (measured in local coordinates). The fluid speed, measured relative to the tank is given by $u(z,t)$.

The first equation comes from the mass conservation:

$$\frac{\partial h}{\partial t} + \frac{\partial}{\partial z}(hu) = 0\,. \tag{6.1}$$

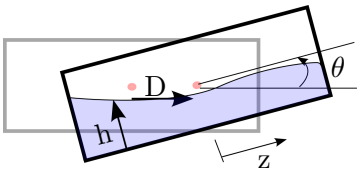

Figure 6.1: Moving tank

The system kinetic energy is given by:

$$T = \int_{z=-a/2}^{a/2} \frac{1}{2}\rho bh \left((u + \dot{D}\cos\theta)^2 + (-\dot{D}\sin\theta + z\dot{\theta})^2 \right) \mathrm{d}z \,, \tag{6.2}$$

where ρ is the fluid density, b is the tank width, a is the tank length, $\dot{D}(t)$ is the tank horizontal speed and $\dot{\theta}(t)$ is the tank rotation rate. Notice that $(u + \dot{D}\cos\theta)$ is the inertial fluid speed in the direction of the tank bottom, $(-\dot{D}\sin\theta + z\dot{\theta})$ is the inertial fluid speed perpendicular to the tank bottom. The term $z\dot{\theta}$ is the component of speed due to the rotation of the tank (around the center of the tank at $z = 0$).

The gravitational energy of the fluid is given by:

$$U = \int_{z=-a/2}^{a/2} \rho bg \left(\frac{h^2}{2}\cos\theta + hz\sin\theta \right) \mathrm{d}z \,, \tag{6.3}$$

where g is the gravitational acceleration.

The system Lagrangian is thus given by:

$$\mathcal{L} = T - U \,. \tag{6.4}$$

In order to find the equations of motion, the minimum of the Lagrangian constrained to mass conservation (Eq. 6.1) is computed:

$$\delta L = \delta(T - U) + \delta \int_{z=-a/2}^{a/2} \lambda(z,t)(\frac{\partial h}{\partial t} + \frac{\partial}{\partial z}(hu))\,\mathrm{d}z = 0 \,. \tag{6.5}$$

After applying the variation with respect to h, u and λ, the following equations are found (see Petit and Rouchon (2002) for a detailed derivation):

$$\begin{aligned} \frac{\partial h}{\partial t} &= -\frac{\partial}{\partial z}(hu) \,, \\ \frac{\partial u}{\partial t} &= -\ddot{D}\cos\theta - \frac{\partial}{\partial z}\left(\frac{u^2}{2} + gz\sin\theta + gh\cos\theta - \frac{z^2\dot{\theta}^2}{2} \right) \,, \end{aligned} \tag{6.6}$$

with boundary conditions given by $u(-a/2, t) = u(a/2, t) = 0$.

These equations can be used for simulation of a tank under prescribed motion, or controlled

by the inputs $D(t)$ and $\theta(t)$. However, coupling these equations with a more complex system does not prove straightforward. That is the reason why they will be rewritten under the port-Hamiltonian formalism in the subsequent subsection.

The step by step derivation presented hereafter will lead (on page 70) to Eqs. 6.38-6.39 and the balance Eq. 6.40 for the same system. This new representation has several advantages compared to Eq. 6.6. Firstly, it presents the equations in a physically structured way. This means that this representation highlights the system conservation laws (mass, momentum and energy conservation). Secondly, boundary and interconnection ports are defined, which allows the fluid to be coupled with a more complex system. Finally, as it will be presented in Part III, the same properties will be preserved in the finite-dimensional approximation with the proposed numerical methods.

6.1.2 Port-Hamiltonian formulation

Here, Eqs. 6.6 is written as an infinite-dimensional pHs such as:

$$\frac{\partial}{\partial t}\begin{bmatrix}\alpha_1\\ \alpha_2\end{bmatrix} = \underbrace{\begin{bmatrix}0 & -\partial_z\\ -\partial_z & 0\end{bmatrix}}_{\mathcal{J}}\begin{bmatrix}e_1\\ e_2\end{bmatrix}, \tag{6.7}$$

where $\mathcal{J}$ is a formally skew-symmetric operator, $\alpha_1(z,t)$ and $\alpha_2(z,t)$ are infinite-dimensional variables, $e_i := \frac{\delta H}{\delta \alpha_i}$ are the variational derivatives of the system Hamiltonian with respect to $\alpha_i(z,t)$.

Before finding the quite involved port-Hamiltonian version of the previous equations, two simplified versions are first addressed in § 6.1.2.1 and § 6.1.2.2: the tank moving horizontally only, and the tank with rotations only. Then, the full system will be presented in § 6.1.2.3.

6.1.2.1 Tank moving horizontally only

Considering that the tank is fixed at horizontal ($\theta(t) = 0$), the equations of the moving tank (Eq. 6.6) simplify to:

$$\begin{aligned}\frac{\partial h}{\partial t} &= -\frac{\partial}{\partial z}(hu)\,,\\ \frac{\partial u}{\partial t} &= -\ddot{D} - \frac{\partial}{\partial z}\left(\frac{u^2}{2} + gh\right),\end{aligned} \tag{6.8}$$

the kinetic and potential energies are given by:

$$T = \int_{z=-a/2}^{a/2} \frac{1}{2}\rho b h (u+\dot{D})^2 \,\mathrm{d}z \quad , \qquad U = \int_{z=-a/2}^{a/2} \rho b g \frac{h^2}{2}\,\mathrm{d}z\,, \tag{6.9}$$

leading to the following total energy (Hamiltonian) $H = T + U$.

First attempt: The following change of variables is proposed: $\alpha_1(z,t) = bh(z,t)$ and $\alpha_2(z,t) = \rho(u(z,t) + \dot{D}(t))$, where α_1 is the fluid section area and α_2 is the fluid momentum by area. Rewriting the Hamiltonian as a function of α_1 and α_2, we get:

$$H[\alpha_1, \alpha_2] = \int_{z=-a/2}^{a/2} \frac{1}{2}\left(\frac{\alpha_1\alpha_2^2}{\rho} + \rho g \frac{\alpha_1^2}{b}\right) \mathrm{d}z \ . \tag{6.10}$$

By computing the variational derivative with respective to α_1 and α_2, it is found:

$$\begin{aligned} e_1 &:= \frac{\delta H}{\delta \alpha_1} = \frac{\alpha_2^2}{2\rho} + \rho g \frac{\alpha_1}{b} = \rho\left(\frac{(u+\dot{D})^2}{2} + gh\right) , \\ e_2 &:= \frac{\delta H}{\delta \alpha_2} = \frac{\alpha_1\alpha_2}{\rho} = bh(u+\dot{D}) . \end{aligned} \tag{6.11}$$

Notice that it is not possible to recover the dynamic Eq. 6.8 using the Hamiltonian framework (as Eq. 6.7):

$$\begin{aligned} \frac{\partial \alpha_1}{\partial t} &= -\frac{\partial}{\partial z}(bhu) \neq -\frac{\partial}{\partial z} e_2 = -\frac{\partial}{\partial z} bh(u+\dot{D}) , \\ \frac{\partial \alpha_2}{\partial t} &= -\frac{\partial}{\partial z}\rho\left(\frac{u^2}{2} + gh\right) \neq -\frac{\partial}{\partial z} e_1 = -\frac{\partial}{\partial z}\rho\left(\frac{(u+\dot{D})^2}{2} + gh\right) . \end{aligned} \tag{6.12}$$

Solution: To overcome this problem, it is necessary to include a kinetic energy term for the tank in addition to the fluid kinetic energy. This can be done by including the term $\frac{1}{2} m_T \dot{D}^2$ in the system Hamiltonian, where m_T is the tank mass:

$$H = \int_{z=-a/2}^{a/2} \frac{1}{2}\left(\rho bh(u+\dot{D})^2 + \rho b g h^2\right) \mathrm{d}z + \frac{1}{2} m_T \dot{D}^2 . \tag{6.13}$$

A new momentum variable for the rigid body translation degree of freedom is defined:

$$p(t) := \frac{\partial H}{\partial \dot{D}} = \int_{z=-a/2}^{a/2} \rho bh(u+\dot{D}) \, \mathrm{d}z + m_T \dot{D} . \tag{6.14}$$

Using the same change of variables (α_1,α_2, as previously defined), $p(t)$ can be written as:

$$p(t) = \underbrace{\int_{z=-a/2}^{a/2} \alpha_1\alpha_2 \, \mathrm{d}z}_{\mathcal{M}[\alpha_1,\alpha_2]} + m_T \dot{D} , \tag{6.15}$$

and rewriting the Hamiltonian as a function of α_1, α_2 and p, we have:

$$H[\alpha_1, \alpha_2, p] = \int_{z=-a/2}^{a/2} \frac{1}{2}\left(\frac{1}{\rho}\,\alpha_1\alpha_2^2 + \frac{\rho g}{b}\,\alpha_1^2\right) \mathrm{d}z + \frac{(p-\mathcal{M})^2}{2m_T} . \tag{6.16}$$

By computing the variational derivatives of H with respect to α_1 and α_2, it is found:

$$\begin{aligned} e_1 := \frac{\delta H}{\delta \alpha_1} &= \frac{\alpha_2^2}{2\rho} + \rho g \frac{\alpha_1}{b} - \frac{(p-\mathcal{M})}{m_T}\frac{\delta \mathcal{M}}{\delta \alpha_1}\,, \\ &= \frac{\alpha_2^2}{2\rho} + \rho g \frac{\alpha_1}{b} - \frac{(p-\mathcal{M})}{m_T}\alpha_2\,, \\ &= \rho \frac{(u+\dot{D})^2}{2} + \rho g h - \dot{D}\rho(u+\dot{D})\,, \\ &= \rho \frac{u^2}{2} + \rho g h - \rho \dot{D}^2\,. \end{aligned} \tag{6.17}$$

$$\begin{aligned} e_2 := \frac{\delta H}{\delta \alpha_2} &= \alpha_1 \frac{\alpha_2}{\rho} - \frac{(p-\mathcal{M})}{m_T}\frac{\delta \mathcal{M}}{\delta \alpha_2}\,, \\ &= bh(u+\dot{D}) - \frac{(p-\mathcal{M})}{m_T}\alpha_1\,, \\ &= bh(u+\dot{D}) - \dot{D}bh\,, \\ &= bhu\,. \end{aligned} \tag{6.18}$$

Now it is possible to rewrite the dynamic equations as:

$$\begin{aligned} \frac{\partial \alpha_1}{\partial t} &= -\frac{\partial}{\partial z}(bhu) = -\frac{\partial}{\partial z} e_2\,, \\ \frac{\partial \alpha_2}{\partial t} &= -\frac{\partial}{\partial z}\rho\left(\frac{u^2}{2} + gh\right) = -\frac{\partial}{\partial z} e_1\,. \end{aligned} \tag{6.19}$$

Differently from Eq. 6.12 obtained in the first attempt, Eq. 6.19 is written in the classical port-Hamiltonian framework, as Eq. 6.7.

In addition, the dynamic equations of the rigid body (tank) can be found. For this, let us first compute the partial derivatives of the Hamiltonian with respect to the finite-dimensional variables D and p:

$$\begin{aligned} e_D := \frac{\partial H}{\partial D} &= 0\,, \\ e_p := \frac{\partial H}{\partial p} &= \frac{p-\mathcal{M}}{m_T} = \dot{D}\,, \end{aligned} \tag{6.20}$$

The dynamic equations for the rigid body are thus given by:

$$\begin{aligned} \frac{\partial p}{\partial t} &= -e_D + F_{\text{ext}}\,, \\ \frac{\partial D}{\partial t} &= e_p\,. \end{aligned} \tag{6.21}$$

The fluid and rigid body equations can then be written as:

$$\frac{\partial}{\partial t}\begin{bmatrix}\alpha_1(z,t)\\ \alpha_2(z,t)\\ p(t)\\ D(t)\end{bmatrix} = \begin{bmatrix}0 & -\partial_z & 0 & 0\\ -\partial_z & 0 & 0 & 0\\ 0 & 0 & 0 & -1\\ 0 & 0 & 1 & 0\end{bmatrix}\begin{bmatrix}e_1\\ e_2\\ e_p\\ e_D\end{bmatrix} + \begin{bmatrix}0\\ 0\\ 1\\ 0\end{bmatrix} F_{\text{ext}}\,, \tag{6.22}$$

and the output is given by:

$$\dot{D} = \begin{bmatrix}0 & 0 & 1 & 0\end{bmatrix}\begin{bmatrix}e_1\\ e_2\\ e_p\\ e_D\end{bmatrix}\,. \tag{6.23}$$

The system power balance is computed:

$$\dot{H} = e_2(-a/2,t)e_1(-a/2,t) - e_2(a/2,t)e_1(a/2,t) + \dot{D}F_{\text{ext}}\,, \tag{6.24}$$

which, as presented in the introduction for the wave equation, motivates the definition of boundary ports: $\boldsymbol{u}_\partial = \begin{bmatrix}e_1(a/2,t)\,, & e_2(-a/2,t)\end{bmatrix}^T$ and $\boldsymbol{y}_\partial = \begin{bmatrix}-e_2(a/2,t)\,, & e_1(-a/2,t)\end{bmatrix}^T$. The energy rate becomes: $\dot{H} = \boldsymbol{u}_\partial^T \boldsymbol{y}_\partial + \dot{D}F_{\text{ext}}$.

In the specific case of a closed tank, the boundary conditions are: $e_2(-a/2,t) = e_2(a/2,t) = 0$ (no volumetric flow through the tank walls) and the power balance reduces to:

$$\dot{H} = \dot{D}F_{\text{ext}}\,. \tag{6.25}$$

Since it has both finite-dimensional ($p(t)$ and $D(t)$), and infinite-dimensional variables ($\alpha_1(z,t)$ and $\alpha_2(z,t)$, the final system (Eqs. 6.22, 6.23 and 6.25) is called a mixed finite-infinite dimensional pHs (m-pHs, as introduced, e.g., in Pasumarthy and van der Schaft (2004), and Macchelli and Melchiorri (2005)).

6.1.2.2 Tank under rotations only

Considering now that the tank can rotate and that the horizontal displacement is $D(t) = 0$, Eq. 6.6 becomes:

$$\begin{aligned}\frac{\partial h}{\partial t} &= -\frac{\partial}{\partial z}(hu)\,,\\ \frac{\partial u}{\partial t} &= -\frac{\partial}{\partial z}\left(\frac{u^2}{2} + gz\sin\theta + gh\cos\theta - \frac{z^2\dot{\theta}^2}{2}\right)\,.\end{aligned} \tag{6.26}$$

The kinetic and potential energies are given by:

$$\begin{aligned} T &= \int_{z=-a/2}^{a/2} \frac{1}{2}\left(\rho b h\left(u^2 + (z\dot{\theta})^2\right)\right) \mathrm{d}z\,, \\ U &= \int_{z=-a/2}^{a/2} \rho b g\left(\frac{h^2}{2}\cos\theta + hz\sin\theta\right) \mathrm{d}z\ . \end{aligned} \tag{6.27}$$

The system Hamiltonian is given by: $H = T + U$. A new moment variable for the rotation motion is defined:

$$p_\theta := \frac{\partial H}{\partial \dot{\theta}} = \underbrace{\left(\int \rho b h z^2 \,\mathrm{d}z\right)}_{\mathcal{I}_f(h)} \dot{\theta}, \tag{6.28}$$

where $\mathcal{I}_f$ is the rotation inertia of the fluid (which is time-dependent, since it depends on $h(z,t)$).

Let us define $\alpha_1 = bh$ and $\alpha_2 = \rho u$ and rewrite the Hamiltonian as a function of α_1, α_2, p_θ and θ:

$$H[\alpha_1, \alpha_2, p_\theta, \theta] = \int_{z=-a/2}^{a/2} \left(\frac{\alpha_1 \alpha_2^2}{2\rho} + \rho g(\frac{\alpha_1^2}{2b}\cos\theta + \alpha_1 z \sin\theta)\right) \mathrm{d}z + \frac{p_\theta^2}{2\mathcal{I}_f}\,. \tag{6.29}$$

By computing the variational derivatives of H with respect to α_1 and α_2, we get:

$$\begin{aligned} e_1 := \frac{\delta H}{\delta \alpha_1} &= \frac{\alpha_2^2}{2\rho} + \rho g(\frac{\alpha_1}{b}\cos\theta + z\sin\theta) - \frac{1}{2}\left(\frac{p_\theta}{\mathcal{I}_f}\right)^2 \frac{\delta \mathcal{I}_f}{\delta \alpha_1}\,, \\ &= \frac{\alpha_2^2}{2\rho} + \rho g(\frac{\alpha_1}{b}\cos\theta + z\sin\theta) - \frac{1}{2}\dot{\theta}^2 \rho z^2)\,, \\ &= \rho\left(\frac{u^2}{2} + gh\cos\theta + gz\sin\theta - \frac{1}{2}\dot{\theta}^2 z^2\right)\,, \end{aligned} \tag{6.30}$$

$$\begin{aligned} e_2 := \frac{\delta H}{\delta \alpha_2} &= \alpha_1 \frac{\alpha_2}{\rho}\,, \\ &= bhu\,. \end{aligned} \tag{6.31}$$

Here, the co-energy variable e_1 includes a negative term related to the rotation of the tank $\frac{1}{2}\rho\dot{\theta}^2 z^2$. This term also appears in the rotating Bernoulli equation (see, e.g., McDonald (2012)).

It is easy to verify that Eqs. 6.26 can now be rewritten using the port-Hamiltonian

framework (Eq. 6.7):

$$\begin{aligned}\frac{\partial \alpha_1}{\partial t} &= -\frac{\partial}{\partial z}(bhu) = -\frac{\partial}{\partial z}e_2\,,\\ \frac{\partial \alpha_2}{\partial t} &= -\frac{\partial}{\partial z}\rho\left(\frac{u^2}{2} + gz\sin\theta + gh\cos\theta - \frac{z^2\dot{\theta}^2}{2}\right) = -\frac{\partial}{\partial z}e_1\,.\end{aligned} \tag{6.32}$$

Finally, it is also possible to write the rotation degree of freedom equations from the Hamiltonian, by computing the partial derivatives with respect to p_θ and θ:

$$\begin{aligned}e_{p\theta} &:= \frac{\partial H}{\partial p_\theta} = \frac{p_\theta}{\mathcal{I}_f} = \dot{\theta}\,,\\ e_\theta &:= \frac{\partial H}{\partial \theta} = \int_{z=-a/2}^{a/2}\rho b g\left(-\frac{h^2}{2}\sin\theta + hz\cos\theta\right)\mathrm{d}z\,,\end{aligned} \tag{6.33}$$

and the dynamic equations are:

$$\begin{aligned}\frac{\partial p_\theta}{\partial t} &= -e_\theta + M_{\text{ext}}\,,\\ \frac{\partial \theta}{\partial t} &= e_{p\theta}\,.\end{aligned} \tag{6.34}$$

Rewriting the fluid and rigid body equations in the matrix form, we have:

$$\frac{\partial}{\partial t}\begin{bmatrix}\alpha_1(z,t)\\ \alpha_2(z,t)\\ p_\theta(t)\\ \theta(t)\end{bmatrix} = \begin{bmatrix}0 & -\partial_z & 0 & 0\\ -\partial_z & 0 & 0 & 0\\ 0 & 0 & 0 & -1\\ 0 & 0 & 1 & 0\end{bmatrix}\begin{bmatrix}e_1\\ e_2\\ e_{p\theta}\\ e_\theta\end{bmatrix} + \begin{bmatrix}0\\ 0\\ 1\\ 0\end{bmatrix}M_{\text{ext}}, \tag{6.35}$$

and the output is:

$$\dot{\theta} = \begin{bmatrix}0 & 0 & 1 & 0\end{bmatrix}\begin{bmatrix}e_1\\ e_2\\ e_{p\theta}\\ e_\theta\end{bmatrix}. \tag{6.36}$$

The system power balance is given by:

$$\dot{H} = \boldsymbol{u}_\partial^T\boldsymbol{y}_\partial + \dot{\theta}M_{\text{ext}}\,, \tag{6.37}$$

where $\boldsymbol{u}_\partial = \begin{bmatrix}e_1(a/2,t)\,, & e_2(-a/2,t)\end{bmatrix}^T$ and $\boldsymbol{y}_\partial = \begin{bmatrix}-e_2(a/2,t)\,, & e_1(-a/2,t)\end{bmatrix}^T$. Again, in the case of a closed tank, the boundary conditions are: $e_2(-a/2,t) = e_2(a/2,t) = 0$ and the power balance reduces to $\dot{H} = \dot{\theta}M_{\text{ext}}$.

6.1.2.3 Tank under both translations and rotation

The procedure for obtaining the port-Hamiltonian equations is exactly the same as the one previously presented for the simplified cases with only translation or rotation. However, due to the fact that the fluid couples with the two rigid-body motions, the mathematical procedure becomes much more tedious and for this reason only the final result is presented in this section. The full development is presented in Appendix A, leading to the following system:

$$\frac{\partial}{\partial t}\begin{bmatrix}\alpha_1(z,t)\\ \alpha_2(z,t)\\ p(t)\\ D(t)\\ p_\theta(t)\\ \theta(t)\end{bmatrix} = \begin{bmatrix}0 & -\partial_z & 0 & 0 & 0 & 0\\ -\partial_z & 0 & 0 & 0 & 0 & 0\\ 0 & 0 & 0 & -1 & 0 & 0\\ 0 & 0 & 1 & 0 & 0 & 0\\ 0 & 0 & 0 & 0 & 0 & -1\\ 0 & 0 & 0 & 0 & 1 & 0\end{bmatrix}\begin{bmatrix}e_1^F\\ e_2^F\\ e_p^F\\ e_D^F\\ e_{p\theta}^F\\ e_\theta^F\end{bmatrix} + \begin{bmatrix}0 & 0\\ 0 & 0\\ 1 & 0\\ 0 & 0\\ 0 & 1\\ 0 & 0\end{bmatrix}\begin{bmatrix}F_{\text{ext}}\\ M_{\text{ext}}\end{bmatrix}, \tag{6.38}$$

where $\alpha_1(z,t) = bh(z,t)$ and $\alpha_2(z,t) = \rho(u(z,t) + \dot{D}(t)\cos\theta(t))$, p and p_θ are the linear and angular momentum, as in the previous sections. The co-energy variables e_i^F are obtained from the variational or partial derivatives of the Hamiltonian with respect to each energy variable (α_1, α_2, p, D, p_θ, θ). The superscript F stands for Fluid.

The outputs are $\dot{D}$ and $\dot{\theta}$, which are conjugated with respect to the inputs F_{ext} and M_{ext}:

$$\begin{bmatrix}\dot{D}\\ \dot{\theta}\end{bmatrix} = \begin{bmatrix}0 & 0 & 0 & 0 & 1 & 0\\ 0 & 0 & 1 & 0 & 0 & 0\end{bmatrix}\begin{bmatrix}e_1^F\\ e_2^F\\ e_p^F\\ e_D^F\\ e_{p\theta}^F\\ e_\theta^F\end{bmatrix}. \tag{6.39}$$

The power balance is:

$$\dot{H}^F = (\boldsymbol{u}_\partial^F)^T\boldsymbol{y}_\partial^F + \dot{D}F_{\text{ext}} + \dot{\theta}M_{\text{ext}}, \tag{6.40}$$

where $\boldsymbol{u}_\partial^F = \begin{bmatrix}e_1^F(a/2,t), & e_2^F(-a/2,t)\end{bmatrix}^T$ and $\boldsymbol{y}_\partial^F = \begin{bmatrix}-e_2^F(a/2,t), & e_1^F(-a/2,t)\end{bmatrix}^T$. Now, new input/output vectors with all the port variables can be defined:

$$\boldsymbol{y}^F = \begin{bmatrix}-e_2^F(a/2,t)\\ e_1^F(-a/2,t)\\ \dot{D}\\ \dot{\theta}\end{bmatrix}, \quad \boldsymbol{u}^F = \begin{bmatrix}e_1^F(a/2,t)\\ e_2^F(-a/2,t)\\ F_{\text{ext}}\\ M_{\text{ext}}\end{bmatrix}, \tag{6.41}$$

such that the power balance is given by $\dot{H}^F = (\boldsymbol{u}^F)^T\boldsymbol{y}^F$.

Assuming a tank with no flow through the walls, the boundary conditions are: $e_2^F(-a/2,t) =$

$e_2^F(a/2,t) = 0$ (since $e_2^F(z,t) = bhu$ is the volumetric flow). In this case:

$$\dot{H}^F = \dot{D}F_{\text{ext}} + \dot{\theta}M_{\text{ext}}. \tag{6.42}$$

Recall that Eqs. 6.38, 6.39 and 6.40 are a new representation of equation 6.6. This new representation (a mixed finite-infinite dimensional pHs) brings several advantages. Eq. 6.38 is presented in a structured way: $\mathcal{J}$ is a formally skew-symmetric matrix operator; the energy rate of change (Eq. 6.40) is related to the interconnection ports; boundary ports define the boundary conditions and are given by the co-energy variables evaluated at the boundary. In particular, the definition of the conjugated input/output ports makes it easy to couple this system with a more complex one.

An additional remark that can be drawn from Eq. 6.38 is that two additional conservation laws are verified. By integrating the infinite-dimensional energy variables $\alpha_1(z,t)$ and $\alpha_2(z,t)$ over the domain:

$$\begin{aligned}\int_{z=-a/2}^{a/2} \dot{\alpha}_1(z,t)\,\mathrm{d}z &= e_2^F(-a/2,t) - e_2^F(a/2,t)\,,\\ \int_{z=-a/2}^{a/2} \dot{\alpha}_2(z,t)\,\mathrm{d}z &= e_1^F(-a/2,t) - e_1^F(a/2,t)\,.\end{aligned} \tag{6.43}$$

The first integral represents the time rate of the total volume inside the domain (since the fluid is incompressible, it expresses the mass conservation law). The second one represents the time rate of the total linear momentum of the fluid. Both equations show that, similarly to the power balance $\dot{H}$, these conservation laws depend only on the co-energy variables evaluated at the boundary.

So far, the mass of the tank was taken into account. Otherwise, the port-Hamiltonian form of the equations could not be obtained, as pointed out in § 6.1.2.1. The additional tank inertias could have been included in the development of the fluid equations (by including their contributions of kinetic energy to the Hamiltonian). However, since we want to emphasize the modularity of the port-Hamiltonian approach, we modeled the rigid tank inertias independently as presented in Appendix B. These inertias are thus coupled with the full system in Chapter 7.

Remark 6.1
No dissipation is included in the previous equations. Recall that for the beam, dissipation was included through distributed ports in § 5.4, together with constitutive relations for a dissipative element. The same procedure is applied for the fluid. A distributed port that acts on the linear momentum $\alpha_2^F(z,t)$ variable is included. The following equations are obtained (the rigid body variables are ignored for simplifying the presentation):

$$\frac{\partial}{\partial t}\begin{bmatrix}\alpha_1(z,t)\\ \alpha_2(z,t)\end{bmatrix} = \begin{bmatrix}0 & -\partial_z\\ -\partial_z & 0\end{bmatrix}\begin{bmatrix}e_1^F\\ e_2^F\end{bmatrix} + \begin{bmatrix}0\\ 1\end{bmatrix} q(z,t) \tag{6.44}$$

with distributed output:

$$y_q(z,t) = \begin{bmatrix} 0 & 1 \end{bmatrix} \begin{bmatrix} e_1^F \\ e_2^F \end{bmatrix} . \tag{6.45}$$

Neglecting the boundary and rigid-body ports, the power balance is given by:

$$\dot{H} = \int_{z=-a/2}^{L/2} y_q(z,t) q(z,t) \, \mathrm{d}z \, . \tag{6.46}$$

Using the constitutive relation, $q(z,t) = -d_1(z) y_q(z,t)$ (with $d_1(z) > 0$), we get

$$\dot{H} = -\int_{z=-a/2}^{L/2} d_1(z) (e_2^F)^2 \, \mathrm{d}z \leq 0 \, , \tag{6.47}$$

and the equations become:

$$\frac{\partial}{\partial t} \begin{bmatrix} \alpha_1(z,t) \\ \alpha_2(z,t) \end{bmatrix} = \begin{bmatrix} 0 & -\partial_z \\ -\partial_z & -d_1(z) \end{bmatrix} \begin{bmatrix} e_1^F \\ e_2^F \end{bmatrix} . \tag{6.48}$$

Remark 6.2
Another possibility to introduce damping is to use a second order differential operator, similar to the Kelvin-Voigt damping presented in § 5.4. Using $q(z,t) = -d_2 \frac{\partial^2}{\partial z^2} y_q(z,t)$, where d_2 is positive, the power balance becomes:

$$\begin{aligned} \dot{H} &= \int_{z=-a/2}^{L/2} e_2^F \, d_2 \, \frac{\partial^2}{\partial z^2} e_2^F \, \mathrm{d}z \, , \\ &= -\int_{z=-a/2}^{L/2} d_2 \left(\frac{\partial}{\partial z} e_2^F \right)^2 \mathrm{d}z + d_2 \left(e_2^F(z,t) \frac{\partial}{\partial z} e_2^F(z,t) \right) \Big|_{z=-a/2}^{L/2} , \end{aligned} \tag{6.49}$$

Since in the case of fluid inside a tank $e_2^F(z,t) = 0$ at the boundaries (no-flow through the walls), $\dot{H} \leq 0$ and the second order differential operator removes energy from the system. The equation with dissipation becomes:

$$\frac{\partial}{\partial t} \begin{bmatrix} \alpha_1(z,t) \\ \alpha_2(z,t) \end{bmatrix} = \begin{bmatrix} 0 & -\partial_z \\ -\partial_z & -d_2 \, \partial_{z^2}^2 \end{bmatrix} \begin{bmatrix} e_1^F \\ e_2^F \end{bmatrix} . \tag{6.50}$$

This second-order dissipative term is similar to the diffusion term in the viscous Burger's equation.

6.2 The 2D Shallow Water Equations

In the subsequent chapters of this thesis, the one-dimensional shallow water model presented in the previous section is used for modeling and control of the fluid-structure system. Still, an extension to bi-dimensional flows is presented here.

A model of the bi-dimensional shallow water equations using the port-Hamiltonian framework was previously presented by Hamroun (2009). In this section, the 2D shallow water equations is firstly used to model the liquid sloshing in the pHs formalism without rigid body motions in § 6.2.1. The main difference in comparison to the work of Hamroun (2009) is that a skew-symmetric matrix $\mathcal{G}$ that represents the gyroscopic forces is introduced. Secondly, following a procedure similar to the previous sections, rigid body motion is included, and a pHs model of the 2D liquid sloshing in moving containers is obtained.

6.2.1 Equations without rigid body motion

The classical shallow water equations, obtained from the mass and momentum conservation laws, are considered in this section. In two dimensions, the mass conservation is written as:

$$\frac{\partial h}{\partial t} = -\mathrm{div}\,(h\vec{\boldsymbol{v}})\ , \tag{6.51}$$

where $h = h(x, y, t)$ is the fluid height, $\vec{\boldsymbol{v}} = \vec{\boldsymbol{v}}(x, y, t)$ is the fluid velocity vector, x and y are the spatial coordinates, t is the time.

The momentum conservation equation is given by:

$$\frac{\partial \rho\vec{\boldsymbol{v}}}{\partial t} + \rho(\vec{\boldsymbol{v}}\cdot\vec{\boldsymbol{\nabla}})\vec{\boldsymbol{v}} = -\vec{\boldsymbol{\nabla}}\,(\rho g h)\ , \tag{6.52}$$

where g is the acceleration of gravity, ρ is the fluid density (assumed constant in time and uniform in space).

Using the following vector calculus identity:

$$(\vec{\boldsymbol{v}}\cdot\vec{\boldsymbol{\nabla}})\vec{\boldsymbol{v}} = \vec{\boldsymbol{\nabla}}(\frac{1}{2}\|\vec{\boldsymbol{v}}\|^2) + (\vec{\boldsymbol{\nabla}}\times\vec{\boldsymbol{v}})\times\vec{\boldsymbol{v}}\,, \tag{6.53}$$

where $\vec{\boldsymbol{\nabla}}\times\vec{\boldsymbol{v}}$ is the rotational of $\vec{\boldsymbol{v}}$ (sometimes denoted $\vec{\mathbf{curl}}\,\vec{\boldsymbol{v}}$), the momentum equation becomes:

$$\frac{\partial \rho\vec{\boldsymbol{v}}}{\partial t} = -\vec{\boldsymbol{\nabla}}\left(\frac{1}{2}\rho\|\vec{\boldsymbol{v}}\|^2 + \rho g h\right) - \rho(\vec{\boldsymbol{\nabla}}\times\vec{\boldsymbol{v}})\times\vec{\boldsymbol{v}}\,, \tag{6.54}$$

where the last term $(\rho(\vec{\boldsymbol{\nabla}}\times\vec{\boldsymbol{v}})\times\vec{\boldsymbol{v}})$ can be rewritten as:

$$\rho(\vec{\boldsymbol{\nabla}}\times\vec{\boldsymbol{v}})\times\vec{\boldsymbol{v}} = \rho\,\omega\begin{bmatrix}0 & -1\\ 1 & 0\end{bmatrix}\vec{\boldsymbol{v}}\,, \tag{6.55}$$

with $\omega(x, y, t) := (\partial_x v - \partial_y u)$ the local vorticity term, $u(x, y, t)$ and $v(x, y, t)$ the components of $\vec{\boldsymbol{v}} = [u, v]^T$.

The system energy is given by the sum of kinetic and potential (gravitational) energies:

$$E[\vec{\boldsymbol{v}}, h] = \frac{1}{2}\int_\Omega \left(\rho h\|\vec{\boldsymbol{v}}\|^2 + \rho g h^2\right)\mathrm{d}\Omega\ . \tag{6.56}$$

The fluid momentum is defined as $\vec{\boldsymbol{\alpha}} := \rho\vec{\boldsymbol{v}}$, and the Hamiltonian as:

$$H[\vec{\boldsymbol{\alpha}}, h] := \frac{1}{2}\int_\Omega \left(\frac{1}{\rho}h\|\vec{\boldsymbol{\alpha}}\|^2 + \rho g h^2\right) \mathrm{d}\Omega \ . \tag{6.57}$$

Rewriting it using the scalar components of $\vec{\boldsymbol{\alpha}} := \begin{bmatrix}\alpha_x, & \alpha_y\end{bmatrix}^T = \begin{bmatrix}\rho u, & \rho v\end{bmatrix}^T$:

$$H[\alpha_x, \alpha_y, h] = \frac{1}{2}\int_\Omega \left(\frac{1}{\rho}h(\alpha_x^2 + \alpha_y^2) + \rho g h^2\right) \mathrm{d}\Omega \,, \tag{6.58}$$

it becomes straightforward to compute the variational derivatives with respect to each variable (h,α_x,α_y):

$$\begin{aligned} e_h(x,y,t) := \frac{\delta H}{\delta h} &= \frac{1}{2\rho}(\alpha_x^2 + \alpha_y^2) + \rho g h \\ &= \frac{1}{2}\rho(u^2 + v^2) + \rho g h \\ e_{\alpha_x}(x,y,t) := \frac{\delta H}{\delta \alpha_x} &= \frac{1}{\rho}h\alpha_x = hu \,, \\ e_{\alpha_y}(x,y,t) := \frac{\delta H}{\delta \alpha_y} &= \frac{1}{\rho}h\alpha_y = hv \,, \end{aligned} \tag{6.59}$$

where u and v are the scalar components of $\vec{\boldsymbol{v}}$. Note that e_h is the total pressure (the sum of the dynamic pressure $\frac{1}{2}\rho(u^2+v^2)$ and the static pressure $\rho g h$), e_{α_x} and e_{α_y} are the volumetric flow (per unit length) in each direction.

It is easy to verify that the Eqs. 6.51 and 6.54 (mass and momentum conservation) can thus be rewritten as:

$$\begin{bmatrix} \frac{\partial h}{\partial t} \\ \frac{\partial \alpha_x}{\partial t} \\ \frac{\partial \alpha_y}{\partial t} \end{bmatrix} = \begin{bmatrix} 0 & -\partial_x & -\partial_y \\ -\partial_x & 0 & \frac{\rho}{h}\omega \\ -\partial_y & -\frac{\rho}{h}\omega & 0 \end{bmatrix} \begin{bmatrix} e_h \\ e_{\alpha_x} \\ e_{\alpha_y} \end{bmatrix} \ , \tag{6.60}$$

or alternatively, in vector form:[1]

$$\begin{bmatrix} \frac{\partial h}{\partial t} \\ \frac{\partial \vec{\boldsymbol{\alpha}}}{\partial t} \end{bmatrix} = \begin{bmatrix} 0 & -\mathrm{div} \\ -\vec{\boldsymbol{\nabla}} & \mathcal{G} \end{bmatrix} \begin{bmatrix} e_h \\ \vec{\boldsymbol{e}}_{\vec{\boldsymbol{\alpha}}} \end{bmatrix} \ , \tag{6.61}$$

where $\vec{\boldsymbol{e}}_{\vec{\boldsymbol{\alpha}}} := \frac{\delta H}{\delta \vec{\boldsymbol{\alpha}}} := \begin{bmatrix} e_{\alpha_x}, & e_{\alpha_y} \end{bmatrix}^T$, and $\mathcal{G}$ is defined as:

$$\mathcal{G}(h,\, \partial_x\alpha_y,\, \partial_y\alpha_x) := \frac{\rho}{h}\omega \begin{bmatrix} 0 & 1 \\ -1 & 0 \end{bmatrix} = \frac{1}{h}(\partial_x\alpha_y - \partial_y\alpha_x) \begin{bmatrix} 0 & 1 \\ -1 & 0 \end{bmatrix} \ . \tag{6.62}$$

The skew-symmetric term $\mathcal{G}$ that depends on the energy variables introduces a nonlinearity in the interconnection matrix. Moreover, this term depends on spatial derivatives of the energy

[1] The operator $\begin{bmatrix} 0 & -\mathrm{div} \\ -\vec{\boldsymbol{\nabla}} & 0 \end{bmatrix}$ is formally skew-symmetric (see, e.g., Zwart and Kurula (2014) for an analysis of this operator on $N-$dimensional spatial domains).

variables ($\partial_x \alpha_y$, $\partial_y \alpha_x$). Thus, equations 6.60 and 6.61 are not in the usual form of infinite-dimensional pHs. A more standard form would be $G(h, \alpha_x, \alpha_y)$, which is not the case here. But still, we can derive useful properties. Let us look at the power balance of the system, by taking the time-derivative of Eq. 6.57:

$$\begin{aligned}
\dot{H}[\vec{\boldsymbol{\alpha}}, h] &= \frac{1}{2}\int_\Omega \left(\dot{h}\frac{\|\vec{\boldsymbol{\alpha}}\|^2}{\rho} + 2h\frac{\vec{\boldsymbol{\alpha}}}{\rho}\cdot\dot{\vec{\boldsymbol{\alpha}}} + 2gh\rho\dot{h} \right) \mathrm{d}\Omega\,, \\
&= \int_\Omega \left(\dot{h}(\frac{1}{2\rho}\|\vec{\boldsymbol{\alpha}}\|^2 + \rho g h) + h\frac{\vec{\boldsymbol{\alpha}}}{\rho}\cdot\dot{\vec{\boldsymbol{\alpha}}} \right) \mathrm{d}\Omega\,, \\
&= \int_\Omega \left(-\mathrm{div}(\vec{\boldsymbol{e}}_{\vec{\boldsymbol{\alpha}}})e_h + \vec{\boldsymbol{e}}_{\vec{\boldsymbol{\alpha}}}\cdot(-\vec{\boldsymbol{\nabla}}(e_h) + \mathcal{G}\vec{\boldsymbol{e}}_{\vec{\boldsymbol{\alpha}}}) \right) \mathrm{d}\Omega\,, \\
&= \int_\Omega \left(-\mathrm{div}(\vec{\boldsymbol{e}}_{\vec{\boldsymbol{\alpha}}})e_h - \vec{\boldsymbol{e}}_{\vec{\boldsymbol{\alpha}}}\cdot\vec{\boldsymbol{\nabla}}(e_h) + \underbrace{\vec{\boldsymbol{e}}_{\vec{\boldsymbol{\alpha}}}\cdot\mathcal{G}\vec{\boldsymbol{e}}_{\vec{\boldsymbol{\alpha}}}}_{0} \right) \mathrm{d}\Omega\,, \\
&= \int_\Omega -\mathrm{div}(e_h\vec{\boldsymbol{e}}_{\vec{\boldsymbol{\alpha}}})\ \mathrm{d}\Omega\,, \\
&= \int_{\partial\Omega} -e_h(\vec{\boldsymbol{e}}_{\vec{\boldsymbol{\alpha}}}\cdot\vec{\boldsymbol{n}})\ \mathrm{d}\Gamma\ .
\end{aligned} \tag{6.63}$$

Notice that the power balance depends only on the boundary values of e_h (the pressure) and $\vec{\boldsymbol{e}}_{\vec{\boldsymbol{\alpha}}}\cdot\vec{\boldsymbol{n}}$ is the flow of fluid in the normal direction of system domain. Similarly to what happened in one-dimensional systems, the previous power balance allows defining boundary ports. In the two-dimensional case, the boundary ports are distributed along the boundary of the domain (and here represented by the pressure and normal direction of fluid).

In the following sections, we introduce the motion of the tank in the 2D fluid equations. The procedure is similar to the one-dimensional case, presented in Section 6.1. For pedagogical reasons, the translation and rotation motions are firstly treated independently in § 6.2.2 and § 6.2.3. Then, the case with both translations and rotations is treated in § 6.2.4.

6.2.2 Equations for a moving tank: translations only

Here the fluid is assumed to be inside of a tank moving with speed $\dot{\vec{\boldsymbol{D}}} = \begin{bmatrix} \dot{D}_x & \dot{D}_y \end{bmatrix}^T$, and with rigid mass m_T. The rigid body motion is assumed to be only on the same plane of surface of the fluid. The Hamiltonian of the moving tank together with the fluid is given by:

$$H[\vec{\boldsymbol{v}}, h, \dot{\vec{\boldsymbol{D}}}] = \frac{1}{2}\int_\Omega \left(\rho h\|\vec{\boldsymbol{v}} + \dot{\vec{\boldsymbol{D}}}\|^2 + \rho g h^2 \right) \mathrm{d}\Omega + \frac{1}{2}m_T\|\dot{\vec{\boldsymbol{D}}}\|^2\,. \tag{6.64}$$

Again, a finite-dimensional momentum variable is defined:

$$\vec{\boldsymbol{p}}(t) := \frac{\partial H}{\partial \dot{\vec{\boldsymbol{D}}}} = \int_\Omega \rho h(\vec{\boldsymbol{v}} + \dot{\vec{\boldsymbol{D}}})\,\mathrm{d}\Omega + m_T\dot{\vec{\boldsymbol{D}}}\,, \tag{6.65}$$

as well as a distributed momentum variable:

$$\vec{\boldsymbol{\alpha}} := \rho(\vec{\boldsymbol{v}} + \dot{\vec{\boldsymbol{D}}})\,. \tag{6.66}$$

From Eq. 6.65, the tank speed can be written as:

$$\dot{\vec{\boldsymbol{D}}} = \frac{\vec{\boldsymbol{p}} - \int_\Omega h\vec{\boldsymbol{\alpha}}\,\mathrm{d}\Omega}{m_T}\,. \tag{6.67}$$

Rewriting the Hamiltonian as a function of these newly defined energy variables, we get:

$$H[\vec{\boldsymbol{\alpha}}, h, \vec{\boldsymbol{p}}] = \frac{1}{2}\int_\Omega \left(\frac{1}{\rho}h\|\vec{\boldsymbol{\alpha}}\|^2 + \rho g h^2\right)\mathrm{d}\Omega + \frac{1}{2m_T}\|\vec{\boldsymbol{p}} - \int_\Omega h\vec{\boldsymbol{\alpha}}\,\mathrm{d}\Omega\,\|^2\,, \tag{6.68}$$

and the variational derivatives with respect to each variable lead to the following co-energy variables:

$$\begin{aligned}
\vec{\boldsymbol{e}}_{\vec{\boldsymbol{\alpha}}} &:= \frac{\delta H}{\delta \alpha} = h\frac{\vec{\boldsymbol{\alpha}}}{\rho} - \dot{\vec{\boldsymbol{D}}}h = h\vec{\boldsymbol{v}}\,,\\
e_h &:= \frac{\delta H}{\delta h} = \frac{1}{2\rho}\|\vec{\boldsymbol{\alpha}}\|^2 + \rho g h - \dot{\vec{\boldsymbol{D}}}\cdot\vec{\boldsymbol{\alpha}}\,,\\
&\qquad = \rho\frac{\|\vec{\boldsymbol{v}}\|^2}{2} + \rho g h - \rho\frac{\|\dot{\vec{\boldsymbol{D}}}\|^2}{2}\,,\\
\vec{\boldsymbol{e}}_{\vec{\boldsymbol{p}}} &:= \frac{\partial H}{\partial \vec{\boldsymbol{p}}} = \dot{\vec{\boldsymbol{D}}}\,.
\end{aligned} \tag{6.69}$$

The mass conservation equation does not change with the rigid body motion and is given by:

$$\frac{\partial h}{\partial t} = -\mathrm{div}(h\vec{\boldsymbol{v}}) = -\mathrm{div}(\vec{\boldsymbol{e}}_{\vec{\boldsymbol{\alpha}}})\,. \tag{6.70}$$

The momentum conservation equation is now given by:

$$\frac{\partial \vec{\boldsymbol{\alpha}}}{\partial t} = -\vec{\boldsymbol{\nabla}}(\rho\frac{\|\vec{\boldsymbol{v}}\|^2}{2} + \rho g h) - \rho(\vec{\boldsymbol{\nabla}}\times\vec{\boldsymbol{v}})\times\vec{\boldsymbol{v}} = -\vec{\boldsymbol{\nabla}}(e_h) + \mathcal{G}\vec{\boldsymbol{e}}_{\vec{\boldsymbol{\alpha}}}\,, \tag{6.71}$$

where:

$$\mathcal{G} := \frac{\rho}{h}(\partial_x v - \partial_y u)\begin{bmatrix}0 & 1\\ -1 & 0\end{bmatrix} = \frac{1}{h}(\partial_x\alpha_y - \partial_y\alpha_x)\begin{bmatrix}0 & 1\\ -1 & 0\end{bmatrix}\,. \tag{6.72}$$

An additional, finite-dimensional, equation for the total momentum $\vec{\boldsymbol{p}}$ can be written as:

$$\dot{\vec{\boldsymbol{p}}} = -\vec{\boldsymbol{e}}_{\vec{\boldsymbol{D}}} + \vec{\boldsymbol{F}} = \vec{\boldsymbol{F}}\,, \tag{6.73}$$

where $\vec{\boldsymbol{F}}$ is the vector of external forces, $\vec{\boldsymbol{e}}_{\vec{\boldsymbol{D}}} := \frac{\partial H}{\partial \vec{\boldsymbol{D}}} = 0$.

Finally, as computed before:

$$\dot{\vec{\boldsymbol{D}}} = \vec{\boldsymbol{e}}_{\vec{\boldsymbol{p}}}\,, \tag{6.74}$$

The fluid-tank equations can thus be written as:

$$\begin{bmatrix} \dot{h} \\ \dot{\vec{\boldsymbol{\alpha}}} \\ \dot{\vec{\boldsymbol{p}}} \\ \dot{\vec{\boldsymbol{D}}} \end{bmatrix} = \begin{bmatrix} 0 & -\mathrm{div} & 0 & 0 \\ -\vec{\boldsymbol{\nabla}} & \mathcal{G} & 0 & 0 \\ 0 & 0 & 0 & -1 \\ 0 & 0 & 1 & 0 \end{bmatrix} \begin{bmatrix} e_h \\ \vec{\boldsymbol{e}}_{\vec{\boldsymbol{\alpha}}} \\ \vec{\boldsymbol{e}}_{\vec{\boldsymbol{p}}} \\ \vec{\boldsymbol{e}}_{\vec{\boldsymbol{D}}} \end{bmatrix} + \begin{bmatrix} 0 \\ 0 \\ \vec{\boldsymbol{F}} \\ 0 \end{bmatrix} . \tag{6.75}$$

Finally, the energy flow can be computed as:

$$\begin{aligned} \dot{H} &= \int_\Omega \left(\dot{h} e_h + \dot{\vec{\boldsymbol{\alpha}}} \cdot \vec{\boldsymbol{e}}_{\vec{\boldsymbol{\alpha}}} \right) \mathrm{d}\Omega + \dot{\vec{\boldsymbol{D}}} \cdot \vec{\boldsymbol{F}} \,, \\ &= \int_{\partial\Omega} (e_h \vec{\boldsymbol{e}}_{\vec{\boldsymbol{\alpha}}} \cdot \vec{\boldsymbol{n}}) \, \mathrm{d}\Gamma + \dot{\vec{\boldsymbol{D}}} \cdot \vec{\boldsymbol{F}} \,. \end{aligned} \tag{6.76}$$

In addition to the distributed boundary ports that were already presented in the previous section, the rigid body motion introduces the force $\vec{\boldsymbol{F}}$ and speed $\dot{\vec{\boldsymbol{D}}}$ as input/output ports of the system. In particular, since we are modeling the fluid sloshing inside tanks, the boundary conditions are such that: $\vec{\boldsymbol{e}}_{\vec{\boldsymbol{\alpha}}} \cdot \vec{\boldsymbol{n}} = 0$ (no flow). Thus: $\dot{H} = \dot{\vec{\boldsymbol{D}}} \cdot \vec{\boldsymbol{F}}$.

6.2.3 Equations for a moving tank: planar (yaw) rotation only

Now, the tank is assumed to rotate with angular speed $\dot{\theta}$ around the center of the tank $(x, y) = (0, 0)$ (the rigid body angular velocity is perpendicular to the tank bottom). The fluid speed with respect to a frame that moves with the tank is given by $\vec{\boldsymbol{v}} = \begin{bmatrix} u, & v \end{bmatrix}^T$. The inertial speed, using the same coordinates is given by $\begin{bmatrix} u - y\dot{\theta}, & v + x\dot{\theta} \end{bmatrix}^T$.

The system Hamiltonian is given by:

$$H = \frac{1}{2} \int_\Omega \left(\rho h \left((u - y\dot{\theta})^2 + (v + x\dot{\theta})^2 \right) + \rho g h^2 \right) \mathrm{d}\Omega + \frac{1}{2} I_T \dot{\theta}^2 \,, \tag{6.77}$$

where I_T is the tank rotation inertia (around the center of the tank). Let us define the rotation momentum $p_\theta(t)$:

$$\begin{aligned} p_\theta(t) &:= \frac{\partial H}{\partial \dot{\theta}} \,, \\ &= \int_\Omega h \left(-y\rho(u - y\dot{\theta}) + x\rho(v + x\dot{\theta}) \right) d\Omega + I_T \dot{\theta} \,, \end{aligned} \tag{6.78}$$

and the distributed momentum variable α:

$$\vec{\boldsymbol{\alpha}}(x, y, t) := \begin{bmatrix} \alpha_x \\ \alpha_y \end{bmatrix} = \begin{bmatrix} \rho(u - y\dot{\theta}) \\ \rho(v + x\dot{\theta}) \end{bmatrix} . \tag{6.79}$$

The variable $p_\theta(t)$ becomes:

$$p_\theta(t) = \underbrace{\int_\Omega h\,(-y\alpha_x + x\alpha_y)d\Omega}_{p_f(t)} + I_T\dot{\theta}\,, \tag{6.80}$$

where the term $p_f[h, \vec{\boldsymbol{\alpha}}]$ is the momentum due to the fluid.

The rotation speed $\dot{\theta}$ is then computed:

$$\dot{\theta} = \frac{p_\theta(t) - p_f[h, \vec{\boldsymbol{\alpha}}]}{I_T}\,, \tag{6.81}$$

and the Hamiltonian is written as a function of these newly defined variables:

$$H[h, \vec{\boldsymbol{\alpha}}, p_\theta] = \frac{1}{2}\int_\Omega \Big(h\|\vec{\boldsymbol{\alpha}}\|^2 + \rho g h^2\Big)d\Omega + \frac{1}{2I_T}(p_\theta(t) - p_f[h, \vec{\boldsymbol{\alpha}}])^2\,. \tag{6.82}$$

The co-energy variables are thus given by:

$$\begin{aligned} e_h &:= \frac{\delta H}{\delta h} \\ &= \frac{1}{2}\|\vec{\boldsymbol{\alpha}}\|^2 + \rho g h - \frac{(p_\theta - p_f)}{I_T}\frac{\delta p_f}{\delta h}\,, \\ &= \frac{1}{2}\|\vec{\boldsymbol{\alpha}}\|^2 + \rho g h - \frac{(p_\theta - p_f)}{I_T}(-y\alpha_x + x\alpha_y)\,, \end{aligned} \tag{6.83}$$

$$\begin{aligned} e_{\alpha_x} &:= \frac{\delta H}{\delta \alpha_x} \\ &= h\alpha_x - \frac{(p_\theta - p_f)}{I_T}\frac{\delta p_f}{\delta \alpha_x} \\ &= h\alpha_x - \frac{(p_\theta - p_f)}{I_T}(-hy) \end{aligned} \tag{6.84}$$

$$\begin{aligned} e_{\alpha_y} &:= \frac{\delta H}{\delta \alpha_y}\,, \\ &= h\alpha_y - \frac{(p_\theta - p_f)}{I_T}\frac{\delta p_f}{\delta \alpha_y}\,, \\ &= h\alpha_y - \frac{(p_\theta - p_f)}{I_T}(hx)\,, \end{aligned} \tag{6.85}$$

$$\begin{aligned} e_{p_\theta} &:= \frac{\partial H}{\partial p_\theta}\,, \\ &= \frac{(p_\theta - p_f)}{I_T}\,. \end{aligned} \tag{6.86}$$

In terms of the original variables, these three co-energy variables become:

$$e_h = \frac{1}{2}\rho\,\|\vec{\boldsymbol{v}}\|^2 + \rho g h - \frac{1}{2}\rho\,\dot{\theta}^2(x^2 + y^2)\,, \tag{6.87}$$

$$e_{\alpha_x} = hu\,, \tag{6.88}$$

$$e_{\alpha_y} = hv\,, \tag{6.89}$$

$$e_{p_\theta} = \dot{\theta}\,, \tag{6.90}$$

As in the other cases, the mass conservation equation is given by:

$$\dot{h} = \mathrm{div}(h\vec{\boldsymbol{v}}) = \mathrm{div}(\vec{\boldsymbol{e}}_{\vec{\boldsymbol{\alpha}}})\,, \tag{6.91}$$

The fluid momentum conservation equation is given by:

$$\dot{\vec{\boldsymbol{\alpha}}} = \vec{\boldsymbol{\nabla}}(e_h) + \mathcal{G}\vec{\boldsymbol{e}}_{\vec{\boldsymbol{\alpha}}}\,, \tag{6.92}$$

where:

$$\mathcal{G} := \frac{\rho}{h}(\partial_y u - \partial_y v)\begin{bmatrix} 0 & 1 \\ -1 & 0 \end{bmatrix} = \frac{1}{h}(\partial_x \alpha_y - \partial_y \alpha_x + 2\rho\dot{\theta})\begin{bmatrix} 0 & 1 \\ -1 & 0 \end{bmatrix}. \tag{6.93}$$

The dynamics of the total momentum is given by:

$$\dot{p}_\theta = M\,, \tag{6.94}$$

where M is the external moment applied to the tank.

Rewriting Eqs. 6.91, 6.92 and 6.94, we get:

$$\begin{bmatrix} \dot{h} \\ \dot{\vec{\boldsymbol{\alpha}}} \\ \dot{p}_\theta \\ \dot{\theta} \end{bmatrix} = \begin{bmatrix} 0 & -\mathrm{div} & 0 & 0 \\ -\vec{\boldsymbol{\nabla}} & \mathcal{G} & 0 & 0 \\ 0 & 0 & 0 & -1 \\ 0 & 0 & 1 & 0 \end{bmatrix} \begin{bmatrix} e_h \\ \vec{\boldsymbol{e}}_{\vec{\boldsymbol{\alpha}}} \\ e_{p_\theta} \\ e_{\dot{\theta}} \end{bmatrix} + \begin{bmatrix} 0 \\ 0 \\ M \\ 0 \end{bmatrix}. \tag{6.95}$$

Finally, the energy flow is given by:

$$\begin{aligned} \dot{H} &= \int_\Omega \left(\dot{h}e_h + \dot{\vec{\boldsymbol{\alpha}}} \cdot \vec{\boldsymbol{e}}_{\vec{\boldsymbol{\alpha}}}\right) \mathrm{d}\Omega + \dot{\theta}M\,, \\ &= \int_{\partial\Omega} (e_h \vec{\boldsymbol{e}}_{\vec{\boldsymbol{\alpha}}} \cdot \vec{\boldsymbol{n}})\, \mathrm{d}\Gamma + \dot{\theta}M\,. \end{aligned} \tag{6.96}$$

Again, together with the boundary ports, the moment M and the rotation speed $\dot{\theta}$ are the ports of this pHs. Furthermore, in the case of the tank, with the condition of no flow through the walls, thus: $\dot{H} = \dot{\theta}M$.

6.2.4 Equations for a moving tank: both translations and planar rotation

Finally, let us treat the case of the moving tank with both translations, given by a translational velocity $\dot{\vec{\boldsymbol{D}}}$, and one rotation, given by an angular speed $\dot{\theta}$. The tank has a mass m_T and a rotation inertia I_T.

The system Hamiltonian (total energy) is given by:

$$H[\vec{\boldsymbol{v}}, h, \dot{\vec{\boldsymbol{D}}}, \dot{\theta}, \theta] = \frac{1}{2}\int_{\Omega}\left(\rho h\left\|\vec{\boldsymbol{v}} + T(\theta)\dot{\vec{\boldsymbol{D}}} + \begin{bmatrix}-y\\ x\end{bmatrix}\dot{\theta}\right\|^2 + \rho g h^2\right)\mathrm{d}\Omega + \frac{1}{2}m_T\|\dot{D}\|^2 + \frac{1}{2}I_T\dot{\theta}^2\,, \tag{6.97}$$

where $\vec{\boldsymbol{v}}$ is written in local (moving) coordinates, $\dot{\vec{\boldsymbol{D}}}$ is written in fixed coordinates, $T(\theta)$ is a transformation matrix from the fixed to local coordinates.

The finite-dimensional momentum variables, due to the rotation and the translations are defined as:

$$\begin{aligned} p_{\dot{\theta}}(t) &:= \frac{\partial H}{\partial \dot{\theta}}\,, \\ &= \int_{\Omega}\rho h\left(\vec{\boldsymbol{v}} + T(\theta)\,, \dot{\vec{\boldsymbol{D}}} + \begin{bmatrix}-y\\ x\end{bmatrix}\dot{\theta}\right)\cdot\begin{bmatrix}-y\\ x\end{bmatrix}d\Omega + I_T\dot{\theta}\,, \end{aligned} \tag{6.98}$$

$$\begin{aligned} \vec{\boldsymbol{p}}_{\dot{\vec{\boldsymbol{D}}}}(t) &:= \frac{\partial H}{\partial \dot{\vec{\boldsymbol{D}}}}\,, \\ &= \int_{\Omega}\rho h T(\theta)^T\left(\vec{\boldsymbol{v}} + T(\theta)\dot{\vec{\boldsymbol{D}}} + \begin{bmatrix}-y\\ x\end{bmatrix}\dot{\theta}\right)d\Omega + m_T\dot{\vec{\boldsymbol{D}}}\,. \end{aligned} \tag{6.99}$$

The distributed momentum variable is given by:

$$\vec{\boldsymbol{\alpha}}(x, y, t) := \rho\left(\vec{\boldsymbol{v}} + T(\theta)\dot{\vec{\boldsymbol{D}}} + \begin{bmatrix}-y\\ x\end{bmatrix}\dot{\theta}\right)\,. \tag{6.100}$$

Thus, the moment variables can be rewritten as:

$$\begin{aligned} p_{\dot{\theta}}(t) &= \underbrace{\int_{\Omega} h\vec{\boldsymbol{\alpha}}\cdot\begin{bmatrix}-y\\ x\end{bmatrix}d\Omega}_{p_{f\theta}[h,\vec{\boldsymbol{\alpha}}]} + I_T\dot{\theta} \\ \vec{\boldsymbol{p}}_{\dot{\vec{\boldsymbol{D}}}}(t) &= \underbrace{\int_{\Omega} hT(\theta)^T\vec{\boldsymbol{\alpha}}d\Omega}_{\vec{\boldsymbol{p}}_f[h,\vec{\boldsymbol{\alpha}}]} + m_T\dot{\vec{\boldsymbol{D}}} \end{aligned} \tag{6.101}$$

Using the newly defined variables, the Hamiltonian reads as:

$$H[\vec{\boldsymbol{v}}, h, \vec{\boldsymbol{p}}_{\dot{\vec{\boldsymbol{D}}}}, p_{\dot{\theta}}] = \frac{1}{2}\int_{\Omega}\left(\frac{h}{\rho}\|\vec{\boldsymbol{\alpha}}\|^2 + \rho g h^2\right)d\Omega + \frac{1}{2m_T}(\vec{\boldsymbol{p}}_{\dot{\vec{\boldsymbol{D}}}}(t) - \vec{\boldsymbol{p}}_f[h,\vec{\boldsymbol{\alpha}}])^2 + \frac{1}{2I_T}(p_{\dot{\theta}}(t) - p_{f\theta}[h,\vec{\boldsymbol{\alpha}}])^2\,, \tag{6.102}$$

and the co-energy variables are given by:

$$\begin{aligned} e_h &:= \frac{\delta H}{\delta h}\,, \\ &= \frac{\|\vec{\boldsymbol{\alpha}}\|^2}{2\rho} + \rho g h - \frac{\vec{\boldsymbol{p}}_{\dot{\vec{\boldsymbol{D}}}} - \vec{\boldsymbol{p}}_f}{m_T} \cdot \frac{\delta p_f}{\delta h} - \frac{p_\theta - p_{f\theta}}{I_T} \frac{\delta p_{f\theta}}{\delta h}\,, \\ &= \frac{\|\vec{\boldsymbol{\alpha}}\|^2}{2\rho} + \rho g h - \frac{\vec{\boldsymbol{p}}_{\dot{\vec{\boldsymbol{D}}}} - \vec{\boldsymbol{p}}_f}{m_T} \cdot T(\theta)^T \vec{\boldsymbol{\alpha}} h - \frac{p_\theta - p_{f\theta}}{I_T} \vec{\boldsymbol{\alpha}} \cdot \begin{bmatrix} -y \\ x \end{bmatrix}\,, \end{aligned} \tag{6.103}$$

$$\begin{aligned} \vec{\boldsymbol{e}}_{\vec{\boldsymbol{\alpha}}} &:= \frac{\delta H}{\delta \vec{\boldsymbol{\alpha}}}\,, \\ &= \frac{h\vec{\boldsymbol{\alpha}}}{\rho} - T(\theta) \frac{\vec{\boldsymbol{p}}_{\dot{\vec{\boldsymbol{D}}}} - \vec{\boldsymbol{p}}_f}{m_T} h - \frac{p_{\dot\theta} - p_{f\theta}}{I_T} h \begin{bmatrix} -y \\ x \end{bmatrix}\,, \end{aligned} \tag{6.104}$$

$$\begin{aligned} \vec{\boldsymbol{e}}_{\vec{\boldsymbol{p}}} &:= \frac{\partial H}{\partial \vec{\boldsymbol{p}}_{\dot{\vec{\boldsymbol{D}}}}}\,, \\ &:= \frac{\vec{\boldsymbol{p}}_{\dot{\vec{\boldsymbol{D}}}} - \vec{\boldsymbol{p}}_f}{m_T}\,, \end{aligned} \tag{6.105}$$

$$\begin{aligned} e_{p_\theta} &:= \frac{\partial H}{\partial p_\theta}\,, \\ &:= \frac{p_\theta - p_{f\theta}}{I_T}\,. \end{aligned} \tag{6.106}$$

Using the original variables, we verify that:

$$\begin{aligned} e_h &= \frac{1}{2}\rho\|\vec{\boldsymbol{v}}\|^2 + \rho g h - \frac{1}{2}\left\| T(\theta)\dot{\vec{\boldsymbol{D}}} + \begin{bmatrix} -y \\ x \end{bmatrix} \dot\theta \right\|^2\,, \\ \vec{\boldsymbol{e}}_{\vec{\boldsymbol{\alpha}}} &= h\vec{\boldsymbol{v}}\,, \\ \vec{\boldsymbol{e}}_{\vec{\boldsymbol{p}}} &= \dot{\vec{\boldsymbol{D}}}\,, \\ e_{p_\theta} &= \dot\theta\,. \end{aligned} \tag{6.107}$$

The full equations of the fluid, with the rotation and the translations, are given by:

$$\begin{bmatrix} \dot h \\ \dot{\vec{\boldsymbol{\alpha}}} \\ \dot{\vec{\boldsymbol{p}}} \\ \dot{\vec{\boldsymbol{D}}} \\ \dot p_\theta \\ \dot\theta \end{bmatrix} = \begin{bmatrix} 0 & -\mathrm{div} & 0 & 0 & 0 & 0 \\ -\vec{\boldsymbol{\nabla}} & \mathcal{G} & 0 & 0 & 0 & 0 \\ 0 & 0 & 0 & -1 & 0 & 0 \\ 0 & 0 & 1 & 0 & 0 & 0 \\ 0 & 0 & 0 & 0 & 0 & -1 \\ 0 & 0 & 0 & 0 & 1 & 0 \end{bmatrix} \begin{bmatrix} e_h \\ \vec{\boldsymbol{e}}_{\vec{\boldsymbol{\alpha}}} \\ \vec{\boldsymbol{e}}_{\vec{\boldsymbol{p}}} \\ e_{\dot{\vec{\boldsymbol{D}}}} \\ e_{p_\theta} \\ e_{\dot\theta} \end{bmatrix} + \begin{bmatrix} 0 & 0 \\ 0 & 0 \\ \vec{\boldsymbol{F}} & 0 \\ 0 & 0 \\ 0 & M \\ 0 & 0 \end{bmatrix}\,, \tag{6.108}$$

where:

$$\mathcal{G} := \frac{\rho}{h}(\partial_y u - \partial_y v) \begin{bmatrix} 0 & 1 \\ -1 & 0 \end{bmatrix} = \frac{1}{h}(\partial_x \alpha_y - \partial_y \alpha_x + 2\rho\dot\theta) \begin{bmatrix} 0 & 1 \\ -1 & 0 \end{bmatrix}\,. \tag{6.109}$$

Finally, the power balance is computed:

$$\begin{aligned} \dot{H} &= \int_{\Omega} \left(\dot{h} e_h + \dot{\vec{\boldsymbol{\alpha}}} \cdot \vec{\boldsymbol{e}}_{\vec{\boldsymbol{\alpha}}} \right) d\Omega + \dot{\vec{\boldsymbol{D}}} \cdot \vec{\boldsymbol{F}} + \dot{\theta} M \,, \\ &= \int_{\partial\Omega} (e_h \vec{\boldsymbol{e}}_{\vec{\boldsymbol{\alpha}}} \cdot \vec{\boldsymbol{n}}) d\Gamma + \dot{\vec{\boldsymbol{D}}} \cdot \vec{\boldsymbol{F}} + \dot{\theta} M \,. \end{aligned} \tag{6.110}$$

Together with the boundary ports, the moment M, the rotation speed $\dot{\theta}$, the force $\vec{\boldsymbol{F}}$ and the velocity $\dot{\vec{\boldsymbol{D}}}$ are the ports of this port-Hamiltonian system. Furthermore, in the case of the tank, with the condition of no flow through the walls ($\vec{\boldsymbol{e}}_{\vec{\boldsymbol{\alpha}}} \cdot \vec{\boldsymbol{n}} = 0$), we get $\dot{H} = \dot{\vec{\boldsymbol{D}}} \cdot \vec{\boldsymbol{F}} + \dot{\theta} M$.

6.3 Limitations of the shallow water model

As evidenced by the name, the *Shallow Water* Equations are obtained with the assumption of a small depth of fluid (in comparison to the free surface dimensions). An alternative model that is also common for the sloshing is provided by the incompressible Euler equations. In the linearized case, analytical transfer functions that relates the acceleration of the tank to the force that the fluid applies in the walls of the tank can be obtained, both for the SWE and incompressible Euler. These transfer functions are recalled in Appendix C for a rectangular tank.

Thus, we can compare the frequency response of the linearized SWE to the depth-dependent linear incompressible Euler equations, leading to the results of Figure 6.2. We find that:

- The frequency response agrees very well for very small filling ratios of fluid;
- For larger filling ratios, only the first resonant frequencies agree.

The SWE are adequate for simulating the fluid in long tanks, and subject to low frequency excitation. Rewriting the incompressible Euler equations in the port-Hamiltonian formalism leads to a few difficulties, as we are going to see in the sequel.

First, let us recall the fluid equations for the compressible inviscid and irrotational fluid:

$$\begin{cases} \text{mass conservation:} \;\; \dot{\rho} + \operatorname{div}(\rho \vec{\boldsymbol{v}}) = 0 \,, \\ \text{momentum conservation:} \;\; \dot{\vec{\boldsymbol{v}}} + \vec{\boldsymbol{\nabla}} \left(\dfrac{||\vec{\boldsymbol{v}}||^2}{2} + \dfrac{P}{\rho} + gz \right) = 0 \,. \end{cases} \tag{6.111}$$

These equations can be rewritten using the port-Hamiltonian framework as (van der Schaft and Maschke, 2001):

$$\begin{bmatrix} \dot{\rho} \\ \dot{\vec{\boldsymbol{v}}} \end{bmatrix} = \begin{bmatrix} 0 & -\operatorname{div} \\ -\vec{\boldsymbol{\nabla}} & 0 \end{bmatrix} \begin{bmatrix} e_1 \\ \vec{\boldsymbol{e}}_2 \end{bmatrix} \,. \tag{6.112}$$

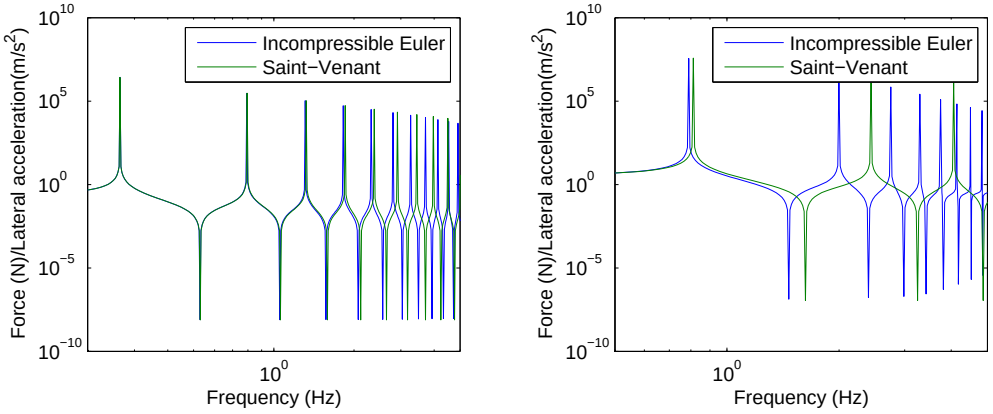

Tank 10% filled. Tank 70% filled.

Figure 6.2: Frequency response of linearized sloshing equations: tank acceleration as input, fluid force on the walls as output. It is easy to note that the agreement between shallow water equations (Saint-Venant) and incompressible Euler is much better for small filling ratios. For larger filling ratios, only the low-frequency behavior is adequately represented.

The Hamiltonian (total energy) is given by:

$$H = \int_\Omega \left(\frac{\rho \, \|\vec{\boldsymbol{v}}\|^2}{2} + \rho U(\rho) + \rho g z \right) \mathrm{d}V \,, \tag{6.113}$$

$U(\rho)$ is the fluid specific internal energy.

The co-energy variables are given by the variational derivatives of the Hamiltonian, i.e.,

$$\begin{aligned} e_1 &:= \frac{\delta H}{\delta \rho} = \frac{||\vec{\boldsymbol{v}}||^2}{2} + \frac{P}{\rho} + g z \,, \\ \vec{\boldsymbol{e}}_2 &:= \frac{\delta H}{\delta \vec{\boldsymbol{v}}} = \rho \vec{\boldsymbol{v}} \,. \end{aligned} \tag{6.114}$$

The power balance is given by:

$$\dot{H} = \int_{\partial\Omega} ((\vec{\boldsymbol{n}} \cdot \vec{\boldsymbol{e}}_2) e_1) \, \mathrm{d}\gamma \,, \tag{6.115}$$

and depends only on the boundary conditions, i.e., the values of the inflow speed $(\vec{\boldsymbol{n}} \cdot \frac{\vec{\boldsymbol{e}}_2}{\rho})$ and pressure ρe_1 at the boundaries.

Now, let us discuss the incompressible case.[2] Defining the pressure $\lambda := \rho \, e_1$, since ρ is constant, the dynamic equation can be rewritten as:

$$\begin{aligned} \rho \dot{\vec{\boldsymbol{v}}} &= 0 \, \vec{\boldsymbol{e}}_2 - \vec{\boldsymbol{\nabla}}(\lambda) \,, \\ 0 &= -\mathrm{div}(\vec{\boldsymbol{e}}_2) \,. \end{aligned} \tag{6.116}$$

[2]For classical Hamiltonian systems, the incompressible fluid equations (without free-surface) was treated, e.g., in Example 7.9 of Olver (1993). There, the equations were rewritten in terms of the vorticity.

Note that the previous equation does not represent a usual infinite-dimensional pHs. Actually, Eq. 6.116 is similar to the constrained pHs, as presented in § 4.1.4 for finite-dimensional pHs. Here, the pressure λ plays the role of a *distributed* Lagrange multiplier. In the incompressible case, the Hamiltonian is given only by the kinetic energy (since the potential energy inside the fluid domain is constant):

$$H = \int_\Omega \rho \frac{\|\vec{\boldsymbol{v}}\|^2}{2} \, \mathrm{d}V \ . \tag{6.117}$$

The power balance gives the same result as before, i.e.:

$$\dot{H} = \int_{\partial\Omega} ((\vec{\boldsymbol{n}} \cdot \vec{\boldsymbol{v}})\lambda) \, \mathrm{d}\gamma \ . \tag{6.118}$$

Note that the free surface interacts with the upper boundary of the fluid domain. Further work should be addressed to properly represent the incompressible equations with free surface using the pHs framework.

6.4 Conclusions

In this chapter, several nonlinear models for liquid sloshing in moving containers were proposed using the port-Hamiltonian framework.

Interconnection ports naturally appears when rewriting the equations as pHs. These ports can be used to couple the fluid with other systems. In addition, the port-Hamiltonian model highlights the conservation laws of the system (energy, mass and momentum conservation).

In Section 6.1, we introduced the port-Hamiltonian model for the fluid assuming one-dimensional flow. Two degrees of freedom were assumed for the rigid body motion: one rotation and one translation. This model will be used in the following chapters to model, simulation and control of the fluid-structure system. The translation of the tank will be coupled with the bending motion, the rotation of the tank will be coupled with the torsion motion.

In Section 6.2, we presented an extension for the bi-dimensional SWE. The rotational term leads to the appearence of a gyroscopic matrix $\mathcal{G}$ in the interconnection structure that does not affect the power balance of the system since it is skew-symmetric. Two translations and one rotation were taken into account. Only planar rotations were taken into account.

The fluid equations presented in this chapter are usually applied for flows in canals, oceans and other cases where the depth of fluid is small in comparison with the free surface dimensions. The use of SWE for modeling sloshing in tanks leads to good results in the low frequency range, but it is limited in high frequency and cases where the depth of fluid is large. As discussed in Section 6.3, the incompressible Euler equations provide a possible alternative that is more accurate in these cases. However, they lead to some difficulties, since the incompressible fluid equations are given by an infinite-dimensional constrained pHs.

Chapter 7

Fluid-structure coupled system

The two previous chapters presented the models of the structural dynamics and fluid dynamics using the port-Hamiltonian representation. A key characteristic of the port-Hamiltonian systems is that interconnection ports are defined and these ports allows coupling the subsystems in a systematic way. In this chapter, these interconnection ports are used to couple the fluid-structure system.

Firstly, the equations, interconnection ports and the power balance of each subsystem of the system are recalled in § 7.1. Then, kinematic and dynamic constraints are obtained, allowing the coupling of the system using the interconnection ports in § 7.2.

7.1 Recall of the equations and interconnection ports of each subsystem

Here we recall the equations and interconnection ports of each model presented in the previous chapters. In the next chapters, the coupled model is used for simulation and control of the fluid-structure device of Chapter 3. In this section, the dissipative ports are ignored for simplifying the presentation.

Bending: The first model is the bending motion of the beam (Eq. 5.15):

$$\frac{\partial}{\partial t}\begin{bmatrix} x_1^B(z,t) \\ x_2^B(z,t) \end{bmatrix} = \begin{bmatrix} 0 & -\partial_{z^2}^2 \\ \partial_{z^2}^2 & 0 \end{bmatrix} \begin{bmatrix} e_1^B(z,t) \\ e_2^B(z,t) \end{bmatrix} + \begin{bmatrix} \partial_{z^2}^2 \\ 0 \end{bmatrix} \Pi_{ab}(z) k_p v(t)\,, \tag{7.1}$$

with the following interconnection ports given by Eq. 5.22:

$$\boldsymbol{y}^B = \begin{bmatrix} \partial_z e_2^B(0,t) \\ -e_2^B(0,t) \\ -e_1^B(L,t) \\ \partial_z e_1^B(L,t) \\ y_v(t) \end{bmatrix} = \begin{bmatrix} \text{force} \\ \text{torque} \\ \text{speed} \\ \text{angular velocity} \\ \text{“current”}^1. \end{bmatrix}, \boldsymbol{u}^B = \begin{bmatrix} e_1^B(0,t) \\ \partial_z e_1^B(0,t) \\ \partial_z e_2^B(L,t) \\ e_2^B(L,t) \\ v(t) \end{bmatrix} = \begin{bmatrix} \text{speed} \\ \text{angular velocity} \\ \text{force} \\ \text{torque} \\ \text{voltage} \end{bmatrix}, \tag{7.2}$$

As we will see in the sequel, the boundary ports at $z = L$ will be used for interconnection between the the beam and the tank with fluid. The boundary ports at $z = 0$ are fixed to

[1] Recall from Remark 5.3 that y_v represents the component of current linked to the electro-mechanical coupling (also known as “motional current”)

define clamped conditions. The voltage will be used as a control port.

The power balance, with appropriate boundary conditions at $z = 0$, is given by (Eq. 5.23):

$$\dot{H}^B = e_2^B(L,t)\,\partial_z e_1^B(L,t) - \partial_z e_2^B(L,t)\,e_1^B(L,t) + y_v(t)\,v(t). \tag{7.3}$$

Torsion: The second model is the torsion motion of the beam (Eq. 5.26):

$$\frac{\partial}{\partial t}\begin{bmatrix} x_1^T(z,t) \\ x_2^T(z,t) \end{bmatrix} = \begin{bmatrix} 0 & -\partial_z \\ -\partial_z & 0 \end{bmatrix}\begin{bmatrix} e_1^T(z,t) \\ e_2^T(z,t) \end{bmatrix}, \tag{7.4}$$

with the following ports as given by Eq. 5.29:

$$\boldsymbol{y}^T = \begin{bmatrix} -e_2^T(L,t) \\ e_1^T(0,t) \end{bmatrix} = \begin{bmatrix} \text{torque} \\ \text{angular velocity} \end{bmatrix}, \boldsymbol{u}^T = \begin{bmatrix} e_1^T(L,t) \\ e_2^T(0,t) \end{bmatrix} = \begin{bmatrix} \text{angular velocity} \\ \text{torque} \end{bmatrix}. \tag{7.5}$$

Again, the boundary ports at $z = L$ are used for interconnection, the boundary at $z = 0$ is set to define fixed boundary conditions. In these conditions, the power balance is given by Eq. 5.30:

$$\dot{H}^T = -e_2^T(L,t)e_1^T(L,t). \tag{7.6}$$

Sloshing: The third model is the fluid in a moving tank (Eq. 6.38):

$$\frac{\partial}{\partial t}\begin{bmatrix} \alpha_1(z,t) \\ \alpha_2(z,t) \\ p(t) \\ D(t) \\ p_\theta(t) \\ \theta(t) \end{bmatrix} = \begin{bmatrix} 0 & -\partial_z & 0 & 0 & 0 & 0 \\ -\partial_z & 0 & 0 & 0 & 0 & 0 \\ 0 & 0 & 0 & -1 & 0 & 0 \\ 0 & 0 & 1 & 0 & 0 & 0 \\ 0 & 0 & 0 & 0 & 0 & -1 \\ 0 & 0 & 0 & 0 & 1 & 0 \end{bmatrix}\begin{bmatrix} e_1^F(z,t) \\ e_2^F(z,t) \\ e_p^F(t) \\ e_D^F(t) \\ e_{p\theta}^F(t) \\ e_\theta^F(t) \end{bmatrix} + \begin{bmatrix} 0 & 0 \\ 0 & 0 \\ 1 & 0 \\ 0 & 0 \\ 0 & 1 \\ 0 & 0 \end{bmatrix}\begin{bmatrix} F_{\text{ext}} \\ M_{\text{ext}} \end{bmatrix}, \tag{7.7}$$

The ports are given by Eq. 6.41:

$$\boldsymbol{y}^F = \begin{bmatrix} -e_2^F(a/2,t) \\ e_1^F(-a/2,t) \\ \dot{D}(t) \\ \dot{\theta}(t) \end{bmatrix} = \begin{bmatrix} \text{volumetric flow} \\ \text{pressure} \\ \text{speed} \\ \text{rotation speed} \end{bmatrix}, \quad \boldsymbol{u}^F = \begin{bmatrix} e_1^F(a/2,t) \\ e_2^F(-a/2,t) \\ F_{\text{ext}}(t) \\ M_{\text{ext}}(t) \end{bmatrix} = \begin{bmatrix} \text{pressure} \\ \text{volumetric flow} \\ \text{force} \\ \text{torque} \end{bmatrix}, \tag{7.8}$$

Here, the boundary ports at both sides are used to set the no-flow condition. The other ports will be used to couple with the structural dynamics. The power balance, from Eq. 6.42:

$$\dot{H}^F = \dot{D}(t)\,F_{\text{ext}}(t) + \dot{\theta}(t)\,M_{\text{ext}}(t). \tag{7.9}$$

Rigid tank: Finally, additional rigid body equations are presented in Appendix B. These equations are used to represent the inertias of the tank and its support, that are assumed to

be rigid bodies. They are given by Eq. B.3:

$$\begin{aligned} \frac{d}{dt}\begin{bmatrix} p_{\theta B}(t) \\ p_{\theta T}(t) \end{bmatrix} &= \begin{bmatrix} 0 & 0 \\ 0 & 0 \end{bmatrix}\begin{bmatrix} e^{RB}_{p_{\theta B}}(t) \\ e^{RB}_{p_{\theta T}}(t) \end{bmatrix} + \begin{bmatrix} 1 & 0 \\ 0 & 1 \end{bmatrix}\begin{bmatrix} M_{\text{ext,B}}(t) \\ M_{\text{ext,T}}(t) \end{bmatrix} \\ \boldsymbol{y}^{RB} &= \begin{bmatrix} \dot{\theta}_B(t) \\ \dot{\theta}_T(t) \end{bmatrix} = \begin{bmatrix} 1 & 0 \\ 0 & 1 \end{bmatrix}\begin{bmatrix} e^{RB}_{p_{\theta B}}(t) \\ e^{RB}_{p_{\theta T}}(t) \end{bmatrix}. \end{aligned} \tag{7.10}$$

The ports are given by Eq. B.6:

$$\boldsymbol{y}^{RB} = \begin{bmatrix} \dot{\theta}_B(t) \\ \dot{\theta}_T(t) \end{bmatrix} = \begin{bmatrix} \text{angular velocity (bending)} \\ \text{angular velocity (torsion)} \end{bmatrix}, \boldsymbol{u}^{RB} = \begin{bmatrix} M_{\text{ext,B}}(t) \\ M_{\text{ext,T}}(t) \end{bmatrix} = \begin{bmatrix} \text{torque (bending)} \\ \text{torque (torsion)} \end{bmatrix}. \tag{7.11}$$

Both ports will be used to interconnect to the structure-fluid system. The power balance is given by (Eq. B.5):

$$\dot{H}^{RB} = \dot{\theta}_B(t)\, M_{\text{ext,B}}(t) + \dot{\theta}_T(t)\, M_{\text{ext,T}}(t)\,. \tag{7.12}$$

7.2 Coupling

Firstly, the kinematic constraints that naturally arise at the interconnection point are written:

- Translation speeds of each subsystem are equal (1 constraint):

$$e^B_1(L,t) = \dot{D}(t) \tag{7.13}$$

- Rotation speeds in bending are equal (1 constraint):

$$\dot{\theta}_B(t) = \frac{\partial e^B_1}{\partial z}(L,t) \tag{7.14}$$

- Rotation speeds in torsion are equal (2 constraints):

$$\dot{\theta}_T(t) = -e^T_2(L,t) = \dot{\theta}_F(t) \tag{7.15}$$

Secondly, the Hamiltonian of the global system is written as the sum of each Hamiltonian component (Eqs. A.5, B.4, 5.23 and 5.27):

$$H = H^F + H^{RB} + H^B + H^T. \tag{7.16}$$

Finally, using the sum of each Hamiltonian component rate of change (Eqs. 7.9, 7.12, 7.3 and 7.6), and imposing the four kinematic constraints from Eqs. 7.13, 7.14 and 7.15, the following

global Hamiltonian rate of change is obtained:

$$\begin{aligned}\dot{H} = &+ \dot{D}(t) \underbrace{\left(-\frac{\partial}{\partial z} e_2^B(L,t) + F_{\text{ext}}(t)\right)}_{F_\Sigma} + \dot{\theta}_B(t) \underbrace{\left(e_2^B(L,t) + M_{\text{ext,B}}(t)\right)}_{M_{\Sigma,B}} \\ &+ \dot{\theta}_T(t) \underbrace{\left(e_1^T(L,t) + M_{\text{ext,T}}(t) + M_{\text{ext}}(t)\right)}_{M_{\Sigma,T}} + y_v(t)v(t)\,. \end{aligned} \tag{7.17}$$

Notice that F_Σ, $M_{\Sigma,B}$ and $M_{\Sigma,T}$ are the sum of external forces/moments applied to each subsystem. From a global system perspective, they are the sum of internal forces/moments at the interconnection point, which should be equal to zero:

$$\begin{aligned} F_\Sigma &= 0\,, \\ M_{\Sigma,B} &= 0\,, \\ M_{\Sigma,T} &= 0\,. \end{aligned} \tag{7.18}$$

Since no damping has been taken into account in the modeling of the different components, the only energy change in the global system is due to the piezoelectric excitation. Hence, when imposing the constraints from Eq. 7.18, the energy flow becomes:

$$\dot{H} = y_v(t)v(t)\,. \tag{7.19}$$

Remark 7.1
Remind that in addition to the boundary conditions that comes from the seven constraints presented before, a few additional boundary conditions are needed for each infinite-dimensional subsystem:

- *No flow through the tank walls:* $e_2^F(-a/2,t) = e_2^F(a/2,t) = 0$*;*
- *Fixed end for torsion:* $e_2^T(0,t) = 0$*;*
- *Fixed end for bending:* $e_1^B(0,t) = \frac{\partial e_1^B}{\partial z}(0,t) = 0$.

Remark 7.2
An alternative, and more precise way, of coupling the elements is possible. In Eq. 7.13 we assumed equal *velocities for the beam deflection and tank with liquid. Using this assumption, we are also considering that the center of gravity of the fluid is at the same point as the interconnection point. This assumption is only exact when the tank is 100% filled (and there is no sloshing). For partial filling ratios of the tank, there is an offset between the center of the tank and the center of gravity of the fluid.*

It is possible to rewrite the interconnection between the beam and the fluid starting with the following kinematic constraint:

$$\dot{D}(t) = e_1^B(L,t) - y_{CG}\,\dot{\theta}_T(t)\,, \tag{7.20}$$

where y_{CG} is the offset between the center of the tank and center of gravity. Thus, the speed of the center of mass of the fluid ($\dot{D}(t)$) depends both on the tip speed of the beam due to bending ($e_1^B(L,t)$), and the rotation speed due to torsion ($\dot{\theta}_T(t)$).

The two other kinematic conditions (Eqs. 7.14 and 7.15) remain unchanged. Finally,

$$\begin{aligned}\dot{H} = &+ \dot{D}(t) \underbrace{\left(-\frac{\partial}{\partial z} e_2^B(L,t) + F_{ext}(t)\right)}_{F'_\Sigma} + \dot{\theta}_B(t) \underbrace{\left(e_2^B(L,t) + M_{ext,B}(t)\right)}_{M'_{\Sigma,B}} \\ &+ \dot{\theta}_T(t) \underbrace{\left(e_1^T(L,t) + M_{ext,T}(t) + M_{ext}(t) + y_{CG}\, F_{ext}(t)\right)}_{M'_{\Sigma,T}} + y_v(t) v(t)\,. \end{aligned} \tag{7.21}$$

Where again: $F'_\Sigma = M'_{\Sigma,B} = M'_{\Sigma,T} = 0$. Note that $M'_{\Sigma,T}$ now includes the moment of force due to the offset of the center of gravity of fluid.

Numerical results for both coupling strategies will be presented in Chapter 10.

7.3 Conclusions

In this short chapter, we recalled the models and the interconnection ports of the port-Hamiltonian systems presented in the previous chapter. These systems are used to model each element of the fluid-structure experimental device.

Thanks to the physically meaningful interconnection ports, coupling the elements becomes straightforward. The kinematic conditions from Eqs. 7.13, 7.14 and 7.15, together with the dynamic conditions from Eq. 7.18 provide a power-preserving interconnection structure between the elements of the system.

One remarkable characteristic of the port-Hamiltonian systems is that this structure is model-independent: it depends only on the interconnection ports. This gives a great modularity to this approach. For instance, if the bi-dimensional shallow water equations are used, instead of the 1D used above, the interconnection structure would be the same (since force/speed, torque/angular speed are the interconnection ports of the 2D shallow water equations). Similarly, both linear and nonlinear models share the same structure.

The final system consists in a mixed finite-infinite dimensional pHs, with 6 distributed, and 6 finite-dimensional energy variables. In the following part of this thesis, each infinite-dimensional model will be approximated in such a way that the interconnection ports above will be preserved using power-preserving semi-discretization methods. After semi-discretization, the relations presented in this chapter will be used for interconnection of each module.

Part III

Structure-preserving semi-discretization

Chapter 8

A recall on power-preserving semi-discretization methods

In the previous chapters, several infinite-dimensional equations were introduced to represent phenomena like structural dynamics and fluid sloshing. Their representation as pHs allows verifying several interesting properties, like power conserving interconnection and stability. However, for practical applications (like simulation and control), obtaining a finite-dimensional approximation of the previous pHs equations is necessary.

In this chapter, we recall two power-preserving spatial discretization methods. The first is the mixed finite element method, proposed by Golo et al. (2004). It divides the domain in small "elements", and uses different low-order basis functions to approximate the energy and co-energy variables. The second is the geometric pseudo-spectral method proposed by Moulla, Lefèvre, and Maschke (2012). Instead of dividing the domain in elements, it uses high-order global basis functions.

This chapter is organized as follows. Firstly, in Section 8.1, we define the power-preserving discretization problem as well as the kind of equation for which the recalled methods were developed. Secondly, the mixed finite elements method is recalled in Section 8.2. Thirdly, the pseudo-spectral method is recalled in Section 8.3. Fourthly, the relationship between the two methods is discussed in Section 8.4. Finally, the main motivations for the extensions that will be proposed in the following chapter are presented in Section 8.5.

Contents

8.1 Definition of the power-preserving semi-discretization problem

As shown in Eq. 4.73, a typical representation of infinite-dimensional port-Hamiltonian is the following:

$$\begin{aligned} \frac{\partial \boldsymbol{\alpha}}{\partial t}(z,t) &= \mathcal{J}\boldsymbol{e}(z,t)\,, \\ \boldsymbol{u}_\partial(t) &= \mathcal{B}\boldsymbol{e}(z,t)\,, \\ \boldsymbol{y}_\partial(t) &= \mathcal{C}\boldsymbol{e}(z,t)\,, \end{aligned} \tag{8.1}$$

such that, thanks to the fact that $\mathcal{J}$ is formally skew-symmetric, a Stokes-Dirac structure can be defined with respect to the power product:

$$P := -\int_{z=0}^{L} \boldsymbol{e}^T \dot{\boldsymbol{\alpha}}\,\mathrm{d}z + \boldsymbol{y}_\partial^T \boldsymbol{u}_\partial = 0\,, \tag{8.2}$$

as presented in the example of § 4.2.2. By including the constitutive relation given by the variational derivative of the Hamiltonian with respect to the energy variables $\boldsymbol{e} = \frac{\delta H}{\delta \boldsymbol{\alpha}}$, the power balance of the system is obtained as:

$$\dot{H} = \int_{z=0}^{L} \left(\frac{\delta H}{\delta \boldsymbol{\alpha}}\right)^T \dot{\boldsymbol{\alpha}}\,\mathrm{d}z = \boldsymbol{y}_\partial^T \boldsymbol{u}_\partial\,. \tag{8.3}$$

We call here power-preserving semi-discretization methods, the methods that approximate Eq. 8.1 and preserve the port-Hamiltonian structure of the system, leading to a finite-dimensional Dirac structure, e.g.:

$$\begin{aligned} \dot{\boldsymbol{x}}(t) &= J\tilde{\boldsymbol{e}}(t) + B\boldsymbol{u}_\partial(t)\,, \\ \boldsymbol{y}_\partial(t) &= B^T\tilde{\boldsymbol{e}}(t) + D\boldsymbol{u}_\partial(t)\,, \end{aligned} \tag{8.4}$$

with power product given by:

$$P_d := -\tilde{\boldsymbol{e}}^T\dot{\boldsymbol{x}} + \boldsymbol{y}_\partial^T\boldsymbol{u}_\partial = 0\,, \tag{8.5}$$

where $\boldsymbol{x}(t)$ is the vector of approximated energy variables, $\boldsymbol{u}_\partial$ and $\boldsymbol{y}_\partial$ are the vectors of boundary ports, J is the interconnection matrix and D is the feed-through matrix, both of them being necessarily skew-symmetric. Moreover, using constitutive relations as $\tilde{\boldsymbol{e}} :=$

$\nabla_{\boldsymbol{x}} H_d(\boldsymbol{x})$, the gradient of the discretized Hamiltonian ($H_d(\boldsymbol{x})$), the continuous power balance of the original system (Eq. 8.3) is preserved:

$$\dot{H}_d = (\nabla_{\boldsymbol{x}} H_d(\boldsymbol{x}))^T \, \dot{\boldsymbol{x}} = \boldsymbol{y}_\partial^T \boldsymbol{u}_\partial \,. \tag{8.6}$$

Both the mixed finite element and geometric pseudo-spectral methods were originally developed for equations such as the wave equation, which has the following form:

$$\begin{bmatrix} \dot{x}_1(z,t) \\ \dot{x}_2(z,t) \end{bmatrix} = \underbrace{\begin{bmatrix} 0 & \partial_z \\ \partial_z & 0 \end{bmatrix}}_{\mathcal{J}_1} \underbrace{\begin{bmatrix} e_1(z,t) \\ e_2(z,t) \end{bmatrix}}_{\boldsymbol{e}} , \; z \in [0\,,\, L]\,, \tag{8.7}$$

with the following boundary ports:

$$\boldsymbol{y}_\partial(t) = \mathcal{B}\boldsymbol{e} = \begin{bmatrix} e_2(L,t) \\ -e_1(0,t) \end{bmatrix} , \quad \boldsymbol{u}_\partial(t) = \mathcal{C}\boldsymbol{e} = \begin{bmatrix} e_1(L,t) \\ e_2(0,t) \end{bmatrix} . \tag{8.8}$$

Together with constitutive relations $e_1(z,t) = \frac{\delta H}{\delta x_1}$ and $e_2(z,t) = \frac{\delta H}{\delta x_2}$, the power balance of the infinite-dimensional system is given by:

$$\dot{H} = \boldsymbol{y}_\partial^T \boldsymbol{u}_\partial \,. \tag{8.9}$$

We recall each of the methods applied to the wave equation in the sequel.

8.2 Mixed finite element method

The mixed finite element method was proposed by Golo et al. (2004). The method divides the domain in small "elements" where $z \in [a, b]$ (with $0 \leq a < b \leq L$). The equations and boundary ports, for each element, are thus given by:

$$\begin{bmatrix} \dot{x}_1(z,t) \\ \dot{x}_2(z,t) \end{bmatrix} = \underbrace{\begin{bmatrix} 0 & \partial_z \\ \partial_z & 0 \end{bmatrix}}_{\mathcal{J}_1} \underbrace{\begin{bmatrix} e_1(z,t) \\ e_2(z,t) \end{bmatrix}}_{\boldsymbol{e}} , \; z \in [a\,,\, b]\,, \tag{8.10}$$

$$\boldsymbol{y}_\partial^{ab}(t) = \begin{bmatrix} e_2(b,t) \\ -e_1(a,t) \end{bmatrix} , \quad \boldsymbol{u}_\partial^{ab}(t) = \begin{bmatrix} e_1(b,t) \\ e_2(a,t) \end{bmatrix} , \tag{8.11}$$

and the power balance inside each element is given by:

$$\dot{H}^{ab} = (\boldsymbol{y}_\partial^{ab})^T \boldsymbol{u}_\partial^{ab} \,. \tag{8.12}$$

The central idea of the discretization method is that, in each element, different approximation bases are used for each energy and co-energy variables. After discretization in space,

a finite-dimensional port-Hamiltonian system for each element is obtained. Finally, the elements are coupled and a port-Hamiltonian representation for the whole domain is obtained.

The method is briefly recalled in this section. For detailed proofs, the reader can check the original paper from Golo et al. (2004). The different approximation bases are presented in § 8.2.1. A finite-dimensional representation and the boundary ports of the system for a single element are obtained in § 8.2.2. Then, we look at the time-derivative of the Hamiltonian, which motivates the definition of alternative co-energy variables in § 8.2.3. A finite-dimensional Dirac structure for each element is thus obtained in § 8.2.4. The discretization of the Hamiltonian gives the constitutive relations that completes the pHs in § 8.2.5. Finally, the coupling of the elements is presented in § 8.2.6.

8.2.1 Approximation bases

The central idea is that different approximation bases are used for the energy (flow) and co-energy (effort) variables inside each element ($a \leq z \leq b$).

Three assumptions are considered with respect to the approximation bases:

Assumption 8.1
Each energy variable (flow space) is spatially discretized using ***one*** *spatial basis function* $w_i^{ab}(z)$ *(for* $i = 1, 2$*):*

$$\dot{x}_i(z,t) \approx \dot{x}_i^{ap}(z,t) := \dot{x}_i^{ab}(t) w_i^{ab}(z)\,, \tag{8.13}$$

where the following normalization assumption on $w_i^{ab}(z)$ *holds:*

$$\int_{z=a}^{b} w_i^{ab}(z)\,\mathrm{d}z = 1\,, \tag{8.14}$$

which means that $\dot{x}_i^{ab}(t)$ *is the integral of* $\dot{x}_i^{ap}(z,t)$ *along the element.*

Assumption 8.2
Each co-energy variable is spatially discretized using ***two*** *different basis functions* $w_i^a(z)$ *and* $w_i^b(z)$ *(for* $i = 1, 2$*):*

$$e_i(z,t) \approx e_i^{ap}(z,t) := e_i^a(t) w_i^a(z) + e_i^b(t) w_i^b(z)\,, \tag{8.15}$$

where the following boundary conditions holds:

$$w_i^a(a) = 1 \quad w_i^b(a) = 0\,, \quad w_i^a(b) = 0\,, \quad w_i^b(b) = 1\,, \tag{8.16}$$

which means that $e_i^a(t)$ *and* $e_i^b(t)$ *are the boundary values of the co-energy variables.*

Assumption 8.3
The basis functions for the energy and co-energy variable must satisfy the original equation

(Eq. 8.7) in the finite-dimensional space, i.e.:

$$\begin{aligned} \dot{x}_1^{ap}(z,t) &= \frac{\partial}{\partial z} e_2^{ap}(z,t)\,, \\ \dot{x}_2^{ap}(z,t) &= \frac{\partial}{\partial z} e_1^{ap}(z,t)\,. \end{aligned} \qquad \forall\, z \in [a,b]\,. \tag{8.17}$$

Using these assumptions, it is straightforward to prove the following relationships must hold:

$$\begin{aligned} w_1^{ab}(z) &= -\frac{\partial w_2^a}{\partial z}(z) = \frac{\partial w_2^b}{\partial z}(z)\,, \\ w_2^{ab}(z) &= -\frac{\partial w_1^a}{\partial z}(z) = \frac{\partial w_1^b}{\partial z}(z)\,. \end{aligned} \tag{8.18}$$

8.2.2 Finite-dimensional equations

Using the previous assumptions, after integration of Eq. 8.17 with respect to z along $[a,b]$ the following finite-dimensional equations are obtained:

$$\begin{aligned} \dot{x}_1^{ab}(t) &= e_2^b(t) - e_2^a(t)\,, \\ \dot{x}_2^{ab}(t) &= e_1^b(t) - e_1^a(t)\,, \end{aligned} \tag{8.19}$$

Additionally, the boundary ports defined in Eq. 8.11, can be set as a linear function of these co-energy variables:

$$\boldsymbol{y}_\partial^{ab} = \begin{bmatrix} f_{1\partial} \\ f_{2\partial} \end{bmatrix} = \begin{bmatrix} e_2^b(t) \\ -e_1^a(t) \end{bmatrix} \quad , \quad \boldsymbol{u}_\partial^{ab} = \begin{bmatrix} e_{1\partial} \\ e_{2\partial} \end{bmatrix} = \begin{bmatrix} e_1^b(t) \\ e_2^a(t) \end{bmatrix}\,. \tag{8.20}$$

Eq. 8.19 cannot be used for defining a Dirac structure, since it presents 2 "flow-like" variables ($\dot{x}_1^{ab}$ and $\dot{x}_2^{ab}$) and 4 "effort-like" variables (e_1^a,e_1^b, e_2^a and e_2^b). In the sequel, we look at the time-derivative of the Hamiltonian. This will motivate the definition alternative co-energy (effort) variables that will allow defining a Dirac structure.

8.2.3 Preserving the power balance

In this subsection, the time-derivative of the Hamiltonian in the finite-dimensional space is analyzed. This analysis will be essential to guarantee that the energy is preserved after discretization.

The time-derivative of the Hamiltonian in $[a,b]$ is given by:

$$\dot{H}^{ab} = \int_{z=a}^{b} (\dot{x}_1 e_1 + \dot{x}_2 e_2)\,\mathrm{d}z\,, \tag{8.21}$$

which can be approximated as:

$$\begin{aligned}\dot{H}^{ab} &\approx \int_{z=a}^{b} (\dot{x}_1^{ap} e_1^{ap} + \dot{x}_2^{ap} e_2^{ap})\,\mathrm{d}z\,,\\ &= \int_{z=a}^{b} \dot{x}_1^{ab}\, w_1^{ab}(z) \left(w_1^a(z) e_1^a(t) + w_1^b(z) e_1^b(t)\right) + \dot{x}_2^{ab}\, w_2^{ab}(z) \left(w_2^a(z) e_2^a(t) + w_2^b(z) e_2^b(t)\right) \mathrm{d}z\,,\end{aligned} \tag{8.22}$$

This motivates the definition of *two* alternative co-energy variables, which are given by a projection of the *four* co-energy variables previously defined:

$$\begin{aligned} e_1^{ab}(t) &:= \underbrace{\int_{z=a}^{b} w_1^{ab}(z) w_1^a(z)\,\mathrm{d}z}_{\alpha_1^a}\; e_1^a(t) \;+ \underbrace{\int_{z=a}^{b} w_1^{ab}(z) w_1^b(z)\,\mathrm{d}z}_{\alpha_1^b}\; e_1^b(t)\,,\\ e_2^{ab}(t) &:= \underbrace{\int_{z=a}^{b} w_2^{ab}(z) w_2^a(z)\,\mathrm{d}z}_{\alpha_2^a}\; e_2^a(t) \;+ \underbrace{\int_{z=a}^{b} w_2^{ab}(z) w_2^b(z)\,\mathrm{d}z}_{\alpha_2^b}\; e_2^b(t)\,, \end{aligned} \tag{8.23}$$

such that the power balance becomes the product of the *two* energy and *two* co-energy variables:

$$\dot{H}^{ab} \approx \dot{x}_1^{ab}(t) e_1^{ab}(t) + \dot{x}_2^{ab}(t) e_2^{ab}(t)\,. \tag{8.24}$$

Thanks to the assumptions of § 8.2.1, it is possible to prove that $\alpha_1^a + \alpha_1^b = 1$, $\alpha_2^a + \alpha_2^b = 1$ and $\alpha_1^a + \alpha_2^a = 1$ (see Proposition 1 of Golo (2002)). Thus, using $\alpha := \alpha_1^a$ as free parameter, Eq. 8.23 rewrites as:

$$\begin{aligned} e_1^{ab}(t) &:= \alpha e_1^a(t) + (1-\alpha) e_1^b(t)\,,\\ e_2^{ab}(t) &:= (1-\alpha) e_2^a(t) + \alpha e_2^b(t)\,. \end{aligned} \tag{8.25}$$

In addition, from the substitution of Eqs. 8.19 and 8.18 in Eq. 8.22, we get:

$$\dot{x}_1^{ab}(t) e_1^{ab}(t) + \dot{x}_2^{ab}(t) e_2^{ab}(t) = -e_1^b(t) e_2^b(t) + e_1^a(t) e_2^a(t) = (\boldsymbol{y}_\partial^{ab})^T \boldsymbol{u}_\partial^{ab}\,. \tag{8.26}$$

8.2.4 Finite-dimensional Dirac structure

Let us define the flow variables as: $\boldsymbol{f} := \begin{bmatrix} -\dot{x}_1^{ab} & -\dot{x}_2^{ab} & f_{1\partial} & f_{2\partial} \end{bmatrix}^T$, the effort variables as: $\boldsymbol{e} := \begin{bmatrix} e_1^{ab} & e_2^{ab} & e_{1\partial} & e_{2\partial} \end{bmatrix}^T$, and the following power product:

$$P := \boldsymbol{f}^T \boldsymbol{e}\,. \tag{8.27}$$

From Eq. 8.26, note that $P = 0$ for all $\boldsymbol{e}$, $\boldsymbol{f}$ that satisfies Eqs. 8.19, 8.25 and 8.23. Using the bilinear form defined in Eq. 4.39, we can verify that these three equations define a Dirac structure.

Alternatively, the Dirac structure can be easily obtained by rewriting the relationship between the flow and effort variables (from Eqs. 8.19, 8.25 and 8.23) using the image representation (as Eq. 4.46):

$$\begin{bmatrix} -\dot{x}_1^{ab} \\ -\dot{x}_2^{ab} \\ f_{1\partial} \\ f_{2\partial} \end{bmatrix} = \underbrace{\begin{bmatrix} 0 & 0 & 1 & -1 \\ 1 & -1 & 0 & 0 \\ 0 & 0 & 0 & 1 \\ -1 & 0 & 0 & 0 \end{bmatrix}}_{F} \begin{bmatrix} e_1^a \\ e_1^b \\ e_2^a \\ e_2^b \end{bmatrix} \quad , \quad \begin{bmatrix} e_1^{ab} \\ e_2^{ab} \\ e_{1\partial} \\ e_{2\partial} \end{bmatrix} = \underbrace{\begin{bmatrix} \alpha & 1-\alpha & 0 & 0 \\ 0 & 0 & 1-\alpha & \alpha \\ 0 & 1 & 0 & 0 \\ 0 & 0 & 1 & 0 \end{bmatrix}}_{E} \begin{bmatrix} e_1^a \\ e_1^b \\ e_2^a \\ e_2^b \end{bmatrix} . \tag{8.28}$$

Since $EF^T + FE^T = 0$ and $\text{rank}[F|E] = 4$, Eq. 8.28 defines an image representation of a Dirac structure.

After manipulations, the equations can also be rewritten using the explicit representation as:

$$\begin{aligned} \begin{bmatrix} \dot{x}_1^{ab} \\ \dot{x}_2^{ab} \end{bmatrix} &= \underbrace{\begin{bmatrix} 0 & \frac{1}{\alpha} \\ -\frac{1}{\alpha} & 0 \end{bmatrix}}_{J^{ab}} \begin{bmatrix} e_1^{ab} \\ e_2^{ab} \end{bmatrix} + \underbrace{\begin{bmatrix} 0 & -\frac{1}{\alpha} \\ \frac{1}{\alpha} & 0 \end{bmatrix}}_{B^{ab}} \boldsymbol{u}_\partial^{ab} , \\ \boldsymbol{y}_\partial^{ab} &= \underbrace{\begin{bmatrix} 0 & \frac{1}{\alpha} \\ -\frac{1}{\alpha} & 0 \end{bmatrix}}_{B^{abT}} \begin{bmatrix} e_1^{ab} \\ e_2^{ab} \end{bmatrix} + \underbrace{\begin{bmatrix} 0 & \frac{\alpha-1}{\alpha} \\ \frac{1-\alpha}{\alpha} & 0 \end{bmatrix}}_{D_\partial^{ab}} \boldsymbol{u}_\partial^{ab} . \end{aligned} \tag{8.29}$$

Note that Eq. 8.29 exhibits a direct feedthrough matrix D_∂^{ab} that is only zero for $\alpha = 1$.

8.2.5 Discretization of the Hamiltonian

Finally, in order to properly define the finite-dimensional port-Hamiltonian system, constitutive relationships are needed to find the values of the co-energy variables e_i^{ab}. To do this, a discretized Hamiltonian that approximates the infinite-dimensional Hamiltonian is defined:

Definition 8.1
The discretized Hamiltonian H_d^{ab} in $[a\,,b]$ is defined as:

$$H_d^{ab}(x_1^{ab}(t), x_2^{ab}(t)) := H\left[x_1(z,t) = {x_1}^{ab}(t) w_1^{ab}(z),\, x_2(z,t) = {x_2}^{ab}(t) w_2^{ab}(z)\right] . \tag{8.30}$$

With this definition, the time-derivative of H_d is given by:

$$\dot{H}_d^{ab} = \frac{\partial H_d^{ab}}{\partial x_1^{ab}} \dot{x}_1^{ab}(t) + \frac{\partial H_d^{ab}}{\partial x_2^{ab}} \dot{x}_2^{ab}(t) . \tag{8.31}$$

Note that using:

$$\begin{aligned} e_1^{ab} &= \frac{\partial H_d^{ab}}{\partial x_1^{ab}}\,, \\ e_2^{ab} &= \frac{\partial H_d^{ab}}{\partial x_2^{ab}}\,, \end{aligned} \tag{8.32}$$

the original power-balance is *exactly* preserved, i.e.:

$$\dot{H}_d^{ab} = e_1^{ab}(t)\dot{x}_1^{ab}(t) + e_2^{ab}(t)\dot{x}_2^{ab}(t) = (\boldsymbol{y}_\partial^{ab})^T \boldsymbol{u}_\partial = \dot{H}^{ab}\,. \tag{8.33}$$

8.2.6 Concatenation of the elements: finding the global equations

Previously, the equations for each element were presented in explicit form in Eq. 8.29. In order to obtain an approximation in the whole domain $z = [0, L]$, the elements must be coupled using the following relationships between the boundary values:

$$e_1^{b(n)} = e_1^{a(n+1)}\,, \tag{8.34}$$

$$e_2^{b(n)} = e_2^{a(n+1)}\,, \tag{8.35}$$

where the index (n) is used to identify each element ($n = 1, 2, \ldots, N_e$, where N_e is the number of elements).

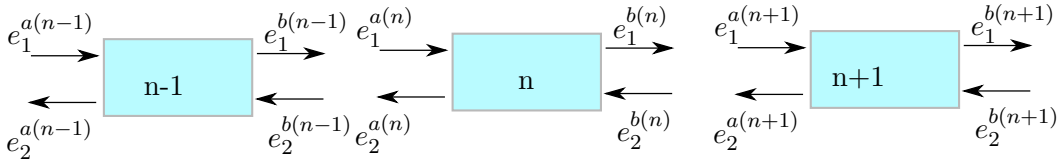

Figure 8.1: Concatenation of the elements. Inward arrows represent the inputs of the elements. Outward arrows represent the outputs.

By successive substitutions, the global equations are found:

$$\begin{aligned} \begin{bmatrix} \dot{\mathbf{x}}_1 \\ \dot{\mathbf{x}}_2 \end{bmatrix} &= \underbrace{\begin{bmatrix} 0 & M \\ -M^T & 0 \end{bmatrix}}_{J} \begin{bmatrix} \boldsymbol{e}_1 \\ \boldsymbol{e}_2 \end{bmatrix} + \underbrace{\begin{bmatrix} 0 & \mathbf{b}_1 \\ \mathbf{b}_2 & 0 \end{bmatrix}}_{B} \boldsymbol{u}_\partial\,, \\ \boldsymbol{y}_\partial &= \underbrace{\begin{bmatrix} 0 & \mathbf{b}_2^T \\ \mathbf{b}_1^T & 0 \end{bmatrix}}_{B^T} \begin{bmatrix} \boldsymbol{e}_1 \\ \boldsymbol{e}_2 \end{bmatrix} + \underbrace{\begin{bmatrix} 0 & \left(\frac{\alpha-1}{\alpha}\right)^{N_e} \\ -\left(\frac{\alpha-1}{\alpha}\right)^{N_e} & 0 \end{bmatrix}}_{D_\partial} \boldsymbol{u}_\partial\,, \end{aligned} \tag{8.36}$$

where $\boldsymbol{x}_i = [x_i^{ab(1)} \quad x_i^{ab(2)} \quad \ldots \quad x_i^{ab(N_e)}]^T$, $\boldsymbol{e}_i = [e_i^{ab(1)} \quad e_i^{ab(2)} \quad \ldots \quad e_i^{ab(N_e)}]^T$, $\boldsymbol{u}_\partial = \begin{bmatrix} e_1(L) & e_2(0) \end{bmatrix}^T$,

$\boldsymbol{y}_\partial = \begin{bmatrix} e_2(L) & -e_1(0) \end{bmatrix}^T$ and:

$$M = \begin{bmatrix} \frac{1}{\alpha} & 0 & 0 & 0 & 0 & 0 \\ -\frac{1}{\alpha^2} & \frac{1}{\alpha} & 0 & 0 & 0 & 0 \\ -\frac{1}{\alpha^2}\left(\frac{\alpha-1}{\alpha}\right) & -\frac{1}{\alpha^2} & \frac{1}{\alpha} & 0 & 0 & 0 \\ -\frac{1}{\alpha^2}\left(\frac{\alpha-1}{\alpha}\right)^2 & -\frac{1}{\alpha^3} - (\alpha-1) & -\frac{1}{\alpha^2} & \frac{1}{\alpha} & 0 & 0 \\ \vdots & \vdots & \vdots & \ddots & \ddots & \vdots \\ -\frac{1}{\alpha^2}\left(\frac{\alpha-1}{\alpha}\right)^{N_e-2} & -\frac{1}{\alpha^2}\left(\frac{\alpha-1}{\alpha}\right)^{N_e-3} & \dots & -\frac{1}{\alpha^2}\left(\frac{\alpha-1}{\alpha}\right) & -\frac{1}{\alpha^2} & \frac{1}{\alpha} \end{bmatrix}, \tag{8.37}$$

$$\mathbf{b}_1 = \begin{bmatrix} -\frac{1}{\alpha} \\ -\frac{1}{\alpha^2}(\alpha-1) \\ -\frac{1}{\alpha^3}(\alpha-1)^2 \\ -\frac{1}{\alpha^4}(\alpha-1)^3 \\ \vdots \\ -\frac{1}{\alpha}\left(\frac{\alpha-1}{\alpha}\right)^{N_e-1} \end{bmatrix}, \quad \mathbf{b}_2 = \begin{bmatrix} \frac{1}{\alpha}\left(\frac{\alpha-1}{\alpha}\right)^{N_e-1} \\ \vdots \\ \frac{1}{\alpha^4}(\alpha-1)^3 \\ \frac{1}{\alpha^3}(\alpha-1)^2 \\ \frac{1}{\alpha^2}(\alpha-1) \\ \frac{1}{\alpha} \end{bmatrix}. \tag{8.38}$$

The total Hamiltonian is given by:

$$H_d(\boldsymbol{x}_1, \boldsymbol{x}_2) = \sum_{n=1}^{N_e} H_d^{ab(n)}(x_1^{ab(n)}, x_2^{ab(n)}), \tag{8.39}$$

and the co-energy variables are given by:

$$\begin{aligned} \boldsymbol{e}_1 :=& \nabla_{\boldsymbol{x}_1} H_d, \\ \boldsymbol{e}_2 :=& \nabla_{\boldsymbol{x}_2} H_d. \end{aligned} \tag{8.40}$$

Remark 8.1
A usual basis function for the mixed finite element method is given by the spline interpolation (used e.g. in (Golo et al., 2004; Hamroun, Lefèvre, and Mendes, 2007; Baaiu et al., 2009), i.e.:

$$w_1^{ab}(z) = w_2^{ab}(z) = \frac{1}{b-a}, \quad a \le z \le b, \tag{8.41}$$

which obviously satisfies assumption 8.1. Then, from Eq. 8.18 and assumption 8.2:

$$w_1^a(z) = w_2^a(z) = \frac{b-z}{b-a}, \quad a \le z \le b, \tag{8.42}$$

$$w_1^b(z) = w_2^b(z) = \frac{z-a}{b-a}, \quad a \le z \le b. \tag{8.43}$$

The value of α can be easily evaluated and is given by $\alpha = \int_{z=a}^{b} w_1^{ab}(z) w_1^a(z)\,\mathrm{d}z = 0.5$.

Remark 8.2
For any *value of α, the finite-dimensional approximation of the system is a Dirac structure. Consequently, together with a choice of constitutive relationship, it leads to the definition of a pHs. Several references (Le Gorrec et al., 2011; Hamroun, 2009; Hamroun et al., 2010) use $\alpha = 1$, even though this value does not come from the choice of a basis function that satisfies the original assumptions of § 8.2.1. Note that with $\alpha = 1$, the matrices M, $\boldsymbol{b}_1$ and $\boldsymbol{b}_2$ become sparser. Additionally, the direct transmission matrix D_∂ becomes equal to zero. As pointed out by Kotyczka (2016), this choice leads to a numerical scheme that is equivalent to finite volumes with staggered grids.*

8.3 Pseudo-spectral method

Here, we recall the approach detailed by Moulla, Lefèvre, and Maschke (2012). As in the case of mixed finite elements, the key idea of the method is that different approximation bases must be used for the energy and co-energy variables. The main difference is that high-order global[1] basis functions are used, instead of subdivising the domain in small elements.

Firstly, the approximation basis for each variable is presented in § 8.3.1. Secondly, a finite-dimensional version of the equations is shown in § 8.3.2. Thirdly, the time-derivative of the Hamiltonian in the finite-dimensional space is analyzed in § 8.3.3: this motivates the definition of boundary port-variables that guarantee the power-conservation of the system. Then, the finite-dimensional equations, together with the definition of the co-energy and port variables are combined to define a finite-dimensional Dirac structure in § 8.3.4. Finally, the discretization of the Hamiltonian gives the constitutive relations that complete the finite-dimensional pHs in § 8.3.5.

8.3.1 Approximation basis

The energy and co-energy variables are approximated into a finite-dimensional space using polynomial interpolation. Different degrees for the polynomial basis are used for each of these variables. For $j = 1, 2$:

$$x_j(z,t) \approx x_j^{ap}(z,t) := \sum_{i=1}^{N} x_j^i(t)\phi^i(z) = \boldsymbol{x}_j{}^T(t)\,\boldsymbol{\phi}(z)\,, 0 < z < L\,, \tag{8.44}$$

$$e_j(z,t) \approx e_j^{ap}(z,t) := \sum_{i=1}^{N+1} e_j^i(t)\psi^i(z) = \boldsymbol{e}_j{}^T(t)\,\boldsymbol{\psi}(z)\,, 0 < z < L\,. \tag{8.45}$$

The energy variables are approximated using N basis functions ($\boldsymbol{x}_j, \boldsymbol{\phi} \in \mathbb{R}^N$) , while the co-energy variables are approximated with $N+1$ ($\boldsymbol{e}_j, \boldsymbol{\psi} \in \mathbb{R}^{N+1}$). Thanks to this particular choice, the spatial derivatives can be exactly computed in the finite-dimensional space, using

[1] valid in all the domain: $z = [0,\, L]$.

polynomial interpolation.

In Moulla, Lefèvre, and Maschke (2012), Lagrange polynomials are used as basis functions, i.e., polynomials such that:

$$\ell^i(z) = \prod_{\substack{0 \leq m \leq N \\ m \neq i}} \frac{z - z_m}{z_i - z_m} \tag{8.46}$$

When using these polynomials (or other cardinal basis function), the coefficients of $\boldsymbol{x_j}$ and $\boldsymbol{e_j}$ are the values of $x_j(z,t)$ and $e_j(z,t)$ evaluated at the collocation points. The collocation points are denoted by z_{xi} for the energy space and z_{ei} for the co-energy space. Note that the basis for the energy variables has N collocation points, while the basis for co-energy variables has $N+1$ points.

8.3.2 Finite-dimensional equations

From Eq. 8.7 and using approximations from Eqs. 8.44 and 8.45, we get:

$$\begin{aligned} \boldsymbol{\phi}^T(z)\dot{\boldsymbol{x}}_1(t) &= {\boldsymbol{\psi}_z}^T(z)\boldsymbol{e}_2(t)\,, \\ \boldsymbol{\phi}^T(z)\dot{\boldsymbol{x}}_2(t) &= {\boldsymbol{\psi}_z}^T(z)\boldsymbol{e}_1(t)\,, \end{aligned} \tag{8.47}$$

where the subscript z in $\boldsymbol{\psi}_z(z)$ denotes the spatial derivative of the vector function $\boldsymbol{\psi}(z)$.

The evaluation of Eq. 8.47 at the N collocation points z_{xi}, leads to the finite-dimensional version of Eq. 8.7:

$$\begin{aligned} \dot{\boldsymbol{x}}_1 &= D_1\boldsymbol{e}_2\,, \\ \dot{\boldsymbol{x}}_2 &= D_1\boldsymbol{e}_1\,, \end{aligned} \tag{8.48}$$

where D_1 is defined as follows:

Definition 8.2
The differentiation matrix D_1, of size $N \times (N+1)$, is defined as:

$$D_1 = \begin{bmatrix} {\boldsymbol{\psi}_z}^T(z_{x1}) \\ {\boldsymbol{\psi}_z}^T(z_{x2}) \\ {\boldsymbol{\psi}_z}^T(z_{x3}) \\ \vdots \\ {\boldsymbol{\psi}_z}^T(z_{x(N)}) \end{bmatrix} \tag{8.49}$$

where z_{xi} are the collocation points related to the finite-dimensional energy variables.

Note that this matrix exactly computes the spatial derivative of the effort variables at the flow variables collocation points. This is very similar to classical collocation (pseudo-spectral) methods (Trefethen, 2000; Boyd, 2001), except that two different bases are being used here. The matrix D_1 is of dimension $N \times (N+1)$.

The boundary ports ($\boldsymbol{u}_\partial$, $\boldsymbol{y}_\partial \in \mathbb{R}^N$) defined in Eq. 8.8 can be set as a linear function of the co-energy variables $\boldsymbol{e}_1$ and $\boldsymbol{e}_2$:

$$\boldsymbol{y}_\partial = \begin{bmatrix} f_{1\partial} \\ f_{2\partial} \end{bmatrix} = \begin{bmatrix} \boldsymbol{\psi}^T(L)\boldsymbol{e}_2 \\ -\boldsymbol{\psi}^T(0)\boldsymbol{e}_1 \end{bmatrix}, \boldsymbol{u}_\partial = \begin{bmatrix} e_{1\partial} \\ e_{2\partial} \end{bmatrix} = \begin{bmatrix} \boldsymbol{\psi}^T(L)\boldsymbol{e}_1 \\ \boldsymbol{\psi}^T(0)\boldsymbol{e}_2 \end{bmatrix}. \tag{8.50}$$

As it happened in the mixed finite element method, the number of discrete energy and co-energy variables is not the same (since $\boldsymbol{e}_1$, $\boldsymbol{e}_2 \in \mathbb{R}^{N+1}$ and $\boldsymbol{x}_1$, $\boldsymbol{x}_2 \in \mathbb{R}^N$). Thus, a projection of the co-energy variables is recalled in the following subsection. Together with the result of the following proposition, it will allow preserving the energy balance after spatial discretization.

Proposition 8.1
Using the polynomial approximation basis defined in § 8.3.1, such that the differential equations are satisfied at the collocation points (Eq. 8.48), the differential equation is also satisfied at all other points of the domain, i.e.:

$$\begin{aligned} \dot{x}_1^{ap}(z,t) &= \frac{\partial}{\partial z} e_2^{ap}(z,t)\,, \\ \dot{x}_2^{ap}(z,t) &= \frac{\partial}{\partial z} e_1^{ap}(z,t)\,. \end{aligned} \qquad \forall\, z \in [0, L]\,. \tag{8.51}$$

Proof. Let $f(z) := \boldsymbol{f}^T\boldsymbol{\phi}(z)$ be a polynomial of degree N, $g(z) := \boldsymbol{g}^T\boldsymbol{\psi}(z)$ a polynomial of degree $N+1$. If $f(z) = \partial_z g(z)$:

$$\boldsymbol{f}^T\boldsymbol{\phi}(z) = \boldsymbol{g}^T\boldsymbol{\psi}_z(z)\,,$$

evaluating the previous expression at each collocation point z_{xi}:

$$\boldsymbol{f} = D_1\boldsymbol{g}\,. \tag{8.52}$$

Since both $\boldsymbol{f}^T\boldsymbol{\phi}(z)$ and $\boldsymbol{g}^T\boldsymbol{\psi}_z(z)$ are polynomials of degree N, the following equation is valid for any $\boldsymbol{g}$ and z:

$$\boldsymbol{g}^T {D_1}^T\boldsymbol{\phi}(z) = \boldsymbol{g}^T\boldsymbol{\psi}_z(z)\,, \tag{8.53}$$

which leads to:

$$\boldsymbol{\phi}^T(z)D_1 = \boldsymbol{\psi}_z^T(z)\,, \forall z \in [0\,,\, L]\,. \tag{8.54}$$

Multiplying Eq. 8.48 by $\boldsymbol{\phi}^T(z)$, we get:

$$\begin{aligned} \boldsymbol{\phi}^T(z)\dot{\boldsymbol{x}}_1 &= \boldsymbol{\phi}^T(z)D_1\boldsymbol{e}_2\,, \\ \boldsymbol{\phi}^T(z)\dot{\boldsymbol{x}}_2 &= \boldsymbol{\phi}^T(z)D_1\boldsymbol{e}_1\,, \end{aligned}, \quad \forall\, z \in [0\,,\, L]\,, \tag{8.55}$$

and thanks to Eq. 8.54:

$$\begin{aligned} \boldsymbol{\phi}^T(z)\dot{\boldsymbol{x}}_1 &= {\boldsymbol{\psi}_z}^T(z)\boldsymbol{e}_2\,, \\ \boldsymbol{\phi}^T(z)\dot{\boldsymbol{x}}_2 &= {\boldsymbol{\psi}_z}^T(z)\boldsymbol{e}_1\,. \end{aligned} \tag{8.56}$$

Finally:

$$\begin{aligned} \dot{x}_1^{ap}(z,t) &= \frac{\partial}{\partial z} e_2^{ap}(z,t)\,, \\ \dot{x}_2^{ap}(z,t) &= \frac{\partial}{\partial z} e_1^{ap}(z,t)\,. \end{aligned} \qquad \forall\, z \in [0,L]\,. \tag{8.57}$$

□

8.3.3 Preserving the power balance

In this section, the time-derivative of the Hamiltonian in the finite-dimensional space will be analyzed. This analysis will be essential to guarantee that the energy is preserved after semi-discretization.

The time-derivative of the Hamiltonian is given by:

$$\begin{aligned} \dot{H} &= \int_{z=0}^{L} \left(\delta_{x_1} H\, \dot{x}_1 + \delta_{x_2} H\, \dot{x}_2\right) \mathrm{d}z\,, \\ &= \int_{z=0}^{L} \left(e_1 \dot{x}_1 + e_2 \dot{x}_2\right) \mathrm{d}z\ . \end{aligned} \tag{8.58}$$

After using the finite-dimensional approximations (Eqs. 8.44 and 8.45) this energy flow becomes:

$$\dot{H} \approx \boldsymbol{e}_1{}^T M_{\psi\phi}\, \dot{\boldsymbol{x}}_1 + \boldsymbol{e}_2{}^T M_{\psi\phi}\, \dot{\boldsymbol{x}}_2\,, \tag{8.59}$$

where

$$M_{\psi\phi} = \int_{z=0}^{L} \boldsymbol{\psi}(z) \boldsymbol{\phi}^T(z)\, \mathrm{d}z\,. \tag{8.60}$$

is an $(N+1) \times N$ matrix.

This motivates the definition of new co-energy variables of the same dimension as the energy variables $\boldsymbol{x}_1$ and $\boldsymbol{x}_2$, namely:

$$\begin{aligned} \tilde{\boldsymbol{e}}_1 &:= M_{\psi\phi}{}^T \boldsymbol{e_1}\,, \\ \tilde{\boldsymbol{e}}_2 &:= M_{\psi\phi}{}^T \boldsymbol{e_2}\,, \end{aligned} \tag{8.61}$$

such that the energy flow is given by the product of these energy and co-energy variables:

$$\dot{H} \approx \tilde{\boldsymbol{e}}_1{}^T \dot{\boldsymbol{x}}_1 + \tilde{\boldsymbol{e}}_2{}^T \dot{\boldsymbol{x}}_2\,. \tag{8.62}$$

After substitution of the finite-dimensional equations (Eq. 8.48) into Eq. 8.62, we get:

$$\begin{aligned} \dot{H} &\approx \boldsymbol{e}_1{}^T M_{\psi\phi} D_1 \boldsymbol{e}_2 + \boldsymbol{e}_2{}^T M_{\psi\phi} D_1 \boldsymbol{e}_1\,, \\ &= \boldsymbol{e}_1{}^T \left(M_{\psi\phi} D_1 + D_1{}^T M_{\psi\phi}{}^T\right) \boldsymbol{e}_2\,, \end{aligned} \tag{8.63}$$

Proposition 8.2
As in the infinite-dimensional case, the energy flow in Eq. 8.63 is related to the boundary conditions only, so that:

$$\boldsymbol{e}_1{}^T \left(M_{\psi\phi} D_1 + D_1{}^T M_{\psi\phi}{}^T \right) \boldsymbol{e}_2 = \boldsymbol{e}_1{}^T \boldsymbol{\psi}(z) \boldsymbol{\psi}(z)^T \boldsymbol{e}_1 \Big|_{z=0}^{L} = \boldsymbol{y}_\partial^T \boldsymbol{u}_\partial \,. \tag{8.64}$$

Proof.

$$\begin{aligned} \boldsymbol{e}_1{}^T \left(M_{\psi\phi} D_1 + D_1{}^T M_{\psi\phi}{}^T \right) \boldsymbol{e}_2 =& \boldsymbol{e}_1{}^T \left(\int_{z=0}^{L} \boldsymbol{\psi}(z) \boldsymbol{\phi}^T(z) D_1 \, \mathrm{d}z \right) \boldsymbol{e}_2 \\ &+ \boldsymbol{e}_2{}^T \left(\int_{z=0}^{L} D_1{}^T \boldsymbol{\phi}(z) \boldsymbol{\psi}_z{}^T(z) \, \mathrm{d}z \right) \boldsymbol{e}_1 \,, \end{aligned} \tag{8.65}$$

but from the proof of Proposition 8.1, we have that $\boldsymbol{\phi}^T(z) D_1 = \boldsymbol{\psi}_z^T(z) \, \forall \, z \in [0, \, L]$, so:

$$\begin{aligned} \boldsymbol{e}_1{}^T \left(M_{\psi\phi} D_1 + D_1{}^T M_{\psi\phi}{}^T \right) \boldsymbol{e}_2 &= \boldsymbol{e}_1{}^T \left(\int_{z=0}^{L} \boldsymbol{\psi}(z) \boldsymbol{\psi}_z{}^T(z) \, \mathrm{d}z \right) \boldsymbol{e}_2 + \boldsymbol{e}_2{}^T \left(\int_{z=0}^{L} \boldsymbol{\psi}_z \boldsymbol{\psi}_z{}^T(z) \, \mathrm{d}z \right) \boldsymbol{e}_1 \,, \\ &= \boldsymbol{e}_1{}^T \left(\int_{z=0}^{L} \partial_z \left(\boldsymbol{\psi}(z) \boldsymbol{\psi}^T(z) \right) \mathrm{d}z \right) \boldsymbol{e}_2 \,, \\ &= \boldsymbol{e}_1{}^T \left(\boldsymbol{\psi}(z) \boldsymbol{\psi}(z)^T \right) \boldsymbol{e}_2 \Big|_{z=0}^{L} = \boldsymbol{y}_\partial^T \boldsymbol{u}_\partial \,. \end{aligned} \tag{8.66}$$

□

8.3.4 Finite-dimensional Dirac structure

The flow and effort variables ($\boldsymbol{f}$ and $\boldsymbol{e}$) are defined as:

$$\boldsymbol{f} := \begin{bmatrix} -\dot{\boldsymbol{x}}_1 & f_{1\partial} & -\dot{\boldsymbol{x}}_2 & f_{2\partial} \end{bmatrix}^T \,, \quad \boldsymbol{e} := \begin{bmatrix} \tilde{\boldsymbol{e}}_1 & e_{1\partial} & \tilde{\boldsymbol{e}}_2 & e_{2\partial} \end{bmatrix}^T \,, \tag{8.67}$$

where both $\boldsymbol{f}$ and $\boldsymbol{e} \in \mathbb{R}^{2N+2}$. A power product is also defined: $P = \boldsymbol{f}^T \boldsymbol{e}$, that is equal to zero for all ($\boldsymbol{e}$, $\boldsymbol{f}$) that satisfy Eqs. 8.48, 8.50 and 8.61.

Using the finite-dimensional Eqs. 8.48, the co-energy variables definition from Eq. 8.61 and the boundary ports from Eq. 8.50, it is possible to write:

$$\begin{bmatrix} -\dot{\boldsymbol{x}}_1 \\ f_{1\partial} \\ -\dot{\boldsymbol{x}}_2 \\ f_{2\partial} \end{bmatrix} = \begin{bmatrix} 0 & -D_1 \\ 0 & \boldsymbol{\psi}^T(L) \\ -D_1 & 0 \\ -\boldsymbol{\psi}^T(0) & 0 \end{bmatrix} \begin{bmatrix} \boldsymbol{e}_1 \\ \boldsymbol{e}_2 \end{bmatrix} \,, \quad \begin{bmatrix} \tilde{\boldsymbol{e}}_1 \\ e_{1\partial} \\ \tilde{\boldsymbol{e}}_2 \\ e_{2\partial} \end{bmatrix} = \begin{bmatrix} M_{\psi\phi}{}^T & 0 \\ \boldsymbol{\psi}^T(L) & 0 \\ 0 & M_{\psi\phi}{}^T \\ 0 & \boldsymbol{\psi}^T(0) \end{bmatrix} \begin{bmatrix} \boldsymbol{e}_1 \\ \boldsymbol{e}_2 \end{bmatrix} \,, \tag{8.68}$$

which is an image representation of a Dirac structure, as defined in Eq. 4.46. This equation

can be rewritten using an explicit representation as:[2]

$$\begin{bmatrix} -\dot{\boldsymbol{x}}_1 \\ f_{1\partial} \\ -\dot{\boldsymbol{x}}_2 \\ f_{2\partial} \end{bmatrix} = \begin{bmatrix} 0 & \begin{pmatrix} -D_1 \\ \boldsymbol{\psi}^T(L) \end{pmatrix} \begin{pmatrix} {M_{\psi\phi}}^T \\ \boldsymbol{\psi}^T(0) \end{pmatrix}^{-1} \\ \begin{pmatrix} -D_1 \\ -\boldsymbol{\psi}^T(0) \end{pmatrix} \begin{pmatrix} {M_{\psi\phi}}^T \\ \boldsymbol{\psi}^T(L) \end{pmatrix}^{-1} & 0 \end{bmatrix} \begin{bmatrix} \tilde{\boldsymbol{e}}_1 \\ e_{1\partial} \\ \tilde{\boldsymbol{e}}_2 \\ e_{2\partial} \end{bmatrix}. \tag{8.69}$$

The skew-symmetry of the matrix in Eq. 8.69 is easily proven by the product of flow and effort variables (Eqs. 8.68), which is equal to zero, thanks to Proposition 8.2.

Finally, Eq. 8.69 can be rewritten in a more classical way (as Eq. 4.8) by simply rearranging its rows and columns:

$$\begin{bmatrix} -\dot{\boldsymbol{x}} \\ \boldsymbol{y}_\partial \end{bmatrix} = \begin{bmatrix} -J & -B \\ B^T & D \end{bmatrix} \begin{bmatrix} \tilde{\boldsymbol{e}} \\ \boldsymbol{u}_\partial \end{bmatrix}, \tag{8.70}$$

where $\dot{\boldsymbol{x}} = \begin{bmatrix} {\dot{\boldsymbol{x}}_1}^T & {\dot{\boldsymbol{x}}_2}^T \end{bmatrix}^T$, $\tilde{\boldsymbol{e}} = \begin{bmatrix} \tilde{\boldsymbol{e}}_1 & \tilde{\boldsymbol{e}}_2 \end{bmatrix}^T$, $\boldsymbol{y}_\partial = \begin{bmatrix} e_2(L,t) & -e_1(0,t) \end{bmatrix}^T$ and $\boldsymbol{u}_\partial = \begin{bmatrix} e_1(L,t) & e_2(0,t) \end{bmatrix}^T$. Finally, J and D are skew-symmetric matrices that can be extracted from Eq. 8.69 by permutations of the appropriate elements.

Remark 8.3
In this thesis, we preferred to use the explicit representation (Eq. 8.69), instead of the image representation (Eq. 8.68). The explicit representation is usually computationally cheaper to simulate, and also more common for control design. However, for large N, the matrices $\begin{pmatrix} M^T \\ \boldsymbol{\psi}^T(L) \end{pmatrix}$ and $\begin{pmatrix} M^T \\ \boldsymbol{\psi}^T(0) \end{pmatrix}$ lose conditioning, and the numerical computation of its inverse might be inaccurate. Thus, the use of the image representation might be preferable in some cases. The image representation is implicit, and Differential-Algebraic methods are needed for simulation.

8.3.5 Discretization of the Hamiltonian

Finally, constitutive relations are needed to find the values of the co-energy variables $\tilde{\boldsymbol{e}}_1$ and $\tilde{\boldsymbol{e}}_2$. To do this, a discretized Hamiltonian that approximates the infinite-dimensional Hamiltonian is defined:

Definition 8.3
The discretized Hamiltonian H_d is defined as:

$$H_d(\boldsymbol{x}_1, \boldsymbol{x}_2) := H\left[x_1(z,t) = {\boldsymbol{x}_1}^T(t)\boldsymbol{\phi}(z),\, x_2(z,t) = {\boldsymbol{x}_2}^T(t)\boldsymbol{\phi}(z)\right]. \tag{8.71}$$

[2] The matrices $\begin{pmatrix} M^T \\ \boldsymbol{\psi}^T(L) \end{pmatrix}$ and $\begin{pmatrix} M^T \\ \boldsymbol{\psi}^T(0) \end{pmatrix}$ are square and supposed invertible.

With this definition, the time-derivative of H_d is given by:

$$\dot{H}_d(\boldsymbol{x}_1, \boldsymbol{x}_2) = (\nabla_{\boldsymbol{x}_1} H_d)^T \dot{\boldsymbol{x}}_1 + (\nabla_{\boldsymbol{x}_1} H_d)^T \dot{\boldsymbol{x}}_2 \,. \tag{8.72}$$

Note that using:

$$\begin{aligned} \tilde{\boldsymbol{e}}_1 &= \nabla_{\boldsymbol{x}_1} H_d(\boldsymbol{x}_1, \boldsymbol{x}_2) \,, \\ \tilde{\boldsymbol{e}}_2 &= \nabla_{\boldsymbol{x}_2} H_d(\boldsymbol{x}_1, \boldsymbol{x}_2) \,, \end{aligned} \tag{8.73}$$

the original power-balance is exactly preserved, i.e.:

$$\dot{H}_d = \tilde{\boldsymbol{e}}_1{}^T(t)\dot{\boldsymbol{x}}_1(t) + \tilde{\boldsymbol{e}}_2(t)\dot{\boldsymbol{x}}_2(t) = \boldsymbol{y}_\partial^T \boldsymbol{u}_\partial = \dot{H} \,. \tag{8.74}$$

8.4 Comparison between the two methods

Both the mixed finite element method and pseudo-spectral method follow the general procedure below:

Firstly, different approximation basis are choosen for the energy and co-energy variables: $\dot{x}_i(z,t) \in \mathcal{F}_i$ is approximated as $\dot{x}_i^{ap}(z,t) \in \mathcal{F}_i^{ap}$ such that $\dot{x}_i^{ap}(z,t) = \sum_{j=1}^{N_{xi}} \dot{x}_i^j(t)\phi_i^j(z)$ and $\dot{e}_i(z,t) \in \mathcal{E}_i$ is approximated as $\dot{e}_i^{ap}(z,t) \in \mathcal{E}_i^{ap}$ such that $\dot{e}_i^{ap}(z,t) = \sum_{j=1}^{N_{ei}} \dot{e}_i^j(t)\psi_i^j(z)$. In addition, the span of the approximated spaces must satisfy the following assumption:

$$\text{span}\{\mathcal{F}^{ap}\} = \text{span}\{\mathcal{J}e | e \in \mathcal{E}^{ap})\} \tag{8.75}$$

In the pseudo-spectral method, this happens by using polynomials of order $N+1$ in the co-energy variables, and N in the energy variables. Thanks to this choice, if the approximated equations are satisfied at N points, i.e.:

$$\begin{aligned} \dot{\boldsymbol{x}}_1 &= D_1 \boldsymbol{e}_2 \,, \\ \dot{\boldsymbol{x}}_2 &= D_1 \boldsymbol{e}_1 \,, \end{aligned} \tag{8.76}$$

then they are also satisfied at all other points, i.e.:

$$\begin{aligned} \dot{x}_1^{ap}(z,t) &= \frac{\partial}{\partial z} e_2^{ap}(z,t) \,, \\ \dot{x}_2^{ap}(z,t) &= \frac{\partial}{\partial z} e_1^{ap}(z,t) \,. \end{aligned} \qquad \forall\, z \in [0, L] \,. \tag{8.77}$$

Secondly, the co-energy variables are redefined in a new space, obtained from a projection of $\mathcal{E}^{ap}$ in $\mathcal{F}^{ap}$. In this newly defined space, thanks to the exact differentiation property (Eq. 8.77) the original power-product is preserved, i.e.: $\int_{z=0}^{L} \dot{x}_1^{ap} e_1^{ap} + \dot{x}_2^{ap} e_2^{ap} dz = \boldsymbol{y}_\partial^T \boldsymbol{y}_\partial$.

While the mixed finite element method uses low-order basis function in each "element" of the domain, the pseudo-spectral method uses high-order global functions. The main ad-

vantage of the second method is that it presents much better convergence properties. Consequently, a reduced number of states is needed to obtain accurate models of the system. This advantage is illustrated by Fig. 8.2, which compares the error in the computation of the first natural frequency using both methods for the linear wave equation. The error of the pseudo-spectral method goes quickly to zero and, using 8 basis functions or more, it is limited by the machine precision.

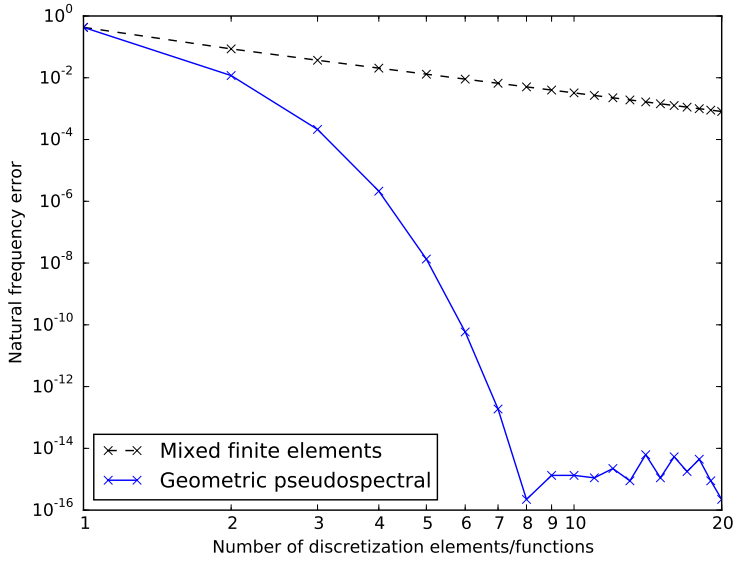

Figure 8.2: Error in the computation of the first natural frequency of the linear wave equation. The pseudo-spectral method converges much faster than the mixed finite element method.

On the other hand, one disadvantage of the pseudo-spectral method is that, for larger N, the "differentiation matrices" have elements with larger values. This causes high-frequency oscillations known as Runge's phenomenon. In this thesis, we used Gauss-Legendre collocation points, which reduces these oscillations.

Remark 8.4
Note that the procedure recalled in Section 8.3 can also be readily used for discretization of only a part the domain (as in Section 8.2). Thus, the pseudo-spectral method can also be written using an "element"-like form. Indeed, if we use spline basis function for the mixed finite elements and $N = 1$ for the pseudo-spectral method with Lagrange polynomials, both methods would give exactly the same finite-dimensional equations.

8.5 Conclusions

The main goal of this chapter was to recall the most used power-preserving methods, namely the mixed finite element, originally proposed by Golo et al. (2004) and the geometrical pseudo-spectral method, originally proposed by Moulla, Lefèvre, and Maschke (2012). We tried to

emphasize the similarities of both methods, and presented the derivation of equations using a similar procedure. In this thesis, the second method will be used for both simulation and control. The main reason for this choice is that the use of pseudo-spectral methods leads to small order state-space models, which is a desirable feature for simulation and control design.

Another approach for the power-preserving spatial discretization of pHs using simplicial complexes was recently proposed by Seslija, Scherpen, and van der Schaft (2014). This method will not be treated in this thesis.

In the next chapter, extensions of the power-preserving pseudo-spectral method are proposed, in order to tackle the particularities of the pHs models presented in Part II of this thesis.

Chapter 9

Extensions of the power-preserving pseudo-spectral method

In the previous chapter, we recalled the power-preserving pseudo-spectral method proposed by Moulla, Lefèvre, and Maschke (2012). In this chapter, we propose several extensions, in order to take into account distributed ports and higher-order derivative operators in $\mathcal{J}$, which are specificities of the pHs models developed in this thesis.

The contributions of the work presented here are the following. Firstly, we extended the discretization method for a modified version of the wave equation presented in the previous chapter. Here, in addition to the boundary ports, the wave equation also have distributed ports. Secondly, we extended it to cases where the differential operator $\mathcal{J}$ has second order spatial derivatives (differently from the wave equation, which has first-order derivatives), which is the case of the beam equation in bending. Thirdly, we proposed a modification of the pseudo-spectral method, by using a weak form of the equations, to deal with an unbounded input operator (presented in Cardoso-Ribeiro, Matignon, and Pommier-Budinger (2016b)).

This chapter is organized as follows. Firstly, the semi-discretization of distributed ports is proposed in Section 9.1. Secondly, the extension for second-order operators and unbounded input ports is proposed in Section 9.2. Conclusions are presented in Section 9.3.

Contents

9.1 First-order pHs with distributed input

Let us consider the equations used to model the beam in torsion and the sloshing in Part II. These equations can be written under the form of an infinite-dimensional pHs:

$$\begin{bmatrix}\dot{x}_1(z,t)\\ \dot{x}_2(z,t)\end{bmatrix} = \begin{bmatrix}0 & \partial_z\\ \partial_z & 0\end{bmatrix}\begin{bmatrix}e_1(z,t)\\ e_2(z,t)\end{bmatrix} + \begin{bmatrix}1\\ 0\end{bmatrix} q(z,t)\,, \tag{9.1}$$

with distributed ports:

$$y_q(z,t) = \begin{bmatrix}1 & 0\end{bmatrix}\begin{bmatrix}e_1(z,t)\\ e_2(z,t)\end{bmatrix}\,, \tag{9.2}$$

boundary ports:

$$\boldsymbol{y}_\partial(t) := \mathcal{B}\boldsymbol{e} := \begin{bmatrix}f_{1\partial}\\ f_{2\partial}\end{bmatrix} := \begin{bmatrix}e_2(L,t)\\ -e_1(0,t)\end{bmatrix}\,, \quad \boldsymbol{u}_\partial(t) = \mathcal{C}\boldsymbol{e} = \begin{bmatrix}e_{1\partial}\\ e_{2\partial}\end{bmatrix} = \begin{bmatrix}e_1(L,t)\\ e_2(0,t)\end{bmatrix}\,, \tag{9.3}$$

and power balance given by:

$$\dot{H} = \boldsymbol{y}_\partial^T\boldsymbol{u}_\partial + \int_{z=0}^{L}\left(q(z,t)y_q(z,t)\right)\mathrm{d}z\ . \tag{9.4}$$

The distributed ports $q(z,t)$ and $y_q(z,t)$ can be used for coupling the pHs with other systems, introducing external forces, or introducing damping (as explained in § 5.4). In this thesis, these ports will be used to include damping in the model.

In the next subsections, a power-preserving semi-discretization method for the Eq. 9.1 is proposed.

Firstly, the approximation basis for each variable is presented in § 9.1.1. Secondly, the equations of motion presented in Eq. 9.1 are presented in a finite-dimensional form with the boundary ports in § 9.1.2. Thirdly, the time-derivative of the Hamiltonian in the finite-dimension space is analyzed: this motivates the definition of new finite-dimensional co-energy variables that guarantee the power-conservation of the system in § 9.1.3. Then, the finite-dimensional equations together with the definition of the co-energy and port variables are combined in § 9.1.4 to define a finite-dimensional Dirac structure of the system. Finally, the discretization of the Hamiltonian gives the constitutive relations needed to define the finite-dimensional port-Hamiltonian system in § 9.1.5.

9.1.1 Approximation bases

The energy and co-energy variables are approximated into a finite-dimensional space using polynomial interpolation, exactly as in the previous chapter (§ 8.3.1, Eqs. 8.44 and 8.45). An alternative approximation for the co-energy variables ($\hat{e}_j^{ap}(z,t)$) using the same approximation

basis as the energy variables is also defined:

$$e_j(z,t) \approx \hat{e}_j^{ap}(z,t) := \sum_{i=1}^{N} \hat{e}_j^i(t)\phi^i(z) = \boldsymbol{e}_j{}^T(t)\boldsymbol{\phi}(z)\,, 0 < z < L\,. \tag{9.5}$$

In addition, the distributed ports also need to be approximated. The same approximation basis used for the energy variables are used for the distributed ports, i.e.:

$$q(z,t) \approx q^{ap}(z,t) := \sum_{i=1}^{N} q^i(t)\phi^i(z) = \boldsymbol{q}^T(t)\boldsymbol{\phi}(z)\,, 0 < z < L\,, \tag{9.6}$$

$$y_q(z,t) \approx y_q^{ap}(z,t) := \sum_{i=1}^{N} y^i(t)\phi^i(z) = \boldsymbol{y}_q{}^T(t)\boldsymbol{\phi}(z)\,, 0 < z < L\,, \tag{9.7}$$

where $\boldsymbol{y}_q$ and $\boldsymbol{q}$ are vectors of size N.

9.1.2 Finite-dimensional equations

From Eq. 9.1 and using approximations from Eqs. 8.44, 8.45 and 9.6, we get:

$$\begin{aligned} \boldsymbol{\phi}^T(z)\dot{\boldsymbol{x}}_1(t) &= \boldsymbol{\psi}_z{}^T(z)\boldsymbol{e}_2(t) + \boldsymbol{\phi}^T(z)\boldsymbol{q}(t)\,, \\ \boldsymbol{\phi}^T(z)\dot{\boldsymbol{x}}_2(t) &= \boldsymbol{\psi}_z{}^T(z)\boldsymbol{e}_1(t)\,. \end{aligned} \tag{9.8}$$

The evaluation of Eq. 9.8 at the N collocation points z_{xi}, leads to the finite-dimensional version of Eq. 9.1:

$$\begin{cases} \dot{\boldsymbol{x}}_1 &= D_1\boldsymbol{e}_2 + \boldsymbol{q}\,, \\ \dot{\boldsymbol{x}}_2 &= D_1\boldsymbol{e}_1\,, \end{cases} \tag{9.9}$$

where D_1 is the same $N \times (N+1)$ matrix as the one defined in Definition 8.2.

The boundary ports (as defined in Eq. 9.3) can be set as a function of the co-energy variables $\boldsymbol{e}_1$ and $\boldsymbol{e}_2$ as Eq. 8.50.

9.1.3 Preserving the power balance

Using the same procedure of § 8.3.3, but using the finite-dimensional equations with distributed ports (Eq. 9.9), we get:

$$\begin{aligned} \dot{H} &\approx \boldsymbol{e}_1{}^T M_{\psi\phi}(D_1\boldsymbol{e}_2 + \boldsymbol{q}) + \boldsymbol{e}_2{}^T M_{\psi\phi} D_1\boldsymbol{e}_1\,, \\ &= \boldsymbol{e}_1{}^T \left(M_{\psi\phi}D_1 + D_1{}^T M_{\psi\phi}{}^T\right)\boldsymbol{e}_2 + \boldsymbol{e}_1{}^T M_{\psi\phi}\boldsymbol{q}\,. \end{aligned} \tag{9.10}$$

Note that Proposition 8.2 (from Chapter 8) is still valid, thus the power balance becomes:

$$\dot{H} \approx \tilde{\boldsymbol{e}}_1{}^T \dot{\boldsymbol{x}}_1 + \tilde{\boldsymbol{e}}_2{}^T \dot{\boldsymbol{x}}_2 \,, \tag{9.11}$$

$$= \boldsymbol{y}_\partial{}^T \boldsymbol{u}_\partial + \boldsymbol{e}_1{}^T M_{\psi\phi} \boldsymbol{q} \,. \tag{9.12}$$

The last term of the power balance ($\boldsymbol{e}_1{}^T M_{\psi\phi}\boldsymbol{q}$) is related to the distributed ports. It readily motivates the definition of the output conjugated to $\boldsymbol{q}$:

$$\boldsymbol{y}_q := M_{\psi\phi}{}^T \boldsymbol{e}_1 = \tilde{\boldsymbol{e}} \,. \tag{9.13}$$

And the power balance becomes:

$$\dot{H} \approx \tilde{\boldsymbol{e}}_1{}^T \dot{\boldsymbol{x}}_1 + \tilde{\boldsymbol{e}}_2{}^T \dot{\boldsymbol{x}}_2 = \boldsymbol{y}_\partial{}^T \boldsymbol{u}_\partial + \boldsymbol{y}_q{}^T \boldsymbol{q} \,. \tag{9.14}$$

Remark 9.1
Note that $\boldsymbol{e}_1 , \boldsymbol{e}_2 \in \mathbb{R}^{N+1}$ have a clear physical meaning: each element of these vectors represents the value of the co-energy variable at a collocation point. The physical meaning of $\tilde{\boldsymbol{e}}_1 , \tilde{\boldsymbol{e}}_2 \in \mathbb{R}^N$ is unclear until this point. Indeed, by approximating the continuous power balance with $e_j(z,t) \approx \hat{\boldsymbol{e}}_j^T \boldsymbol{\phi}$, it becomes:

$$\begin{aligned} \dot{H} &= \int_{z=0}^{L} (e_1 \dot{x}_1 + e_2 \dot{x}_2) \, \mathrm{d}z \,, \\ &\approx \hat{\boldsymbol{e}}_1{}^T \left(\int_{z=0}^{L} \boldsymbol{\phi}\boldsymbol{\phi}^T \, \mathrm{d}z \right) \dot{\boldsymbol{x}}_1 + \hat{\boldsymbol{e}}_2{}^T \left(\int_{z=0}^{L} \boldsymbol{\phi}\boldsymbol{\phi}^T \, \mathrm{d}z \right) \dot{\boldsymbol{x}}_2 \,, \\ &= \hat{\boldsymbol{e}}_1{}^T M_\phi \dot{\boldsymbol{x}}_1 + \hat{\boldsymbol{e}}_2{}^T M_\phi \dot{\boldsymbol{x}}_2 \,. \end{aligned} \tag{9.15}$$

In order to satisfy both Eq. 9.15 and Eq. 9.11, the following equality must hold:

$$\hat{\boldsymbol{e}}_j = M_\phi^{-1} \tilde{\boldsymbol{e}}_j \text{ for } j = 1,2. \tag{9.16}$$

Thus, Eq. 9.16 provides a relationship between the point-wise value of the co-energy variables $\hat{\boldsymbol{e}}_j(t) \in \mathbb{R}^N$ and $\tilde{\boldsymbol{e}}_j(t) \in \mathbb{R}^N$. Moreover, note that the discretization of the output: $y_q(z,t) = e_1(z,t)$ leads to:

$$y_q^{ap}(z,t) = \hat{e}_1^{ap}(z,t) \,, \tag{9.17}$$

which is equivalent to:

$$\hat{\boldsymbol{y}}_q(t) = \hat{\boldsymbol{e}}_1(t) \,. \tag{9.18}$$

Thus, thanks to 9.13 and 9.16, the term $(\boldsymbol{y}_q)^T \boldsymbol{q}$ of Eq. 9.14 can be rewritten as:

$$\boldsymbol{y}_q{}^T \boldsymbol{q} = \hat{\boldsymbol{y}}_q{}^T M_\phi \boldsymbol{q} = \int_{z=0}^{L} y_q^{ap}(z,t) \, q^{ap}(z,t) \, \mathrm{d}z \,. \tag{9.19}$$

9.1.4 Finite-dimensional Dirac structure

The flow and effort variables ($\boldsymbol{f}$ and $\boldsymbol{e}$) are defined as:

$$\boldsymbol{f}^T := \begin{bmatrix} -\dot{\boldsymbol{x}}_1 & f_{1\partial} & -\dot{\boldsymbol{x}}_2 & f_{2\partial} & \boldsymbol{q} \end{bmatrix}, \quad \boldsymbol{e}^T := \begin{bmatrix} \tilde{\boldsymbol{e}}_1 & e_{1\partial} & \tilde{\boldsymbol{e}}_2 & e_{2\partial} & \boldsymbol{y}_q \end{bmatrix}, \tag{9.20}$$

where both $\boldsymbol{f}$ and $\boldsymbol{e} \in \mathbb{R}^{3N+2}$. A power product is also defined: $P := \boldsymbol{f}^T\boldsymbol{e}$, that is equal to zero thanks to Eq. 9.14 for all ($\boldsymbol{e}$, $\boldsymbol{f}$) satisfying Eqs. 9.9, 8.50, 8.61 and 9.13.

Using the finite-dimensional Eqs. 9.9, the boundary ports from Eq. 8.50, the co-energy variables definition from Eq. 8.61 and the output definition from Eq. 9.13, it is possible to write:

$$\begin{bmatrix} -\dot{\boldsymbol{x}}_1 \\ f_{1\partial} \\ -\dot{\boldsymbol{x}}_2 \\ f_{2\partial} \\ \boldsymbol{y}_q \end{bmatrix} = \begin{bmatrix} 0 & -D_1 & -I \\ 0 & \boldsymbol{\psi}^T(L) & 0 \\ -D_1 & 0 & 0 \\ -\boldsymbol{\psi}^T(0) & 0 & 0 \\ M_{\psi\phi} & 0 & 0 \end{bmatrix} \begin{bmatrix} \boldsymbol{e}_1 \\ \boldsymbol{e}_2 \\ \boldsymbol{q} \end{bmatrix}, \quad \begin{bmatrix} \tilde{\boldsymbol{e}}_1 \\ e_{1\partial} \\ \tilde{\boldsymbol{e}}_2 \\ e_{2\partial} \\ \boldsymbol{q} \end{bmatrix} = \begin{bmatrix} {M_{\psi\phi}}^T & 0 & 0 \\ \boldsymbol{\psi}^T(L) & 0 & 0 \\ 0 & {M_{\psi\phi}}^T & 0 \\ 0 & \boldsymbol{\psi}^T(0) & 0 \\ 0 & 0 & I \end{bmatrix} \begin{bmatrix} \boldsymbol{e}_1 \\ \boldsymbol{e}_2 \\ \boldsymbol{q} \end{bmatrix}, \tag{9.21}$$

which is an image representation of a Dirac structure, as defined in Eq. 4.46. This equation can be rewritten using an explicit representation as:[1]

$$\begin{bmatrix} -\dot{\boldsymbol{x}}_1 \\ f_{1\partial} \\ -\dot{\boldsymbol{x}}_2 \\ f_{2\partial} \\ \boldsymbol{y}_q \end{bmatrix} = \begin{bmatrix} 0 & \begin{pmatrix} -D_1 \\ \boldsymbol{\psi}^T(L) \end{pmatrix} \begin{pmatrix} {M_{\psi\phi}}^T \\ \boldsymbol{\psi}^T(0) \end{pmatrix}^{-1} & -I \\ \begin{pmatrix} -D_1 \\ -\boldsymbol{\psi}^T(0) \end{pmatrix} \begin{pmatrix} {M_{\psi\phi}}^T \\ \boldsymbol{\psi}^T(L) \end{pmatrix}^{-1} & 0 & 0 \\ I \quad 0 & 0 & 0 \end{bmatrix} \begin{bmatrix} \tilde{\boldsymbol{e}}_1 \\ e_{1\partial} \\ \tilde{\boldsymbol{e}}_2 \\ e_{2\partial} \\ \boldsymbol{q} \end{bmatrix}. \tag{9.22}$$

The skew-symmetry of the matrix in Eq. 9.22 is easily proven by the product of flow and effort variables, which is equal to zero, since $P = 0$.

Finally, Eq. 9.22 can be rewritten in a more classical way (as Eq. 4.6) by simply rearranging its rows and columns:

$$\begin{bmatrix} -\dot{\boldsymbol{x}} \\ \boldsymbol{y}_\partial \\ \boldsymbol{y}_q \end{bmatrix} = \begin{bmatrix} -J & -B_\partial & -I \\ B_\partial^T & D_\partial & 0 \\ I & 0 & 0 \end{bmatrix} \begin{bmatrix} \tilde{\boldsymbol{e}} \\ \boldsymbol{u}_\partial \\ \boldsymbol{q} \end{bmatrix}, \tag{9.23}$$

where $\dot{\boldsymbol{x}} = \begin{bmatrix} {\dot{\boldsymbol{x}}_1}^T & {\dot{\boldsymbol{x}}_2}^T \end{bmatrix}^T$, $\tilde{\boldsymbol{e}} = \begin{bmatrix} \tilde{\boldsymbol{e}}_1 & \tilde{\boldsymbol{e}}_2 \end{bmatrix}^T$, $\boldsymbol{y}_\partial = \begin{bmatrix} e_2(L,t) & -e_1(0,t) \end{bmatrix}^T$ and $\boldsymbol{u}_\partial = \begin{bmatrix} e_1(L,t) & e_2(0,t) \end{bmatrix}^T$. The matrices J and D_∂ are skew-symmetric and they can be extracted from Eq. 9.22 by permutation of rows and columns.

[1] The matrices $\begin{pmatrix} M^T \\ \boldsymbol{\psi}^T(L) \end{pmatrix}$ and $\begin{pmatrix} M^T \\ \boldsymbol{\psi}^T(0) \end{pmatrix}$ are square and supposed to be invertible.

Remark 9.2
We used $\boldsymbol{y}_q$ as output of the system. Alternatively, it is possible to use $\hat{\boldsymbol{y}}_q$ as output (the vector of point-wise values $y(z,t)$). In this case, the flow and effort variables are defined as:

$$\boldsymbol{f}^T := \begin{bmatrix} -\dot{\boldsymbol{x}}_1 & f_{1\partial} & -\dot{\boldsymbol{x}}_2 & f_{2\partial} & \boldsymbol{q} \end{bmatrix}, \quad \check{\boldsymbol{e}}^T := \begin{bmatrix} \tilde{\boldsymbol{e}}_1 & e_{1\partial} & \tilde{\boldsymbol{e}}_2 & e_{2\partial} & \hat{\boldsymbol{y}}_q \end{bmatrix}. \tag{9.24}$$

The power product, however, must be redefined as:

$$P := \boldsymbol{f}^T \begin{bmatrix} I & 0 & 0 & 0 & 0 \\ 0 & 1 & 0 & 0 & 0 \\ 0 & 0 & I & 0 & 0 \\ 0 & 0 & 0 & 1 & 0 \\ 0 & 0 & 0 & 0 & M_\phi \end{bmatrix} \check{\boldsymbol{e}}, \tag{9.25}$$

thus, the matrix M_ϕ appears in the definition of power product.

9.1.5 Discretization of the Hamiltonian

Finally, constitutive relations are needed to find the values of the co-energy variables $\tilde{\boldsymbol{e}}_1$ and $\tilde{\boldsymbol{e}}_2$. The same procedure of § 8.3.5 is used. In the case of the system with distributed port, the power balance of the semi-discretized system becomes:

$$\dot{H}_d = \tilde{\boldsymbol{e}}_1{}^T(t)\, \dot{\boldsymbol{x}}_1(t) + \tilde{\boldsymbol{e}}_2{}^T(t)\, \dot{\boldsymbol{x}}_2(t) = \boldsymbol{y}_\partial{}^T\, \boldsymbol{u}_\partial + \boldsymbol{y}_q{}^T\, \boldsymbol{q}\,. \tag{9.26}$$

9.2 Second-order pHs with unbounded distributed input operator

Recall from § 5.1.2 that the piezoelectric beam equations are given by:

$$\begin{bmatrix} \dot{x}_1(z,t) \\ \dot{x}_2(z,t) \end{bmatrix} = \begin{bmatrix} 0 & -\partial_{z^2}^2 \\ \partial_{z^2}^2 & 0 \end{bmatrix} \begin{bmatrix} e_1(z,t) \\ e_2(z,t) \end{bmatrix} + \begin{bmatrix} \partial_{z^2}^2 \\ 0 \end{bmatrix} \Pi_{ab}(z) k_p v(z,t)\,, \quad 0 < z < L\,, \tag{9.27}$$

with distributed output:

$$y_v(z,t) = k_p\, \partial_{z^2}^2 e_1\,, \quad a < z < b\,, \tag{9.28}$$

boundary ports:

$$\boldsymbol{y}_\partial^B := \begin{bmatrix} f_{1\partial}^B \\ f_{2\partial}^B \\ f_{3\partial}^B \\ f_{4\partial}^B \end{bmatrix} := \begin{bmatrix} \partial_z e_2^B(0) \\ -e_2^B(0) \\ -e_1^B(L) \\ \partial_z e_1^B(L) \end{bmatrix}, \boldsymbol{u}_\partial^B = \begin{bmatrix} e_{1\partial}^B \\ e_{2\partial}^B \\ e_{3\partial}^B \\ e_{4\partial}^B \end{bmatrix} = \begin{bmatrix} e_1^B(0) \\ \partial_z e_1^B(0) \\ \partial_z e_2^B(L) \\ e_2^B(L) \end{bmatrix}, \tag{9.29}$$

and energy flow given by:

$$\dot{H} = \boldsymbol{y}_\partial{}^T \boldsymbol{u}_\partial + \int_{z=a}^{b} v(z,t) y_v(z,t)\,\mathrm{d}z\ . \tag{9.30}$$

The previous equation has two major differences with respect to the system semi-discretized by Moulla, Lefèvre, and Maschke (2012). Firstly, the differential operator has a second-order spatial derivative (instead of a first-order). Secondly, the term $\partial^2_{z^2}(\Pi_{ab}(z) k_p v(z,t))$ is unbounded and the direct use of collocation methods is not possible. To deal with the second difficulty, a weak formulation is needed, as already pointed out in Remark 5.8.

In the next subsections, a power-preserving semi-discretization method for the piezoelectric beam equation (Eq. 9.27) is presented.

Firstly, the approximation basis for each variable is presented in § 9.2.1. Secondly, the equations of motion presented in Eq. 9.27 are rewritten in a weak form and then spatially discretized in § 9.2.2. Thirdly, the time-derivative of the Hamiltonian in the finite-dimension space is analyzed: this motivates the definition of new finite-dimensional co-energy variables that guarantee the power-conservation of the system in § 9.2.3. Then, the finite-dimensional equations together with the definition of the co-energy and port variables are combined in § 9.2.4 to define a finite-dimensional Dirac structure of the system. Finally, the discretization of the Hamiltonian gives the closure equations to define the finite-dimensional port-Hamiltonian system in § 9.2.5.

9.2.1 Approximation bases

The energy variables are approximated using N polynomial basis functions as (for $j = 1, 2$):

$$x_j(z,t) \approx x_j^{ap}(z,t) := \sum_{i=1}^{N} x_j^i(t)\phi^i(z) = \boldsymbol{x}_j{}^T(t)\boldsymbol{\phi}(z)\,, \quad 0 < z < L\,, \tag{9.31}$$

where $\boldsymbol{x}_j(t)$, $\boldsymbol{\phi}(z) \in \mathbb{R}^N$.

Two different approximation bases are proposed for the co-energy variables. For $j = 1, 2$:

$$e_j(z,t) \approx e_j^{ap}(z,t) := \sum_{i=1}^{N+2} e_j^i(t)\psi^i(z) = \boldsymbol{e}_j{}^T(t)\boldsymbol{\psi}(z)\,, \quad 0 < z < L\,, \tag{9.32}$$

$$e_j(z,t) \approx \hat{e}_j^{ap}(z,t) := \sum_{i=1}^{N} \hat{e}_j^i(t)\phi^i(z) = \hat{\boldsymbol{e}}_j{}^T(t)\boldsymbol{\phi}(z)\,, \quad 0 < z < L\,, \tag{9.33}$$

where $\boldsymbol{e}_j(t)$, $\boldsymbol{\psi}(z) \in \mathbb{R}^{N+2}$ and $\hat{\boldsymbol{e}}_j(t) \in \mathbb{R}^N$.

In Eq. 9.32, a basis with $N+2$ elements is used. This choice allows the original differential equation to be exactly fulfilled in the finite-dimensional space, since Eq. 9.27 has a second-

order derivative. In addition, Eq. 9.33 uses a basis of order N, that is chosen to deal with the distributed ports (as it happened in Section 9.1).

Secondly, the distributed external input $v(z,t)$ is approximated using a polynomial basis with K functions:

$$v(z,t) \approx v^{ap}(z,t) := \sum_{i=1}^{K} v^i(t)\theta^i(z) = \boldsymbol{v}^T(t)\boldsymbol{\theta}(z)\,, \quad a < z < b\,, \tag{9.34}$$

where $\boldsymbol{v}(t)$, $\boldsymbol{\theta}(z) \in \mathbb{R}^K$. The same basis will be used to approximate the distributed output $y_v(z,t)$.

Lagrange polynomials are used as approximation basis. Thus, the values of the coefficients $\boldsymbol{x_j}(t)$, $\boldsymbol{e_j}(t)$ and $\boldsymbol{v}(t)$ are the values of $x_j(z,t)$, $e_j(z,t)$ and $v(z,t)$ evaluated at the collocation points. The collocation points are denoted as z_{xi} for the energy space, z_{ei} for the co-energy space and z_{vi} for the distributed input. Note that the energy variables are approximated using N points, the co-energy variables using $N+2$ points, and the distributed external input using K collocation points.

9.2.2 Finite-dimensional equations

The pseudo-spectral method used by Moulla, Lefèvre, and Maschke (2012) cannot be applied here because of the unbounded term $\partial_{z^2}^2 \left(\Pi_{ab}(z) k_p v(z,t)\right)$ in Eq. 9.27. For this reason, we propose to use an integral formulation, with an arbitrary smooth test function $c(z)$ of class $\mathcal{C}^2$, such that Eq. 9.27 is rewritten as:

$$\int_{z=0}^{L} c(z) \begin{bmatrix} \dot{x}_1 \\ \dot{x}_2 \end{bmatrix} \mathrm{d}z = \int_{z=0}^{L} c(z) \begin{bmatrix} 0 & -\partial_{z^2}^2 \\ \partial_{z^2}^2 & 0 \end{bmatrix} \begin{bmatrix} e_1 \\ e_2 \end{bmatrix} \mathrm{d}z + \int_{z=0}^{L} c(z) \begin{bmatrix} \partial_{z^2}^2 \\ 0 \end{bmatrix} \Pi_{ab}(z) k_p v(z,t)\, \mathrm{d}z\ .$$

After integrating the last term by parts twice, the weak formulation of the original problem is found to be:

$$\int_{z=0}^{L} c(z) \begin{bmatrix} \dot{x}_1 \\ \dot{x}_2 \end{bmatrix} \mathrm{d}z = \int_{z=0}^{L} c(z) \begin{bmatrix} 0 & -\partial_{z^2}^2 \\ \partial_{z^2}^2 & 0 \end{bmatrix} \begin{bmatrix} e_1 \\ e_2 \end{bmatrix} \mathrm{d}z + \int_{z=a}^{b} \partial_{z^2}^2 \left(c(z)\right) \begin{bmatrix} 1 \\ 0 \end{bmatrix} k_p v(z,t)\, \mathrm{d}z\ . \tag{9.35}$$

Now, the second order derivative is applied to the smooth function $c(z)$. We use the particular choice of $c(z) = \boldsymbol{c}^T\boldsymbol{\phi}(z)$, for an arbitrary vector $\boldsymbol{c}$.

From the weak form Eq. 9.35, using the approximations from Eqs. 9.31, 9.32, 9.34, we get:

$$\begin{aligned} \left(\int_{z=0}^{L} \boldsymbol{\phi}\boldsymbol{\phi}^T \mathrm{d}z\right) \dot{\boldsymbol{x}}_1 &= -\left(\int_{z=0}^{L} \boldsymbol{\phi}\boldsymbol{\psi}_{zz}{}^T \mathrm{d}z\right) \boldsymbol{e}_2 + \left(\int_{z=a}^{b} \boldsymbol{\phi}_{zz}\boldsymbol{\theta}^T \mathrm{d}z\right) k_p \boldsymbol{v}\,, \\ \left(\int_{z=0}^{L} \boldsymbol{\phi}\boldsymbol{\phi}^T \mathrm{d}z\right) \dot{\boldsymbol{x}}_2 &= \left(\int_{z=0}^{L} \boldsymbol{\phi}\boldsymbol{\psi}_{zz}{}^T \mathrm{d}z\right) \boldsymbol{e}_1\,, \end{aligned} \tag{9.36}$$

where $\boldsymbol{\psi}_{zz}(z)$ and $\boldsymbol{\phi}_{zz}(z)$ are the second-order spatial derivatives $\boldsymbol{\psi}(z)$ and $\boldsymbol{\phi}(z)$, respectively.

In order to simplify the presentation, the following notations are introduced:

$$M_\phi := \int_{z=0}^{L} \boldsymbol{\phi}\boldsymbol{\phi}^T \,\mathrm{d}z\,, \quad \bar{D}_2 := \int_{z=0}^{L} \boldsymbol{\phi}{\boldsymbol{\psi}_{zz}}^T \,\mathrm{d}z\,, \quad \bar{B} := k_p \int_{z=a}^{b} \boldsymbol{\phi}_{zz}\boldsymbol{\theta}^T \,\mathrm{d}z\,, \tag{9.37}$$

M_ϕ is a symmetric positive-definite $N \times N$ matrix, $\bar{D}_2$ is an $N \times (N+2)$ matrix and $\bar{B}$ is an $N \times K$ matrix.

The finite-dimensional equations (Eqs. 9.36) thus become:

$$\begin{aligned} M_\phi \dot{\boldsymbol{x}}_1 &= -\bar{D}_2 \boldsymbol{e}_2 + \bar{B}\boldsymbol{v} \\ M_\phi \dot{\boldsymbol{x}}_2 &= \bar{D}_2 \boldsymbol{e}_1 \end{aligned} \tag{9.38}$$

Definition 9.1
The differentiation matrix D_2 is defined as:

$$D_2 := \begin{bmatrix} {\boldsymbol{\psi}_{zz}}^T(z_{x1}) \\ {\boldsymbol{\psi}_{zz}}^T(z_{x2}) \\ {\boldsymbol{\psi}_{zz}}^T(z_{x3}) \\ \vdots \\ {\boldsymbol{\psi}_{zz}}^T(z_{xN}) \end{bmatrix}, \tag{9.39}$$

where z_{xi} are the collocation points related to the energy variables approximation basis. D_2 is an $N \times (N+2)$ matrix.

Proposition 9.1
The differentiation matrix D_2 is related to the matrix obtained from the weak formulation method $\bar{D}_2$, by the following expression:

$$D_2 = M_\phi^{-1} \bar{D}_2\,. \tag{9.40}$$

Proof. Let $f(z) := \boldsymbol{f}^T\boldsymbol{\phi}(z)$ be a polynomial of degree N, $g(z) := \boldsymbol{g}^T\boldsymbol{\psi}(z)$ a polynomial of degree $N+2$. If $f(z) = \partial_{z^2}^2 g(z)$:

$$\boldsymbol{f}^T\boldsymbol{\phi}(z) = \boldsymbol{g}^T\boldsymbol{\psi}_{zz}(z)\,,$$

evaluating the previous expression at each collocation point z_{xi}:

$$\boldsymbol{f} = D_2\boldsymbol{g}\,,$$

$$\boldsymbol{g}^T {D_2}^T \boldsymbol{\phi}(z) = \boldsymbol{g}^T\boldsymbol{\psi}_{zz}(z)\,. \tag{9.41}$$

Since both $\boldsymbol{f}^T\boldsymbol{\phi}(z)$ and $\boldsymbol{g}^T\boldsymbol{\psi}_{zz}(z)$ are polynomials of degree N, the previous equation is exact for any $\boldsymbol{g}$ and:

$$\boldsymbol{\phi}^T D_2 = {\boldsymbol{\psi}_{zz}}^T\,. \tag{9.42}$$

Eq. 9.42 is multiplied by $\boldsymbol{\phi}$ and integrated over $(0, L)$:

$$\int_{z=0}^{L} \boldsymbol{\phi}\boldsymbol{\phi}^T \,\mathrm{d}z\, D_2 = \int_{z=0}^{L} \boldsymbol{\phi}\boldsymbol{\psi}_z{}^T \,\mathrm{d}z \;. \tag{9.43}$$

$$M_\phi D_2 = \bar{D}_2 \,. \tag{9.44}$$

Finally:

$$D_2 = M_\phi^{-1} \bar{D}_2 \,. \tag{9.45}$$

□

Proposition 9.1 means that the finite-dimensional weak-form and collocation methods are equivalent, when discretizing the $\mathcal{J}_2$ operator. This occurs thanks to the choice of different basis functions for the energy and co-energy variables.

Multiplying Eq. 9.38 by M_ϕ^{-1} and using Proposition 9.1, the following finite-dimensional equations are obtained:

$$\begin{aligned} \dot{\boldsymbol{x}}_1 &= -D_2 \boldsymbol{e}_2 + B\boldsymbol{v} \,, \\ \dot{\boldsymbol{x}}_2 &= D_2 \boldsymbol{e}_1 \,, \end{aligned} \tag{9.46}$$

where:

$$B := M_\phi^{-1} \bar{B} \,. \tag{9.47}$$

The boundary ports (as defined in Eq. 9.29) can be set as a linear function of the co-energy variables $\boldsymbol{e}_1$ and $\boldsymbol{e}_2$:

$$\boldsymbol{y}_\partial = \begin{bmatrix} f_{1\partial} \\ f_{2\partial} \\ f_{3\partial} \\ f_{4\partial} \end{bmatrix} = \begin{bmatrix} \boldsymbol{\psi}_z{}^T(0)\boldsymbol{e}_2 \\ -\boldsymbol{\psi}^T(0)\boldsymbol{e}_2 \\ -\boldsymbol{\psi}^T(L)\boldsymbol{e}_1 \\ \boldsymbol{\psi}_z{}^T(L)\boldsymbol{e}_1 \end{bmatrix} , \; \boldsymbol{u}_\partial = \begin{bmatrix} e_{1\partial} \\ e_{2\partial} \\ e_{3\partial} \\ e_{4\partial} \end{bmatrix} = \begin{bmatrix} \boldsymbol{\psi}^T(0)\boldsymbol{e}_1 \\ \boldsymbol{\psi}_z{}^T(0)\boldsymbol{e}_1 \\ \boldsymbol{\psi}_z{}^T(L)\boldsymbol{e}_2 \\ \boldsymbol{\psi}^T(L)\boldsymbol{e}_2 \end{bmatrix} \,. \tag{9.48}$$

9.2.3 Preserving the power balance

The energy flow of the Hamiltonian can be obtained from the definition of the variational derivative as:

$$\begin{aligned} \dot{H} &= \int_{z=0}^{L} \left(\delta_{x_1} H \, \dot{x}_1 + \delta_{x_2} H \, \dot{x}_2\right) \mathrm{d}z \,, \\ &= \int_{z=0}^{L} \left(e_1 \dot{x}_1 + e_2 \dot{x}_2\right) \mathrm{d}z \;. \end{aligned} \tag{9.49}$$

After substitution of the finite-dimensional versions of $x_j(z,t)$ (Eq. 9.31) and $e_j(z,t)$ (Eq. 9.32), it is found:

$$\dot{H} \approx \boldsymbol{e}_1{}^T M_{\psi\phi} \dot{\boldsymbol{x}}_1 + \boldsymbol{e}_2{}^T M_{\psi\phi} \dot{\boldsymbol{x}}_2 \,, \tag{9.50}$$

where:

$$M_{\psi\phi} := \int_{z=0}^{L} \boldsymbol{\psi}(z)\boldsymbol{\phi}^T(z)\,\mathrm{d}z \tag{9.51}$$

is an $(N+2)\times N$ matrix.

This motivates the definition of new co-energy variables of same dimension as the energy variables, namely:

$$\begin{aligned} \tilde{\boldsymbol{e}}_1 &:= M_{\psi\phi}^T \boldsymbol{e}_1\,, \\ \tilde{\boldsymbol{e}}_2 &:= M_{\psi\phi}^T \boldsymbol{e}_2\,, \end{aligned} \tag{9.52}$$

such that the energy flow is given by the product of these energy and co-energy variables:

$$\dot{H} \approx \tilde{\boldsymbol{e}}_1{}^T \dot{\boldsymbol{x}}_1 + \tilde{\boldsymbol{e}}_2{}^T \dot{\boldsymbol{x}}_2\,. \tag{9.53}$$

After substitution of the finite-dimensional equations (Eqs. 9.46) in Eq. 9.53:

$$\begin{aligned} \tilde{\boldsymbol{e}}_1{}^T \dot{\boldsymbol{x}}_1 + \tilde{\boldsymbol{e}}_2{}^T \dot{\boldsymbol{x}}_2 &= -\tilde{\boldsymbol{e}}_1{}^T \left(D_2 \boldsymbol{e}_2 + M_\phi^{-1} \bar{B} \boldsymbol{v} \right) + \tilde{\boldsymbol{e}}_2{}^T D_2 \boldsymbol{e}_1\,, \\ &= -\boldsymbol{e}_1{}^T \left(M_{\psi\phi} D_2 \boldsymbol{e}_2 + M_{\psi\phi} M_\phi^{-1} \bar{B} \boldsymbol{v} \right) + \boldsymbol{e}_2{}^T M_{\psi\phi} D_2 \boldsymbol{e}_1\,, \\ &= \boldsymbol{e}_1{}^T \left(-M_{\psi\phi} D_2 + D_2{}^T M_{\psi\phi}^T \right) \boldsymbol{e}_2 + \boldsymbol{e}_1{}^T M_{\psi\phi} B \boldsymbol{v}\,. \end{aligned} \tag{9.54}$$

Proposition 9.2
As for the infinite-dimensional case (Eq. 5.16), the first part of the energy flow in Eq. 9.54 is related to the boundary conditions only, i.e.:

$$\boldsymbol{e}_1{}^T \left(-M_{\psi\phi} D_2 + D_2{}^T M_{\psi\phi}^T \right) \boldsymbol{e}_2 = \boldsymbol{y}_\partial^T \boldsymbol{u}_\partial\,.$$

Proof.

$$\begin{aligned} &\boldsymbol{e}_1{}^T \left(-M_{\psi\phi} D_2 + D_2{}^T M_{\psi\phi}^T \right) \boldsymbol{e}_2 \\ &= \boldsymbol{e}_1{}^T \left(-\int_{z=0}^{L} \boldsymbol{\psi}(z)\boldsymbol{\phi}^T(z)\,\mathrm{d}z D_2 + D_2{}^T \int_{z=0}^{L} \boldsymbol{\phi}(z)\boldsymbol{\psi}^T(z)\,\mathrm{d}z \right) \boldsymbol{e}_2\,, \\ &= \boldsymbol{e}_1{}^T \left(-\int_{z=0}^{L} \boldsymbol{\psi}(z)\boldsymbol{\phi}^T(z) D_2\,\mathrm{d}z + \int_{z=0}^{L} D_2{}^T \boldsymbol{\phi}(z)\boldsymbol{\psi}^T(z)\,\mathrm{d}z \right) \boldsymbol{e}_2\,. \end{aligned} \tag{9.55}$$

Since $\boldsymbol{\phi}^T D_2 = \boldsymbol{\psi}_{zz}{}^T$ (Eq. 9.42):

$$\begin{aligned} &\boldsymbol{e}_1{}^T \left(-M_{\psi\phi} D_2 + D_2{}^T M_{\psi\phi}^T \right) \boldsymbol{e}_2 \\ &= \boldsymbol{e}_1{}^T \left(-\int_{z=0}^{L} \boldsymbol{\psi}(z)\boldsymbol{\psi}_{zz}\,\mathrm{d}z + \int_{z=0}^{L} \boldsymbol{\psi}_{zz}\boldsymbol{\psi}^T(z)\,\mathrm{d}z \right) \boldsymbol{e}_2\,, \\ &= \boldsymbol{e}_1{}^T \left(\int_{z=0}^{L} \partial_z \left(-\boldsymbol{\psi}(z)\boldsymbol{\psi}_z^T(z) + \boldsymbol{\psi}_z(z)\boldsymbol{\psi}^T(z) \right) \mathrm{d}z \right) \boldsymbol{e}_2\,, \\ &= \boldsymbol{e}_1{}^T \left(-\boldsymbol{\psi}(z)\boldsymbol{\psi}_z^T(z) + \boldsymbol{\psi}_z(z)\boldsymbol{\psi}^T(z) \right) \boldsymbol{e}_2 \Big|_{z=0}^{L} = \boldsymbol{y}_\partial^T \boldsymbol{u}_\partial\,. \end{aligned}$$

□

The approximated Hamiltonian time derivative is thus written as:

$$\dot{H} \approx \tilde{\boldsymbol{e}}_1{}^T \dot{\boldsymbol{x}}_1 + \tilde{\boldsymbol{e}}_2{}^T \dot{\boldsymbol{x}}_2 = \boldsymbol{y}_\partial{}^T \boldsymbol{u}_\partial + \tilde{\boldsymbol{e}}_1{}^T B \boldsymbol{v} \,. \tag{9.56}$$

The second part of the power balance ($\tilde{\boldsymbol{e}}_1{}^T B\boldsymbol{v}$) is related to the distributed ports. The previous expression readily motivates the definition of the output conjugated to $\boldsymbol{v}$:

$$\boldsymbol{y}_v := B^T \tilde{\boldsymbol{e}}_1 \,, \tag{9.57}$$

leading to the following power balance:

$$\dot{H} \approx \tilde{\boldsymbol{e}}_1{}^T \dot{\boldsymbol{x}}_1 + \tilde{\boldsymbol{e}}_2{}^T \dot{\boldsymbol{x}}_2 = \boldsymbol{y}_\partial{}^T \boldsymbol{u}_\partial + \boldsymbol{y}_v{}^T \boldsymbol{v} \,. \tag{9.58}$$

Remark 9.3
As presented in Remark 9.1, using the approximation $e_j(z,t) \approx \hat{e}_j(z,t) := \hat{\boldsymbol{e}}_j^T \boldsymbol{\phi}$, we can also find a relationship between $\tilde{\boldsymbol{e}}_i$ and the vector of point-wise values of the co-energy variables $\hat{\boldsymbol{e}}_i$:

$$\hat{\boldsymbol{e}}_j = M_\phi^{-1} \tilde{\boldsymbol{e}}_j \text{ for } j = 1,2. \tag{9.59}$$

These variables will prove useful in the sequel.

Remark 9.4
Similarly, using the approximation $y_v(z,t) \approx y_v^{ap}(z,t) := \hat{\boldsymbol{y}}_v{}^T \boldsymbol{\theta}$, we can define a relationship between $\boldsymbol{y}_v$ and the vector of point-wise values of the output $\hat{\boldsymbol{y}}_v$:

$$\hat{\boldsymbol{y}}_v := M_\theta^{-1} \boldsymbol{y}_v \,, \tag{9.60}$$

where $M_\theta := \int_{z=a}^{b} \boldsymbol{\theta}\boldsymbol{\theta}^T \,\mathrm{d}z$ is a symmetric positive-definite $K \times K$ matrix.

This choice preserves the continuous power balance related to the distributed ports in the finite-dimensional space, i.e.:

$$\begin{aligned} \int_{z=a}^{b} y_v^{ap}(z,t) v^{ap}(z,t) \,\mathrm{d}z &= \int_{z=a}^{b} \hat{\boldsymbol{y}}_v{}^T \boldsymbol{\theta}\boldsymbol{\theta}^T \boldsymbol{v} \,\mathrm{d}z \,, \\ &= \hat{\boldsymbol{y}}_v{}^T M_\theta \, \boldsymbol{v} \,, \\ &= \boldsymbol{y}_v{}^T \boldsymbol{v} \,. \end{aligned}$$

Remark 9.5
The previous conjugated output $\boldsymbol{y}_v$ (Eq. 9.57) can also be obtained from the spatial discretization of the integral form of the continuous output: $y_v(z,t) = k_p \partial_{z^2}^2 e_1(z,t)$. Indeed, the approximation of:

$$\int_{z=a}^{b} c(z) y_v(z,t) \,\mathrm{d}z = \int_{z=a}^{b} c(z) k_p \partial_{z^2}^2 e_1(z,t) \,\mathrm{d}z \qquad \forall c(z) \tag{9.61}$$

implies:

$$\boldsymbol{y}_v = B^T \tilde{\boldsymbol{e}}_1 \,, \tag{9.62}$$

with the particular choice $c(z) = \boldsymbol{c}^T\boldsymbol{\theta}(z)$.

Proof. Let us approximate $e_1(z,t)$ using the $N-$dimensional basis $\boldsymbol{\phi}(z)$:

$$e_1(z,t) \approx \hat{\boldsymbol{e}}_1^{ap}(z,t) = \hat{\boldsymbol{e}}_1{}^T(t)\boldsymbol{\phi}(z)\,,$$

$y(z,t)$ using the $K-$dimensional basis $\boldsymbol{\theta}(z)$:

$$y_v(z,t) \approx y_v^{ap}(z,t) = \hat{\boldsymbol{y}}_v{}^T(t)\boldsymbol{\theta}(z)\,,$$

and choosing $c(z) = \boldsymbol{c}^T\,\boldsymbol{\theta}(z)$. Thus, the approximated version of Eq. 9.61 is given by:

$$\underbrace{\left(\int_{z=a}^{b}\boldsymbol{\theta}\boldsymbol{\theta}^T\,\mathrm{d}z\right)}_{M_\theta}\hat{\boldsymbol{y}}_v = \underbrace{k_p\left(\int_{z=a}^{b}\boldsymbol{\theta}\boldsymbol{\phi}_{zz}{}^T\,\mathrm{d}z\right)}_{\bar{B}}\hat{\boldsymbol{e}}_1\,,$$
$$M_\theta\,\hat{\boldsymbol{y}}_v = \bar{B}^T\hat{\boldsymbol{e}}_1\,,$$

Since $\hat{\boldsymbol{e}}_1 = M_\phi^{-1}\tilde{\boldsymbol{e}}_1$ and $\hat{\boldsymbol{y}}_v = M_\theta^{-1}\tilde{\boldsymbol{y}}_v$, we find:

$$\begin{aligned}\boldsymbol{y}_v = M_\theta\,\hat{\boldsymbol{y}}_v &= \bar{B}^T M_\phi^{-1}\tilde{\boldsymbol{e}}_1\,,\\ &= B^T\tilde{\boldsymbol{e}}_1\,.\end{aligned}$$

□

9.2.4 Finite-dimensional Dirac structure

Let us define the flow variables as

$$\boldsymbol{f}^T := \left[-\dot{\boldsymbol{x}}_1\,,\quad f_{1\partial}\,,\quad f_{2\partial}\,,\quad -\dot{\boldsymbol{x}}_2\,,\quad f_{3\partial}\,,\quad f_{4\partial}\,,\quad \boldsymbol{y}_v\right]^T\,, \tag{9.63}$$

and the effort variables as

$$\boldsymbol{e}^T := \left[\tilde{\boldsymbol{e}}_1\,,\quad e_{1\partial}\,,\quad e_{2\partial}\,,\quad \tilde{\boldsymbol{e}}_2\,,\quad e_{3\partial}\,,\quad e_{4\partial}\,,\quad \boldsymbol{v}\right]^T\,, \tag{9.64}$$

where both $\boldsymbol{f}$ and $\boldsymbol{e} \in \mathbb{R}^{2N+4+K}$. Defing the following power product:

$$P := \boldsymbol{f}^T\boldsymbol{e}\,, \tag{9.65}$$

thanks to Eq. 9.58, $P = 0$ for all $(\boldsymbol{f}, \boldsymbol{e})$ satisfying Eqs. 9.46, 9.52 and 9.48.

Using the finite-dimensional Eqs. 9.46, the co-energy variables definition from Eq. 9.52, the boundary-ports definition from Eq. 9.48 and the distributed ports definition from Eq.

9.57, it is possible to write:

$$\begin{bmatrix} -\dot{\boldsymbol{x}}_1 \\ f_{1\partial} \\ f_{2\partial} \\ -\dot{\boldsymbol{x}}_2 \\ f_{3\partial} \\ f_{4\partial} \\ \boldsymbol{y}_v \end{bmatrix} = \underbrace{\begin{bmatrix} 0 & D_2 & -M_\phi^{-1}\bar{B} \\ 0 & \boldsymbol{\psi}_z{}^T(0) & 0 \\ 0 & -\boldsymbol{\psi}^T(0) & 0 \\ -D_2 & 0 & 0 \\ -\boldsymbol{\psi}^T(L) & 0 & 0 \\ \boldsymbol{\psi}_z{}^T(L) & 0 & 0 \\ \bar{B}^T M_\phi^{-1} M_{\psi\phi}^T & 0 & 0 \end{bmatrix}}_{F} \begin{bmatrix} \boldsymbol{e}_1 \\ \boldsymbol{e}_2 \\ \boldsymbol{v} \end{bmatrix}, \quad \begin{bmatrix} \tilde{\boldsymbol{e}}_1 \\ e_{1\partial} \\ e_{2\partial} \\ \tilde{\boldsymbol{e}}_2 \\ e_{3\partial} \\ e_{4\partial} \\ \boldsymbol{v} \end{bmatrix} = \underbrace{\begin{bmatrix} M_{\psi\phi}^T & 0 & 0 \\ \boldsymbol{\psi}^T(0) & 0 & 0 \\ \boldsymbol{\psi}_z{}^T(0) & 0 & 0 \\ 0 & M_{\psi\phi}^T & 0 \\ 0 & \boldsymbol{\psi}_z{}^T(L) & 0 \\ 0 & \boldsymbol{\psi}^T(L) & 0 \\ 0 & 0 & I \end{bmatrix}}_{E} \begin{bmatrix} \boldsymbol{e}_1 \\ \boldsymbol{e}_2 \\ \boldsymbol{v} \end{bmatrix}, \tag{9.66}$$

which provides an image representation of a Dirac structure as presented in Eq. 4.46. Note that the matrices

$$\begin{pmatrix} M^T \\ \boldsymbol{\psi}_z{}^T(0) \\ \boldsymbol{\psi}^T(0) \end{pmatrix} \quad \text{and} \quad \begin{pmatrix} M_{\psi\phi}^T \\ \boldsymbol{\psi}^T(L) \\ \boldsymbol{\psi}_z{}^T(L) \end{pmatrix}$$

are square and supposed to be invertible. Thus by inverting the block-diagonal matrix E,[2] Eq. 9.66 can be rewritten in explicit form as:

$$\boldsymbol{f} = \tilde{J}\boldsymbol{e}\,, \tag{9.67}$$

where:

$$\tilde{J} = \begin{bmatrix} 0 & \begin{pmatrix} D_2 \\ \boldsymbol{\psi}_z{}^T(0) \\ -\boldsymbol{\psi}^T(0) \end{pmatrix} \begin{pmatrix} M_{\psi\phi}^T \\ \boldsymbol{\psi}_z{}^T(L) \\ \boldsymbol{\psi}^T(L) \end{pmatrix}^{-1} & -M_\phi^{-1}\bar{B} \\ \begin{pmatrix} -D_2 \\ -\boldsymbol{\psi}^T(L) \\ \boldsymbol{\psi}_z{}^T(L) \end{pmatrix} \begin{pmatrix} M_{\psi\phi}^T \\ \boldsymbol{\psi}^T(0) \\ \boldsymbol{\psi}_z{}^T(0) \end{pmatrix}^{-1} & 0 & 0 \\ \bar{B}^T M_\phi^{-1} \quad 0 \quad 0 & 0 & 0 \end{bmatrix}. \tag{9.68}$$

The skew-symmetry of $\tilde{J}$ is easily verified, since $P = \boldsymbol{f}^T\boldsymbol{e} = 0$.

Finally, it is possible to rewrite Eq. 9.67 in a more classical way, by simply rearranging

[2] The elements of the block-diagonal matrix E are: the $(N+2)\times(N+2)$ matrices $\begin{pmatrix} M^T \\ \boldsymbol{\psi}_z{}^T(0) \\ \boldsymbol{\psi}^T(0) \end{pmatrix}$ and $\begin{pmatrix} M_{\psi\phi}^T \\ \boldsymbol{\psi}^T(L) \\ \boldsymbol{\psi}_z{}^T(L) \end{pmatrix}$, and the $K \times K$ identity I.

its rows and columns:

$$\begin{bmatrix} -\dot{\boldsymbol{x}} \\ \boldsymbol{y}_\partial \\ \boldsymbol{y}_v \end{bmatrix} = \begin{bmatrix} -J & -B_\partial & -B_d \\ B_\partial^T & D_\partial & 0 \\ B_d^T & 0 & 0 \end{bmatrix} \begin{bmatrix} \tilde{\boldsymbol{e}} \\ \boldsymbol{u}_\partial \\ \boldsymbol{v} \end{bmatrix}, \tag{9.69}$$

where $\dot{\boldsymbol{x}} = \begin{bmatrix} \dot{\boldsymbol{x}}_1{}^T & \dot{\boldsymbol{x}}_2{}^T \end{bmatrix}^T$, $\tilde{\boldsymbol{e}} = \begin{bmatrix} \tilde{\boldsymbol{e}}_1 & \tilde{\boldsymbol{e}}_2 \end{bmatrix}^T$, $\boldsymbol{u}_\partial$ and $\boldsymbol{y}_\partial$ are the boundary inputs and outputs, $\boldsymbol{v}$ and $\boldsymbol{y}_v$ are the discretized distributed input/outputs. The matrices J and D_∂ are skew-symmetric.

9.2.5 Hamiltonian discretization

As in the previous cases, the Hamiltonian is approximated as follows:

Definition 9.2
The discretized Hamiltonian H_d is defined as:

$$H_d(\boldsymbol{x}_1, \boldsymbol{x}_2) := H[x_1(x,t) = \boldsymbol{x}_1{}^T \boldsymbol{\phi}(z), x_2(x,t) = \boldsymbol{x}_2{}^T \boldsymbol{\phi}(z)] \,.$$

The time-derivative of H_d is given by:

$$\dot{H}_d(\boldsymbol{x}_1, \boldsymbol{x}_1) = (\nabla_{\boldsymbol{x}_1} H)^T \dot{\boldsymbol{x}}_1 + (\nabla_{\boldsymbol{x}_2} H)^T \dot{\boldsymbol{x}}_2 \,. \tag{9.70}$$

By choosing the following constitutive relationships:

$$\begin{aligned} \tilde{\boldsymbol{e}}_1 &= \nabla_{\boldsymbol{x}_1} H_d(\boldsymbol{x}_1, \boldsymbol{x}_2) \,, \\ \tilde{\boldsymbol{e}}_2 &= \nabla_{\boldsymbol{x}_2} H_d(\boldsymbol{x}_1, \boldsymbol{x}_2) \,, \end{aligned} \tag{9.71}$$

the finite-dimensional power-balance is given by:

$$\dot{H}_d = \tilde{\boldsymbol{e}}_1{}^T(t) \dot{\boldsymbol{x}}_1(t) + \tilde{\boldsymbol{e}}_2{}^T(t) \dot{\boldsymbol{x}}_2(t) = \boldsymbol{y}_\partial{}^T \boldsymbol{u}_\partial + \boldsymbol{y}_v{}^T \boldsymbol{v} \,. \tag{9.72}$$

Recall that from Remark 9.4 (page 122) that the term $(\boldsymbol{y}_v)^T \boldsymbol{v} = \int_{z=a}^{b} y_v^{ap}(z,t)\, u^{ap}(z,t)\, \mathrm{d}z$:

$$\dot{H}_d = \boldsymbol{y}_\partial^T \boldsymbol{u}_\partial + \int_{z=a}^{b} y_v^{ap}(z,t)\, u^{ap}(z,t)\, \mathrm{d}z \,. \tag{9.73}$$

9.3 Conclusions

This chapter provides some extensions for the power-preserving pseudo-spectral method, originally proposed by Moulla, Lefèvre, and Maschke (2011). Firstly, we included distributed input ports for first-order pHs in Section 9.1. These ports will be used in subsequent chapters to introduce damping on the fluid and torsion equations. Although not presented in this chapter for simplicity, the same approach is also used to include this type of distributed ports in the bending equations.

The second proposed extension is the discretization of the second-order differential operator, that appears in the bending equations. In this case, the system has four pairs of boundary ports.

Finally, the most tricky extension is related to the fact that the bending equations with piezoelectric actuators exhibit an unbounded input operator $\partial_{z^2}^2(\Pi_{ab}(z)k_p v(z,t))$ (which includes a second-order derivative of the discontinuous function $\Pi_{ab}(z)$). Thus, the use of pseudo-spectral methods is not straightforward. We used a weak form of the partial differential equations to overcome this issue.

Chapter 10

Numerical and experimental results

In the previous chapters, structure-preserving semi-discretization methods for port-Hamiltonian systems were presented. In Chapter 9, the pseudo-spectral methods were extended to take into account the specifities of the models presented in Part II: fluid and torsion beam with dissipative ports; piezoelectric beam with distributed ports.

In this chapter, these models are now discretized with the schemes of Chapter 9. Firstly, some practical aspects about the implementation of the numerical schemes are presented in Section 10.1. Secondly, in order to validate the numerical approach and verify the convergence of the method, each of the subsystems (beam in bending, torsion and fluid) is first analyzed separately in Section 10.2. Once the individual models are validated, they are coupled to obtain the fluid-structure interactions model. The procedure for coupling the numerical models is recalled in 10.3. Section 10.4 shows numerical and experimental results in the frequency domain. Section 10.5 presents the time-domain simulation results for the nonlinear coupled fluid-structure system. Finally, conclusions are presented in Section 10.6.

Contents

10.1 Implementation of the pseudo-spectral numerical scheme: difficulties and tricks

10.1.1 Computation of the "differentiation" and "mass" matrices

In order to implement the numerical schemes of Chapter 9, it is necessary to compute the "differentiation" and "mass" matrices, defined for example in Eqs. 9.39, 9.37 and 9.51. The "differential" D_i matrices are obtained by evaluation of the derivatives of polynomials of the effort basis in the flow basis collocation points; the "mass" matrices M_i are obtained from the integral formulas of the product of the two basis polynomial vectors; weak-form matrices $\tilde{B}$ and $\tilde{D}_2$ are obtained from the integral of basis polynomials vectors spatially derived.

For implementation, two different approaches have been tested:

1. Using a computer algebra software: this leads to exact computation of these matrices when using polynomial basis, which can be quickly done for N up to about 10. On the other hand, for larger values of N, the computational burden becomes too expensive.
2. Since the approximation basis are polynomials, the integrals can be exactly computed by Gaussian quadrature, and the derivatives can be exactly computed using automatic differentiation methods.[1]

The results presented in this thesis use the second method, since it leads to a very precise solution with very small computational cost (even for large N).

10.1.2 Computation of the discretized Hamiltonian

Once the finite-dimensional approximation interconnection matrices J,B and D are obtained, the next step is compute the approximate Hamiltonian. Notice that all the Hamiltonians presented in Part II are defined by integrals. For example, in the case of a quadratic H (which is the case of the torsion and bending equations):

$$H[x_1(z,t), x_2(z,t)] = \int \left(a x_1^2 + b x_2^2 \right) \mathrm{d}z \,, \tag{10.1}$$

its approximation is obtained by substitution of $x_i(z,t)$ by its finite-dimensional approximation $x_i^{ap}(z,t) = \boldsymbol{x}_i^T(t)\boldsymbol{\phi}(z)$:

$$H_d(\boldsymbol{x}_1, \boldsymbol{x}_2) = \int \left(a(x_1^{ap})^2 + b(x_2^{ap})^2 \right) \mathrm{d}z \,, \tag{10.2}$$

$$= a\boldsymbol{x}_1^T(t) \left(\int \boldsymbol{\phi}(z)\boldsymbol{\phi}^T(z)\,\mathrm{d}z \right) \boldsymbol{x}_1 + b\boldsymbol{x}_2^T(t) \left(\int \boldsymbol{\phi}(z)\boldsymbol{\phi}^T(z)\,\mathrm{d}z \right) \boldsymbol{x}_2 \,. \tag{10.3}$$

[1] We used the package ForwardDiff: http://www.juliadiff.org, which uses the forward mode automatic differentiation method.

We have not yet made any hypothesis about the collocation points z_{xi} and z_{ei}, so until now any grid could be used. Gauss-Legendre collocation points are chosen for z_{xi}, since in this case $\int \boldsymbol{\phi}(z)\boldsymbol{\phi}^T(z)\,\mathrm{d}z$ becomes a diagonal matrix. The previous integral can be exactly computed as a weighted sum:

$$H_d(\boldsymbol{x}_1, \boldsymbol{x}_2) = \sum (a{x_{1,i}}^2 + b{x_{2,i}}^2) w_i \,. \tag{10.4}$$

In addition, the integral of more general nonlinear functions $f(z)$ can be approximated using Gaussian integration as:

$$\int f(z)\,\mathrm{d}z \approx \sum_i f(z_i) w_i \,, \tag{10.5}$$

with very good precision when $f(z)$ can be approximated by a polynomial. Indeed, for N degree collocation points, the previous formula allows computing the integral of a $2N+1$ degree polynomial exactly. In our case, all the integrands of the approximate Hamiltonian are actually polynomials of z (even in the non-quadratic case of nonlinear fluid (Eq. A.5)). For this reason, the quadrature formula leads to extremely precise computation of H_d. This makes the computation of the approximate Hamiltonians quite simple.

In addition, another advantage of the Gauss-Legendre collocation points is that they also reduce the high frequency oscillations, known as Runge's phenomenon, since these points are more densely distributed near the edges of the interval (see, e.g., Trefethen (2000)).

Finally, the gradient of the Hamiltonians is computed using two different methods:

1. Analytically.

2. Using automatic differentiation methods (as we did for the differentiation matrices).

The first method is straightforward for simple Hamiltonians, but it can be tedious (and error-prone) for complicated cases (as the nonlinear fluid equations). For this reason, the automatic differentiation method is preferable for nonlinear equations as the fluid Hamiltonian (Eq. A.5) and is used to compute the results of the following sections.

10.1.3 Including damping

After discretization, a set of equations of the following form is obtained:

$$\begin{aligned}
\dot{\boldsymbol{x}}^i &= J^i \tilde{\boldsymbol{e}}^i + B^i_\partial \boldsymbol{u}^i_\partial + B^i_d \boldsymbol{u}^i_d + B^i_R \boldsymbol{u}^i_R \,, \\
\boldsymbol{y}^i_\partial &= (B^i_\partial)^T \tilde{\boldsymbol{e}}^i + D^i_\partial \boldsymbol{u}^i_\partial \,, \\
\boldsymbol{y}^i_d &= (B^i_d)^T \tilde{\boldsymbol{e}}^i \,, \\
\boldsymbol{y}^i_R &= (B^i_R)^T \tilde{\boldsymbol{e}}^i \,,
\end{aligned} \tag{10.6}$$

where the superscript i stands for B, T and F (bending, torsion and fluid equations, as used in Part II), $\boldsymbol{x}^i(t)$ and $\tilde{\boldsymbol{e}}^i$ are the vectors of energy and co-energy variables, J^i and D^i are skew-symmetric matrices, $\boldsymbol{u}^i_\partial(t)$ and $\boldsymbol{y}^i_\partial(t)$ are respectively the input and output boundary ports, $\boldsymbol{u}^i_d$ and $\boldsymbol{y}^i_d$ are distributed ports (that are related to the piezoelectric voltage, in the case of beam equations), and $\boldsymbol{u}^i_R(t)$ and $\boldsymbol{y}^i_R(t)$ are the distributed resistive (ou dissipative) ports.

In order to include damping, as explained in § 4.1.3, it is possible to use constitutive relations as: $\boldsymbol{u}_R = -D\boldsymbol{y}_R$, where D is a positive definite matrix. Then, the dynamic equations can be written without the dissipative ports as:

$$\begin{aligned}
\dot{\boldsymbol{x}}^i &= (J^i - R^i)\tilde{\boldsymbol{e}}^i + B^i_\partial \boldsymbol{u}^i_\partial + B^i_d \boldsymbol{u}^i_d \,, \\
\boldsymbol{y}^i_\partial &= (B^i_\partial)^T \tilde{\boldsymbol{e}}^i + D^i_\partial \boldsymbol{u}^i_\partial \,, \\
\boldsymbol{y}^i_d &= (B^i_d)^T \tilde{\boldsymbol{e}}^i \,,
\end{aligned} \tag{10.7}$$

where $R^i = B^i_R D (B^i_R)^T$.

Any positive semi-definite matrix D leads to the introduction of damping in the system. Appendix D describes how this matrix was chosen in this thesis.

10.2 Validation of the individual numerical models

In this section, the pHs models of each individual system (beam in torsion and bending, and fluid) and the discretization scheme are validated. Firstly, in the case of homogeneous versions of the PDEs, the validation is performed in § 10.2.1 by comparing the natural frequencies obtained from the discretized pHs models and known analytical results. Then, in § 10.2.2, we show that in the inhomogeneous case, where no analytical solution is known, the validation is performed by comparing the numerical frequency response with experimental results.

10.2.1 Case of pHs models considering homogeneous parameters and comparison with analytical results

In the case of the linearized partial differential equations for the fluid and the beam with homogeneous parameters, analytical solutions exist and thus they provide a valuable tool for validation of the numerical schemes proposed in this thesis. The analytical solutions for the linearized fluid and beam equations are presented in Appendix C.

In Eq. 10.7, the co-energy variables $\tilde{\boldsymbol{e}}^i$ are obtained from the gradient of the discretized Hamiltonian, i.e.: $\tilde{\boldsymbol{e}}^i = \nabla_{\boldsymbol{x}^i} H^i_d$. In the case of linear systems, the Hamiltonian is quadratic: $H^i_d = \frac{1}{2}(\boldsymbol{x}^i)^T Q^i \boldsymbol{x}^i$, and $\tilde{\boldsymbol{e}}^i = Q^i \boldsymbol{x}^i$. Thus, the equations become:

$$\begin{aligned}
\dot{\boldsymbol{x}}^i &= (J^i - R^i) Q^i \boldsymbol{x}^i + B^i_\partial \boldsymbol{u}^i_\partial \,, \\
\boldsymbol{y}^i_\partial &= (B^i_\partial)^T Q^i \boldsymbol{x}^i + D^i_\partial \boldsymbol{u}^i_\partial \,,
\end{aligned} \tag{10.8}$$

Both in the cases of the bending and torsion beam, the fixed-free boundary conditions are satisfied if $\boldsymbol{u}^i_\partial = 0$. Neglecting the dissipation, the autonomous equations become:

$$\dot{\boldsymbol{x}}^i = J^i Q^i \boldsymbol{x}^i \,. \tag{10.9}$$

Consequently, in order to find the approximated natural frequencies of these systems, it is enough to find the eigenvalues of $J^i Q^i$. These results are presented in Tables 10.1 and 10.2.

In the case of fluid equations, the no-flow boundary condition introduces a constraint to the system, since one of the outputs is equal to zero,i.e.:

$$\begin{aligned} \dot{\boldsymbol{x}}^F &= J^F Q^F \boldsymbol{x}^F + B^F_\partial u^F_{1\partial} \,, \\ 0 = y^F_{1\partial} &= (B^F_{1\partial})^T Q^F \boldsymbol{x}^F \,, \end{aligned} \tag{10.10}$$

for this reason it must be written as a descriptor system (see, e.g., Verghese, Lévy, and Kailath (1981)):

$$\underbrace{\begin{bmatrix} I & 0 \\ 0 & 0 \end{bmatrix}}_{E} \begin{bmatrix} \dot{\boldsymbol{x}}^F \\ \dot{u}^F_{1\partial} \end{bmatrix} = \underbrace{\begin{bmatrix} J^F Q^F & B^F_\partial \\ (B^F_{1\partial})^T Q^F & 0 \end{bmatrix}}_{A} \begin{bmatrix} \boldsymbol{x}^F \\ u^F_{1\partial} \end{bmatrix} \,. \tag{10.11}$$

The natural frequencies of the sloshing problem presented in Table 10.3 are obtained by linearizing the system[2] and computing the generalized eigenvalues of the pair of matrices (E,A).

From Tables 10.1 to 10.3, the convergence of the method can be easily verified. The relative errors of the numerical results with respect to the exact ones are presented. It is possible to see that, when using only 9 basis functions, the error of the first frequency is limited by the numerical precision. Using 12 basis functions, the first 7 natural frequencies have a relative error smaller than 1% for all the three tested cases.

In the case of the bending beam, the state-space obtained from the numerical method is used to find the frequency response and compared with known exact results for a beam with uniform parameters presented in Appendix C. These results are presented in Fig. 10.1. Only 12 basis functions were used in the numerically obtained system. The numerical results agree very well with the exact transfer function.

[2]The linearization is obtained by computing the Hessian matrix of the Hamiltonian at the equilibrium point, which can be easily done using automatic differentiation. In this case: $Q^F = \frac{\partial^2 H^F_d}{\partial \boldsymbol{x}^2}(\boldsymbol{x}_{\text{eq}})$.

Table 10.1: Torsion equation: approximated natural frequencies obtained from the semi-discretization model computed for different number of (N) basis functions and comparison with the exact frequencies computed by the analytical expression.

	N = 3		N = 6		N = 9		N = 100		Exact
Mode	Freq.	Error	Freq.	Error	Freq.	Error	Freq.	Error	Freq.
1	35.2	1e-04	35.2	4e-11	35.2	8e-16	35.2	2e-14	35.2
2	111.2	5e-02	105.6	1e-05	105.6	2e-10	105.6	1e-14	105.6
3	345.0	1e+00	176.5	3e-03	176.0	9e-07	176.0	7e-15	176.0
4			257.9	5e-02	246.5	2e-04	246.4	1e-16	246.4
5			414.0	3e-01	318.3	5e-03	316.8	1e-15	316.8
6			1203.5	2e+00	402.9	4e-02	387.2	1e-16	387.2
7					541.6	2e-01	457.7	2e-16	457.7

Table 10.2: Bending equation: approximated natural frequencies obtained from the semi-discretization model computed for different number of (N) basis functions and comparison with the exact frequencies computed by the analytical expression.

	N = 3		N = 6		N = 9		N = 12		Exact
Mode	Freq.	Error	Freq.	Error	Freq.	Error	Freq.	Error	Freq.
1	2.2	6e-04	2.2	2e-10	2.2	2e-14	2.2	6e-15	2.2
2	14.0	2e-02	13.8	3e-05	13.8	1e-11	13.8	5e-15	13.8
3	199.1	4e+00	38.5	6e-04	38.5	2e-06	38.5	2e-12	38.5
4			82.6	9e-02	75.5	3e-05	75.5	1e-07	75.5
5			146.7	2e-01	125.9	9e-03	124.7	2e-06	124.7
6			3446.4	2e+01	190.5	2e-02	186.5	9e-04	186.3
7					364.5	4e-01	261.0	3e-03	260.3

Table 10.3: Linearized sloshing equation: approximated natural frequencies obtained from the semi-discretization model computed for different number of (N) basis functions and comparison with the exact frequencies computed by the analytical expression.

	N = 3		N = 6		N = 9		N = 12		Exact
Mode	Freq.	Error	Freq.	Error	Freq.	Error	Freq.	Error	Freq.
1	0.46	7e-03	0.45	1e-07	0.45	1e-13	0.45	9e-15	0.45
2	1.12	2e-01	0.91	3e-04	0.91	2e-08	0.91	1e-12	0.91
3			1.38	1e-02	1.36	2e-05	1.36	2e-09	1.36
4			2.05	1e-01	1.82	1e-03	1.82	1e-06	1.82
5			3.93	7e-01	2.31	2e-02	2.27	9e-05	2.27
6					2.97	9e-02	2.73	2e-03	2.73

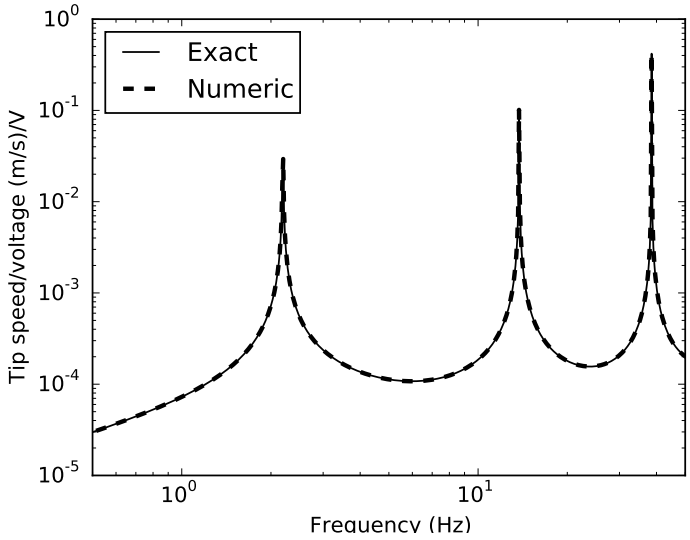

Figure 10.1: Frequency response of the bending beam: comparison between the numerical model and the exact transfer function. The beam is assumed to have uniform rigidity and mass distributions. The number of basis functions used in the semi-discretization method is $N = 12$.

10.2.2 Case of pHs model considering inhomogeneous beam with piezoelectric patch: numerical model and comparison with experimental results

The results in 10.2.1 assume that the beam has uniformly distributed parameters. This assumption are useful for theoretical validation since in this case closed-form expressions exist. In practice, however, the piezoelectric patches change the local rigidity and mass distribution of the beam. This effect is presented in Fig. 10.2, which shows a comparison between the numerical and experimental results of the beam frequency response. The experimental results are obtained from a frequency sweep excitation of the piezoelectric patches. The tip speed is measured using an accelerometer placed near the free-tip of beam. Two different numerical results are presented: 1) the beam is considered without piezoelectric patch; 2) the mass and rigidity of the piezoelectric patches are taken into account in the computation of the beam Hamiltonian. The results show in general a good agreement between the numerical and experimental frequency response. However, the curve using the second numerical method agrees better with experiments for small frequencies, since it introduces the mass and rigidity of the patch. No damping is included in the numerical method, which explains the larger amplitudes of the peaks.

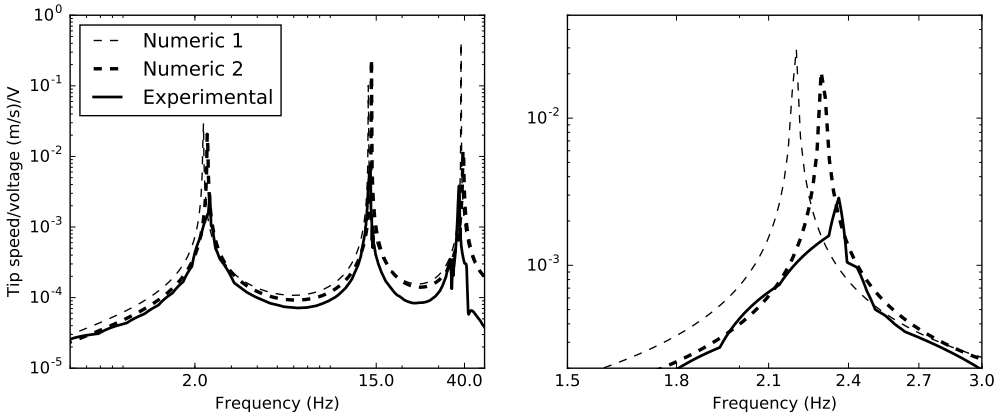

Figure 10.2: Frequency response: comparison between two numerical models and the experimental results. The curve labeled as *numeric 1* was obtained using a model in which the piezoelectric patches are not taken into account. *Numeric 2* takes into account the piezoelectric patches mass and rigidity. The figure on the right focuses on the first natural frequency. By including the patches properties, both the amplitude and natural frequency shift and a better agreement with experimental result is obtained for small frequencies. The number of basis functions used in the semi-discretization method is $N = 12$.

10.3 FSI: coupling of the numerical models

The fluid-structure system of Part II is modeled by four different subsystems:

1. Piezoelectric beam with bending motion;
2. Piezoelectric beam with torsion motion;
3. Fluid equations;
4. Rigid body equations to represent the tank and other rigid appendices.

By concatenating the state-variables of each subsystem as: $\boldsymbol{x} = \begin{bmatrix} \boldsymbol{x}^B & \boldsymbol{x}^T & \boldsymbol{x}^F & \boldsymbol{x}^{RB} \end{bmatrix}^T$, it is possible to rewrite the full model using exactly the same framework as for each component individually (which is one strength of the pHs modeling). Thus we get:

$$\begin{aligned} \dot{\boldsymbol{x}}(t) &= (J - R)\nabla_{\boldsymbol{x}} H_d + B\boldsymbol{u}\,, \\ \boldsymbol{y}(t) &= B^T \nabla_{\boldsymbol{x}} H_d + D\boldsymbol{u}\,, \end{aligned} \tag{10.12}$$

where J,R, B and D are the block-diagonal matrices obtained from each component J^i, R^i, B^i and D^i matrices. The discrete global Hamiltonian $H_d(\boldsymbol{x}(t))$ is the sum of each $H_d^i(\boldsymbol{x^i}(t))$. The input and output vectors are obtained from Eqs. 5.22, 5.29, 6.41 and B.6:

$$\begin{aligned} \boldsymbol{u}(t) &= \left[\; e_1^B(0) \quad \partial_z e_1^B(0) \quad \partial_z e_2^B(L) \quad e_2^B(L) \quad v \;\middle|\; e_1^T(L) \quad e_2^T(0) \;\middle|\; e_1^F(a/2) \quad e_2^F(-a/2) \quad F_{ext}^F \quad M_{ext}^F \;\middle|\; M_{ext,B}^{RB} \quad M_{ext,T}^{RB} \;\right]^T, \\ \boldsymbol{y}(t) &= \left[\; \partial_z e_2^B(0) \quad -e_2^B(0) \quad -e_1^B(L) \quad \partial_z e_1^B(L) \quad v^* \;\middle|\; -e_2^T(L) \quad e_1^T(0) \;\middle|\; -e_2^F(a/2) \quad e_1^F(-a/2) \quad \dot{D} \quad \dot{\theta}^F \;\middle|\; \dot{\theta}_B^{RB} \quad \dot{\theta}_T^{RB} \;\right]^T. \end{aligned} \tag{10.13}$$

The coupling between all the equations is given by the four kinematic and three dynamic constraints (Eqs. 7.13, 7.14, 7.15, 7.18).

There are also five fixed boundary conditions: $e_2^F(-a/2) = e_2^F(a/2) = 0$ (no flow through the tank walls) and $e_1^B(0) = \partial_z e_1^B(0) = 0$ for the bending fixed-end and $e_2^T(0) = 0$ for the torsion fixed-end. Four of these boundary conditions are related to variables of the input vector $\boldsymbol{u}$. Only $e_2^F(a/2) = 0$ is related to an output and, for this reason, will represent one additional constraint to the problem. Finally, the piezoelectric applied voltage is also related to an input: $v = V(t)$.

We can reorganize the input and output vector to keep only the constrained port-variables $\boldsymbol{u}_c$ and $\boldsymbol{y}_c$, such that Eq. 10.12 becomes:

$$\begin{cases} \dot{\boldsymbol{x}} &= J\nabla_{\boldsymbol{x}} H_d + B_c \boldsymbol{u}_c + B_v v\,, \\ \boldsymbol{y}_c &= {B_c}^T \nabla_{\boldsymbol{x}} H_d\,, \end{cases} \tag{10.14}$$

where:

$$\begin{aligned} \boldsymbol{u}_c(t) &= \left[\ \partial_z e_2^B(L) \quad e_2^B(L) \ \middle|\ e_1^T(L) \ \middle|\ e_1^F(a/2) \quad F_{ext}^F \quad M_{ext}^F \ \middle|\ M_{ext,B}^{RB} \quad M_{ext,T}^{RB} \ \right]^T , \\ \boldsymbol{y}_c(t) &= \left[\ -e_1^B(L) \quad \partial_z e_1^B(L) \ \middle|\ -e_2^T(L) \ \middle|\ -e_2^F(a/2) \quad \dot{D} \quad \dot{\theta}^F \ \middle|\ \dot{\theta}_B^{RB} \quad \dot{\theta}_T^{RB} \ \right]^T . \end{aligned} \tag{10.15}$$

Notice that the four kinematic constraints (Eqs. 7.13, 7.14, 7.15) and the no-flow condition ($e_2^F(a/2) = 0$) are linear functions of the output variables. So it is possible to write them as:

$$\mathcal{M}\boldsymbol{y}_c = 0\,, \tag{10.16}$$

where $\mathcal{M}$ is a 5×8 matrix. Similarly, the three dynamic constraints (Eq. 7.18) are linear functions of the input variables:

$$\mathcal{N}\boldsymbol{u}_c = 0\,, \tag{10.17}$$

where $\mathcal{N}$ is a 3×8 matrix. Since $\boldsymbol{u}_c$ represents a vector of 8 unknowns subject to 3 constraints, it is possible to rewrite it as a function of only 5 unknowns: $\boldsymbol{u}_c = G\boldsymbol{\lambda}$, where $\lambda \in \mathbb{R}^5$ is the vector of Lagrange multipliers.

Additionally, since the interconnections are power-preserving ($\boldsymbol{u}_c^T \boldsymbol{y}_c = 0$), it is easy to verify that $\mathcal{M} = G^T$. Thus, the coupled equations can be written as:

$$\begin{aligned} \dot{\boldsymbol{x}}(t) &= J\nabla_{\boldsymbol{x}} H_d + B_v v + B_c G\boldsymbol{\lambda}\,, \\ 0 &= G^T {B_c}^T \nabla_{\boldsymbol{x}} H_d\,. \end{aligned} \tag{10.18}$$

These equations can be used for simulation using numerical integration methods for differential-algebraic equations (DAEs) (Kunkel and Mehrmann, 2006; Ascher and Petzold, 1998). Additionally, several manipulations are possible, as recalled in § 4.3.2, leading to an explicit set of ordinary differential equations, which can be used for nonlinear time-domain simulation thanks to classical numerical methods for ODEs.

Now, in order to analyze the frequency response of the experimental set up, the linearized version of Eq. 10.18 has to be taken into account. In this case, the coupled system can be

written using a linear descriptor state-space (DSS) formulation:

$$\underbrace{\begin{bmatrix} I & 0 \\ 0 & 0 \end{bmatrix}}_{E} \frac{\partial}{\partial t} \begin{bmatrix} \boldsymbol{x} \\ \boldsymbol{\lambda} \end{bmatrix} = \underbrace{\begin{bmatrix} JQ & B_c G \\ G{B_c}^T Q & 0 \end{bmatrix}}_{A} \begin{bmatrix} \boldsymbol{x} \\ \boldsymbol{\lambda} \end{bmatrix} + \begin{bmatrix} B_v \\ 0 \end{bmatrix} v(t)\,. \tag{10.19}$$

This linearized system can also be used for simulation. In addition, from the generalized eigenvalues of (E,A), it is possible to find the modes of the coupled system and to compare them to experimentally measured natural frequencies. Finally, the output matrix (C) of the DSS is chosen such that the output of the system is the tip speed or acceleration. Then, the resulting system is used to compare with experimental results (frequency response, for example).

Remark 10.1
The matrix G of the coupled equations (Eq. 10.18) can be obtained manually from the constraints established in Chapter 7.

In practice, each subsystem is implemented in the computer as an individual "module" (an object, in object-oriented programming paradigm). Furthermore, the procedures described in § 4.3 are implemented, allowing the manipulation of the modules. Thus, the derivation of Eq. 10.18 is automatically done, using the following procedure:

1. *Concatenation of bending and torsion models;*
2. *Coupling between beam model (in torsion and bending) with the fluid dynamics;*
3. *Coupling of the model obtained in step 2 with the rigid body dynamics.*

Using pseudo-code, the procedure is as follows:

1. *structural model = concatenate(bending model, torsion model)*
2. *FSI model = interconnection(structural model, fluid model)*
3. *FSI model with RB = interconnection (FSI model, RB model)*

This pseudo-code highlights the systematic and modular characteristics of the pHs approach. The final system can be also easily manipulated using tools like constraint removals (from § 4.3.2), linearization (by simply evaluating the Hessian of the Hamiltonian at equilibrium), etc. We implemented all the tools for discretization and manipulation of pHs in the programming language Julia. The codes are available at:
`https://github.com/flavioluiz/PortHamiltonian.jl`.

10.4 Results for FSI: frequency response

The fully coupled system is validated by comparing the frequency response of the discretized finite-dimensional model with the measured frequency response.

The natural frequencies of the coupled system, obtained from generalized eigenvalues of the (E, A) matrices (Eq. 10.19) are presented for two filling ratios in Tables 10.4 and 10.5. The frequency responses for the same filling ratios are presented in Figs. 10.3 and 10.4. The input is the voltage applied to the piezoelectric patches and the output is the speed of the tank. All the results are compared with the experimental ones.

The first five modes of Tables 10.4 and 10.5 are mainly due to the coupling between the sloshing dynamics and the first bending mode of the structure. The sixth mode is dominated by the torsion dynamics. The seventh and eighth modes are bending modes.

The fluid dynamics also introduces modes that are symmetric with respect to the center of the tank. The natural frequencies of these modes are not presented in Tables 10.4 and 10.5 since they do not interact with the structure (they are not observable nor controllable).

Notice that a quite good agreement with experimental results is obtained. For the 25% filling ratio, most modes agree with an error less than 7%. Larger errors appears for larger filling ratios, specially for modes 3 to 5: one of the reasons is that the fluid equations used in this paper assume the shallow water hypothesis, which is more accurate for small filling ratios of the tank.

Remark 10.2
Recall that in Remark 7.2, another interconnection structure was defined. The offset between the center of gravity of the fluid and the torsion axis of the beam was taken into account. The frequency responses for this improved interconnection are presented in Figs. 10.5 and 10.6. We note that now the torsion mode (mode number 6) now appears in the frequency response.

Table 10.4: Coupled fluid-structure with 25% filled tank: approximated natural frequencies obtained from the semi-discretization model computed for different values of N basis functions and comparison with the experimental results.

	N = 3		N = 6		N = 9		N = 12		Experimental
Mode	Freq. (Hz)	Error (%)	Freq. (Hz)	Error (%)	Freq. (Hz)	Error (%)	Freq. (Hz)	Error (%)	Freq. (Hz)
1	0.44	6.5	0.43	7.0	0.43	7.0	0.43	7.0	0.47
2	1.24	7.9	1.18	3.2	1.18	3.1	1.18	3.1	1.15
3			1.45	3.4	1.43	4.9	1.43	4.9	1.50
4			3.99	67.7	2.32	2.3	2.29	3.8	2.38
5					4.32	46.9	3.24	10.4	2.94
6	8.42	5.1	8.42	5.1	8.42	5.1	8.42	5.1	8.01
7	9.64	0.3	9.52	0.9	9.51	1.0	9.51	1.0	9.61
8	25.40	3.1	23.64	4.0	23.63	4.1	23.63	4.1	24.63

Table 10.5: Coupled fluid-structure with 50% filled tank: approximated natural frequencies obtained from the semi-discretization model computed for different values of N basis functions and comparison with the experimental results.

	N = 3		N = 6		N = 9		N = 12		Experimental
Mode	Freq. (Hz)	Error (%)	Freq. (Hz)	Error (%)	Freq. (Hz)	Error (%)	Freq. (Hz)	Error (%)	Freq. (Hz)
1	0.59	6.6	0.59	6.2	0.59	6.2	0.59	6.2	0.55
2	1.31	9.1	1.26	5.6	1.26	5.6	1.26	5.6	1.20
3			2.16	13.4	2.13	11.4	2.12	11.4	1.91
4			6.05	124.6	3.49	29.5	3.43	27.3	2.69
5					6.47	98.1	4.85	48.3	3.27
6	6.95	0.4	6.95	0.5	6.95	0.5	6.95	0.4	6.92
7	9.61	3.9	9.54	3.1	9.52	2.9	9.52	2.9	9.25
8	25.39	9.9	23.64	2.3	23.63	2.3	23.64	2.3	23.10

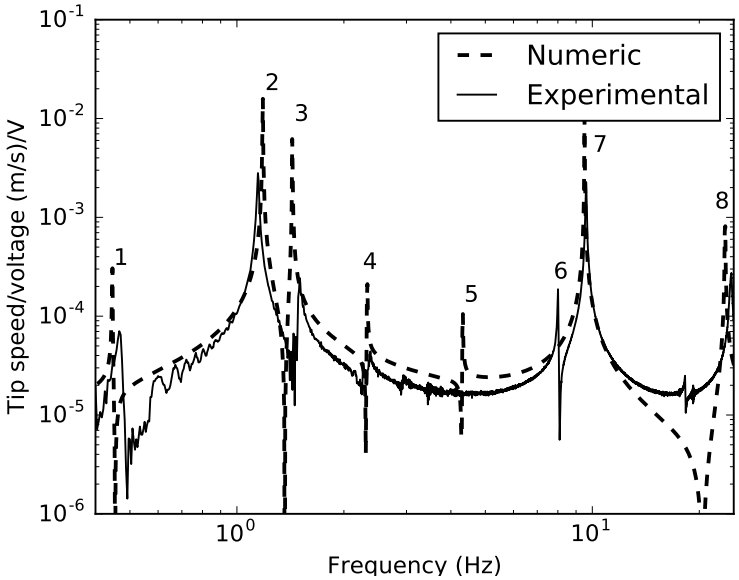

Figure 10.3: Frequency response of the fluid-structure coupled system: comparison between the numerical model with experimental results (tank 25% filled). The numbers indicate the mode number as in Table 10.4. A good agreement is observed for the first four coupled sloshing-structure modes. The number of basis functions used in the semi-discretization method is $N = 9$ (for each subsystem).

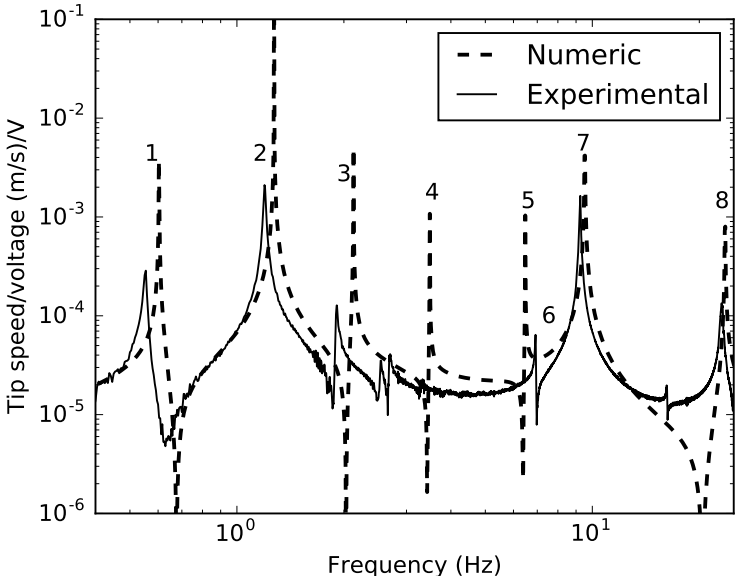

Figure 10.4: Frequency response of the fluid-structure coupled system: comparison between the numerical model with experimental results (tank 50% filled). The numbers indicate the mode number as in Table 10.5. Only the first two sloshing modes are well represented. The larger discrepancy is explained by the use of shallow water hypothesis, which validity is reduced for larger filling ratios. The number of basis functions used in the semi-discretization method is $N = 9$ (for each subsystem).

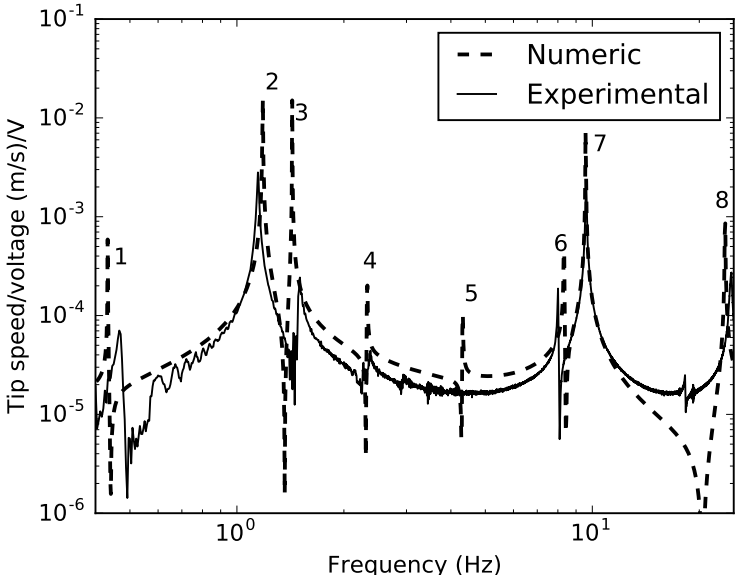

Figure 10.5: Frequency response of the fluid-structure coupled system: comparison between the numerical model with experimental results (tank 25% filled). Differently from Fig. 10.3, here the offset of the position of the fluid center of gravity with respect to the torsion is taken into account. The torsion mode (6) appears in the numerical frequency response. The number of basis functions used in the semi-discretization method is $N = 9$ (for each subsystem).

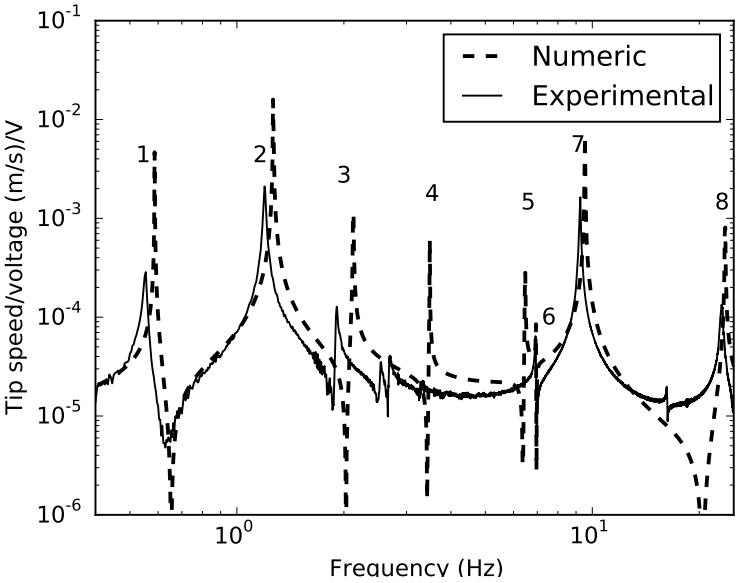

Figure 10.6: Frequency response of the fluid-structure coupled system: comparison between the numerical model with experimental results (tank 50% filled). Differently from Fig. 10.4, here the offset of the position of the fluid center of gravity with respect to the torsion is taken into account. The torsion mode (6) appears in the numerical frequency response. The number of basis functions used in the semi-discretization method is $N = 9$ (for each subsystem).

10.5 Results for FSI: time response and nonlinear behavior

One of the main interests of using the port-Hamiltonian formulation is that it allows representing nonlinear systems. Although the fluid equations presented in this paper are nonlinear, the numerical results presented above were obtained after linearizing the equations. Hereafter, an example of nonlinear simulation is presented.

Fig. 10.7 shows the snapshots of the fluid height in a moving tank. The fluid starts in still condition and is excited using harmonic voltages for the piezoelectric patches, with a frequency close to the first natural frequency of sloshing. Moreover, the simulations are run for two different amplitudes of the voltages to generate small and large fluid motion amplitudes. Fig. 10.7 shows the result after 11 seconds of simulation. The amplitude of the oscillations are 100 times larger in Fig. 10.7 - Right, which corresponds to the higher voltage simulation. In each figure, two curves are presented: one from the simulation using the nonlinear equations and the other using a linearized version of the fluid model. For small amplitude motions (Fig. 10.7 - Left), the linear and nonlinear simulations coincide and the shape of the waves is similar to the first modal deformation of the fluid. For large amplitude motions (Fig. 10.7 - Right), a nonlinear wave behavior appears: the linear and nonlinear results are clearly different. Fig. 10.8 shows the time response of the tip speed of the beam for these same simulations. For large amplitudes (Fig. 10.8 - Right), the fluid nonlinear behavior affects the structural dynamics response, reducing the amplitude of the vibrations, which is observed in practice on the real experimental set up.

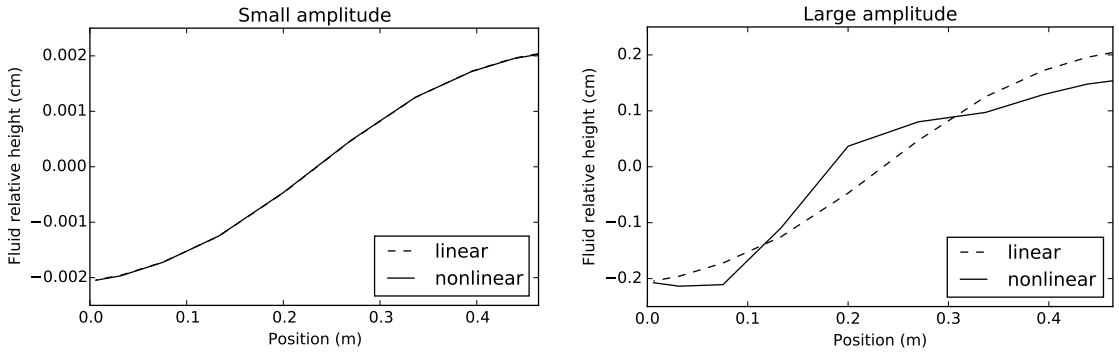

Figure 10.7: Sloshing-structure simulation: the system starts in still condition and is harmonically excited with frequency close to the first natural frequency. The figures show a snapshot of the fluid height after 11 seconds of simulation. On the left with small amplitude excitation, linear and nonlinear simulations give the same results. On the right with 100 times larger amplitude excitation, two different behaviors can be observed: a nonlinear sloshing wave appears. The number of basis functions used in the semi-discretization method is $N = 10$ (for each subsystem).

Additional simulation results, as well as videos with comparison between the numerical and experimental results can be found on our website.[3]

[3] `https://github.com/flavioluiz/port-hamiltonian`

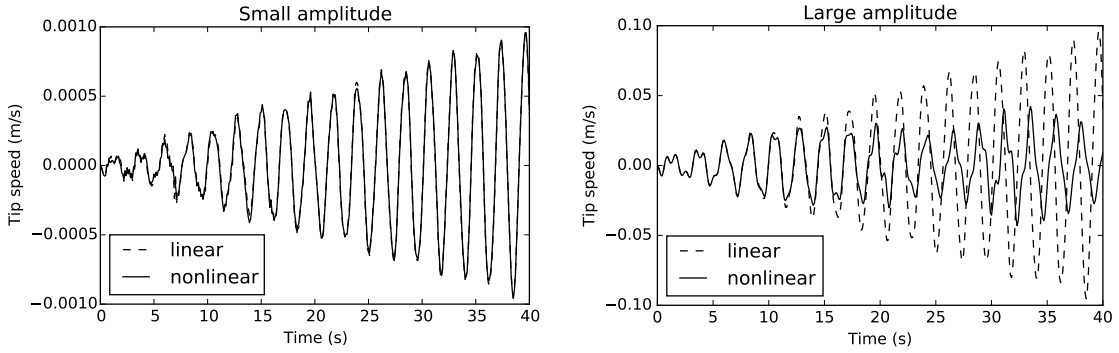

Figure 10.8: Sloshing-structure simulation: the system starts in still condition and is harmonically excited with frequency close to the first natural frequency. The figures show the time-response of the beam tip speed. On the left with small amplitude excitation, linear and nonlinear simulations give the same results. On the right with 100 times larger amplitude excitation, two different behaviors can be observed: the fluid nonlinear behavior reduces the amplitude of the structure vibration. The number of basis functions used in the semi-discretization method is $N = 10$ (for each subsystem).

10.6 Conclusions

In this chapter, the fluid-structure models proposed in Part II, as well as the numerical methods proposed in Chapter 9 were implemented and validated.

Firstly, the numerical scheme was validated by comparing results of the individual models with known analytical results in § 10.2. Thanks to the convergence characteristics of the pseudo-spectral methods, a small number of states is needed to accurately predict the exact natural frequencies. Furthermore, the numerical scheme was able to represent well the frequency response of piezoelectric beam, obtained in the experimental device.

Secondly, the fluid-structure system was analyzed. The frequency response of the coupled system was presented in § 10.4, both for numerical and experimental results. Again, a good agreement was obtained between these results: the first coupled sloshing modes are well represented, specially for small filling ratios of fluid. For higher frequencies, and larger filling ratios, however, the *shallow water* model exhibits spurious natural frequencies, that do not match with good precision the experimental results. This issue is a limitation of the fluid model, as commented in § 6.3.

Finally, time-domain response was used to simulate the non-linear behavior of the fluid, that occurs when exciting the piezoelectric patches at larges amplitudes of voltage.

Part IV

Control

Chapter 11

A recall on active vibrations control

Mechanical vibrations can impose several detrimental effects on systems from different engineering fields. In aircraft (and other transportation vehicles), for example, vibrations can reduce comfort due to the body vibration and noise (Zuziak et al., 2010). These issues can even negatively impact the health and work performance of flight attendants and pilots (Mellert et al., 2008).

Vibrations also impose restrictions in the design of precision instruments (Rivin, 1995). This is the case of large telescopes, that experience mechanical micro vibrations that must be attenuated (Di Lieto et al., 2007).

Moreover, vibrations can be a main cause of structural failure. One example is the excessive strain due to external perturbation as earthquakes, which might cause the collapse of buildings (Soong and Costantinou, 1994). In the aerospace field, the coupling of aerodynamic forces and structural dynamics might cause flutter (Hodges and Pierce, 2011). Furthermore, vibrations also cause material fatigue (Alan, 1958) and reduce the lifetime of the structure.

All these examples motivate the research of methods for vibration mitigation. As pointed out by Preumont (2011), the most common ways to reduce vibrations are stiffening, damping and isolation. *Stiffening* consists in increase the structural stiffness, which shifts the resonance frequency of the structure. *Damping* consists in dissipating the vibration energy, which reduces the amplitude of oscillations near the natural frequencies. *Isolation* consists in preventing the propagation of vibrations to sensitive parts of the systems.

Vibration reduction methods are usually classified as either *passive* or *active* control methods. The *passive* methods consist in including physical components that change the dynamic behavior of the system (e.g., by introducing fluid dampers and dynamic vibration absorbers). *Active* control involves using sensors, actuators, and a control algorithm. Differently from the passive control methods, active control methods have an external power source for the actuator. This might lead to increased performance characteristics but might also lead to issues like instability due to poor control design.

The main goal of this chapter is to present a brief recall of *active* vibration control methods. Since it is a broad field, we focus on the control using piezoelectric actuators. First, we recall some control applications of piezoelectric materials in Section 11.1. Then, usual strategies for vibration control are recalled in Section 11.2.

11.1 Piezoelectric actuators and examples of applications to active control

Most materials have a direct coupling between the deformation (strain) and the stress applied to the material. This coupling is determined by the constitutive equations related to each material. *Smart* materials are materials for which the deformation is not only related to the external material stress, but it is also strongly coupled to other mechanisms like temperature, electric and magnetic field. Thanks to this coupling, these materials can be used for active control of vibrations (Preumont, 2011). For example, *Magnetostrictive* materials deform under a magnetic field. *Magneto-rheological* and *electro-rheological* fluids, which are fluids that change the apparent viscosity when subject to magnetic and electric fields, respectively. *Shape Memory Alloy* is an alloy that, when deformed, returns to its pre-deformed shape when heated.

Among smart materials, piezoelectric materials are widely used for active vibration control in the most diverse fields. As described in Chapter 5, these materials deform under an electric field. Conversely, they also produce an electric field when deformed. Thus, they can be used both as actuators and sensors. Two main classes of piezoelectric materials exist: ceramics and polymers. Piezoceramics are widely used as both sensors and actuators. One of the most popular piezoceramics is the PZT (Lead Zirconate Titanate), which is used in our experimental device in the form of patches glued to the structure. Piezopolymers are mainly used as sensors, since they v have a limited control authority.

There are many examples of applications of piezoelectric actuators for active vibrations control. For instance, Aglietti et al. (1997) studied the use of piezoelectric patches, with the goal of actively reduce spacecraft microvibrations. Onawola and Sinha (2011) used patches as sensors and actuators for flutter suppression. Cobb et al. (2009) designed and tested an active controller for fin-buffet alleviation in the F-16 fighter aircraft. Grewal et al. (2000) used piezoelectric actuators for reducing cabin noise and vibrations in a turboprop airplane. Cesnik and Brown (2003) proposed the use of piezoelectric materials for active wing warping and control of the rolling motion of the airplane. Other applications outside of aerospace domain include vibrations control of a flexible robotic link (Shin and Choi, 2001) and a kitchen hood (Previdi et al., 2014).

11.2 Design of control laws for active control

There are many different control strategies for active vibration reduction. *Feed-forward* controllers attempt to cancel disturbances by generating a secondary signal of opposite phase. *Feedback* controllers use the signals measured by sensors, that are compared to reference signals, passed into a compensator and applied to the system actuators. Here, we focus on feedback control laws.

Active vibration control systems are usually also classified depending on the relative posi-

tion of the actuators and sensors since it has a major influence on the stability and robustness characteristics of the controlled system. The actuator/sensor pair is said to be *collocated* if the effort applied by the actuator acts over the same degree of freedom as the measure obtained by the sensor. This is the case, for example, when a force is applied at a point of the structure and the deflection speed is measured at the same point. Better robustness characteristics are obtained when using *collocated* actuators/sensors, than *non-collocated*. The reason for this can be easily understood when we notice that for mechanical systems, the power balance is given by the product of two variables: applied force and local speed, for example. Given an energy function for the system V, the power balance is given by:

$$\dot{V} = uy\,, \tag{11.1}$$

where u is the actuator input (force, for example), and y is the sensor output (speed, for example). Note that, thanks to Lyapunov's second method for stability, a simple negative output feedback $u = -ky$ (with positive k) leads to a stable closed-loop system, since $\dot{V} = -ky^2 \leq 0$ (assuming that the energy function V is lower-bounded). Such a control law removes energy from the system, and (assuming ideal actuators and sensors) will never destabilize the closed-loop system.

Figures 11.1 and 11.2 highlight the different root locus of this negative output feedback control law when using collocated and non-collocated controllers. The plant represented in the first figure is the piezoelectric beam of our experimental device using the input/output pair v and y_v. The second figure uses the voltage applied to the piezoelectric actuators (v) as input and the tip speed $\dot{w}(L,t)$. Note that when using the collocated pair, the open-loop plant poles and zeros appears in intercalated order near the imaginary axis. Thanks to this pattern, any feedback gain may lead to a stable closed-loop behavior of the plant. On the other hand, for non-collocated pairs, this control law leads to unstable closed-loop behavior and more complicated control laws are needed.

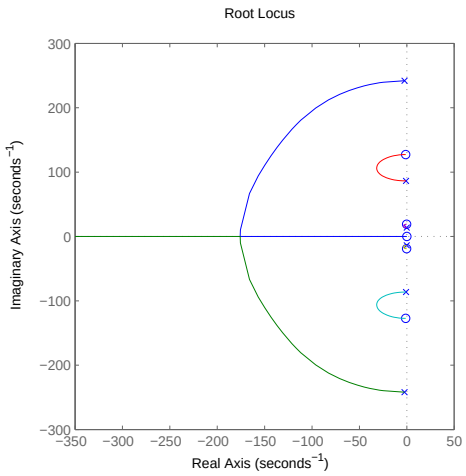

Figure 11.1: Root locus - collocated input/output pair.

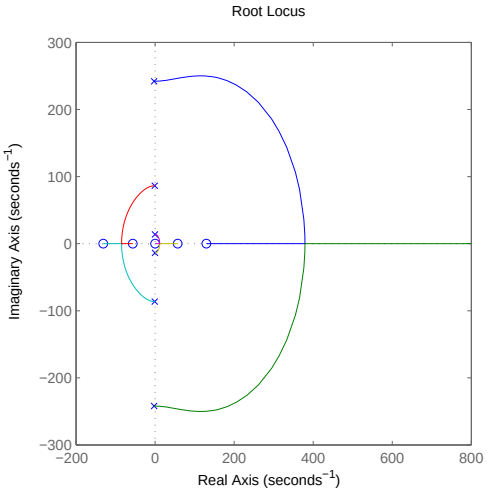

Figure 11.2: Root locus - non-collocated input/output pair.

The control law $u = -ky$ is commonly called *Direct Velocity Feedback* (DVF). Other common control laws for collocated pairs, that are also robustly stable, include:

- Positive Position Feedback (PPF): the structural position is fed on a second order compensator, and fed back on the collocated actuator. This approach was originally developed for control of large space structures by Goh and Caughey (1985) . Among other applications, PPF was also used to buffet alleviation using piezoelectric patches by Ono (2012); Cobb et al. (2009)

- Integral force feedback (IFF): a force sensor is fed on an integrator, and fed back on the collocated actuator (Fleming and Leang, 2010).

Remark 11.1
Systems that satisfy Eq. 11.1 are called passive systems (in a mathematical point of view). PHs are passive systems since the time derivative of the Hamiltonian (which is usually the energy function) is given by $\dot{H} = \boldsymbol{y}^T\boldsymbol{u}$. *The DVF control law* $\boldsymbol{u} = -K\boldsymbol{y}$ *(where* K *is a positive-definite matrix) dissipates energy from the system. In the energy-based control jargon, DVF is called damping injection or damping assignment.*

Since the coupling of a pHs with another pHs is still a pHs, any controller structured as a pHs can be used to control systems with collocated input/output pairs with robust stability properties. This includes both linear and nonlinear controllers. Thus, the pHs framework is largely used for control design (Ortega et al., 2002).

The use of *collocated* input/output pairs favors very simple control laws with guaranteed robustness characteristics. Moreover, a mathematical model of the open-loop plant is not even necessary.

Many times, however, collocated actuator/sensor pairs are not available. In this case, more complicated feedback control laws are usually needed. Again, many different control strategies are available. In most cases, the design of feedback laws for non-collocated pairs require a (precise) mathematical model of the plant. Modeling inaccuracies might even cause unstable behavior of the closed-loop plant.

One of the most used control strategies is the Linear Quadratic Regulator (LQR), which consists in finding the state feedback matrix gain K that minimizes the following integral:

$$J = \int_{t=0}^{\infty} \left(\boldsymbol{x}^T Q \boldsymbol{x} + \boldsymbol{u}^T R \boldsymbol{u} \right) \mathrm{d}t \,, \tag{11.2}$$

where $\boldsymbol{x}(t)$ is the vector of state variables, $\boldsymbol{u}$ is the vector of control variables, Q and R are weighting design matrices. For controllable linear state-space systems, the state feedback gain that optimizes Eq. 11.2 can be obtained from the Riccati equation. Since the states are usually not available, a state observer is needed. One common strategy is to design the state estimator using the Linear Quadratic Estimator (LQE) approach (Kalman Filter). The control scheme with state observer is recalled in Figure 11.3.

This combined approach (also known as Linear Quadratic Gaussian - LQG control) was to improve the damping characteristics of piezoelectric beams by many authors, e.g.: Aglietti et al. (1997); Vasques and Dias Rodrigues (2006); Zhang, He, and Wang (2010); Zhang et al. (2009); Zhang et al. (2008). Furthermore, the active control for buffet alleviation implemented in the F-16 aircraft was also implemented using LQG (Ono, 2012; Cobb et al., 2009).

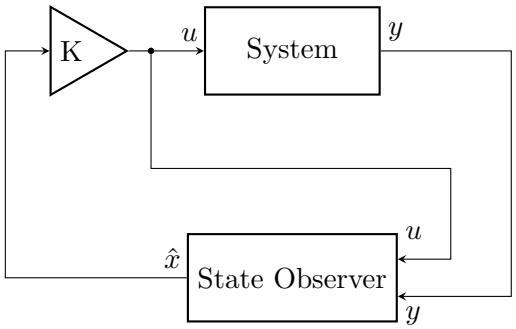

Figure 11.3: Observer-based control with state feedback.

Another popular strategy for active vibration control is the H_∞ synthesis method. Consider the scheme of the general control design problem of Fig. 11.4. The method consists in finding a control dynamics $K(s)$ that minimizes the H_∞ norm of the transfer function between disturbances $\boldsymbol{d}$ and outputs $\boldsymbol{z}$ of the system (Gu, Petkov, and Konstantinov, 2013):

$$\min_{K(s) \quad \underbrace{\text{stabilizing}}} ||T_{zd}||_\infty \,. \tag{11.3}$$

The first solution for this problem was proposed by Doyle et al. (1989), leading to optimal controllers with the same number of states as the plant P. More recently, Apkarian and Noll (2006) proposed a numerical method that allows designing optimal controllers with fixed-structure, instead of full-order. Both algorithms are implemented in *MATLAB Robust Control Toolbox* (functions HINFSYN for the first one, HINFSTRUCT and SYSTUNE for the latter).

Two typical schemes for defining the generalized plant P, in the case of structural dynamics control are presented in Figs. 11.6, 11.7:

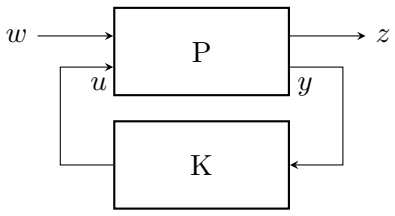

Figure 11.4: Scheme for the general control design problem

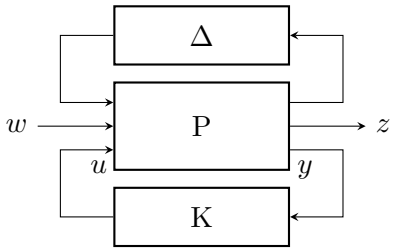

Figure 11.5: Scheme for the control design problem for a plant with parametric uncertainties

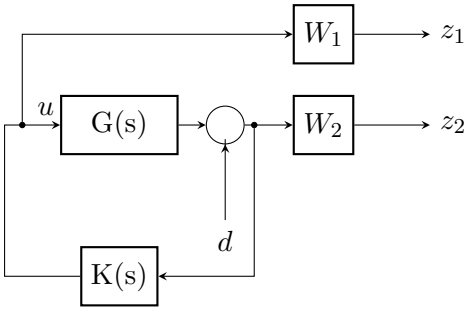

Figure 11.6: Control scheme with disturbance in output

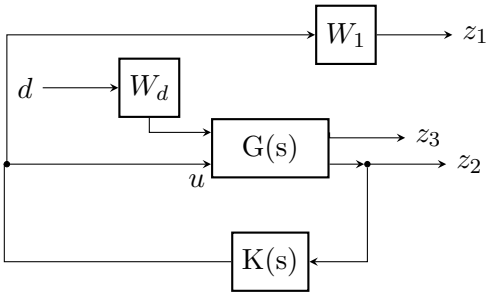

Figure 11.7: Control scheme with disturbance in input

- Fig. 11.6 uses a disturbance applied in the output of the plant; the control signal as well as the output signal are multiplied by weights, leading to the outputs z_1 and z_2. Usually, weight W_1 is chosen in order to ensure that the control signal will not excite high frequency dynamics (working as a roll-off filter). Weight W_2 is related to the sensibility function of the system, and defines the closed-loop performance. In order to increase the damping of structural modes, a usual approach is to choose W_2 trying to reduce sensitivity near these frequencies. This strategy was used for active vibrations control by Leleu (2002) and Zhang et al. (2009).
- Fig. 11.7 uses a disturbance applied in the input of the plant (which can be caused by an external actuator, like a shaker for example). The outputs are given by the weighted control signal (as in previous case), and the plant outputs (which can be weighted or not). The idea is to minimize the effect of disturbances in specific responses (like displacements, accelerations). This approach is used by Kar, Miyakura, and Seto (2000), Robu (2010) and Robu et al. (2012).

Finally, a more general problem of control is to design a controller $K(s)$ that minimizes a performance objective (like the H_∞ norm), but considering the plant parametric uncertainties (so that it should be stable and have good performance characteristics in the uncertainty envelope). A scheme that represents this problem is given in Figure 11.5. The μ-synthesis method is the usual approach for this problem (D-K or D-K-G algorithms). Such schemes were studied for active vibrations control, e.g., by Moutsopoulou, Stavroulakis, and Pouliezos (2011).

11.3 Conclusions

The goal of this chapter was to briefly recall a few of the most used methods for vibrations control. Since it is a broad subject, we focused on active control using piezoelectric actuators. Among the active control laws, we have seen that there are several simple strategies when using collocated input/output pairs. In the next chapter, a method for applying damping injection to non-collocated input/output pairs is proposed.

Chapter 12

Observer-based damping injection with non-collocated input/output actuators

In the Parts II and III of this thesis, we emphasized on the interest of using port-Hamiltonian systems from a modeling point of view. The framework also provides natural strategies for passivity-based control techniques. Indeed, since the energy flow is given by $\dot{H} = \boldsymbol{y}^T \boldsymbol{u}$, a negative output-feedback such as $\boldsymbol{u} = -K\,\boldsymbol{y}$ (where K is a positive semidefinite matrix) gives:

$$\dot{H}(\boldsymbol{x}) = -\boldsymbol{y}^T\, K\, \boldsymbol{y} \leq 0\,,\, \forall\, \boldsymbol{y}\,. \tag{12.1}$$

Provided that $H(\boldsymbol{x})$ is lower-bounded, this simple control law (called damping-injection) stabilizes the system. Mechanical systems can be controlled using this technique if the inputs and outputs are power-conjugated (the power flow is given by their product), which implies that they are collocated, i.e. the actuators and the sensors are located at the same place. Note that, conversely, collocated actuators and sensors do not necessarily give rise to power conjugated inputs and outputs. Due to the robustness properties, implementing control laws using collocated actuators and sensors is classical in the control of flexible structures (Preumont, 2011). However, there are limitations to this approach when the inputs/outputs are not collocated and consequently not power-conjugated. For instance, in our fluid-structure application, the actuators are piezoelectric patches near the clamped end, and the sensors are accelerometers near the free end of the structure.

The use of passivity-based control techniques for non-passive linear systems was studied by Kelkar and Joshi (1997), Kelkar and Joshi (1998) and Kelkar and Joshi (2004). They proposed "passivation" techniques by including series, feedback and feedforward compensators. Kelkar, Mao, and Joshi (2000) suggested an LMI-based method to find compensators that allow using PBC to non-passive systems. The design of state observers for a class of non-linear PHS has been addressed by Venkatraman and van der Schaft (2010).

This chapter proposes a method for damping injection in linear mechanical systems with non-collocated input/outputs. The idea is to write the system using the port-Hamiltonian formulation (with all conjugated input/outputs). Then, a state observer is implemented to estimate the actuators conjugate output.

In Section 12.1, an observer-based controller is presented for non-conjugated mechanical

systems. Firstly, the use of the port-Hamiltonian formalism allows identifying the conjugated inputs/outputs in a straightforward way. A state observer is implemented to estimate the actuators conjugated output. Secondly, Section 12.2 applied the technique for increasing the damping ratio of the beam, and the fluid-structure system. Finally, thanks to the symmetry of the transfer function matrix, an alternative controller is proposed in Section 12.3. This controller gives results that are equivalent to including a physical damper near the tip of the plate. Experimental results are used to validate both controllers.

Contents

12.1 Observer-based control by damping injection

This section is divided as follows. Firstly, the class of linear port-Hamiltonian systems that is treated in this chapter is presented in § 12.1.1. Secondly, a state observer is presented in § 12.1.2. Thirdly, the damping injection control law is recalled in § 12.1.3. Finally, the observer-based controller equations are presented in § 12.1.4.

12.1.1 Defining a port-Hamiltonian system

This study will be limited to linear port-Hamiltonian systems. For these systems, the Hamiltonian is given by the quadratic form: $H(\boldsymbol{x}) = \frac{1}{2}\boldsymbol{x}^T Q\boldsymbol{x}$, where $\boldsymbol{x} \in \mathbb{R}^n$ is the energy variables vector and Q is an $n \times n$ symmetric positive-definite matrix. The Hamiltonian gradient is given by $\nabla_{\boldsymbol{x}} H(\boldsymbol{x}) = Q\boldsymbol{x}$. We assume that the system dynamics is given by:

$$\begin{aligned} \dot{\boldsymbol{x}} =& (J-R)Q\boldsymbol{x} + B_a\boldsymbol{u}_a\,, \\ \boldsymbol{y}_s =& B_s^T Q\boldsymbol{x}\,, \end{aligned} \tag{12.2}$$

where J is an $n \times n$ skew-symmetric matrix and R is an $n \times n$ positive semidefinite matrix; $\boldsymbol{u}_a \in \mathbb{R}^{n_a}$ is the actuators input vector, hence subscript "a" stands for actuators; $\boldsymbol{y}_s \in \mathbb{R}^{n_s}$ is the sensors output vector, similarly subscript "s" stands for sensors; B_a and B_s are $n \times n_a$ and $n \times n_s$ matrices, respectively. Note that the previous system is not strictly speaking port-Hamiltonian, since $B_a \neq B_s$. Note also that the input $\boldsymbol{u}_a$ and output $\boldsymbol{y}_s$ are not conjugated.

If we compute the Hamiltonian time-derivative, we find:

$$\dot{H} = \left(\boldsymbol{x}^T Q B_a\right) \boldsymbol{u}_a - \boldsymbol{x}^T Q R Q \boldsymbol{x} \leq \left(\boldsymbol{x}^T Q B_a\right) \boldsymbol{u}_a \neq \boldsymbol{y}_s^T \boldsymbol{u}_a \,. \tag{12.3}$$

This motivates us to define $\boldsymbol{y}_a := B_a^T Q \boldsymbol{x} \in \mathbb{R}^{n_a}$, which is the conjugated output of $\boldsymbol{u}_a$. Since this variable cannot actually be measured, we call it a *virtual* output. In order to write the equations using the classical port-Hamiltonian formalism, we also introduce another *virtual* variable, $\boldsymbol{u}_s \in \mathbb{R}^{n_s}$ which is the conjugated input of the sensors (actually $\boldsymbol{u}_s = 0$). With these extra *virtual* ports at hand, the original system (Eq. 12.2) now takes the more classical pHs form below:

$$\begin{aligned} \dot{\boldsymbol{x}} =& (J - R) Q \boldsymbol{x} + \begin{bmatrix} B_a & B_s \end{bmatrix} \begin{bmatrix} \boldsymbol{u}_a \\ \boldsymbol{u}_s \end{bmatrix} \,, \\ \begin{bmatrix} \boldsymbol{y}_a \\ \boldsymbol{y}_s \end{bmatrix} =& \begin{bmatrix} B_a^T \\ B_s^T \end{bmatrix} Q \boldsymbol{x} \,, \end{aligned} \tag{12.4}$$

which is written as Eq. 4.6. The time derivative of the Hamiltonian is then:

$$\dot{H} = \boldsymbol{y}_a^T \boldsymbol{u}_a + \boldsymbol{y}_s^T \boldsymbol{u}_s - \boldsymbol{x}^T Q R Q \boldsymbol{x} \,. \tag{12.5}$$

Since $\boldsymbol{u}_s = 0$:

$$\dot{H} = \boldsymbol{y}_a^T \boldsymbol{u}_a - \boldsymbol{x}^T Q R Q \boldsymbol{x} \,. \tag{12.6}$$

12.1.2 Designing an observer

In Eq. 12.4, $\boldsymbol{y}_a$ is not being measured. For using passivity-based control, it is necessary to estimate it. For this purpose, a state observer of the system is computed.

Assumption 12.1
The pair $\left((J - R)Q, B_s^T Q\right)$ *is assumed to be observable.*

The classical Luenberger continuous state observer is given by:

$$\begin{aligned} \dot{\hat{\boldsymbol{x}}} =& (J - R) Q \hat{\boldsymbol{x}} + B_a \boldsymbol{u}_a + L(\boldsymbol{y}_s - B_s^T Q \hat{\boldsymbol{x}}) \,, \\ \hat{\boldsymbol{y}}_a =& B_a^T Q \hat{x} \,, \qquad\qquad \hat{\boldsymbol{x}}(0) = 0 \,. \end{aligned} \tag{12.7}$$

The observer error ($\boldsymbol{e} = \boldsymbol{x} - \hat{\boldsymbol{x}}$) dynamics is given by:

$$\dot{\boldsymbol{e}} = (J - R - L B_s^T) Q \boldsymbol{e} \,. \tag{12.8}$$

The matrix L should be designed such that the error dynamics be asymptotically stable (e.g. using pole placement). The fact that Eq. 12.8 is independent of the control input leads to the well-known principle of separation of estimation and control (Luenberger, 1966).

12.1.3 Designing a control law

The damping injection control law is given by $\boldsymbol{u}_a = -K_a \boldsymbol{y}_a = -K_a B_a^T Q \boldsymbol{x}$, where K_a is an $n_a \times n_a$ matrix. Using this law with the *theoretical* system (Eq. 12.4), the closed-loop dynamics becomes:

$$\dot{\boldsymbol{x}} = \left(J - R - B_a K_a B_a^T\right) Q \boldsymbol{x} \,. \tag{12.9}$$

Property 12.1
The closed-loop system is stable for any symmetric positive semidefinite matrix K_a.

Proof. The Hamiltonian rate of change of Eq. 12.6, with $\boldsymbol{u}_a = -K_a \boldsymbol{y}_a$ and $\boldsymbol{y}_a = B_a^T Q \boldsymbol{x}$ is given by:

$$\dot{H}(\boldsymbol{x}) = -\boldsymbol{y}_a^T K_a \boldsymbol{y}_a - \boldsymbol{x}^T Q R Q \boldsymbol{x} \,, \tag{12.10}$$

$$= -(Q\boldsymbol{x})^T \left(B_a K_a B_a^T + R\right) (Q\boldsymbol{x}) \leq 0 \,. \tag{12.11}$$

Using this control law, we can guarantee that the system energy will never increase. Since the Hamiltonian has a lower bound, it guarantees that the system is stable. In addition, Eq. 12.11 shows that $B_a K_a B_a^T + R \geq 0$ is a sufficient condition for stability. □

12.1.4 Observer-based controller

Since $\boldsymbol{y}_a$ is not being measured, we will use its estimate $\hat{\boldsymbol{y}}_a$ to define the new control law:

$$\boldsymbol{u}_a := -K_a \hat{\boldsymbol{y}}_a = -K_a B_a^T Q \hat{\boldsymbol{x}} \,, \tag{12.12}$$

with positive semidefinite matrix K_a. Fig. 12.1 shows a scheme of this control law with the state observer.

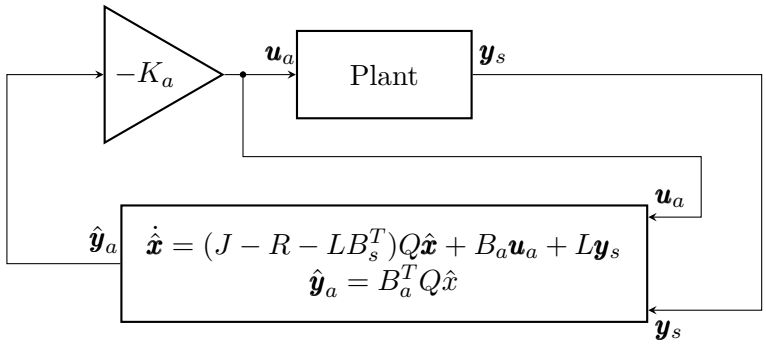

Figure 12.1: Observer-based controller for damping injection.

Property 12.2
The dynamical system (Eq. 12.2) together with the state observer (Eq. 12.7) and the controller (Eq. 12.12) is stable for any positive semidefinite K_a.

Proof. This can be easily verified from the separation principle. For the sake of completeness, we recall the proof here. The closed-loop equations are given by:

$$\begin{bmatrix} \dot{\boldsymbol{e}} \\ \dot{\boldsymbol{x}} \end{bmatrix} = \begin{bmatrix} (J - R - LB_s^T)Q & 0 \\ -B_a K_a B_a^T Q & (J - R - B_a K_a B_a^T)Q \end{bmatrix} \begin{bmatrix} \boldsymbol{e} \\ \boldsymbol{x} \end{bmatrix} . \tag{12.13}$$

Note that since the state matrix is block-triangular, the eigenvalues of the full system are given by the eigenvalues of the observer $(J-R-LB_s^T)Q$ and of the closed-loop plant without the observer $(J - R - B_a K_a B_a^T)Q$. For this reason, provided that the observer is stable by design, and the closed-loop plant without observer is stable (Property 12.1), the closed-loop system with observer is also stable. □

Remark 12.1
The proposed controller can be seen as a particular case of state feedback, with a reduced number of degrees of freedom. Note that usual state feedback is given by $\boldsymbol{u}_a = -K\hat{\boldsymbol{x}}$*, where* K *is an* $n_a \times n$ *matrix. Our controller implies the following structure for the gain* $K = K_a B_a^T Q$*. The structure of the state feedback gain is physically motivated to remove energy from the system (increase damping). Since* K_a *is an* $n_a \times n_a$ *positive semidefinite matrix, a diagonal matrix with positive elements stabilizes the system, making the control design simpler, from a control practitioner perspective. For instance, any diagonal matrix* K_a *with positive elements can be used.*

12.2 Application to damping injection with non-collocated actuators/sensors

The technique presented in the previous section is applied here for the fluid-structure system described in the previous parts of this thesis. Let us assume the following linear port-Hamiltonian system, obtained after semi-discretization (Chapter 9), coupling of all the modules (as described in Chapters 7 and 10) and after removing the constraints (as described in § 4.3.2):

$$\begin{aligned} \boldsymbol{x} &= (J - R)Q\boldsymbol{x} + B\boldsymbol{u} \,, \\ \boldsymbol{y} &= B^T Q\boldsymbol{x} \,, \end{aligned} \tag{12.14}$$

where the inputs and outputs are given by:

$$\boldsymbol{y} = \begin{bmatrix} y_v \\ \dot{w}^B(L,t) \end{bmatrix} , \qquad \boldsymbol{u} = \begin{bmatrix} v \\ F \end{bmatrix} , \tag{12.15}$$

v is the input voltage, $\dot{w}^B(L,t)$is the measured tip speed. F is the *virtual* input force applied at the position of the sensor that measures the speed. y_v is the *virtual* output.

The technique suggested in the previous section can be directly applied to the FSI system, described by Eq. 12.14, using the non-conjugate input/output pair given by the voltage as

input and tip speed as output. Thus, the control law is written as:

$$v(t) = -k\hat{y}_v(t)\,, \tag{12.16}$$

where $k > 0$ and $\hat{y}_v(t)$ is the estimate of $y_v(t)$, obtained using a state observer.

The proposed observer based controller was tested on the experimental device. The controller was implemented using MATLAB Simulink, on Real-time Windows Target, with an NI 6024-E board. A sample time of 0.001 s was chosen. One 4371 Bruel & Kjaer accelerometer was used (located near the plate free tip), together with a charge amplifier (Type 2635). The amplifier can give directly the speed measurements but only for frequencies above 1 Hz. The two PZT piezoelectric actuators were actuated symmetrically.

The controller was designed for two different plant set-ups. Firstly, only the beam was taken into account (without the tank). Secondly, a controller was designed for the beam coupled with the tank 25% filled of water. In each case, once the observer was designed, the plant behavior was tested for different values of the controller gain k_a. Large values of gain lead to large reduction of the peaks. However, if the value of the gain is too large, two phenomena can happen: 1) the actuators become saturated; 2) the closed-loop system becomes unstable.

Frequency response from 1 to 45 Hz is shown in the case of the beam only case (Fig. 12.2). A reduction of the peaks when using the controller shows that it introduces damping in the system.

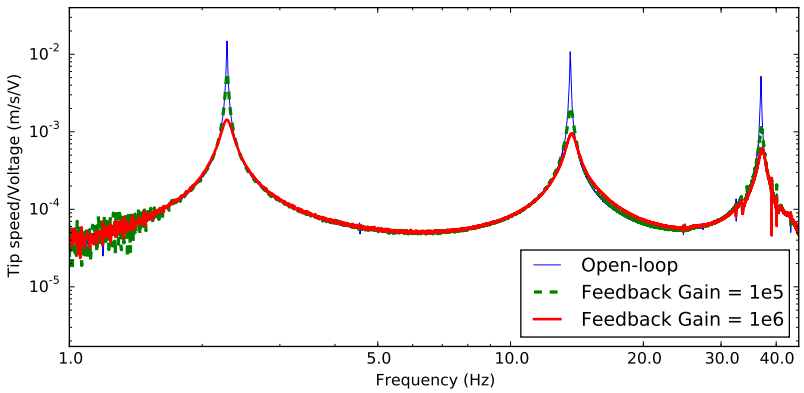

Figure 12.2: Experimental frequency response for different gains - beam only.

In the case of the fluid-structure system (beam with partially filled tank), the frequency response from 1 to 25 Hz is shown in Fig. 12.3. The numbering of the modes is the same as previously used in § 10.4. As it happened with only the beam, the peaks of several fluid-structure modes were reduced. The damping ratios of three modes that are attenuated by the controllers are presented in Table 12.1.

Figures 12.4 and 12.5 show the time response of the system initially excited during 20 seconds with no control using a harmonic voltage, at two different frequencies (near the

natural frequencies of modes 2 and 9, respectively), and then controlled according to the proposed strategy. The time-response shows the decrease of the speed for different values of k_a. These time responses were used to compute the damping ratios of Table 12.1.

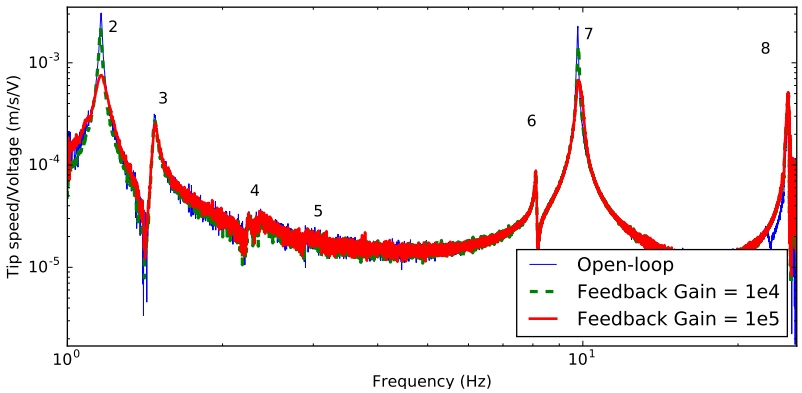

Figure 12.3: Experimental frequency response for different gains - fluid-structure system (25% filled tank).

Mode	Description	Damping ratio		
		Open-loop	Closed-loop	
			Gain = 10^4	Gain = 10^5
2	2nd sloshing + 1st bending	0.0045	0.0054	0.0150
3	3rd sloshing + 1st bending	0.0053	0.0058	0.0090
7	2nd bending	0.0020	0.0035	0.0095

Table 12.1: Comparison between damping ratios obtained experimentally on the beam with the partially-filled tank.

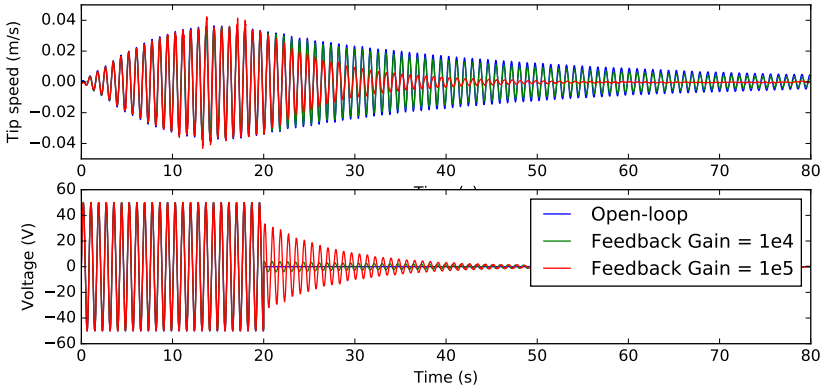

Figure 12.4: Experimental time response for different gains: the system is excited using a sinusoidal voltage at 1.2 Hz for the first 20 seconds; then, the control law is activated. Top: tip deflection speed; Bottom: Actuator voltage.

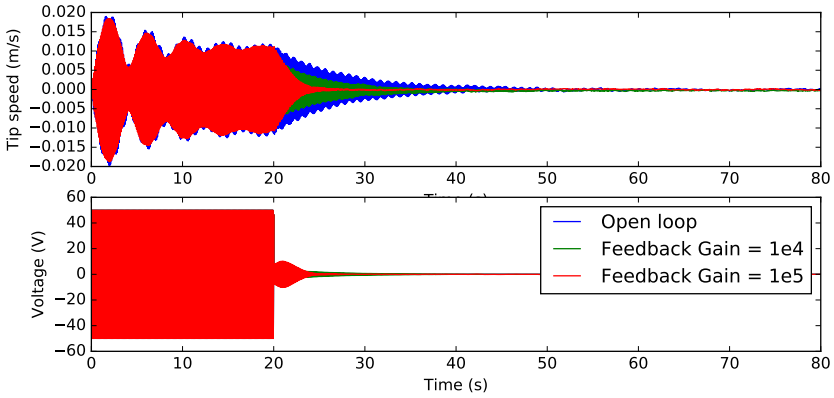

Figure 12.5: Experimental time response for different gains: the system is excited using a sinusoidal voltage at 9.5 Hz for the first 20 seconds; then, the control law is activated. Top: tip deflection speed; Bottom: Actuator voltage.

12.3 Alternative observer-based controller: "virtual" speed feedback

One interesting property about linear mechanical systems written as port-Hamiltonian systems is that their transfer function matrix is usually symmetric. This happens under some conditions that are usually satisfied by mechanical systems (and are satisfied by the systems presented in this thesis) as presented in the following proposition.

Proposition 12.1
Let us consider linear port-Hamiltonian systems written as Eq. 12.14. In the case of mechanical systems, the energy variables can be split in two vectors: $\boldsymbol{x} = [\boldsymbol{x}_1\,, \boldsymbol{x}_2]^T$*, which are momentum and position variables (one vector is related to kinetic and the other to potential energy). Similarly, the Q matrix is usually block-diagonal (there is no energetic coupling between the kinetic and potential energy). The damping matrix R, as well as the input matrix B usually interferes only in the momentum variable.*

Under these assumptions, Eq. 12.14 can be written as:

$$\begin{aligned} \begin{bmatrix} \dot{\boldsymbol{x}}_1 \\ \dot{\boldsymbol{x}}_2 \end{bmatrix} &= \begin{bmatrix} -R & -J \\ J^T & 0 \end{bmatrix} \begin{bmatrix} Q_1 & 0 \\ 0 & Q_2 \end{bmatrix} \begin{bmatrix} \boldsymbol{x}_1 \\ \boldsymbol{x}_2 \end{bmatrix} + \begin{bmatrix} B \\ 0 \end{bmatrix} \boldsymbol{u}\,, \\ \boldsymbol{y} &= \begin{bmatrix} B^T & 0 \end{bmatrix} \begin{bmatrix} Q_1 & 0 \\ 0 & Q_2 \end{bmatrix} \begin{bmatrix} \boldsymbol{x}_1 \\ \boldsymbol{x}_2 \end{bmatrix}. \end{aligned} \tag{12.17}$$

If, in addition, we assume that Q_1*,* Q_2 *and R are symmetric matrices, then, the transfer function matrix between the inputs* $\tilde{\boldsymbol{u}}$ *and outputs* $\tilde{\boldsymbol{y}}$ *(where* $\tilde{\boldsymbol{u}}(s)$ *and* $\tilde{\boldsymbol{y}}(s)$ *are the Laplace transforms of* $\boldsymbol{u}(t)$ *and* $\boldsymbol{y}(t)$*), i.e.,* $G(s)$ *in:*

$$\tilde{\boldsymbol{y}} = G(s)\tilde{\boldsymbol{u}} \tag{12.18}$$

is symmetric.

Proof. Eq. 12.17 can be rewritten as a second-order ODE:

$$\begin{aligned} \ddot{\boldsymbol{x}}_2 &= J^T Q_1 \dot{\boldsymbol{x}}_1\,, \\ &= J^T Q_1(-RQ_1\boldsymbol{x}_1 - JQ_2\boldsymbol{x}_2 + B\boldsymbol{u})\,, \end{aligned} \tag{12.19}$$

but $\boldsymbol{x}_1 = Q_1^{-1}J^{-T}\dot{\boldsymbol{x}}_2$, so:

$$\ddot{\boldsymbol{x}}_2 + J^T Q_1 R J^{-T}\dot{\boldsymbol{x}}_2 + J^T Q_1 J Q_2 \boldsymbol{x}_2 = J^T Q_1 B\boldsymbol{u}\,. \tag{12.20}$$

Applying the Laplace transform with zero initial conditions, we get:

$$\tilde{\boldsymbol{x}}_2 = (s^2 I + sJ^T Q_1 R J^{-T} + J^T Q_1 J Q_2)^{-1} J^T Q_1 B\tilde{\boldsymbol{u}}\,. \tag{12.21}$$

From the Laplace transform of the output, we have $\tilde{\boldsymbol{y}} = B^T Q_1 \tilde{\boldsymbol{x}}_1 = sB^T J^{-T} \tilde{\boldsymbol{x}}_2$. After substitution in Eq. 12.21, we find the transfer function:

$$\begin{aligned}
\tilde{\boldsymbol{y}} &= sB^T J^{-T}(s^2 I + sJ^T Q_1 R J^{-T} + J^T Q_1 J Q_2)^{-1} J^T Q_1 B\tilde{\boldsymbol{u}}\,, \\
\tilde{\boldsymbol{y}} &= sB^T(s^2 J^T + sJ^T Q_1 R + J^T Q_1 J Q_2 J^T)^{-1} J^T Q_1 B\tilde{\boldsymbol{u}}\,, \\
\tilde{\boldsymbol{y}} &= sB^T(s^2 Q_1^{-1} + sR + JQ_2 J^T)^{-1} B\tilde{\boldsymbol{u}}\,.
\end{aligned} \tag{12.22}$$

Since Q_1, R and Q_2 are symmetric, the term $(s^2 Q_1^{-1} + sR + JQ_2 J^T)$ is also symmetric, as well as its inverse. □

The previous proposition leads to the following interesting property of the system with piezolectric actuators: since the transfer function matrix is symmetric, the behavior of the system with piezoelectric voltage $v(t)$ as input and tip speed $\dot{w}^B(L,t)$ as output is the same as the behavior of the system in which the force F *would be* the input and y_v the output.

Therefore, it is possible to design a control law for a “virtual” system with $F(t)$ as input and $y_v(t)$ as an output.

For this “virtual” system, the technique presented in Section 12.1 was used, and a state observer was designed. The damping injection law in this case is given by:

$$F(t) = -k\hat{\dot{w}}(L,t)\,. \tag{12.23}$$

This control law is equivalent to including a physical damper at the tip of the plate. We called here this control law “virtual” speed feedback.

This controller was implemented on the real system for the fluid-structure plant with 25% filled tank. The frequency response from 1 to 25 Hz is shown in Fig. 12.6, exhibiting an additional reduction of the amplitudes of the first peaks compared to the results of Section 12.2.

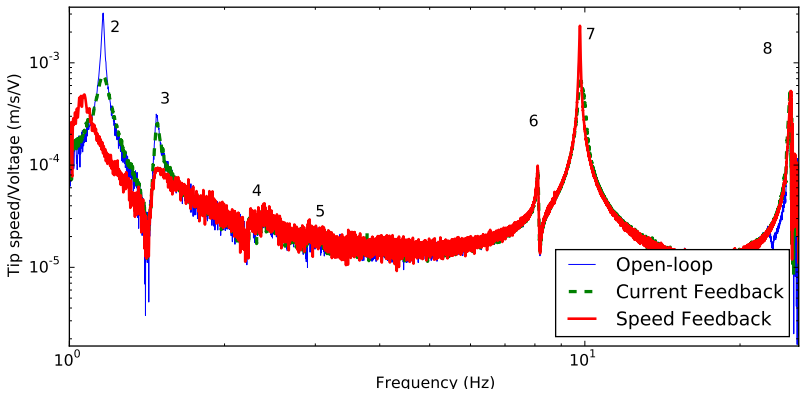

Figure 12.6: Experimental frequency response using the two different control strategies.

Mode	Description	Damping ratio		
		Open-loop	Closed-loop	
			"Virtual" speed Feedback	$\hat{y}_v$ feedback
2	2nd sloshing + 1st bending	0.0045	0.0255	0.0150
3	3rd sloshing + 1st bending	0.0053	0.0160	0.0090
7	2nd bending	0.0020	0.0020	0.0095

Table 12.2: Comparison between damping ratios obtained experimentally - The "virtual" speed feedback significantly increases the damping of the first modes.

The time-response with this new controller, obtained using the same conditions as in the previous section, is presented in Figure 12.7.

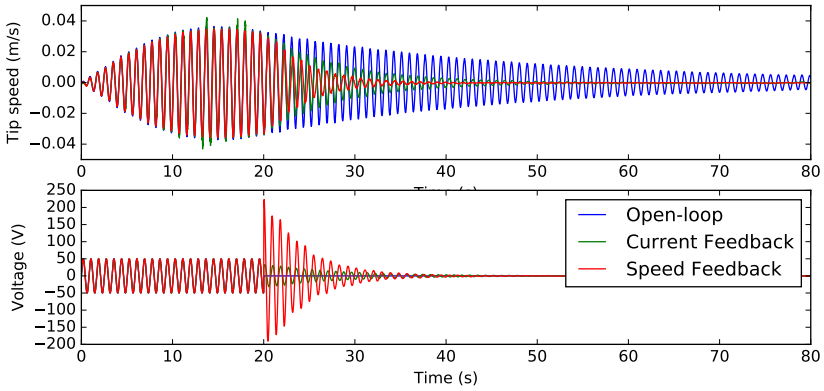

Figure 12.7: Experimental time response for different gains: the system is excited using a sinusoidal voltage at 1.2 Hz for the first 20 seconds; then, the control law is activated. Top: tip deflection speed; Bottom: Actuator voltage.

12.4 Conclusions

This chapter presents a simple technique for damping-injection in mechanical systems with non-collocated inputs/outputs. The idea is to take advantage of the structured representation provided by the port-Hamiltonian framework and to use a state observer that allows estimating the conjugated ports of the actuators. Then, classical damping injection techniques are used.

It is important to recall that the proposed controller is a usual state feedback with state observer, presented in Fig. 11.3. The specificity of this controller lies in the fact that the observer is written in such a way that the state vector is the vector of energy variables (Eq. 12.7). The control gain K is now strongly structured as $K = k_a B_a^T Q$, and the closed-loop system proves to be stable for any positive k_a. This choice of gain is physically motivated to increase the structural damping. The method is an alternative way of finding the feedback gain K, with a reduced number of degrees of freedom.

Furthermore, a second control law was presented in Section 12.3. Thanks to the symmetry of the matrix transfer function, it is possible to assume that the input of the open-loop system is given by an external force, and the output is given by the y_v (the output conjugated to the voltage). Thus, the previous observer-based controller can be applied, and the resulting closed-loop response is equivalent to a system with a physical damper placed near the tip of the plate.

Both control laws were tested on the experimental device and promising results were obtained, with good attenunation of the first coupled fluid-structure modes. Although only one input and one output were used in the experiment, the methodology can also be used for MIMO systems.

Conclusions and further work

Conclusions and further work

Contributions

As pointed out in Chapter 1, new paradigms for aircraft design, the increased flexibility of recent aircraft projects, together with the use of new smart materials bring new challenges that motivate the development of multidisciplinary tools that allows modeling, simulating and controlling complex systems. The port-Hamiltonian framework goes into this direction, providing a modular approach for multi-physics modeling. Furthermore, energy-based control methods come naturally from this approach. The main goal of this thesis was to bring this framework to the aerospace context. We used the port-Hamiltonian framework to model, simulate and control a fluid-structure system that consists of a beam with piezoelectric actuators coupled to a tank partially filled with water. This structure has resonance modes similar to the modes of an aircraft wing. In order to achieve this objective, this thesis presented contributions in the modeling, discretization, and control of pHs. These contributions are recalled in the sequel.

Modeling

Part II focused on the port-Hamiltonian models of each part of the system and the following contributions can be highlighted:

- PHs model of a simple cantilever beam with piezoelectric actuators, considering both the bending and torsion motions of the beam (Chapter 5).
  In the proposed model, the voltage is assumed to be distributed along the domain, providing distributed control ports. The boundary ports are given by the forces, moments and their conjugate values (translation and angular speeds);

- Extension of nonlinear 1D and 2D shallow water equations in a moving tank as a mixed finite-infinite port-Hamiltonian system (Chapter 6).
  The originality of the models comes from the rigid body motion of the tank that is taken into account, and that is coupled to the motion of the fluid. The interconnection ports are given by the external forces and moments applied to the tank, and their conjugate outputs (translation and angular speeds).

Then, the interconnection ports that appear in the pHs models are used to couple the systems in a systematic way (Chapter 7).

Partial results of the modeling part were presented in Cardoso-Ribeiro, Matignon, and Pommier-Budinger (2015b).

Discretization

Part III focused on the power-preserving spatial discretization. Thanks to the use of pseudo-spectral methods, the finite-dimensional models have excellent convergence properties. We extended these methods (presented in Cardoso-Ribeiro, Matignon, and Pommier-Budinger (2016b)) in Chapter 9 to take into account the specific characteristics of the models proposed in Part II:

- Specificities of the distributed control. In particular, the piezoelectric voltage leads to an unbounded input operator. Thus, the pseudo-spectral methods cannot be used directly. A weak formulation had to be used to overcome this issue.
- Second-order differential. In this case, four boundary ports are needed. These boundary ports represent the usual boundary conditions of the Euler-Bernoulli beam.

Chapter 10 presented the numerical results. Among the contributions of this chapter, we can cite:

- The shallow water equations discretized using the power-preserving pseudo-spectral method. Differently from previous work that used this method to discretize the wave equation (Moulla, Lefèvre, and Maschke, 2012), the shallow water equations are non-linear. The source of the nonlinearities is the Hamiltonian of the system (which is non-quadratic). The discretization of the Hamiltonian was obtained using Gaussian quadrature. The gradients were computed using automatic differentiation methods.
- The equation of the beam with piezoelectric actuators discretized using the proposed power-preserving pseudo-spectral method.

Moreover, each subsystem was validated by comparison with theoretical and experimental results. Then, the coupled system was validated against experimental data.

Control

Part IV focused on the control of the FSI system. An observer-based controller was proposed and tested in the experimental device in Chapter 12 (presented in Cardoso-Ribeiro, Matignon, and Pommier-Budinger (2016a)). The structure of the controller is the same as the usual state feedback with state observer. The difference lies in the fact that, thanks to the pHs model, the new state feedback gain of the controller is physically structured to remove energy from the system. From a practitioner point of view, the method provides a simple way to find the feedback gain, with a reduced number of degrees of freedom.

Furthermore, thanks to the symmetry of the transfer function matrix of the linearized pHs, an alternative design was investigated. In this case, the closed-loop response gives a response that is equivalent to introducing a physical damper in the system.

An application of H_∞ robust control techniques to the linearized system was also implemented as presented in Appendix E (presented in Cardoso-Ribeiro, Matignon, and Pommier-Budinger (2015a)).

The controllers were tested on the experimental device, successfully increasing the damping ratio of the fluid-structure system.

Further work

Modeling

Structural dynamics: The structural dynamics model used in this thesis is quite simple. It neglects the bending rotation inertia and shear stresses. Since the cross-section of our beam has small dimensions (in comparison to the beam length), and as we were only interested on the low-frequency behavior, this model exhibited a good agreement with experimental results. Further work should treat more advanced beam models like the Timoshenko beam and beams with geometrically nonlinear deflections (Macchelli and Melchiorri, 2004; Voss and Scherpen, 2014; Trivedi, Banavar, and Kotyczka, 2016). Additionally, instead of using two models, one for the bending and other for the torsion, the use of plate models could provide more accurate results.

Furthermore, the dynamic effects of the magnetic field were neglected in the modeling of piezoelectric patches in this thesis (contrary to, e.g. Voss and Scherpen (2014)). Voss and Scherpen (2011a) verified that including the magnetic field is necessary to derive finite-dimensional models that are controllable. In this thesis, this controllability issue was avoided by using the voltage as an input[1]. From a practical point of view, it is still unclear why such dynamic model should be included, since the structural dynamics and the magnetic field dynamics have time scales that are very different. Further work should verify the accuracy impact, if any, of the inclusion of dynamic magnetic field equations in the global model.

Fluid dynamics: In the case of sloshing equations, many improvements are foreseen. Firstly, for the proposed 2D model, only two translations and one rotation were taken into account. Further work should include all degrees of freedoms for the rigid body motion.

The 2D shallow water equations obtained as pHs in Chapter 6 exhibits an unusual interconnection operator that depends on the spatial derivatives of the energy variables. A possible way to find a more usual operator might be using the vorticity as an extra energy variable (instead of the vector of velocities, see, e.g., example 7.9 of Olver (1993)).

Furthermore, the shallow water equations in pHs framework can be extended in a number of ways. A few ideas include: consider the bottom topography of the tank (instead of assuming

[1] In previous work, the electric field - and, consequently, the voltage - is an energy variable of the system.

a straight bottom); using several layers of fluid (to simulate containers with several immiscible fluids).

As presented in § 6.3, the *shallow water* equations represent well the fluid motion in moving containers for low frequency excitation, and for small filling ratios of the tank (since a small depth is assumed, with respect to the free surface dimensions). This limitation was confirmed by the experimental results presented in § 10.4. One possible alternative to the SWE is given by the incompressible Euler equations. However, as discussed in § 6.3, these equations are not in the usual infinite-dimensional port-Hamiltonian form. Further work should explore how to properly write the incompressible Euler equations with free surface using the port-Hamiltonian formalism.

Coupling: The coupling between the components of the system was point-wise. The boundary ports of the beam equations were used to interconnect with the rigid-body inputs/outputs of the tank equation. In future work, more complex interconnections should be investigated. For instance, the distributed ports, described in this thesis for including damping, could be employed to interconnect the structural dynamics with fluids that are distributed along the surface.

Finally, another subject concerning the coupling that was not treated in this thesis is the well-posedness of the coupled port-Hamiltonian models.

Discretization

One disadvantage of the pseudo-spectral method is that the "differentiation matrices" can have elements with large values for polynomials of high degree (causing the well-known Runge's phenomenon). This problem was avoided in this thesis by the use of Gauss-Legendre collocation points. Another strategy that could be investigated is the following. As pointed out in Remark 8.4, the pseudo-spectral method can also be written using an "element"-like form. The combined use of pseudo-spectral methods with elements would make it possible to use moderate degree polynomials, avoiding the numerical issues related to polynomials of high degree.

In this thesis, we used Lagrange polynomials as basis functions for the pseudo-spectral discretization method. Further work should study other choices of basis functions: for instance, Chebyshev polynomials, eigenfunctions of the linearized equations, or problem-specific basis like the Bessel functions (see, e.g., Vu et al. (2013)).

The power-preserving semi-discretization methods used in this thesis are used only for 1D systems. The extension of these methods for 2D and 3D is foreseen. The main difficulty is how to perform exact differentiation in spatial dimensions larger than one. Other power-preserving methods, like the explicit simplicial discretization (Seslija, Scherpen, and van der Schaft, 2014) seem to be more appropriate for discretization of 2D and 3D systems.

We only worked on the power-preserving *spatial* discretization. To perform time integration, classical ODE and DAE integration tools were used. Further work should also take advantage of the port-Hamiltonian structure of the finite-dimensional systems to perform power-preserving time integration using symplectic numerical schemes (see, e.g., Leimkuhler and Reich (2005)).

Control

Although only one input and one output were used in the experiment, the methodology can also be used for MIMO systems. One limitation of the proposed method is that a precise dynamical model of the plant is necessary to compute the observer dynamics. Further work should be done to analyze the robustness characteristics of this control technique. In particular, we should focus on how to design the state observer to improve the system robustness to modeling uncertainties.

Another interest would be on developing more complex passivity-based control laws. Other passivity-based techniques can be applied (instead of the simple damping injection). For instance, the system can be coupled with another pHs (in order to control specific modes, for example).

Toward more complex systems and flexible airplane modeling using pHs?

In this thesis, we focused on the modeling of a relatively simple fluid-structure coupled system. One of the main characteristics of the pHs, that motivated this work, is that it intrinsically provides a modular framework for modeling. Each subsystem has an independent model, that can be substituted according to necessity. For instance, if we need a better modeling of the fluid dynamics, there is no need to restart the modeling process from the very beginning. Since the interconnection structure between the components remains the same, only the modified subsystem must be changed.

Therefore, once the tools to semi-discretize and manipulate the port-Hamiltonian systems are implemented, modeling systems of arbitrary complexity becomes straightforward.

Furthermore, the use of efficient semi-discretization methods (like pseudo-spectral methods) leads to models of relatively low dimension, which are suitable for simulation and control design.

One interesting and almost straightforward application of the methods presented here is the modeling of complex flexible space structures and flexible robotic manipulators.

The increased structural flexibility in most recent airplane designs and the trend for even more flexible structures in the future were motivations for the studies performed in this thesis.

The methods proposed in this work could be used for modeling the flight dynamics of flexible airplanes after implementing a few additional extensions (rigid body degrees of freedom in the beam equations, aerodynamic forces, etc.).

Appendix A

Detailed derivation of full fluid equations as a port-Hamiltonian system

The goal of this appendix is to rewrite the Eqs. 6.6 using the port-Hamiltonian formalism. First, we have to write the Hamiltonian, given by the sum of the fluid kinetic and potential energies (Eqs. 6.2 and 6.3), and the tank kinetic energy $\frac{1}{2}m_T\dot{D}^2$:

$$\begin{aligned} H = \int_{z=-a/2}^{a/2} \Bigg(& \rho b g (\frac{h^2}{2}\cos\theta + hz\sin\theta) + \\ & + \frac{1}{2}\rho b h \left((u + \dot{D}\cos\theta)^2 + (-\dot{D}\sin\theta + z\dot{\theta})^2 \right) \Bigg) \mathrm{d}z + \frac{1}{2}m_T\dot{D}^2, \end{aligned} \tag{A.1}$$

then, two new moment variables are defined, one for the translation p and other for the rotation p_θ:

$$\begin{aligned} p := \frac{\partial H}{\partial \dot{D}} &= \int_{z=-a/2}^{a/2} bh\rho(u + \dot{D}\cos\theta)\,\mathrm{d}z\cos\theta + (m_T + m_F\sin\theta)\dot{D} \\ &\quad - \int_{z=-a/2}^{a/2} \rho b h z\,\mathrm{d}z\sin\theta\dot{\theta}\,, \\ p_\theta := \frac{\partial H}{\partial \dot{\theta}} &= -\int_{z=-a/2}^{a/2} \rho b h z\,\mathrm{d}z\cos\theta\dot{D} + \int_{z=-a/2}^{a/2} \rho b h z^2\,\mathrm{d}z\dot{\theta}\,, \end{aligned}$$

where m_F is the fluid mass: $m_F = \int_{z=-a/2}^{a/2} \rho b h\,\mathrm{d}z$, which is constant.

By using the following change of variables: $\alpha_1(z,t) = bh(z,t)$ and $\alpha_2(z,t) = \rho(u(z,t) + \dot{D}(t)\cos\theta(t))$, the moment variables become:

$$\begin{aligned} p &= \int_{z=-a/2}^{a/2} \alpha_1\alpha_2\,\mathrm{d}z\cos\theta + (m_T + m_F\sin\theta)\dot{D} - \int_{z=-a/2}^{a/2} \rho\alpha_1 z\,\mathrm{d}z\sin\theta\dot{\theta}\,, \\ p_\theta &= -\int_{z=-a/2}^{a/2} \rho\alpha_1 z\,\mathrm{d}z\cos\theta\dot{D} + \int_{z=-a/2}^{a/2} \rho\alpha_1 z^2\,\mathrm{d}z\,\dot{\theta}\,. \end{aligned} \tag{A.2}$$

We can write $\dot{D}$ and $\dot{\theta}$ as function of the new moment variables:

$$\begin{aligned}\dot{D} &= \frac{\mathcal{A}\mathcal{D} + \mathcal{C}p_\theta - \mathcal{D}p}{\mathcal{C}^2 - \mathcal{B}\mathcal{D}},\\ \dot{\theta} &= -\frac{\mathcal{A}\mathcal{C} + \mathcal{B}p_\theta - \mathcal{C}p}{\mathcal{C}^2 - \mathcal{B}\mathcal{D}},\end{aligned} \tag{A.3}$$

where $\mathcal{A}$, $\mathcal{B}$, $\mathcal{C}$ and $\mathcal{D}$ are defined as follow:

$$\begin{aligned}\mathcal{A}[\alpha_1, \alpha_2, \theta] &:= \int_{z=-a/2}^{a/2} \alpha_1\alpha_2 \,\mathrm{d}z \cos\theta\,,\\ \mathcal{B}(\theta) &:= m_T + m_F \sin\theta\,,\\ \mathcal{C}[\alpha_1, \theta] &:= -\int_{z=-a/2}^{a/2} \rho\alpha_1 z \,\mathrm{d}z \sin\theta\,,\\ \mathcal{D}[\alpha_1] &:= \int_{z=-a/2}^{a/2} \rho\alpha_1 z^2 \,\mathrm{d}z\,.\end{aligned} \tag{A.4}$$

The new Hamiltonian, as function of $\alpha_1(z,t)$, $\alpha_2(z,t)$, $p(t)$, $D(t)$, $p_\theta(t)$, $\theta(t)$ is then given by:

$$\begin{aligned}H^F\left[\alpha_1, \alpha_2, D, p, \theta, p_\theta\right] = \int_{z=-a/2}^{a/2} &\left[\rho g(\frac{\alpha_1^2}{2b}\cos\theta + \alpha_1 z \sin\theta) + \frac{1}{2\rho}\alpha_1\alpha_2^2\right]\mathrm{d}z\\ &- \frac{\mathcal{D}\mathcal{A}^2 - 2\mathcal{D}\mathcal{A}p + 2\mathcal{C}\mathcal{A}p_\theta + \mathcal{D}p^2 - 2\mathcal{C}pp_\theta + \mathcal{B}p_\theta^2}{2(\mathcal{C}^2 - \mathcal{B}\mathcal{D})}\end{aligned} \tag{A.5}$$

Computing the variational derivatives of the Hamiltonian with respect to each energy variable:

$$\begin{aligned}\frac{\delta H^F}{\delta\alpha_2} &= \alpha_1\frac{\alpha_2}{\rho} + \frac{\partial H}{\partial\mathcal{A}}\frac{\delta\mathcal{A}}{\delta\alpha_2},\\ \frac{\delta H^F}{\delta\alpha_1} &= \rho g(\frac{\alpha_1}{b}\cos\theta + z\sin\theta) + \frac{\alpha_2^2}{2\rho} + \frac{\partial H}{\partial\mathcal{A}}\frac{\delta\mathcal{A}}{\delta\alpha_1} + \frac{\partial H}{\partial\mathcal{C}}\frac{\delta\mathcal{C}}{\delta\alpha_1} + \frac{\partial H}{\partial\mathcal{D}}\frac{\delta\mathcal{D}}{\delta\alpha_1},\end{aligned} \tag{A.6}$$

The partial derivatives of the H with respect to $\mathcal{A}$, $\mathcal{B}$, $\mathcal{C}$ and $\mathcal{D}$ are computed as:

$$\begin{aligned}\frac{\partial H^F}{\partial\mathcal{A}} &= -\frac{\mathcal{D}(\mathcal{A} - p) + \mathcal{C}p_\theta}{\mathcal{C}^2 - \mathcal{B}\mathcal{D}} = -\dot{D}\,,\\ \frac{\partial H^F}{\partial\mathcal{B}} &= -\frac{\mathcal{A}^2\mathcal{D}^2 + 2\mathcal{A}\mathcal{C}\mathcal{D}p_\theta - 2\mathcal{A}\mathcal{D}^2p + \mathcal{C}^2p_\theta^2 - 2\mathcal{C}\mathcal{D}pp_\theta + \mathcal{D}^2p^2}{2(\mathcal{C}^2 - \mathcal{B}\mathcal{D})^2} = -\frac{\dot{D}^2}{2}\,,\\ \frac{\partial H^F}{\partial\mathcal{C}} &= \frac{\mathcal{D}\mathcal{A}^2\mathcal{C} + \mathcal{A}\mathcal{C}^2p_\theta - 2\mathcal{D}\mathcal{A}\mathcal{C}p + \mathcal{B}\mathcal{D}\mathcal{A}p_\theta - \mathcal{C}^2pp_\theta + \mathcal{D}\mathcal{C}p^2 + \mathcal{B}\mathcal{C}p_\theta^2 - \mathcal{B}\mathcal{D}p\theta}{(\mathcal{C}^2 - \mathcal{B}\mathcal{D})^2} = -\dot{D}\dot{\theta}\,,\\ \frac{\partial H^F}{\partial\mathcal{D}} &= -\frac{\mathcal{A}^2\mathcal{C}^2 + 2\mathcal{A}\mathcal{B}\mathcal{C}p_\theta - 2\mathcal{A}\mathcal{C}^2p + \mathcal{B}^2p_\theta^2 - 2\mathcal{B}\mathcal{C}pp_\theta + \mathcal{C}^2p^2}{2(\mathcal{C}^2 - \mathcal{B}\mathcal{D})^2} = -\frac{\dot{\theta}^2}{2}\,,\end{aligned} \tag{A.7}$$

and the variational derivatives of $\mathcal{A}$, $\mathcal{B}$, $\mathcal{C}$ and $\mathcal{D}$ with respect to α_1 and α_2 are given by:

$$\frac{\delta\mathcal{A}}{\delta\alpha_1}(\alpha_1,\alpha_2,\theta) = \alpha_2\cos\theta\,, \qquad \frac{\delta\mathcal{A}}{\delta\alpha_2}(h,v,\theta) = \alpha_1\cos\theta\,, \tag{A.8}$$

$$\frac{\delta\mathcal{B}}{\delta\alpha_1}(\theta) = 0\,, \qquad \frac{\delta\mathcal{B}}{\delta\alpha_2}(\theta) = 0\,, \tag{A.9}$$

$$\frac{\delta\mathcal{C}}{\delta\alpha_1}(\alpha_1,\theta) = -\rho z\sin\theta, \qquad \frac{\delta\mathcal{C}}{\delta\alpha_2}(\alpha_1,\theta) = 0\,, \tag{A.10}$$

$$\frac{\delta\mathcal{D}}{\delta\alpha_1}(\alpha_1) = \rho z^2\,, \qquad \frac{\delta\mathcal{D}}{\delta\alpha_2}(\alpha_1) = 0\,, \tag{A.11}$$

So we the variational derivatives from Eq. A.6 can be rewritten as:

$$\begin{aligned} e_2^F &:= \frac{\delta H^F}{\delta\alpha_2} = \frac{\alpha_1\alpha_2}{\rho} - \dot{D}\alpha_1\cos\theta = bh(u+\dot{D}\cos\theta) - \dot{D}bh\cos\theta = bhu\,,\\ e_1^F &:= \frac{\delta H^F}{\delta\alpha_1} = \rho g(\frac{\alpha_1}{b}\cos\theta + z\sin\theta) + \frac{\alpha_2^2}{2\rho} - \dot{D}\alpha_2\cos\theta + \dot{D}\dot{\theta}\rho z\sin\theta - \rho\frac{(\dot{\theta}z)^2}{2}\,,\\ &= \rho g(h\cos\theta + z\sin\theta) + \rho\frac{u^2}{2} + \dot{D}\dot{\theta}\rho z\sin\theta - \frac{1}{2}\rho\left((\dot{D}\cos\theta)^2 + (\dot{\theta}z)^2\right)\,. \end{aligned} \tag{A.12}$$

Finally, the dynamic Equations 6.6 can be written as:

$$\begin{aligned} \frac{\partial\alpha_1}{\partial t}(z,t) &= -\frac{\partial}{\partial z}\left(e_2^F\right)\,,\\ \frac{\partial\alpha_2}{\partial t}(z,t) &= -\frac{\partial}{\partial z}\left(e_1^F\right)\,. \end{aligned} \tag{A.13}$$

In addition, the rigid body equations can be found. First, the partial derivatives of the Hamiltonian with respect to each rigid body variable must be computed:

$$\begin{aligned} e_p^F &:= \frac{\partial H^F}{\partial p} = \frac{\mathcal{A}\mathcal{D} + \mathcal{C}p_\theta - \mathcal{D}p}{\mathcal{C}^2 - \mathcal{B}\mathcal{D}} = \dot{D}\,,\\ e_{p\theta}^F &:= \frac{\partial H^F}{\partial p_\theta} = -\frac{\mathcal{A}\mathcal{C} + \mathcal{B}p_\theta - \mathcal{C}p}{\mathcal{C}^2 - \mathcal{B}\mathcal{D}} = \dot{\theta}\,. \end{aligned} \tag{A.14}$$

Thus, the rigid body equations are given by:

$$\begin{aligned} \frac{\partial p}{\partial t}(t) &= -e_D^F + F_{ext}\,,\\ \frac{\partial D}{\partial t}(t) &= e_p^F\,,\\ \frac{\partial p_\theta}{\partial t}(t) &= -e_\theta^F + M_{ext}\,,\\ \frac{\partial\theta}{\partial t}(t) &= e_{p\theta}^F\,. \end{aligned} \tag{A.15}$$

The fluid and rigid body equations can be rewritten using a matrix form:

$$\frac{\partial}{\partial t}\begin{bmatrix}\alpha_1(z,t)\\ \alpha_2(z,t)\\ p\\ D\\ p_\theta(t)\\ \theta(t)\end{bmatrix} = \begin{bmatrix}0 & -\partial_z & 0 & 0 & 0 & 0\\ -\partial_z & 0 & 0 & 0 & 0 & 0\\ 0 & 0 & 0 & -1 & 0 & 0\\ 0 & 0 & 1 & 0 & 0 & 0\\ 0 & 0 & 0 & 0 & 0 & -1\\ 0 & 0 & 0 & 0 & 1 & 0\end{bmatrix}\begin{bmatrix}e_1^F\\ e_2^F\\ e_p^F\\ e_D^F\\ e_{p\theta}^F\\ e_\theta^F\end{bmatrix} + \begin{bmatrix}0 & 0\\ 0 & 0\\ 1 & 0\\ 0 & 0\\ 0 & 1\\ 0 & 0\end{bmatrix}\begin{bmatrix}F_{ext}\\ M_{ext}\end{bmatrix}, \tag{A.16}$$

and outputs:

$$\begin{bmatrix}\dot{D}\\ \dot{\theta}\end{bmatrix} = \begin{bmatrix}0 & 0 & 0 & 0 & 1 & 0\\ 0 & 0 & 1 & 0 & 0 & 0\end{bmatrix}\begin{bmatrix}e_1^F\\ e_2^F\\ e_p^F\\ e_D^F\\ e_{p\theta}^F\\ e_\theta^F\end{bmatrix}. \tag{A.17}$$

The power balance of this system is given by:

$$\frac{\mathrm{d}\,H^F}{\mathrm{d}t} = \boldsymbol{u}_\partial^{F\,T}\boldsymbol{y}_\partial^F + \dot{D}F_{ext} + \dot{\theta}M_{ext}, \tag{A.18}$$

where $\boldsymbol{u}_\partial^F = \begin{bmatrix}e_1^F(a/2,t) & e_2^F(-a/2,t)\end{bmatrix}^T$ and $\boldsymbol{y}_\partial^F = \begin{bmatrix}-e_2^F(a/2,t) & e_1^F(-a/2,t)\end{bmatrix}^T$.

Appendix B

Rigid body as a pHs

Two additional degrees of freedom are needed to include the inertias of the tank that were not taken into account during the modeling of the sloshing in moving tanks: rotation due to bending $\theta_B(t)$ and rotation due to torsion $\theta_T(t)$.

The equations of motion are given directly by Newton's second law:

$$I_B^{RB}\,\ddot{\theta}_B(t) = M_{\text{ext,B}}, \tag{B.1}$$
$$I_T^{RB}\,\ddot{\theta}_T(t) = M_{\text{ext,T}}, \tag{B.2}$$

where I_B^{RB} and I_T^{RB} are the tank rotational inertias. The superscript RB stands for Rigid Body. $M_{\text{ext,B}}$ is the sum of moments in bending direction and $M_{\text{ext,T}}$ is the sum of moments in torsion direction.

Defining the following moment variables: $p_{\theta B} := I_B^{RB}\dot{\theta}_B$, and $p_{\theta T} := I_T^{RB}\dot{\theta}_T$, the previous equations are rewritten as:

$$\begin{aligned} \frac{d}{dt}\begin{bmatrix} p_{\theta B} \\ p_{\theta T} \end{bmatrix} &= 0 \begin{bmatrix} \frac{\partial H^{RB}}{\partial p_{\theta B}} \\ \frac{\partial H^{RB}}{\partial p_{\theta T}} \end{bmatrix} + \begin{bmatrix} 1 & 0 \\ 0 & 1 \end{bmatrix} \begin{bmatrix} M_{\text{ext,B}} \\ M_{\text{ext,T}} \end{bmatrix} \\ y^{RB} &= \begin{bmatrix} \dot{\theta}_B \\ \dot{\theta}_T \end{bmatrix} = \begin{bmatrix} 1 & 0 \\ 0 & 1 \end{bmatrix} \begin{bmatrix} \frac{\partial H^{RB}}{\partial p_{\theta B}} \\ \frac{\partial H^{RB}}{\partial p_{\theta T}} \end{bmatrix} \end{aligned} \tag{B.3}$$

where the Hamiltonian is equal to the kinetic energy:

$$H^{RB}(p_{\theta B}, p_{\theta T}) = \frac{1}{2}\left(\frac{p_{\theta B}^2}{I_B^{RB}} + \frac{p_{\theta T}^2}{I_T^{RB}}\right), \tag{B.4}$$

and its rate of change is given by:

$$\begin{aligned} \dot{H}^{RB} &= \dot{\theta}_B \dot{p}_{\theta B} + \dot{\theta}_T \dot{p}_{\theta T} \\ &= \dot{\theta}_B M_{\text{ext,B}} + \dot{\theta}_T M_{\text{ext,T}}\,. \end{aligned} \tag{B.5}$$

Notice that these equations also represent a port-Hamiltonian system, with port variables given by:

$$\boldsymbol{y}^{RB} = \begin{bmatrix} \dot{\theta}_B\,, & \dot{\theta}_T \end{bmatrix}^T, \boldsymbol{u}^{RB} = \begin{bmatrix} M_{\text{ext,B}}\,, & M_{\text{ext,T}} \end{bmatrix}^T. \tag{B.6}$$

Appendix C

Analytical solutions of sloshing and beam equations

Here we recall some analytical solutions that exist for the linear PDEs used to model the sloshing and beam motion. These analytical solutions were used to verify the limitations of the shallow water model in § 6.3, and to validate the numerical schemes in § 10.2.

C.1 Sloshing models

C.1.1 Linearized Shallow Water Equations under translation

The linearized SWE are simply given by the wave equation:

$$\frac{\partial^2 \tilde{h}}{\partial t^2}(z,t) = g\bar{h}\frac{\partial^2 \tilde{h}}{\partial z^2}(z,t)\,, \qquad -a/2 < z < a/2\,, \tag{C.1}$$

where $\tilde{h}(z,t)$ is the fluid height with respect to the equilibrium height $\bar{h}$ at time t and position z. The boundary conditions for a tank moving horizontally are given by:

$$g\frac{\partial \tilde{h}}{\partial z}(-a/2,t) = g\frac{\partial \tilde{h}}{\partial z}(a/2,t) = -A(t)\,, \tag{C.2}$$

where $A(t)$ is the tank lateral acceleration.

Applying the Laplace transform to Eq. C.1, with respect to time variable and assuming zero initial conditions, we get:

$$s^2\,\mathcal{L}\tilde{h}(z,s) = g\bar{h}\frac{\partial^2}{\partial z^2}\,\mathcal{L}\tilde{h}(z,s)\,, \tag{C.3}$$

where s is the Laplace variable, $\mathcal{L}\tilde{h}(s,x)$ is the Laplace transform of $\tilde{h}(z,t)$.

The general solution of the second-order ODE (Eq. C.3) is given by:

$$\mathcal{L}\tilde{h}(z,t) = c_1 \cosh\left(\frac{sz}{\sqrt{g\bar{h}}}\right) + c_2 \sinh\left(\frac{sz}{\sqrt{g\bar{h}}}\right), \tag{C.4}$$

where the coefficients of c_1 and c_2 depend on the boundary conditions (Eq. C.2). We find:

$$c_1 = 0 \qquad c_2 = -\frac{\sqrt{g\bar{h}}}{gs\cosh\left(\frac{sa}{2\sqrt{g\bar{h}}}\right)}\mathcal{L}A(s)\,, \tag{C.5}$$

where $\mathcal{L}A(s)$ is the Laplace transform of the tank acceleration.

Thus, the transfer function between lateral accelerations and the fluid height at a position z is given by:

$$\frac{\mathcal{L}\tilde{h}}{\mathcal{L}A}(z,s) = -\frac{\sqrt{g\bar{h}}\sinh\left(\frac{sz}{\sqrt{g\bar{h}}}\right)}{gs\cosh\left(\frac{as}{2\sqrt{g\bar{h}}}\right)}, \tag{C.6}$$

We can compute the pressure at any point of the fluid as: $P = \rho g(\tilde{h} + \bar{h} - y)$ (so that the pressure is zero at free surface, and increases downward).

The force due to fluid is obtained from the integration of the pressure over walls:

$$\begin{aligned}\mathcal{L}F(s) &= \int_{y=0}^{\bar{h}} bP(z = a/2, y, s)\,\mathrm{d}y - \int_{y=0}^{\bar{h}} bP(z = -a/2, y, s)\,\mathrm{d}y,\\ &= -\frac{2}{s}bh\rho\sqrt{gh}\tanh\left(\frac{as}{2\sqrt{gh}}\right)\mathcal{L}A(s).\end{aligned} \tag{C.7}$$

Finally, the transfer function that relates the tank acceleration to the fluid force on the walls is given by:

$$\boxed{\frac{\mathcal{L}F}{\mathcal{L}A}(s) = -\frac{2}{s}bh\rho\sqrt{gh}\tanh\left(\frac{as}{2\sqrt{gh}}\right).} \tag{C.8}$$

Furthermore, the poles of the previous transfer function are all in the imaginary axis and are given by $p = \pm\omega_n j$, where ω_n are the natural frequencies:

$$\boxed{\omega_n^{SW} = \pi(2n+1)\frac{\sqrt{gh}}{a}\,, \qquad n = 0, 1, 2, \ldots} \tag{C.9}$$

C.1.2 Incompressible Euler equations

The incompressible Euler equations with dynamic boundary conditions to represent the free surface allow a better modeling of the sloshing for tanks with large depth of fluid. Here we only present the final transfer function and natural frequencies (used in § 6.3 to expose the limitation of the shallow water model). See, e.g., Abramson (1966) and Cardoso-Ribeiro et al. (2014) for the derivation of the transfer function and more complete results.

As presented for the SWE in the previous section, the following transfer function represents the relationship between the acceleration of the fluid A and the forces applied to the wall by the fluid F:

$$\boxed{\frac{\mathcal{L}F}{\mathcal{L}A}(s) = -\left(ab\bar{h}\rho - \sum_{n=0}^{\infty} \frac{8a^3b\rho\omega_n^2}{g\pi^4(2n+1)^4} \frac{s^2}{s^2+(\omega_n^{IE})^2}\right)} \tag{C.10}$$

where ω_n^{IE} is the natural frequency:

$$\boxed{\omega_n^{IE} = \sqrt{g\frac{(2n+1)\pi}{a}\tanh\left(\frac{(2n+1)\pi}{a}\bar{h}\right)}\,.} \tag{C.11}$$

Remark C.1
Note that for a fixed n, $\omega_n^{IE} \sim \omega_n^{SE}$ for small $\frac{\bar{h}}{a}$.

C.2 Beam models

Here we recall the analytical solutions of the homogeneous Euler-Bernoulli and torsion equations, used for validation of the numerical methods in § 10.2. More details can be obtained, e.g., in Leleu (2002) and Cardoso-Ribeiro et al. (2014).

C.2.1 Bending equations

The bending equations with piezoelectric actuators were obtained in Eq. 5.10. We recall it here (now with uniform coeficients):

$$\mu\ddot{w} = -\partial_{z^2}^2\left(\kappa\partial_{z^2}^2 w\right) + \partial_{z^2}^2\left(\Pi_{ab}(z)k_p v(t)\right)\,, \tag{C.12}$$

The dynamic equations can be solved using separation of variables, which leads to an infinite set of independent ordinary differential equations. The solution $w(z,t)$ is given as an infinite sum and approximating by truncating on the "n-th" term, we get:

$$w(z,t) = \sum_{i=1}^{\infty} W_i(z)T_i^w(t) \approx \sum_{i=1}^{n} W_i(z)T_i^w(t)\,, \tag{C.13}$$

where $T_i^w(t)$ is $i-th$ bending mode displacement, $W_i(z)$ are the modal shapes, which are given by (for fixed-free boundary conditions):

$$\begin{aligned} W_i(x) = -\frac{1}{\sinh(\beta_i L) - \sin(\beta_i L)}\,[&(\cos(\beta_i x) - \cosh(\beta_i x))\cosh(\beta_i L) + \\ &(\cos(\beta_i x) - \cosh(\beta_i x))\cos(\beta_i L)] \end{aligned} \tag{C.14}$$

The modal displacement can be computed from the following ODEs (for $i = 1, 2, \dots$):

$$\ddot{T}_i^w(t) + (\omega_i^B)^2 T_i^w(t) = k_p(\frac{\partial W_i(a)}{\partial z} - \frac{\partial W_i(b)}{\partial z})v(t), \tag{C.15}$$

where ω_i^B is the i-th bending mode's natural frequency, given by:

$$\boxed{\omega_i^B = \beta_i^2 \sqrt{\frac{EI}{\mu}}\,,} \tag{C.16}$$

where β_i are the solutions of the following transcendental equation:

$$\cos(\beta L)\,\cosh(\beta L) + 1 = 0\,. \tag{C.17}$$

Finally, using the first N dynamic modal equations (Eq. C.15), and truncating Eq.C.13, we can easily find a state space model, with $v(t)$ as input and tip deflection as output:

$$\begin{aligned} \dot{\boldsymbol{x}} &= A\boldsymbol{x} + \boldsymbol{B}v(t)\,. \\ w(L,t) &= C\boldsymbol{x}\,. \end{aligned} \tag{C.18}$$

C.2.2 Torsion dynamics

Similarly, analytical results for the torsion dynamics (Eq. 5.25) can be obtained using separation of variables. Here we recall just the natural frequencies:

$$\boxed{\omega_i^T = i\frac{\pi}{2}\sqrt{\frac{GJ}{IL^2}}, \quad i = 1, 3, \dots\,.} \tag{C.19}$$

Appendix D

Including damping in the discretized systems

As presented in § 4.1.3, it is possible to include dissipation in the pHs by introducing *dissipative ports* together with appropriate constitutive relations. Although even a linear constitutive relation given by a diagonal matrix with negative values can be used, we observed that such choice might cause problems in the simulations and control design of semi-discretized pHs. The goal of this appendix is to present strategies of how to choose these constitutive relations in the semi-discretized pHs.

D.1 Semi-discretized pHs

All the semi-discretized models presented in this thesis can be written as:

$$\begin{bmatrix} -\boldsymbol{x}_1 \\ -\boldsymbol{x}_2 \\ \boldsymbol{y} \\ \boldsymbol{y}_R \end{bmatrix} = \begin{bmatrix} 0 & -J_{12} & -B_1 & -B_R \\ -J_{21} & 0 & -B_2 & 0 \\ B_1^T & B_2^T & D_u & 0 \\ B_R^T & 0 & 0 & 0 \end{bmatrix} \begin{bmatrix} \nabla_{\boldsymbol{x}_1} H_d \\ \nabla_{\boldsymbol{x}_2} H_d \\ \boldsymbol{u} \\ \boldsymbol{u}_R \end{bmatrix}, \tag{D.1}$$

where $J_{12} = -{J_{21}}^T$, $\boldsymbol{u}$ and $\boldsymbol{y}$ include the boundary and the distributed input/output ports; $\boldsymbol{u}_R$ and $\boldsymbol{y}_R$ and distributed resistive ports, used specifically to introduce damping in the system. To simplify, let us assume that $\boldsymbol{u} = 0$:

$$\begin{aligned} \begin{bmatrix} \boldsymbol{x}_1 \\ \boldsymbol{x}_2 \end{bmatrix} &= \begin{bmatrix} 0 & J_{12} \\ J_{21} & 0 \end{bmatrix} \begin{bmatrix} \nabla_{\boldsymbol{x}_1} H_d \\ \nabla_{\boldsymbol{x}_2} H_d \end{bmatrix} + \begin{bmatrix} I \\ 0 \end{bmatrix} \boldsymbol{u}_R, \\ \boldsymbol{y}_R &= \begin{bmatrix} I & 0 \end{bmatrix} \begin{bmatrix} \nabla_{\boldsymbol{x}_1} H_d \\ \nabla_{\boldsymbol{x}_2} H_d \end{bmatrix} \end{aligned} \tag{D.2}$$

Notice a linear constitutive relation $\boldsymbol{u}_R = -D\boldsymbol{y}_R$, with positive-definite D, removes energy from the system, since the power balance is given by:

$$\dot{H} = -\left(\nabla_{\boldsymbol{x}_1} H_d\right)^T D \, \nabla_{\boldsymbol{x}_1} H_d \, . \tag{D.3}$$

For instance, a simple D matrix like:

$$D = cI \tag{D.4}$$

where I is the identity matrix and c a positive constant should work to introduce damping in the system. However, we observed that this choice leads to small damping in higher frequencies. For this reason, better choices of D based in the linearized equations are proposed in the following subsection.

D.2 Damping choices that preserve the eigenstructure of the linear system

In this section, the linearized equations will be considered. In the nonlinear case, the equations can be easily linearized around an equilibrium by computing the Hessian of the Hamiltonian at the equilibrium point:

$$Q = \frac{\partial^2 H}{\partial(\boldsymbol{x}_1, \boldsymbol{x}_2)^2}(\boldsymbol{x}_{1\text{eq}}, \boldsymbol{x}_{2\text{eq}})\,. \tag{D.5}$$

In the structural and **linearized** fluid equations, there is no direct coupling between these two energy variables in the Hamiltonian (the coupling occurs only in the interconnection matrix J). For this reason, it is possible to rewrite Q as:

$$Q = \begin{bmatrix} Q_1 & 0 \\ 0 & Q_2 \end{bmatrix}, \tag{D.6}$$

and the (linearized) equations with dissipation become:

$$\begin{aligned} \dot{\boldsymbol{x}}_1 &= -DQ_1\boldsymbol{x}_1 + J_{12}Q_2\boldsymbol{x}_2\,, \\ \dot{\boldsymbol{x}}_2 &= J_{21}Q_1\boldsymbol{x}_1\,, \end{aligned} \tag{D.7}$$

which can be rewritten as a single second-order differential equation:

$$\underbrace{I}_{M}\ddot{\boldsymbol{x}}_2 + \underbrace{J_{21}Q_1D(J_{21})^{-1}}_{C}\dot{\boldsymbol{x}}_2 \underbrace{-J_{21}Q_1J_{12}Q_2}_{K}\boldsymbol{x}_2 = 0\,. \tag{D.8}$$

It is well known (Rayleigh damping) that any combination such:

$$C = \alpha M + \beta K \tag{D.9}$$

preserves the eigenstructure of original system (see, e.g., Caughey (1960), Caughey and O'Kelly (1965) and Matignon and Hélie (2013)). This motivates two possible choices of D:

$$\boxed{D_1 = \alpha(Q_1)^{-1},} \tag{D.10}$$

such that the equation becomes:

$$\ddot{\boldsymbol{x}}_2 + \underbrace{\alpha I}_{C=\alpha M} \dot{\boldsymbol{x}}_2 - J_{21}Q_1J_{12}Q_2\boldsymbol{x}_2 = 0 \tag{D.11}$$

and

$$\boxed{D_2 = -J_{12}Q_2J_{21},} \tag{D.12}$$

such that the equation becomes:

$$\ddot{\boldsymbol{x}}_2 \underbrace{-\beta J_{21}Q_1J_{12}Q_2}_{C=\beta K}\dot{\boldsymbol{x}}_2 - J_{21}Q_1J_{12}Q_2\boldsymbol{x}_2 = 0\,. \tag{D.13}$$

Finally, a damping matrix D based on the modal decomposition of the linearized system is also possible. This choice allows specifying the values of damping ratio for each mode, preserving the eigenvectors of the original system.

Assuming that Σ^2 is a diagonal matrix with the eigenvalues of $-J_{21}Q_1J_{12}Q_2$ and W is a matrix with the respective eigenvectors as columns, it is possible to decompose $-J_{21}Q_1J_{12}Q_2$ as:

$$-J_{21}Q_1J_{12}Q_2 = W\Sigma^2W^{-1}\,. \tag{D.14}$$

Using the following change of coordinates: $Wz = q$, Eq. 8 can be rewritten as:

$$\ddot{\boldsymbol{z}} = -W^{-1}J_{21}Q_1D(J_{21})^{-1}W\dot{\boldsymbol{z}} - W^{-1}W\Sigma^2W^{-1}W\boldsymbol{z}\,, \tag{D.15}$$

which simplifies to:

$$\ddot{\boldsymbol{z}} = -W^{-1}J_{21}Q_1D(J_{21})^{-1}W\dot{\boldsymbol{z}} - \Sigma^2\boldsymbol{z}\,. \tag{D.16}$$

To specify the damping of each mode, the following equation must hold:

$$W^{-1}J_{21}Q_1D(J_{21})^{-1}W = 2\Xi\sqrt{\Sigma^2}, \tag{D.17}$$

where Ξ is a diagonal matrix with the individual damping ratios of each mode. Eq. D.17 holds for the following damping matrix D:

$$\boxed{D_3 = 2{Q_1}^{-1}{J_{21}}^{-1}W\Xi\sqrt{\Sigma^2}W^{-1}J_{21}\,.} \tag{D.18}$$

Remark D.1
In this thesis, the damping model of Eq. D.18 was used since it allows specifying the damping ratio for each mode of the system. This choice is important:

1. *To improve the stability characteristics of the time-domain numerical integration, since it mitigates spurious high-frequency oscillations (see simulations of the fluid-structure system, in § 10.5).*

2. *For control design in Chapter 12. If damping is not taken into account or not well mod-*

eled, the controller may cause an unstable behavior of the plant. For instance, a simple damping model (as Eq. D.4) might cause instability, since the high-frequency modes exhibit small damping ratios (thus, the controller may excite high-frequency unmodeled dynamics).

Appendix E

Multi-model H_∞ control application to FSI

This appendix shows three methodologies that are tested for control design with the goal of improving the damping characteristics of the fluid-structure system. The results were previously presented in Cardoso-Ribeiro, Matignon, and Pommier-Budinger (2015a). The three methodologies are based on fixed-structure H_∞ synthesis method (Apkarian and Noll, 2006). First, a controller is designed for a nominal plant considering a partially filled tank (50% filled). Secondly, a controller is designed based on a multi-model approach, considering three operating points of the plant. Thirdly, an uncertain sloshing model is taken into account and an iterative multi-model robust design is implemented (inspired by Alazard et al. (2013) and Apkarian, Dao, and Noll (2014)). All designs are simulated for different fillings of fluid.

Section E.1 motivates the use of robust control techniques, showing how fluid sloshing affects the system frequency response. Different uncertainty modeling approaches are presented. Section E.2 briefly reviews the control strategies and the design choices. Finally, Section E.3 presents the results and comparisons between the different control designs.

E.1 Uncertainties

Uncertainties of structural dynamic models come from several sources. The most well known is the unmodeled high frequency dynamics: when modeling structural dynamics, we represent a finite dimensional approximation of infinite-dimensional equations. This means that inevitably we are neglecting high-frequency dynamics, which will not be well represented by the nominal model. Designing a control law for a low order system without this in mind can lead to instability (the so-called "spill-over" effect), by excitation of modes that were not predicted by nominal plant. Most robust control applications (not only for flexible structures) use some kind of roll-off filter, to avoid the excitation of unmodeled high order dynamics.

Many other uncertainties appear during the modeling process (uncertain material and geometrical properties, non-ideal boundary conditions, and many simplification hypothesis during the modeling process). All these factors can lead to uncertainties even in the low-frequency range. For our coupled fluid-plate system, an additional uncertainty is the filling of the tank, which changes considerably the frequency response of the system.

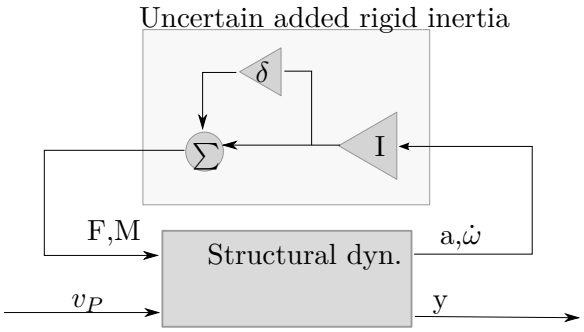

Figure E.1: Structural dynamics coupled with uncertain rigid body

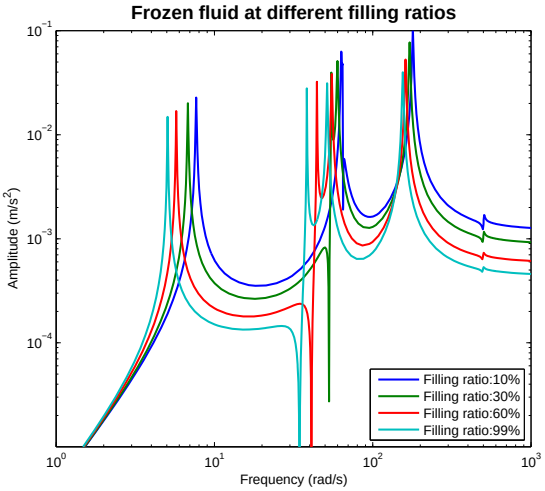

Figure E.2: Frequency response for the tank filled with frozen liquid. Input given by excitation of one piezoelectric patch, output given by acceleration near the plate free tip.

A simple approach would be to consider that the fluid is a rigid body (frozen liquid). In this case, we substitute the sloshing equations into a variable inertia (as represented in Fig. E.1). Fig. E.2 shows the frequency response for several filling of frozen liquid.

Figure E.3 shows that such a simplification might be problematic. It shows the frequency response for different fillings of water. A comparison with the ice case is also presented. We can see that for small fillings, the rigid body approximation proves adequate. However, for intermediate fillings, not only the first structural modes move considerably, but also new modes appear due to sloshing. The behavior near the first structural mode is the most complex one: the first mode (bending) is strongly coupled with sloshing modes, so that it actually "splits" in several "coupled" modes in the frequency response. The most complicated scenario happens when the tank is partially filled (from about 50% to 80%): in these cases, the first structural mode is split in two high amplitude coupled modes.The sloshing dynamics doesn't affect the higher order structural modes considerably[1].

The finite-dimensional sloshing model was used to develop an uncertain model for the sloshing dynamics, considering the typical variations of sloshing natural frequencies (Table E.1) from 25% to 75% of tank filling. The following expressions was used:

$$\omega_{i,\delta} = \omega_{i,n}(1 + v_i\delta_i), \tag{E.1}$$

where $\omega_{i,n}$ is the nominal natural frequency of $i-th$ sloshing mode, $\omega_{i,\delta}$ is the uncertain natural frequency, δ_i is a parametric uncertainty such that $\delta_i \leq 1$ and v_i is a constant value

[1]This is true for the theoretical linear sloshing model. However, nonlinear sloshing waves affects higher order structural modes: in Ref. Cardoso-Ribeiro et al. (2014), we verified that nonlinear sloshing waves appear when exciting the system near the second bending mode.

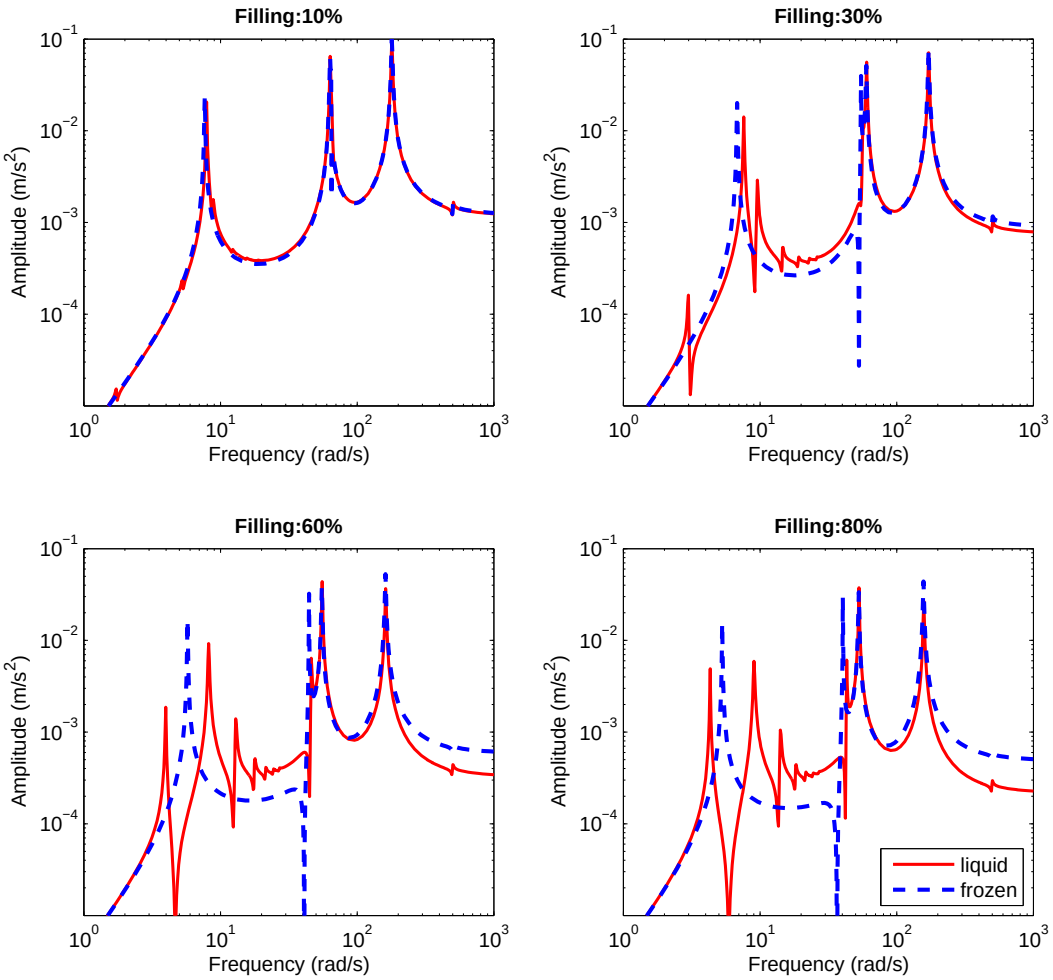

Figure E.3: Frequency response of fluid-structure system vs ice simplification. Input given by excitation of one piezoelectric patch, output given by acceleration near the plate free tip.

Table E.1: Comparison of natural frequencies (in Hz) for different fillings and modeling approaches

0 % ice	25% ice	25% slosh	50% ice	50% slosh	75% ice	75% slosh	100% ice
		0.4362		0.5939		0.6748	
1.2658	1.1165	1.1938	0.9613	1.261	0.8568	1.3992	0.8053
		1.407		1.9144		2.211	
		2.1541		2.7271		2.8859	
		2.8618		3.3479		3.4147	
		3.4767		3.8433		3.8687	
		4.0068		4.2658		4.2749	
10.2333	9.0874	9.3078	7.5205	7.7863	6.5578	6.9618	6.105
10.8059	9.6718	9.7317	9.0055	9.0647	8.4829	8.5191	8.1964
28.9622	27.5728	27.5841	26.116	26.1843	25.1382	25.2647	24.6623
80.1058	79.689	79.692	79.3792	79.3945	79.2203	79.268	79.1535

for each mode, representing the amount of uncertainty in each parameter. Similar uncertain models are used to represent uncertain fluid inertia (considering a variation from 25% to 75% of tank filling) and damping ratio (considering values from 0.005 to 0.015). The nominal values are those for a half-filled tank. The uncertain model, used for control design, takes into account the first 3 sloshing modes, 3 bending modes and 2 torsion modes.

The coupled model with parametric uncertainty can be represented as in Fig. E.4, where Δ is a diagonal matrix with elements δ_i. A set of resulting resulting dynamics (for random Δ) is presented in Fig. E.5.

E.2 Control design

In this work, SYSTUNE was used to find a fixed-order optimal controller, considering the scheme of Fig. E.6. In addition to minimizing chosen H_∞ norms, this tool allows the definition of constraints. The following control design problem is then considered:

$$\underbrace{\min}_{K(s) \quad \text{stabilizing}} \quad ||T_{z_1 d_1}||_\infty, \tag{E.2}$$

constrained to: $||T_{z_2 d_2}||_\infty \leq 1$.

The weight W_1 is used to shape the maximum bounds of the controller. This allow shaping the controller crossover frequency (avoiding spill-over) and maximum amplitude (avoiding saturation of actuators). The resulting controller will usually use the maximum available control ($||T_{z_2 d_2}||_\infty$ near to 1), that minimizes the effect of input disturbance ($||T_{z_1 d_1}||$) on output z_1 (deflections near the plate tip).

Three different strategies are presented: first, the problem is solved for the nominal plant

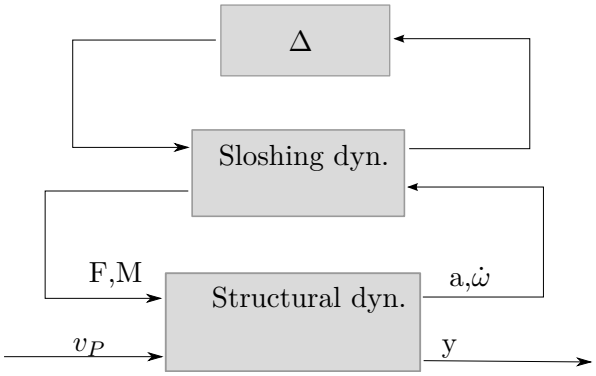

Figure E.4: Structural dynamics coupled with uncertain slosh model

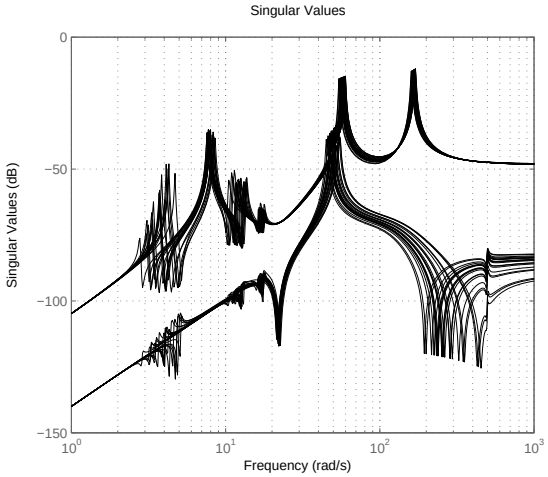

Figure E.5: Singular values for the uncertain plants. Accelerations as outputs, piezoelectric patches voltages as inputs.

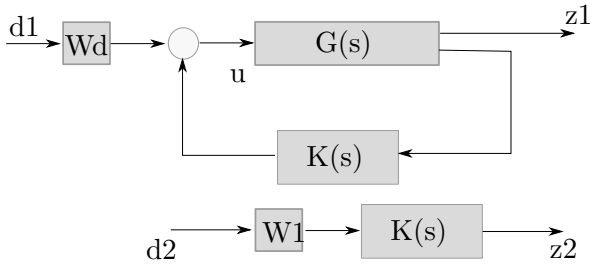

Figure E.6: Control scheme with disturbance in input and control shaping in parallel

and the computed controller is tested for other plants. Secondly, a multi-model approach considering several nominal plants was tested (presented in Section E.2.2). Thirdly, a robust design approach is tested (presented in Section E.2.3).

For all these three design strategies, the performance weights were chosen as presented in the following section.

E.2.1 Choice of performance weights

The key idea of H_∞ control synthesis is to shape closed-loop characteristics by an appropriate choice of weight functions. As explained before, W_1 weights the actuators signals. By increasing this weight, the allowed input signals (voltages) applied in the plant are reduced. In addition, by choosing an appropriate frequency response for this weight, high-frequency excitation and the spill-over effect can be avoided.

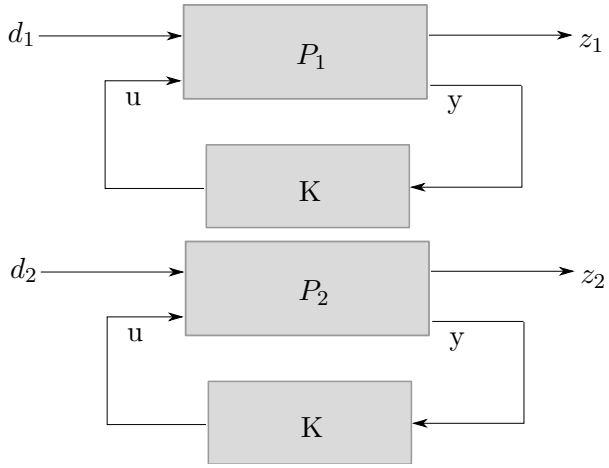

Figure E.7: Multi-model control design

Weight W_1 is chosen as:

$$W_1(s) = k_0 \left(\frac{s/(2\pi f_1) + 1}{s/(2\pi f_2) + 1} \right)^n \tag{E.3}$$

where $n = 4$, $f_1 = 10Hz$, $f_2 = 200Hz$, $k_0 = 0.0001$.

Weight W_d represents usual disturbances applied to the plant. Since the objective is to reduce the effect of disturbances in the first modes, a low-pass filter is appropriate:

$$W_d(s) = \left(\frac{1}{s/(2\pi f_d) + 1} \right), \tag{E.4}$$

where $f_d = 15Hz$, chosen since the goal is to attenuate the vibration of the first modes.

E.2.2 Multi-model design using several nominal plants with different fillings of fluid

Using H_∞ design techniques with fixed-structure controller (like those implemented in the Matlab function SYSTUNE) allows finding a controller that optimizes the H_∞ norm for several plants at the same time. The idea is to put several different plants in parallel, with the same controller, as presented in Fig. E.7 for two plants P_1 and P_2. In this work, the nominal dynamics of three different fillings of fluid (25%, 50% and 75%) are used. For all plants, the performance weights are the same as presented in Section E.2.1.

E.2.3 Multi-model design for robust control using the uncertain plant

A more general problem of control is to design a controller $K(s)$ that minimizes a performance objective (like the H_∞ norm), but considering the plant parametric uncertainties (so that it should be stable and have good performance characteristics in the uncertainty envelope). A scheme that represents this problem is given in Fig.11.5. The μ-synthesis method is the usual

approach for this problem (D-K or D-K-G algorithms).

In this work, we use a recently developed approach (Refs. Apkarian, Dao, and Noll (2014), Alazard et al. (2013)) that uses an iterative multi-model design, based on worst-case analysis. The idea of the algorithm consists in:

1. Solving the problem for the nominal plant;
2. Verifying if the uncertain closed-loop system is robustly stable. If it is not, take the plant parametric values for the worst-case uncertain plant Δ_{wc}. Use this model together with the nominal plant, for multi-model H_∞ design. Repeat the process until the resulting controller leads to a robustly stable closed loop.
3. Verifying if the desired performance goals are achieved for all the closed loop. If it is not, include the worst case in the multi-model design approach.
4. Repeating the process until the system has robust stability and performance characteristics.

For robust stability check, it is possible to use Matlab function ROBUSTSTAB, which calculates the stability margin of uncertain systems and gives the parametric values of uncertainty that causes instability. However, for the problem studied here, this function gives worst-case values that are much bigger than the uncertainty ranges of this problem (which would lead to a too conservative design), even for plants that are clearly not robustly stable. For this reason, a Monte Carlo approach has been implemented: 100 closed loop systems which are inside the uncertainty envelope are randomly generated; if some of them are unstable, the one with largest uncertainty is added to the multi-model design process. The process is stopped when the designed controller is stable to all randomly generated systems.

E.3 Results

As explained in the previous section, three different controllers were designed for this plant. First, a fixed-order controller was designed for the nominal plant, considering the tank half filled. Secondly, a multi-model approach based on three nominal models for the plant was designed. Thirdly, a multi-model approach based on the worst-case uncertainty was tested. In this section, the three controllers are called non-robust, multi-model and robust design, respectively.

All controllers were obtained using a fixed-structure (a 5th order state-space representation). The controlled dynamical system has two-inputs (voltage at two piezoelectric actuators) and two outputs (measurements of accelerations at two points near the plate tip). Figures E.9 and E.10 show the singular values frequency responses for the three closed loop-systems, in comparison with the open loop. Similar results are obtained for the three controllers. However, the non-robust design works only for the nominal plant: using almost any other plant in the uncertainty envelope leads to instability. Fig. E.11 shows the singular values for

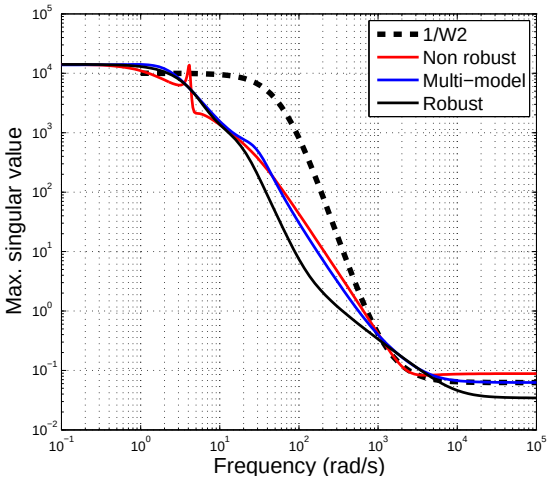

Figure E.8: Maximum singular values for each controller and comparison with upper boundary $1/W_2$.

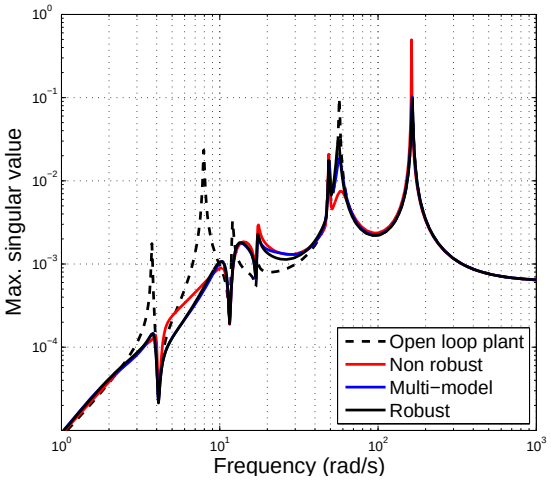

Figure E.9: Singular values for the nominal reduced order plant (filling = 50%), using different control strategies

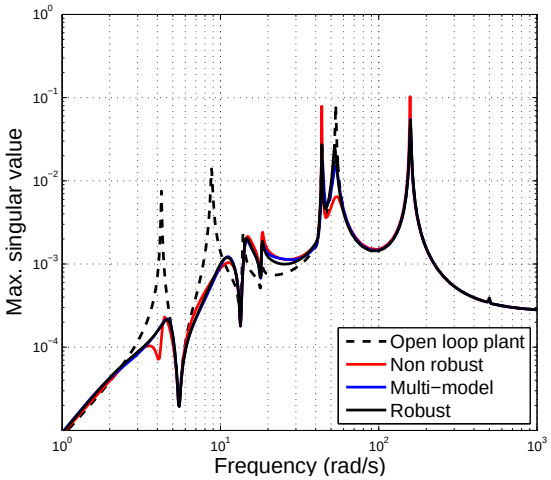

Figure E.10: Singular values for the reduced order plant with filling = 75%, using different control strategies

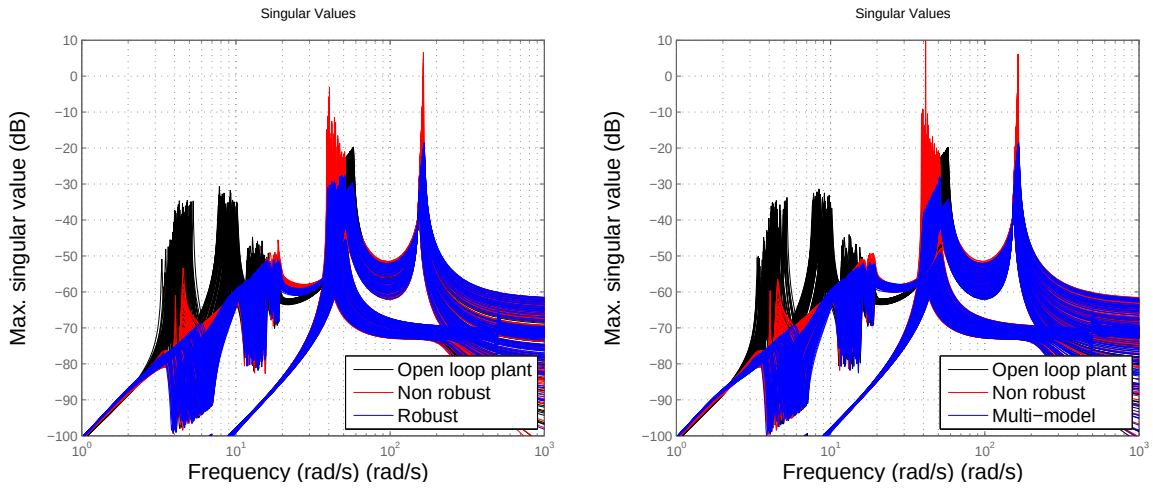

Figure E.11: Singular values for the uncertain reduced order plant - 100 hundred random samples for each case are presented

the closed loop of the uncertain plants. While the multi-model and robust design shows good attenuation characteristics for all the randomly generated plants, several undesired peaks appear when using the non-robust controller. The two multi-design models happen to be robust, working well both on the uncertainty envelope as well as when using a higher-order model of the plant, with different fillings of fluid. Singular value frequency responses of high order plant using these two controllers are presented in Figs. E.12 and E.13, considering fillings of 25% and 75%.

The proposed controllers were tested on the experimental device. The controllers were implemented using MATLAB Simulink, on Real time Windows Target, with a NI 6024-E board. A sample time of 0.001 s was used. The accelerations were measured by two 4371 Bruel & Kjær accelerometers (located near the plate free tip), with two charge amplifiers (Type 2635). The two PZT piezoelectric actuators were saturated at 150 V.

One experimental time response is presented in Fig. E.14 for the robust controller. Open-loop and closed-loop systems were both excited during 60 seconds with a 100 V sine wave at the first resonance frequency (0.7 Hz). In the closed-loop case, controller is activated only after the sine wave excitation. It is possible to see from acceleration measurements that the proposed controller significantly increases the system damping.

Frequency response for experimental results is presented in Fig. E.15 for a filling ratio of 75 %. The controller used in this figure is the robust one. It is possible to see that, as predicted, the first three modes are very well attenuated when using the control. Similar results were obtained for other filling ratios and using the multi-model control design.

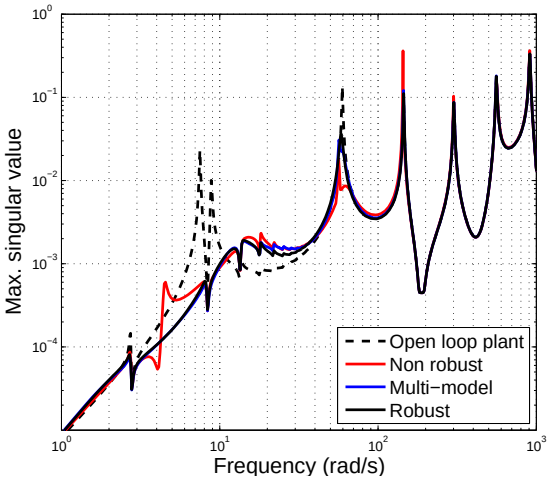

Figure E.12: Singular values for the high order plant (filling = 25%), using different control strategies

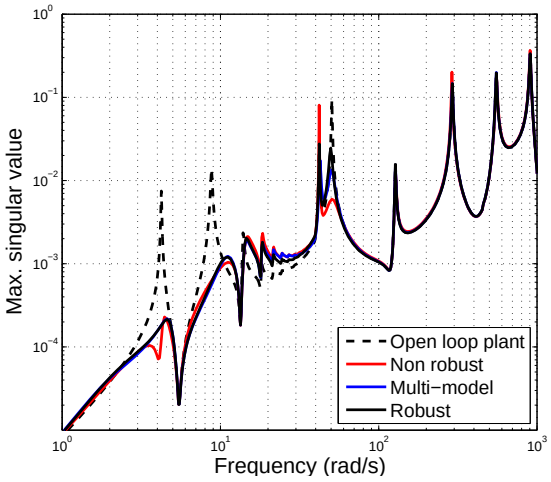

Figure E.13: Singular values for high order plant (filling = 75%), using different control strategies

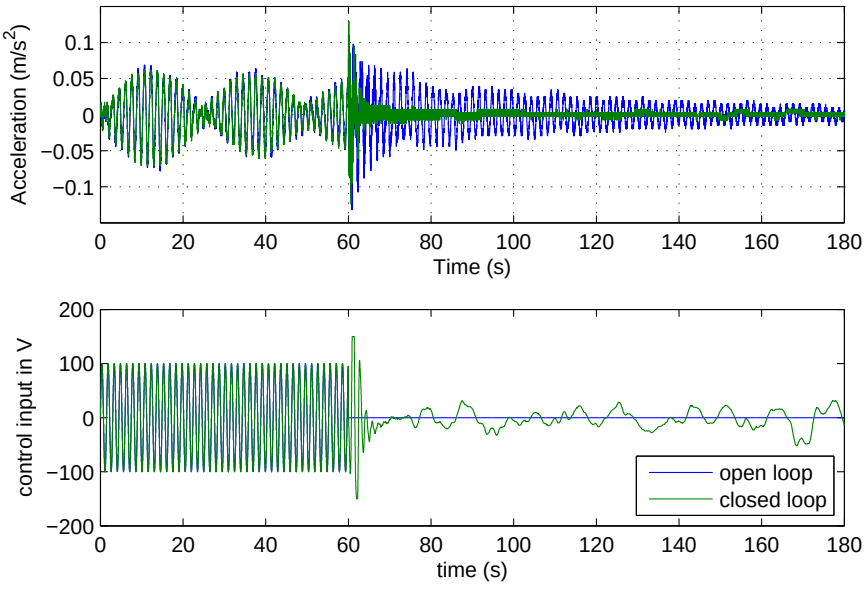

Figure E.14: Open-loop and closed-loop experimental time-response - robust design - 75 % filled tank

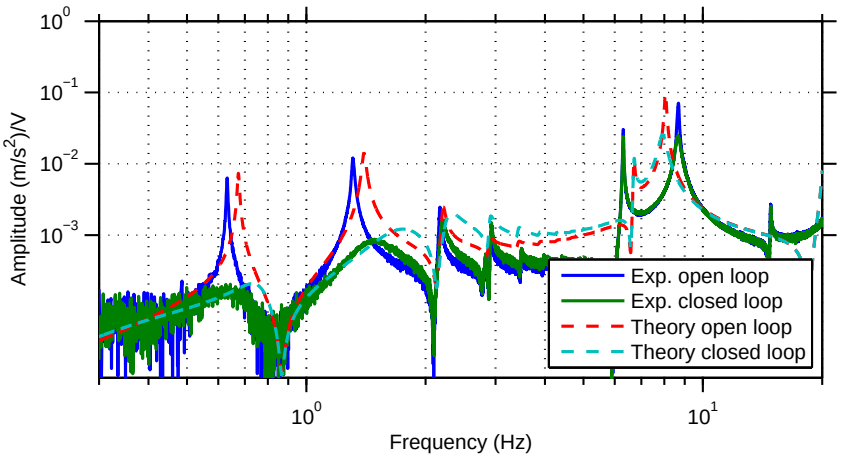

Figure E.15: Experimental vs. theoretical results - frequency response - input: symmetric piezoelectric actuations; output: acceleration measurement near plate free tip. Closed-loop system uses robust design - 75 % filled tank

E.4 Conclusions

This appendix presented three control strategies for improving the damping characteristics of the fluid-structure system:

- design directly from the nominal plant (called "non-robust");
- a multi-model design, considering three operating points of the plant;
- a robust iterative method, that uses the uncertain model with multi-model design.

The results, presented in Section E.3 are promising: except for the non-robust design, the two others exhibited good stability and performance characteristics in the uncertainty envelope and using a high-order model. Experimental results showed that the proposed designs improved damping characteristics of the actual plant.

Bibliography

Abramson, H. N. (1966). *The Dynamic Behaviour of Liquids in Moving Containers. NASA SP-106*. Ed. by H. N. Abramson. NASA (cit. on pp. 3, 9, 178).

Abzug, M. J. (1996). "Fuel Slosh in Skewed Tanks." In: *Journal of Guidance Control and Dynamics* 19(5), pp. 1172–1177 (cit. on p. 9).

Abzug, M. J. and E. E. Larrabee (2002). *Airplane Stability and Control*. Cambridge University Press (cit. on p. 3).

Aglietti, G. S., S. B. Gabriel, R. S. Langley, and E. Rogers (1997). "A modeling technique for active control design studies with application to spacecraft microvibrations." In: *The Journal of the Acoustical Society of America* 102(4), pp. 2158–66 (cit. on pp. 47, 146, 149).

Alan, P. (1958). "On the Fatigue Failure of Structures due to Vibrations Excited by Random Pressure Fields." In: *The Journal of the Acoustical Society of America* 30(12), pp. 1130–1135 (cit. on p. 145).

Alazard, D., T. Loquen, H. de Plinval, and C. Cumer (2013). "Avionics/Control co-design for large flexible space structures." In: *Proceedings of the AIAA Guidance, Navigation, and Control (GNC) Conference*. American Institute of Aeronautics and Astronautics: Boston, MA, pp. 1–15 (cit. on pp. 185, 191).

Alemi Ardakani, H. (2016). "A symplectic integrator for dynamic coupling between nonlinear vessel motion with variable cross-section and bottom topography and interior shallow-water sloshing." In: *Journal of Fluids and Structures* 65, pp. 30–43 (cit. on pp. 11, 61).

Alemi Ardakani, H. and T. J. Bridges (2010). "Dynamic coupling between shallow-water sloshing and horizontal vehicle motion." In: *European Journal of Applied Mathematics* 21(06), pp. 479–517 (cit. on pp. 11, 61).

Alemi Ardakani, H. and T. J. Bridges (2011). "Shallow-water sloshing in vessels undergoing prescribed rigid-body motion in three dimensions." In: *Journal of Fluid Mechanics* 667, pp. 474–519 (cit. on p. 11).

Alemi Ardakani, H. and T. J. Bridges (2012). "Shallow-water sloshing in vessels undergoing prescribed rigid-body motion in two dimensions." In: *European Journal of Mechanics - B/Fluids* 31, pp. 30–43 (cit. on p. 11).

Allen, R. R. (1978). "Bond graph models for plant biosystems." In: *Computer Programs in Biomedicine* 8(3-4), pp. 149–164 (cit. on p. 11).

Apkarian, P., M. N. Dao, and D. Noll (2014). "Parametric robust structured control design." In: *arXiv preprint*. arXiv: `1405.4202` (cit. on pp. 185, 191).

Apkarian, P. and D. Noll (2006). "Nonsmooth H_∞ Synthesis." In: *IEEE Transactions on Automatic Control* 51(1), pp. 71–86 (cit. on pp. 149, 185).

Armenio, V. and L. R. Michele (1996). "On the analysis of sloshing of water in rectangular containers: numerical study and experimental validation." In: *Ocean Engineering* 23(8), pp. 705–739 (cit. on pp. 10, 11).

Ascher, U. M. and L. R. Petzold (1998). *Computer Methods for Ordinary Differential Equations and Differential-Algebraic Equations*. SIAM (cit. on pp. 40, 135).

Baaiu, A., F. Couenne, L. Lefèvre, Y. Le Gorrec, and M. Tayakout (2009). "Structure-preserving infinite dimensional model reduction: Application to adsorption processes." In: *Journal of Process Control* 19(3), pp. 394–404 (cit. on pp. 13, 101).

Banks, H. T., R. C. Smith, and Y. Wang (1996). *Smart material structures: modeling, estimation, and control*. Wiley, p. 304 (cit. on pp. 47, 59).

Bassi, L., A. Macchelli, and C. Melchiorri (2007). "An Algorithm to Discretize One-Dimensional Distributed Port Hamiltonian Systems." In: *Proceedings of the Lagrangian and Hamiltonian Methods for Nonlinear Control 2006*. Springer, pp. 61–73 (cit. on p. 13).

Bauer, H. F. (1960). *Propellant Sloshing Problems of Saturn Test Flight SA-1 (U)*. Tech. rep. November. NASA (cit. on p. 3).

Bisplinghoff, R. L., H. Ashley, and R. L. Halfman (1996). *Aeroelasticity*. Dover (cit. on p. 11).

Boyd, J. P. (2001). *Chebyshev and Fourier Spectral Methods: Second Revised Edition*. Dover, p. 668 (cit. on pp. 13, 103).

Breedveld, P. C. (2004). "Port-based modeling of mechatronic systems." In: *Mathematics and Computers in Simulation* 66(2-3), pp. 99–128 (cit. on p. 5).

Cardoso-Ribeiro, F. L., D. Matignon, and V. Pommier-Budinger (2016a). "Modeling by interconnection and control by damping injection of a fluid-structure system with non-collocated actuators and sensors." In: *Proceedings of the International Conference on Noise and Vibration Engineering ISMA*. Leuven, Belgium (cit. on p. 166).

Cardoso-Ribeiro, F. L., D. Matignon, and V. Pommier-Budinger (2016b). "Piezoelectric beam with distributed control ports : a power-preserving discretization using weak formulation." In: *2nd IFAC Workshop on Control of Systems Governed by Partial Differential Equations*. Bertinoro, Italy, pp. 290–297 (cit. on pp. 111, 166).

Cardoso-Ribeiro, F. L., V. Pommier-Budinger, J.-S. Schotté, and D. Arzelier (2014). "Modeling of a coupled fluid-structure system excited by piezoelectric actuators." In: *Proceedings of the 2014 IEEE/ASME International Conference on Advanced Intelligent Mechatronics*. IEEE: Besançon, France, pp. 216–221 (cit. on pp. 178, 179, 186).

Cardoso-Ribeiro, F. L., D. Matignon, and V. Pommier-Budinger (2015a). "Control design for a coupled fluid-structure system with piezoelectric actuators." In: *Proceedings of the 3rd CEAS EuroGNC*. Toulouse, France (cit. on pp. 167, 185).

Cardoso-Ribeiro, F. L., D. Matignon, and V. Pommier-Budinger (2015b). "Modeling of a Fluid-structure coupled system using port-Hamiltonian formulation." In: *Proceedings of the 5th IFAC Workshop on Lagrangian and Hamiltonian Methods for Nonlinear Control LHMNC (Invited Session)*. Vol. 48. 13. Lyon, France, pp. 217–222 (cit. on p. 165).

Caughey, T. K. (1960). "Classical Normal Modes in Damped Linear Dynamic Systems." In: *Journal of Applied Mechanics* 27(2), p. 269 (cit. on p. 182).

Caughey, T. K. and M. E. J. O'Kelly (1965). "Classical Normal Modes in Damped Linear Dynamic Systems." In: *Journal of Applied Mechanics* 32(3), p. 583 (cit. on p. 182).

Celebi, M. S. and H. Akyildiz (2002). "Nonlinear modeling of liquid sloshing in a moving rectangular tank." In: *Ocean Engineering* 29, pp. 1527–1553 (cit. on p. 10).

Cesnik, C. and E. Brown (2003). "Active Warping Control of a Joined Wing/Tail Airplane Configuration." In: *Proceedings of the 44th AIAA/ASME/ASCE/AHS/ASC Structures, Structural Dynamics, and Materials Conference*. April, pp. 1–15 (cit. on p. 146).

Chen, Y. G., K Djidjeli, and W. G. Price (2009). "Numerical simulation of liquid sloshing phenomena in partially filled containers." In: *Computers and Fluids* 38(4), pp. 830–842 (cit. on p. 10).

Cho, S. and N. H. McClamrocht (2000). "Feedback control of a space vehicle with unactuated fuel slosh dynamics." In: *Proceedings of the AIAA Guidance, Navigation, and Control (GNC) Conference*. August. Denver, USA (cit. on p. 10).

Cobb, R. G., J. Browning, R. Canfield, and S. Miller (2009). "F-16 Ventral Fin Buffet Alleviation Using Piezoelectric Actuators." In: *Proceedings of the 50th AIAA/ASME/ASCE/AHS/ ASC Structures, Structural Dynamics, and Materials Conference*. May. Palm Springs, USA, pp. 1–16 (cit. on pp. 146, 148, 149).

Curtain, R. F. and H. Zwart (1995). *An Introduction to Infinite-Dimensional Linear Systems Theory*. Vol. 21. Texts in Applied Mathematics. Springer New York: New York, NY (cit. on p. 38).

Di Lieto, N., J. Sahlmann, A. Wallander, and G. Vasisht (2007). "An Approach to Stabilizing Large Telescopes for Stellar Interferometry." In: *Proceedings of the 11th International Conference on Accelerator and Large Experimental Control Systems (ICALEPCS 2007)*, pp. 497–499 (cit. on p. 145).

Dodge, F. T. (2000). *The new" dynamic behavior of liquids in moving containers"*. Southwest Research Inst (cit. on p. 9).

Doyle, J. C., K. Glover, P. P. Khargonekar, and B. A. Francis (1989). "State-space solutions to standard H_2 and H_∞ control problems." In: *IEEE Transactions on Automatic Control* 34(8), pp. 831–847 (cit. on p. 149).

Duindam, V., A. Macchelli, S. Stramigioli, and H. Bruyninckx (2009). *Modeling and Control of Complex Physical Systems: The Port-Hamiltonian Approach*. Springer Berlin Heidelberg: Berlin, Heidelberg, p. 442 (cit. on pp. 5, 12, 32).

Duindam, V. (2006). "Port-Based Modeling and Control for Efficient Bipedal Walking Robots." PhD thesis. Universiteit Twente (cit. on p. 12).

Duindam, V., G. Blankenstein, and S. Stramigioli (2004). "Port-based modeling and analysis of snakeboard locomotion." In: *16th International Symposium on Mathematical Theory of Networks and Systems* 1, pp. 1–7 (cit. on p. 12).

Escobar, G., A. J. van der Schaft, and R. Ortega (1999). "Hamiltonian viewpoint in the modeling of switching power converters." In: *Automatica* 35(3), pp. 445–452 (cit. on p. 12).

Falaize, A. (2016). "Modélisation, simulation, génération de code et correction de systèmes multi-physiques audios: approche par réseau de composants et formulation hamiltonienne à ports." PhD thesis. Université Pierre et Marie Curie (cit. on p. 13).

Farhat, C., E. K. Chiu, D. Amsallem, J.-S. Schotté, and R. Ohayon (2013). "Modeling of Fuel Sloshing and its Physical Effects on Flutter." In: *AIAA Journal* 51(9), pp. 2252–2265 (cit. on p. 11).

Feng, G. C. (1973). "Dynamic loads due to moving tank." In: *Proceedings of the AIAA, ASME, SAE 14th Structures, Structural Dynamics, and Materials Conference*. Williamsburg, USA (cit. on p. 10).

Firouz-Abadi, R., P. Zarifian, and H. Haddadpour (2014). "Effect of Fuel Sloshing in the External Tank on the Flutter of Subsonic Wings." In: *Journal of Aerospace Engineering* 27(5) (cit. on pp. 10, 11).

Fleming, A. J. and K. K. Leang (2010). "Integrated strain and force feedback for high-performance control of piezoelectric actuators." In: *Sensors and Actuators, A: Physical* 161(1-2), pp. 256–265. arXiv: 1005.4881v1 (cit. on p. 148).

Goh, C. J. and T. K. Caughey (1985). "On the stability problem caused by finite actuator dynamics in the collocated control of large space structures." In: *International Journal of Control* 41(3), pp. 787–802 (cit. on p. 148).

Golo, G. (2002). "Interconnection Structures in Port-Based Modelling : Tools for Analysis and Simulation." PhD thesis. University of Twente (cit. on pp. 29, 98).

Golo, G., V. Talasila, A. J. van der Schaft, and B. Maschke (2004). "Hamiltonian discretization of boundary control systems." In: *Automatica* 40(5), pp. 757–771 (cit. on pp. 13, 93, 95, 96, 101, 109).

Graham, E. W. and A. M. Rodriguez (1951). *The characteristics of fuel motion which affect airplane dynamics*. Tech. rep. DTIC Document (cit. on p. 9).

Granda, J. J. (1985). "Computer Generation of Physical System Differential Equations Using Bond Graphs." In: *Journal of the Franklin Institute* 319(1-2), pp. 243–255 (cit. on p. 12).

Granda, J. and R. Montgomery (2003). "Automated Modeling and Simulation Using the Bond Graph Method for the Aerospace Industry." In: *Proceedings of the AIAA Modeling and Simulation Technologies Conference and Exhibit*. Austin, USA (cit. on p. 12).

Grewal, A., D. G. Zimcik, L. Hurtubise, and B. Leigh (2000). "Active cabin noise and vibration control for turboprop aircraft using multiple piezoelectric actuators." In: *Journal of Intelligent Materials Systems and Structures* 11(6), pp. 438–447 (cit. on p. 146).

Gu, D.-W., P. H. Petkov, and M. M. Konstantinov (2013). *Robust Control Design with MATLAB®*. Advanced Textbooks in Control and Signal Processing. Springer: London (cit. on p. 149).

Hamroun, B. (2009). "Approche hamiltonienne à ports pour la modélisation, la réduction et la commande des systèmes non linéaires à paramètres distribués: application aux écoulements." PhD thesis. Grenoble INP, France (cit. on pp. 12, 13, 25, 73, 102).

Hamroun, B., L. Lefèvre, and E. Mendes (2007). "Port-based modelling and geometric reduction for open channel irrigation systems." In: *Proceedings of the 46th IEEE Conference on Decision and Control*. IEEE: New Orleans, USA, pp. 1578–1583 (cit. on pp. 13, 61, 101).

Hamroun, B., A. Dimofte, L. Lefèvre, and E. Mendes (2010). "Control by Interconnection and Energy-Shaping Methods of Port Hamiltonian Models. Application to the Shallow Water Equations." In: *European Journal of Control* 16(5), pp. 545–563 (cit. on pp. 13, 61, 102).

Hirt, C. W. and J. L. Cook (1970). "A Lagrangian Method for Calculating the Dynamics of an Incompressible Fluid with Free Surface." In: *Journal of Computational Physics*(5), pp. 103–124 (cit. on p. 10).

Hodges, D. H. and G. A. Pierce (2011). *Introduction to Structural Dynamics and Aeroelasticity*. Cambridge University Press, p. 247 (cit. on pp. 11, 53, 145).

Ibrahim, R. A. (2005). *Liquid Sloshing Dynamics: Theory and Applications*. Cambridge University Press, p. 970 (cit. on p. 9).

Jacob, B. and H. Zwart (2012). *Linear Port-Hamiltonian Systems on Infinite-dimensional Spaces*. Springer, p. 220 (cit. on p. 38).

Jeltsema, D. and A. Dòria-Cerezo (2012). "Port-hamiltonian formulation of systems with memory." In: *Proceedings of the IEEE* 100(6), pp. 1928–1937 (cit. on p. 12).

Kar, I. N., T. Miyakura, and K. Seto (2000). "Bending and torsional vibration control of a flexible plate structure using H_∞-based robust control law." In: *IEEE Transactions on Control Systems Technology* 8(3), pp. 545–553 (cit. on p. 150).

Karnopp, D. (1976). "Bond Graphs for Vehicle Dynamics." In: *Vehicle System Dynamics* 5(3), pp. 171–184 (cit. on p. 11).

Karnopp, D. C., D. L. Margolis, and R. C. Rosenberg (2012). *System Dynamics*. John Wiley & Sons, Inc.: Hoboken, NJ, USA (cit. on p. 5).

Kelkar, A. G. and S. M. Joshi (1998). "Robust passification and control of non-passive systems." In: *Proceedings of the 1998 American Control Conference (ACC)*. IEEE: Philadelphia, PA, United States, 3133–3137 vol.5 (cit. on p. 151).

Kelkar, A. G. and S. M. Joshi (2004). "Control of Elastic Systems via Passivity-Based Methods." In: *Journal of Vibration and Control* 10(11), pp. 1699–1735 (cit. on p. 151).

Kelkar, A. G. and S. N. Joshi (1997). "Robust control of non-passive systems via passification." In: *Proceedings of the 1997 American Control Conference (ACC)*. IEEE: Albuquerque, United States, 2657–2661 vol.5 (cit. on p. 151).

Kelkar, A. G., Y. Mao, and S. M. Joshi (2000). "LMI-based passification for control of non-passive systems." In: *Proceedings of the 2000 American Control Conference (ACC)*. IEEE: Chicago, IL, United States, 1271–1275 vol.2 (cit. on p. 151).

Kiefling, L. and G. C. Feng (1976). "Fluid-Structure Finite Element Vibrational Analysis." In: *AIAA Journal* 14(2), pp. 199–203 (cit. on p. 10).

Kotyczka, P. (2016). "Finite Volume Structure-Preserving Discretization of Distributed-Parameter Port-Hamiltonian Systems." In: *Proceedings of the 2nd IFAC Workshop on Control of Systems Governed by Partial Differential Equations (CPDE)*. Vol. 49. 8. Elsevier B.V.: Bertinoro, Italy, pp. 298–303 (cit. on p. 102).

Kunkel, P. and V. Mehrmann (2006). *Differential-Algebraic Equations: Analysis and Numerical Solution*. European Mathematical Society, p. 377 (cit. on pp. 40, 135).

Lanczos, C. (1970). *The Variational Principles of Mechanics*. University of Toronto Press: Toronto (cit. on p. 22).

Le Gorrec, Y., H. Zwart, and B. Maschke (2005). "Dirac structures and Boundary Control Systems associated with Skew-Symmetric Differential Operators." In: *SIAM Journal on Control and Optimization* 44(5), pp. 1864–1892 (cit. on pp. 34, 38).

Le Gorrec, Y., H. Peng, L. Lefèvre, B. Hamroun, and F. Couenne (2011). "Systèmes hamiltoniens à ports de dimension infinie. Réduction et propriétés spectrales." In: *Journal Européen des Systèmes Automatisés* 45(7-10), pp. 645–664 (cit. on pp. 13, 102).

Leimkuhler, B. and S. Reich (2005). *Simulating Hamiltonian Dynamics*. Cambridge University Press: Cambridge (cit. on pp. 23, 35, 169).

Leleu, S. (2002). "Amortissement actif des vibrations d'une structure flexible de type plaque à l'aide de transducteurs piézoélectriques." PhD thesis. ENS Cachan (cit. on pp. 150, 179).

Liu, W. K. and R. A. Uras (1988). "Variational approach to fluid-structure interaction with sloshing." In: *Nuclear Engineering and Design* 106(1), pp. 69–85 (cit. on p. 10).

Lopes, N. (2016). "Approche passive pour la modélisation, la simulation et l'étude d'un banc de test robotisé pour les instruments de type cuivre." PhD. Université Pierre et Marie Curie - Paris VI (cit. on p. 13).

Luenberger, D. (1966). "Observers for multivariable systems." In: *IEEE Transactions on Automatic Control* 11(2), pp. 190–197 (cit. on p. 153).

Macchelli, A. and C. Melchiorri (2005). "Control by interconnection of mixed port Hamiltonian systems." In: *IEEE Transactions on Automatic Control* 50(11), pp. 1839–1844 (cit. on pp. 12, 38, 67).

Macchelli, A, C. Melchiorri, and S. Stramigioli (2007). "Port-based modeling of a flexible link." In: *IEEE Transactions on Robotics* 23(4), pp. 650–660 (cit. on p. 13).

Macchelli, A., A. J. van der Schaft, and C. Melchiorri (2004a). "Multi-variable port Hamiltonian model of piezoelectric material." In: *IEEE/RSJ International Conference on Intelligent Robots and Systems (IROS)*. Vol. 1. Sendai, Japan (cit. on pp. 12, 47).

Macchelli, A., A. J. van der Schaft, and C. Melchiorri (2004b). "Port Hamiltonian formulation of infinite dimensional systems I. Modeling." In: *Proceedings of the 43rd IEEE Conference on Decision and Control*. IEEE: Atlantis, Paradise Island, Bahamas, pp. 3762–3767 (cit. on p. 12).

Macchelli, A., A. J. van der Schaft, and C. Melchiorri (2004c). "Port Hamiltonian formulation of infinite dimensional systems II. Boundary control by interconnection." In: *Proceedings of the 43rd IEEE Conference on Decision and Control*. Ieee: Atlantis, Paradise Island, Bahamas, 3768–3773 Vol.4 (cit. on p. 12).

Macchelli, A. (2012). "Energy-Based Control of Spatially-Discretized Distributed Port Hamiltonian Systems." In: *Proceedings of the 7th Vienna International Conference on Mathematical Modelling*. Vol. 45. 2, pp. 786–791 (cit. on p. 13).

Macchelli, A. and C. Melchiorri (2004). "Modeling and Control of the Timoshenko Beam. The Distributed Port Hamiltonian Approach." In: *SIAM Journal on Control and Optimization* 43(2), pp. 743–767 (cit. on pp. 12, 30, 167).

Marsden, J. E. and T. S. Ratiu (1999). *Introduction to Mechanics and Symmetry*. Vol. 17. Texts in Applied Mathematics. Springer New York: New York, NY (cit. on p. 22).

Maschke, B. and A. van der Schaft (2013). "On alternative Poisson brackets for fluid dynamical systems and their extension to Stokes-Dirac structures." In: *Proceedings of the 1st IFAC Workshop on Control of Systems Governed by Partial Differential Equations (CPDE)*. Vol. 46. 26. IFAC: Paris, France, pp. 109–114 (cit. on p. 12).

Maschke, B. M. and A. J. van der Schaft (1992). "Port-controlled Hamiltonian systems: modelling and system theoretic properties." In: *Proceedings of the IFAC Nonlinear Control Systems Design*. Bordeaux, France, pp. 359–365 (cit. on p. 12).

Maschke, B. M., A. J. van der Schaft, and P. C. Breedveld (1995). "An Intrinsic Hamiltonian Formulation of the Dynamics of LC-Circuits." In: *IEEE Transactions on Circuits and Systems I: Fundamental Theory and Applications* 42(2), pp. 73–82 (cit. on p. 12).

Maschke, B. M., A. J. van der Schaft, and P. C. Breedveld (1992). "An Intrinsic Hamiltonian formulation of Network Dynamics: Non-standard Poisson Structures and Gyrators." In: *Journal of the Franklin Institute* 329(5), pp. 923–966 (cit. on p. 23).

Maschke, B. M. J. and a. J. van der Schaft (2000). "Port controlled Hamiltonian representation of distributed parameter systems." In: *IFAC Workshop on modeling and Control of Lagrangian and Hamiltonian Systems*. January. Princeton, NJ, USA (cit. on pp. 12, 32).

Maschke, B., R. Ortega, and A. J. van der Schaft (2000). "Energy-Based Lyapunov Functions for Forced Hamiltonian Systems with Dissipation." In: *IEEE Transactions on Automatic Control* 45(8), pp. 1498–1502 (cit. on p. 12).

Matignon, D. and T. Hélie (2013). "A class of damping models preserving eigenspaces for linear conservative port-Hamiltonian systems." In: *European Journal of Control* 19(6), pp. 486–494 (cit. on pp. 57, 182).

McDonald, K. T. (2012). *Bernoulli's Equation for a Rotating Fluid (Lecture notes)*. Available at `http://www.physics.princeton.edu/~mcdonald/examples/bernoulli_rot.pdf`. Princeton, USA (cit. on p. 68).

Mellert, V., I. Baumann, N. Freese, and R. Weber (2008). "Impact of sound and vibration on health, travel comfort and performance of flight attendants and pilots." In: *Aerospace Science and Technology* 12(1), pp. 18–25 (cit. on p. 145).

Morris, K. and A. O. Ozer (2013). "Strong stabilization of piezoelectric beams with magnetic effects." In: *Proceedings of the 52nd IEEE Conference on Decision and Control*. Florence, Italy, pp. 3014–3019 (cit. on p. 47).

Moulla, R. (2010). "Méthodes Géometriques d'Intégration pour les Systèmes Dynamiques." PhD thesis. Université Claude Bernard Lyon 1 (cit. on p. 13).

Moulla, R., L. Lefèvre, and B. Maschke (2012). "Pseudo-spectral methods for the spatial symplectic reduction of open systems of conservation laws." In: *Journal of Computational Physics* 231(4), pp. 1272–1292 (cit. on pp. 13, 93, 102, 103, 109, 111, 117, 118, 166).

Moulla, R., L. Lefèvre, and B. Maschke (2011). "Geometric pseudospectral method for spatial integration of dynamical systems." In: *Mathematical and Computer Modelling of Dynamical Systems* 17(1), pp. 85–104 (cit. on pp. 13, 125).

Moutsopoulou, A., G. E. Stavroulakis, and A. Pouliezos (2011). "Uncertainty Modeling and Robust Control for Smart Structures." In: *Computational Methods in Earthquake Engineering*. Ed. by M. Papadrakakis, M. Fragiadakis, and N. D. Lagaros. Vol. 21. Springer Netherlands: Dordrecht, pp. 331–356 (cit. on p. 150).

Noll, T. E., J. M. Brown, M. E. Perez-davis, S. D. Ishmael, G. C. Tiffany, and M. Gaier (2004). *Investigation of the Helios Prototype Aircraft Mishap*. Tech. rep. January. NASA (cit. on p. 4).

Noorian, M. A., R. D. Firouz-Abadi, and H. Haddadpour (2012). "A reduced order model for liquid sloshing in tanks with flexible baffles using boundary element method." In: *International Journal for Numerical Methods in Engineering* 89(13), pp. 1652–1664. arXiv: `1010.1724` (cit. on p. 10).

Olver, P. J. (1993). *Applications of Lie groups to differential equations*. Springer-Verlag (cit. on pp. 32, 83, 167).

Onawola, O. O. and S. C. Sinha (2011). "A Feedback Linearization Approach for Panel Flutter Suppression With Piezoelectric Actuation." In: *Journal of Computational and Nonlinear Dynamics* 6(3), p. 031006 (cit. on p. 146).

Ono, T. D. (2012). "Application of Multi-input Multi-Output Feedback Control for F-16 Ventral Fin Buffet Alleviation Using Piezoelectric Actuators." Master thesis. Air Force Institute of Technology (cit. on pp. 148, 149).

Ortega, R., A. J. van der Schaft, and B. Maschke (2001). "Putting Energy Back in Control." In: *IEEE Control Systems Magazine*(April), pp. 18–33 (cit. on p. 12).

Ortega, R., A. J. van der Schaft, B. Maschke, and G. Escobar (2002). "Interconnection and damping assignment passivity-based control of port-controlled Hamiltonian systems." In: *Automatica* 38, pp. 585–596 (cit. on pp. 12, 148).

Pasumarthy, R., V. R. Ambati, and A. J. van der Schaft (2012). "Port-Hamiltonian discretization for open channel flows." In: *Systems & Control Letters* 61(9), pp. 950 –958 (cit. on p. 13).

Pasumarthy, R. and A. J. van der Schaft (2004). "On Interconnections of Infinite-dimensional Port-Hamiltonian Systems." In: *Proceedings of the 16th International Symposium on Mathematical Theory of Networks and Systems*. Leuven, Belgium, pp. 1–12 (cit. on p. 67).

Pasumarthy, R. (2006). "On Analysis and Control of Interconnected Finite- and Infinite-dimensional Physical Systems ." PhD thesis. University of Twente (cit. on pp. 12, 13, 38).

Paynter, H. M. (1961). *Analysis and Design of Engineering Systems: Class Notes for M.I.T. Course 2.751*. M.I.T. Press (cit. on p. 11).

Perelson, A. S. (1976). "Description of electrical networks using bond graphs." In: *Circuit Theory and Applications* 4(June 1975), pp. 107–123 (cit. on p. 11).

Petit, N. and P. Rouchon (2002). "Dynamics and solutions to some control problems for water-tank systems." In: *IEEE Transactions on Automatic Control* 47(4), pp. 594–609 (cit. on pp. 11, 61–63).

Preumont, A. (2011). *Vibration Control of Active Structures*. Vol. 179. Springer, p. 432 (cit. on pp. 47, 145, 146, 151).

Previdi, F., C. Spelta, M. Madaschi, D. Belloli, S. M. Savaresi, F. Faginoli, and E. Silani (2014). "Active vibration control over the flexible structure of a kitchen hood." In: *Mechatronics* 24(3), pp. 198–208 (cit. on p. 146).

Ramirez, H., B. Maschke, and D. Sbarbaro (2013). "Irreversible port-Hamiltonian systems: A general formulation of irreversible processes with application to the CSTR." In: *Chemical Engineering Science* 89, pp. 223–234 (cit. on p. 12).

Rivin, E. I. (1995). "Vibration isolation of precision equipment." In: *Precision Engineering* 17(1), pp. 41–56 (cit. on p. 145).

Robles, R. R. and J. P. Serrano (2014). "Sloshing mechanical model for stability and handling qualities evaluation of the C295 aircraft with the OSD system." In: *Proceedings of 29th Congress of the International Council of the Aeronautical Sciences*. St. Petersburg, Russia (cit. on p. 10).

Robu, B. (2010). "Active vibration control of a fluid/plate system." PhD thesis. Université Toulouse III-Paul Sabatier (cit. on pp. 10, 150).

Robu, B., L. Baudouin, C. Prieur, and D. Arzelier (2012). "Simultaneous H_∞ Vibration Control of Fluid/Plate System via Reduced-Order Controller." In: *IEEE Transactions on Control Systems Technology* 20(3), pp. 700–711 (cit. on p. 150).

Rodriguez, H., A. J. van der Schaft, and R. Ortega (2001). "On stabilization of nonlinear distributed parameter port-controlled Hamiltonian systems via energy shaping." In: *Proceedings of the 40th IEEE Conference on Decision and Control*. Vol. 1. IEEE: Orlando, USA, pp. 131–136 (cit. on p. 12).

Schotté, J. S. and R. Ohayon (2003a). "Effect of gravity on a free-free elastic tank partially filled with incompressible liquid." In: *Journal of Fluids and Structures* 18(2), pp. 215–226 (cit. on p. 10).

Schotté, J.-S. and R. Ohayon (2003b). "Representation of liquid sloshing in elastic 3D tanks by equivalent mechanical systems and symmetric reduced models." In: *Proceedings of the 2nd MIT Conference on Compurational Fluid and Solid Mechanics*. Elsevier: Boston, USA, pp. 1506–1509 (cit. on p. 10).

Schotté, J.-S. and R. Ohayon (2009). "Various modelling levels to represent internal liquid behaviour in the vibration analysis of complex structures." In: *Computer Methods in Applied Mechanics and Engineering* 198(21-26), pp. 1913–1925 (cit. on p. 10).

Schy, A. A. (1952). *A Theoretical Analysis of the Effects of Fuel Motion on Airplane Design*. Tech. rep. NACA, NACA–TR–1080 (cit. on p. 9).

Seslija, M., J. M. A. Scherpen, and A. J. van der Schaft (2014). "Explicit simplicial discretization of distributed-parameter port-Hamiltonian systems." In: *Automatica* 50(2), pp. 369–377 (cit. on pp. 13, 110, 168).

Shin, H. C. and S. B. Choi (2001). "Position control of a two-link flexible manipulator featuring piezoelectric actuators and sensors." In: *Mechatronics* 11(6), pp. 707–729 (cit. on p. 146).

Smith Jr., C. C. (1948). *The effects of fuel sloshing on the lateral stability of a free-flying airplane model*. Tech. rep. NACA RM No. L8C16. NACA (cit. on p. 9).

Soong, T. T. and M. C. Costantinou (1994). *Passive and Active Structural Vibration Control in Civil Engineering*. Ed. by T. T. Soong and M. C. Costantinou. Vol. 345. CISM International Centre for Mechanical Sciences. Springer Vienna: Vienna (cit. on p. 145).

SpaceX (2007). *Falcon Demo Flight 2: Flight Review Update*. Tech. rep. SpaceX (cit. on p. 3).

Sueur, C. and G. Dauphin-Tanguy (1991). "Bond-graph approach for structural analysis of MIMO linear systems." In: *Journal of the Franklin Institute* 328(1), pp. 55–70 (cit. on p. 11).

Trefethen, L. N. (2000). *Spectral Methods in MATLAB*. Society for Industrial and Applied Mathematics (cit. on pp. 13, 103, 129).

Trivedi, M. V., R. N. Banavar, and P. Kotyczka (2016). "Hamiltonian modelling and buckling analysis of a nonlinear flexible beam with actuation at the bottom." In: *Mathematical and Computer Modelling of Dynamical Systems* 22(5), pp. 475–492 (cit. on p. 167).

van der Schaft, A. J. (1989). "System Theory and Mechanics." In: *Three decades of mathematical system theory*. Springer Berlin Heidelberg, pp. 426–452 (cit. on p. 23).

van der Schaft, A. J. (2005). *Network Modeling and Control of Physical Systems: Theory of Port-Hamiltonian systems*. Course notes, University of Twente (cit. on p. 25).

van der Schaft, A. J. (2013). "Port-Hamiltonian Differential-Algebraic Systems." In: *Surveys in Differential-Algebraic Equations I*. Springer, pp. 173–226 (cit. on p. 41).

van der Schaft, A. J. and D. Jeltsema (2014). "Port-Hamiltonian Systems Theory: An Introductory Overview." In: *Foundations and Trends® in Systems and Control* 1(2), pp. 173–378 (cit. on p. 30).

van der Schaft, A. J. and B. M. Maschke (2001). "Fluid dynamical systems as Hamiltonian boundary control systems." In: *Proceedings of the 40th IEEE Conference on Decision and Control*. Vol. 5. IEEE: Orlando, USA, pp. 4497–4502 (cit. on pp. 12, 82).

van der Schaft, A. J. and B. M. Maschke (2002). "Hamiltonian formulation of distributed-parameter systems with boundary energy flow." In: *Journal of Geometry and Physics* 42(1-2), pp. 166–194 (cit. on p. 12).

Vasques, C. M. A. and J. Dias Rodrigues (2006). "Active vibration control of smart piezoelectric beams: Comparison of classical and optimal feedback control strategies." In: *Computers & Structures* 84(22-23), pp. 1402–1414 (cit. on p. 149).

Venkatraman, A. and A. J. van der Schaft (2010). "Full-order observer design for a class of port-Hamiltonian systems." In: *Automatica* 46(3), pp. 555–561 (cit. on p. 151).

Verghese, G. C., B. C. Lévy, and T. Kailath (1981). "A Generalized State-Space for Singular Systems." In: *IEEE Transactions on Automatic Control* 26(4), pp. 811–831 (cit. on p. 131).

Villegas, J. A. (2007). "A port-Hamiltonian approach to distributed parameter systems." PhD thesis. University of Twente (cit. on p. 38).

Voss, T. and J. M. A. Scherpen (2011a). "Stability analysis of piezoelectric beams." In: *Proceedings of the 50th IEEE Conference on Decision and Control and European Control Conference*. Orlando, USA, pp. 3758–3763 (cit. on p. 167).

Voss, T. and J. M. A. Scherpen (2011b). "Stabilization and shape control of a 1D piezoelectric Timoshenko beam." In: *Automatica* 47(12), pp. 2780–2785 (cit. on p. 12).

Voss, T. and J. M. A. Scherpen (2011c). "Structure preserving spatial discretization of a 1-D piezoelectric Timoshenko beam." In: *Multiscale Modeling & Simulation* 9(1), pp. 129–154 (cit. on pp. 13, 47).

Voss, T. and J. M. A. Scherpen (2014). "Port-Hamiltonian Modeling of a Nonlinear Timoshenko Beam with Piezo Actuation." In: *SIAM Journal on Control and Optimization* 52(1), pp. 493–519 (cit. on pp. 47, 167).

Voss, T., J. M. A. Scherpen, and P. R. Onck (2008). "Modeling for control of an inflatable space reflector, the nonlinear 1-D case." In: *Proceedings of the 47th IEEE Conference on Decision and Control*, pp. 1777–1782 (cit. on p. 47).

Voss, T., J. M. A. Scherpen, and A. J. van der Schaft (2008). "Modeling for control of an inflatable space reflector , the linear 1-D case." In: *Proceedings of the 18th International Symposium on Mathematical Theory of Networks & Systems*. Blacksburg, Virginia, USA (cit. on p. 47).

Voss, T. and S. Weiland (2011). "Structure preserving spatial discretization of 1D convection-diffusion port-Hamiltonian systems." In: *Proceedings of the 50th IEEE Conference on Decision and Control and European Control Conference*. Orlando, USA, pp. 6979–6984 (cit. on p. 13).

Voss, T. (2010). "Port-Hamiltonian Modeling and Control of Piezoelectric Beams and Plates: Application to Inflatable Space Structures." PhD thesis. University of Groningen (cit. on pp. 13, 47).

Voss, T. and J. M. A. Scherpen (2009). "Structure preserving port-Hamiltonian discretization of a 1-D inflatable space reflector." In: *Proceedings of the 10th European Control Conference*, pp. 850–855 (cit. on p. 13).

Vu, N. M. T. (2014). "Approche hamiltonienne à ports pour la modélisation , la réduction et la commande des dynamiques des plasmas dans les tokamaks." PhD thesis. Université de Grenoble (cit. on p. 13).

Vu, N. M. T., L. Lefèvre, R. Nouailletas, and S. Bremond (2013). "Geometric Discretization for a Plasma Control Model." In: *Proceedings of the 5th IFAC Symposium on System Structure and Control*. Grenoble, France, pp. 755–760 (cit. on p. 168).

Wu, Y., B. Hamroun, Y. Le Gorrec, and B. Maschke (2014). "Port Hamiltonian System in Descriptor Form for Balanced Reduction: Application to a Nanotweezer." In: *Proceedings of the 19th World Congress of the International Federation of Automatic Control*. Cape Town, South Africa (cit. on pp. 13, 41).

Zhang, J., L. He, E. Wang, and R. Gao (2008). "A LQR Controller Design for Active Vibration Control of Flexible Structures." In: *Proceedings of the 2008 IEEE Pacific-Asia Workshop on Computational Intelligence and Industrial Application*, pp. 127–132 (cit. on p. 149).

Zhang, J., L. He, and E. Wang (2010). "Active Vibration Control of Piezoelectric Intelligent Structures." In: *Journal of Computers* 5(3), pp. 401–409 (cit. on p. 149).

Zhang, J., L. He, E. Wang, and R. Gao (2009). "Active Vibration Control of Flexible Structures Using Piezoelectric Materials." In: *Proceedings of the 2009 International Conference on Advanced Computer Control*. Ieee, pp. 540–545 (cit. on pp. 149, 150).

Zuziak, P., Z. Šika, M. Valášek, T. Vampola, and T. Klimmek (2010). "Vibration Control of Flexible Aircraft with Respect to Passengers Comfort." In: *Proceedings of the ISMA International Conference on Noise and Vibration Engineering*. Leuven, Belgium, pp. 495–508 (cit. on p. 145).

Zwart, H. and M. Kurula (2014). "The linear wave equation on N-dimensional spatial domains." In: *Proceedings of the 21st International Symposium on Mathematical Theory of Networks and Systems*. Vol. 2. 3. Groningen, The Netherlands, pp. 1157–1160 (cit. on p. 74).